Seismic Surveys at Alabama Electric Cooperative's Proposed Damascus, Alabama Site

Richard D. Miller
Jianghai Xia

Kansas Geological Survey
1930 Constant Avenue
Lawrence, Kansas 66047

Final Report to

Burns & McDonnell WCI
Kansas City, Missouri

Open-file Report No. 99-12

June 15, 1999

The Kansas Geological Survey makes no warranty or representation, either express or implied, with respect to the data, documentation, or interpretations or decisions based on the use of this data including the quality, performance, merchantability, or fitness for a particular purpose. In no event will the Kansas Geological Survey be liable for direct, indirect, special, incidental, punitive, or consequential damages arising out of the use of or inability to use the database or documentation whether as a result of contract, negligence, strict liability, or otherwise.

Seismic Surveys at Alabama Electric Cooperative's Damascus, Alabama Site

INTRODUCTION

Shallow seismic reflection and surface wave imaging techniques were used to delineate subsidence-prone areas at Alabama Electric Cooperative's proposed power generation plant site near Damascus, Alabama (Figure 1). Discussions in this report will be limited to the seven seismic reflection profiles (lines 1, 2, 3, 6, 8, 9, and 10) and the thirteen shear wave velocity field cross-sections (lines 1-13) (Figure 2). A feasibility survey (Miller and Xia, 1999) conducted during mid-December 1998 provided conclusive evidence that shallow seismic reflection surveying had the potential at this site to delineate dissolution features tens of feet in diameter. The shear wave velocity field was shown to provide valuable information in areas that might be subsidence risks. Areas studied with "young" sinkholes directly tied to karst features consistently produced velocity inversions in proximity to large velocity gradients (generally forming a closure on contoured cross-sections). These characteristic anomalous areas were interpreted to indicate high stress associated with either roof rock loading over rubble zones or void areas or loading over roof support structures or pillars. Shot gathers and shear wave profiles from the feasibility study and stacked reflection sections and shear wave cross-sections possessed several unique features that are likely related to dissolution and subsidence. A complete preliminary discussion of the techniques, limitations, and resolution potential is included in the preliminary report (Miller and Xia, 1999).

GEOLOGY

Near-surface geology (the upper 600 ft) in this area is characterized by relatively flat-laying predominantly limestone and shale (clay) sequences overlain by a relatively thin veneer of highly variable sand and clay layers (Figure 3). Unconsolidated materials at this site are predominantly clay and sandy-clay with the Bucatunna Clay separating River Terrace Deposits from the sculptured surface of the Glendon Limestone (bedrock). Dissolution and erosion have left the bedrock surface with the short wavelength pinnacle-type topography observed in outcrop and suggested in drill data. This highly irregular bedrock surface provided a challenge to both reflection and surface wave imaging with neither able to confidently resolve the pinnacle features

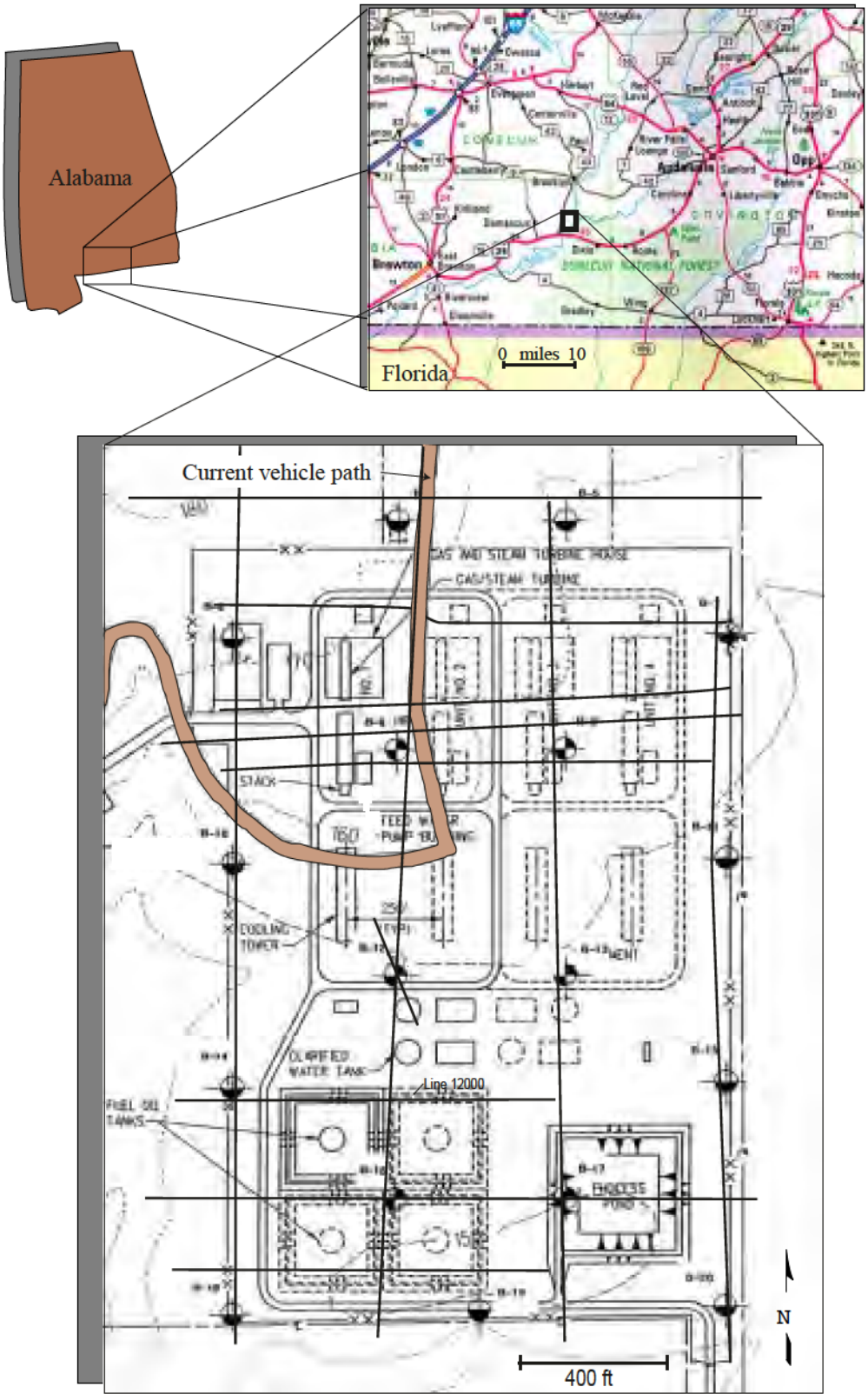

Proposed AEC Site

Figure 1

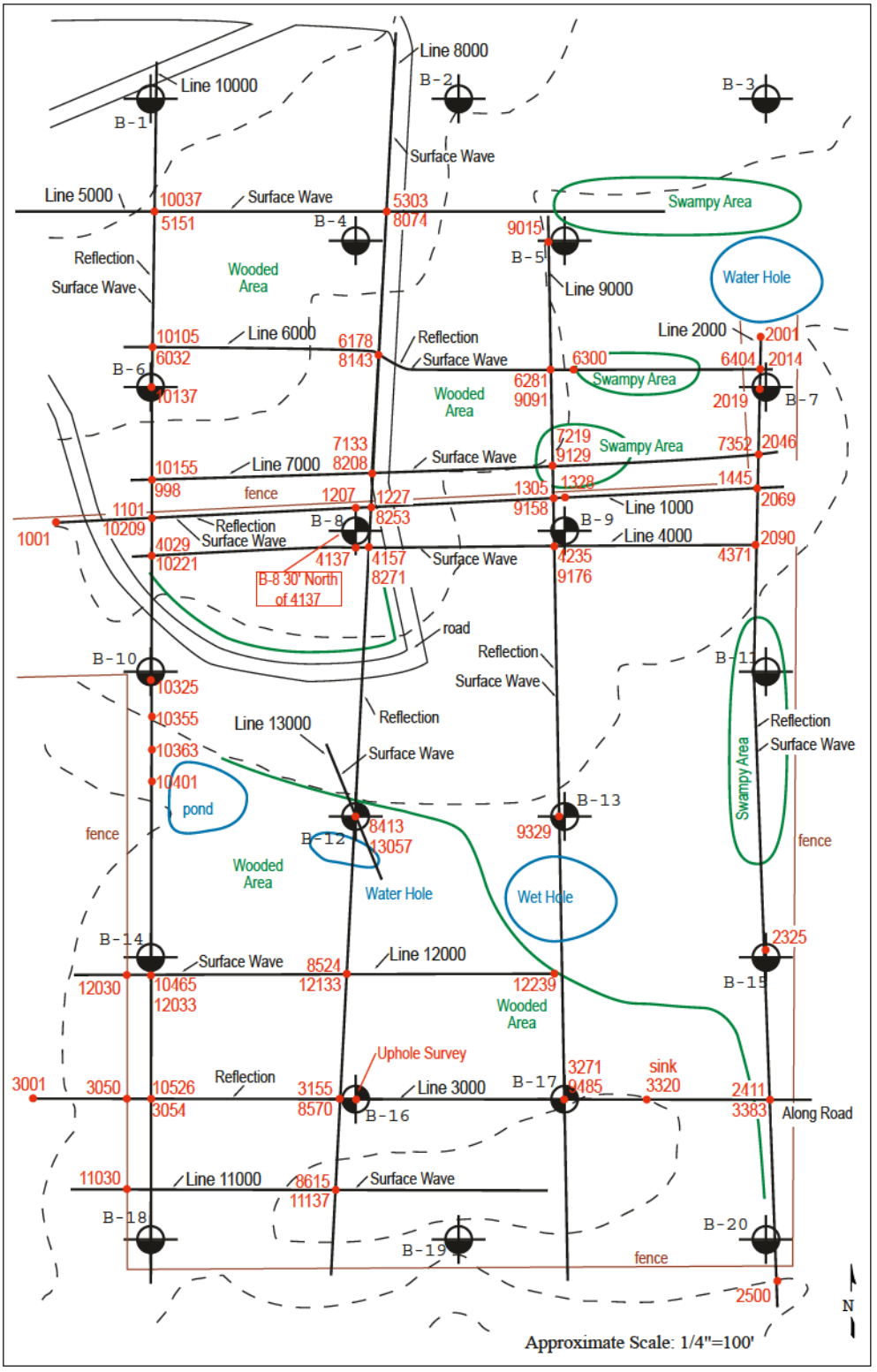

Figure 2. Station location ties between lines and surface features. Lines are located on this diagram in approximate relative locations.

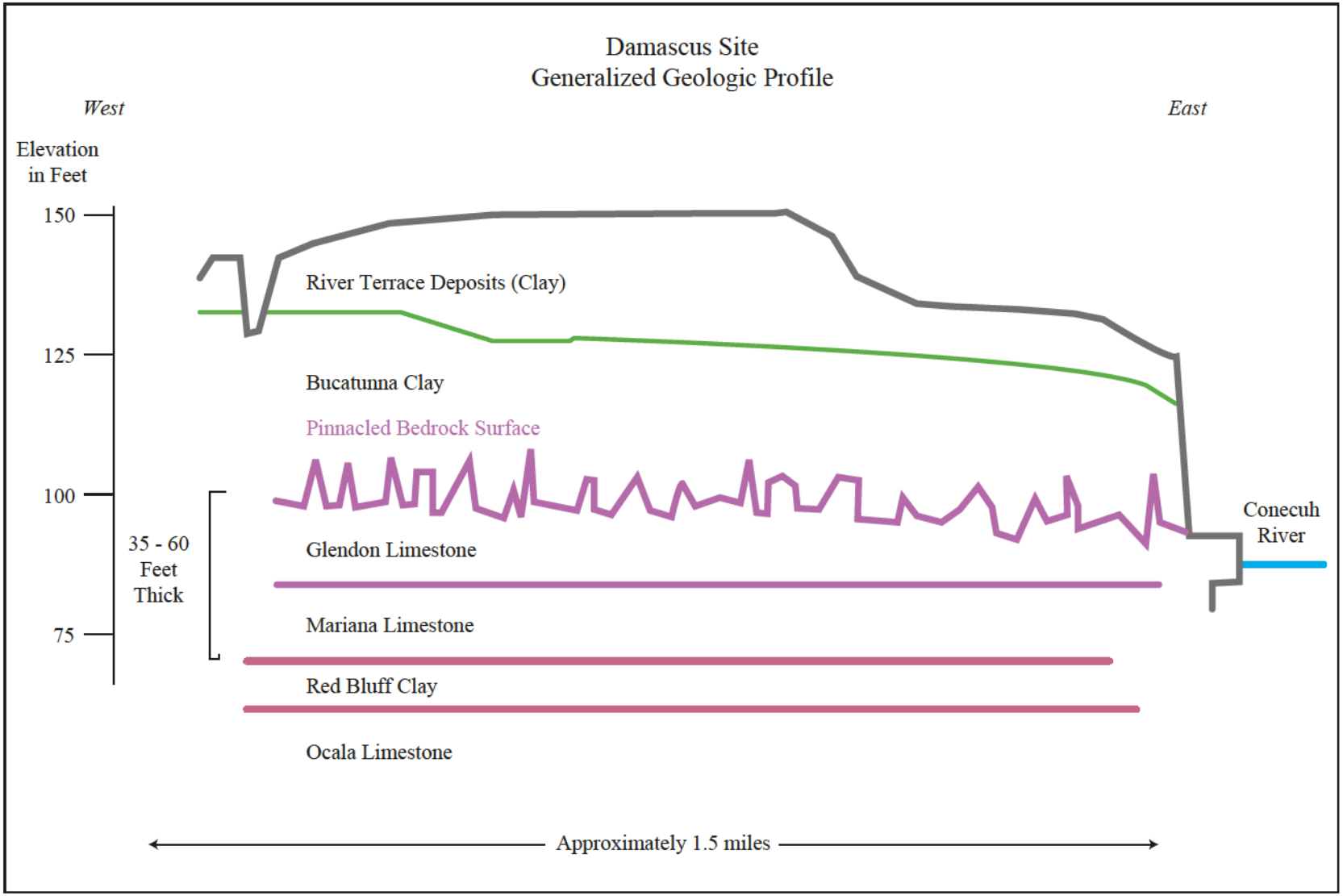
Damascus Site
Generalized Geologic Profile
West
East
Elevation in Feet
150
125
100
75
River Terrace Deposits (Clay)
Bucatunna Clay
Pinnacled Bedrock Surface
35 - 60 Feet Thick
Glendon Limestone
Mariana Limestone
Red Bluff Clay
Ocala Limestone
Conecuh River
Approximately 1.5 miles

Figure 3

observed in outcrop. The Glendon Limestone overlays the Mariana Limestone and together are around 35 to 60 ft thick. The Mariana Limestone is in direct contact with the Red Bluff Clay and which overlays the Ocala Limestone. The top of the Ocala Limestone is generally thought to be around 100 ft below ground surface at this site and represents the shallowest sitewide consistent seismic marker on all the seismic reflection sections.

Limestone units encountered during drilling at this site lacked uniform competence. Rock layers sampled during drilling showed extremely altered rock and resulted in only minimal core recovery. Lithologies have been identified based on drill characteristics (such as changes in stiffness) and general make-up of the highly altered samples recovered during drilling/coring. No unique sitewide geologic interfaces (units) were identified within 150 to 200 ft of the ground surface from drill cutting at this site. Every borehole drilled in association with this study encountered zones with fractures, voids, extremely low blow counts, water loss, and/or vugs. Considering the regional continuity of the near-surface geologic units expected to be present at this site, the lack of any consistently distinguishable limestone and clay units is evidence for a highly altered near-surface (upper 200 ft).

METHODOLOGIES

High resolution seismic reflection is a powerful method of imaging the shallow sub-surface (Appendix A). The successful use of the technique depends on several key conditions. Foremost among these is the existence of acoustic velocity and/or density contrasts generally corresponding to geologic interfaces in the subsurface. The second relates to the ability of the near surface to propagate high frequency seismic signals. Finally, the acquisition parameters, recording equipment, and processing flow must be compatible with the proposed target and resolution requirements of the survey. Seismic reflection and surface wave imaging were used coincidently at this site to allow disturbed strata and anomalous zones (faults, fractures, sub-sidence features, etc.) identified at depth (50 ft and deeper—reflection) to be extended into the shallow subsurface (0 to 100 ft—surface wave).

Continuous surface wave imaging (Park et al., 1999a; Xia et al., 1999a; Park et al., 1999b; Xia et al., 1999b; Xia et al., 1998; Xia et al., 1997; Park et al., 1996) is a new adaptation of a well founded geophysical technique (Nazarian et al., 1983; Stokoe et al., 1994) used for years on civil engineering projects to determine shear wave velocity as a function of depth

(Appendix B). Mapping the two- or three-dimensional shear wave velocity field can provide insight into the variability of subsurface materials. This imaging method can be applied with no assumptions necessary about the subsurface (i.e., layered earth, increasing velocity with depth, geologic/hydrogeologic contacts/interfaces possessing a velocity and/or a density contrast, etc.).

The shear wave velocity field mapping technique, as applied here, is especially sensitive to abrupt changes in near-surface materials (e.g., bedrock interface, voids, fracture zones, etc.). Changes in shear wave velocity are generally directly related to changes in material properties. During the feasibility study (Miller and Xia, 1999), a distinctive localized high velocity signature immediately above a lower velocity zone appeared consistent with the presence of sinkholes in the Auburn University's Solon Dixon Forestry Research Center. This observation is consistent with previous interpretations of voids on shear wave velocity data in coal mine areas. Probably most important to this study is the sensitivity of the technique to the absence or alteration of competent rock below the bedrock surface.

ACQUISITION

Data were acquired with state-of-the-art near-surface imaging equipment. A Geometrics StrataView R60 seismograph was used in a 240-channel configuration for the shallow reflection data and in a 48-channel configuration with a 240-channel roll-along switch to record the surface wave data. Receivers for the shallow reflection survey were a group of three Mark Products L28E 40 Hz geophones wired in series with 5-inch spikes. For the surface wave surveys, single Geospace GS-11D 4.5 Hz geophones with 3-inch spikes were deployed. Station spacing for both reflection surveying and surface wave profiles were the same with receiver stations spaced at 4 ft and source stations at 8 ft. Three ground impacts from a rubber band accelerated weight drop (RAWD) were vertically stacked by the seismograph at each source location for the surface wave profiles, while a single shot from a 50-cal downhole rifle provided the energy for most shallow reflection data. Two shots from a downhole 30.06 rifle, each saved as a separate file in the seismograph supplied the energy pulse for part of line 9 and all of line 10. The data were acquired with equipment and parameters optimized for the available equipment and the site conditions and targets.

PROCESSING

Processing of these data drew on all currently proven and effective methodologies and flows using software specially designed and written for shallow seismic data. Shallow reflection data were processed into CMP stacked sections using *WinSeis*, a commercially available software package. The shallow reflection data are nominal 120 fold with the actual fold ranging from 2 to over 240. This level of redundancy provided ample traces within the optimum window for recording reflections from depths as shallow as 40 ft and events from in excess of 1000 ft. Shallow seismic reflection processing flows must be optimized/customized for each data set and target objective (Table 1). Processing the reflection data for this survey required extreme detail and attention to statics and a variable velocity structure. Static variability on the order of several milliseconds was observed between adjacent traces. Since these data possess dominant frequencies as high as 200 Hz in some locations, less than 3 ms of mismatch between stacked traces would result in cancellation of reflected wavelets for near-vertical traces and less than that with longer offsets.

Table 1

SEG2 to SEGY
Roundup into 240 channels
Bad trace edit
First arrival mute
Air wave/ground roll mute
Time break static adjustment
Match trace polarity
Spectral analysis
Spectral balance (30-80—200-300)
Amplitude balance (100 ms)
F-k filter to remove events with refraction slope after first arrival mute
Define geometry
CMP sort
Velocity analysis
Surface consistent statics
Common offset statics
Velocity analysis
Normal moveout correction
Residual statics
CMP stack
Frequency filter
AGC scale
Migration filter
Time-depth conversion
Display

Surface wave data processing required fewer individual steps and involved about one-fifth as many traces as the reflection data; therefore it was completed in a much shorter time (Table 2). Surface wave data were processed into shear wave velocity field cross-sections with *SurfSeis*, a proprietary set of algorithms developed by the Kansas Geological Survey. Processing of surface wave data involves the transformation of the time-distance shot gathers into a frequency-phase velocity domain curve (dispersion curve). Once displayed as a dispersion curve the appropriate frequency band can be selected and dispersion curve inverted into a shear wave velocity trace (shear wave velocity as a function of depth). After a shear wave velocity trace has been defined for each spread, a 2-D contour map of the velocity field as a function of station location and depth could be generated for each profile line.

Table 2

SEG2 to SEGY
Calculate dispersion curve from phase velocity and frequency
Estimate initial model (5.5 Hz to 24 Hz—30 to 200 ft wavelength)
Invert to solve for shear wave velocity
Contour velocity field (Surfer)

INTERPRETATION

Reflection data from this survey possesses excellent resolution potential down to depths in excess of 1000 ft. Several high quality reflection events can be interpreted in the upper 250 ft. Time-to-depth conversions are based on stacking velocities that average around 4000 ft/sec at around 25 ms, 5000 ft/sec at 100 ms, 6000 ft/sec at 200 ms, and 7000 ft/sec at 300 ms. These velocities provide gross estimations of the depths to interpreted reflectors. Reflection events as shallow as 25 ms (~40 ft) are interpretable on most lines. The 100 ms reflector (~250 ft) provides the reference (datum) for structures interpreted in the shallow portion of the sections. This high amplitude, continuous (at least within the survey area) reflection allows shallower structures to be distinguished from static resulting from ultra-shallow variations in stratigraphy or structure. Interpretation of these data will be broken up according to each individual line, with coincident interpretations of the reflection and shear wave data made when possible.

Surface waves are affected by the shear wave velocity (Xia et al., 1999b). Critical to interpreting the shear wave velocity field when calculated using surface waves is appreciation for the resolution potential of the inverted data. Each wavelength/frequency component of the surface waves penetrates to a depth influenced by the phase velocity of the material. As the wavelengths get longer and longer, the depth of energy penetration increases linearly. The effects of localized changes in shear wave velocity (anomalies) will therefore be averaged over a larger area than actually occupied by the anomaly. It should be expected that anomaly smearing will be elongated downward and away from the source. The highest resolution will be at the top and source side of the image. Keeping this data characteristic in mind, shear wave velocity field interpretations correlated quite well to drilling and provided an excellent overall measure of the sediment uniformity in the upper 100 ft. It is not possible to tell what materials are present within low velocity zones and therefore interpretation of the surface wave (shear wave velocity field) data presented here does not try to correlate with stratigraphy. It is only possible to detect the absence of the "native" materials and the presence of materials anomalous to their surroundings.

Several distinctive features interpretable on the shear wave velocity cross-sections must be future investigated prior to and during the design of any surface structure at this site. A low velocity zone seems to be present generally around the site at a depth of around 20 ft. This low velocity zone is likely consistent with a sand or gravel layer sandwiched between clay-rich layers. Bedrock is interpreted to approximately correlate with the 800 ft/sec contour. The high velocity gradient (indicative of a rapid vertical change in shear wave velocity) sitewide between 20 and 40 ft below ground surface at velocities around 800 ft/sec is characteristic of an abrupt or impulsive change in lithology. In most places around this site the velocity contours change very rapidly and relatively uniformly between about 700 ft/sec and 1000 ft/sec. The actual lithologic boundary interpreted as the bedrock surface in boreholes should very closely correlate to the onset of the large gradient zone. Unless a relatively large portion (at least one spread length, 188 ft) of the bedrock surface is missing and/or replaced by lower velocity unconsolidated materials a distinctive low velocity chimney feature will be difficult to confidently identify. Within bedrock anomalous zones in general will be elongated downward and away from the source laterally. This elongation artifact of this process will impact how well each line ties in the presence of anomalies and the severity of the velocity change. Velocity changes associated with anomalies can be confidently interpreted using a shorter spread length.

Line 1

Reflection (Figures 4 and 5)

Several features significant to this study are evident on the CMP stacked section of line 1. Probably the most striking is the paleosinkhole centered around station 1390. This bowl shaped depression in the reflectors shallower than 250 ft is striking evidence that supports this being an active subsidence area in the past. The lack of flat-laying undisturbed reflection events above this paleosinkhole prohibits estimation of subsidence rates, length of activity, or even when subsidence ended. Careful analysis of the relative location of the various coherent reflection events present within the depression suggests this sinkhole was active at several different times in the past. Subsidence rates cannot be estimated with these data; it is, however possible to estimate the extent of this depression when it was exposed at the ground surface. With no current surface expression of this dissolution feature it is reasonable to suggest the dissolution process responsible for this paleosinkhole is currently experiencing a period of inactivity. However, with the clear indication that several periods of dissolution, subsidence, dormancy, and reactivation, this feature should not be completely dismissed as a potential threat.

Based on seismic stacking velocities, and keeping in mind that these data have not been migrated, it is reasonable to suggest this sinkhole can account for 60 to 70 ft subsidence. It appears to have been active at least twice prior to the current state of inactivity. Interpretations using this line alone suggests this feature was about 200 ft across and 50 ft deep prior to the infilling with sediments.

Other noteworthy features include the disturbed reflection events between stations 1115 and 1190 within the 40 to 80 ms (80 and 200 ft) time window. Chaotic-looking reflection events are present within the same time interval on the west end that the signature of the sinkhole is in on the east end of the line. It is reasonable to suggest that the dissolution responsible for the paleosinkhole is or has been active within this portion of the profile, but not to the same extent. Between station 1130 and about 1240 the shallowest reflector (30 to 40 ft) appears to be either missing or extremely disturbed. This could be from dissolution, bedrock erosion (channel) prior to burial by the overlying unconsolidated sediments, or simply this portion of the bedrock lacked sufficient lateral coherency to be mapped as a continuous unit with this resolution seismic data.

Several small diffraction events are interpreted on the stacked sections. These diffrac tions are key indicators of point source features, which are generally bed terminations, extreme

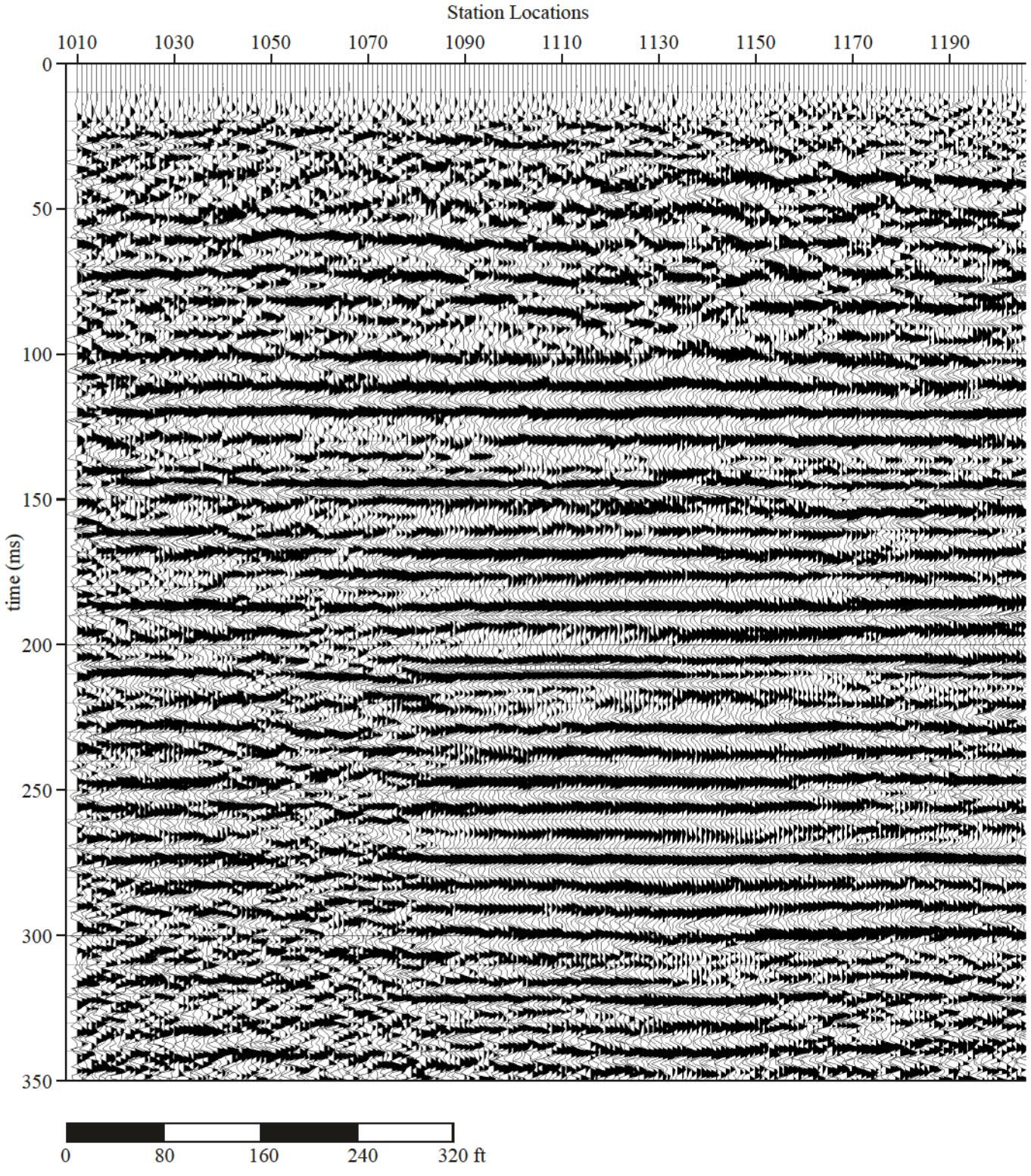

Figure 4a. CMP stacked section of line 1.

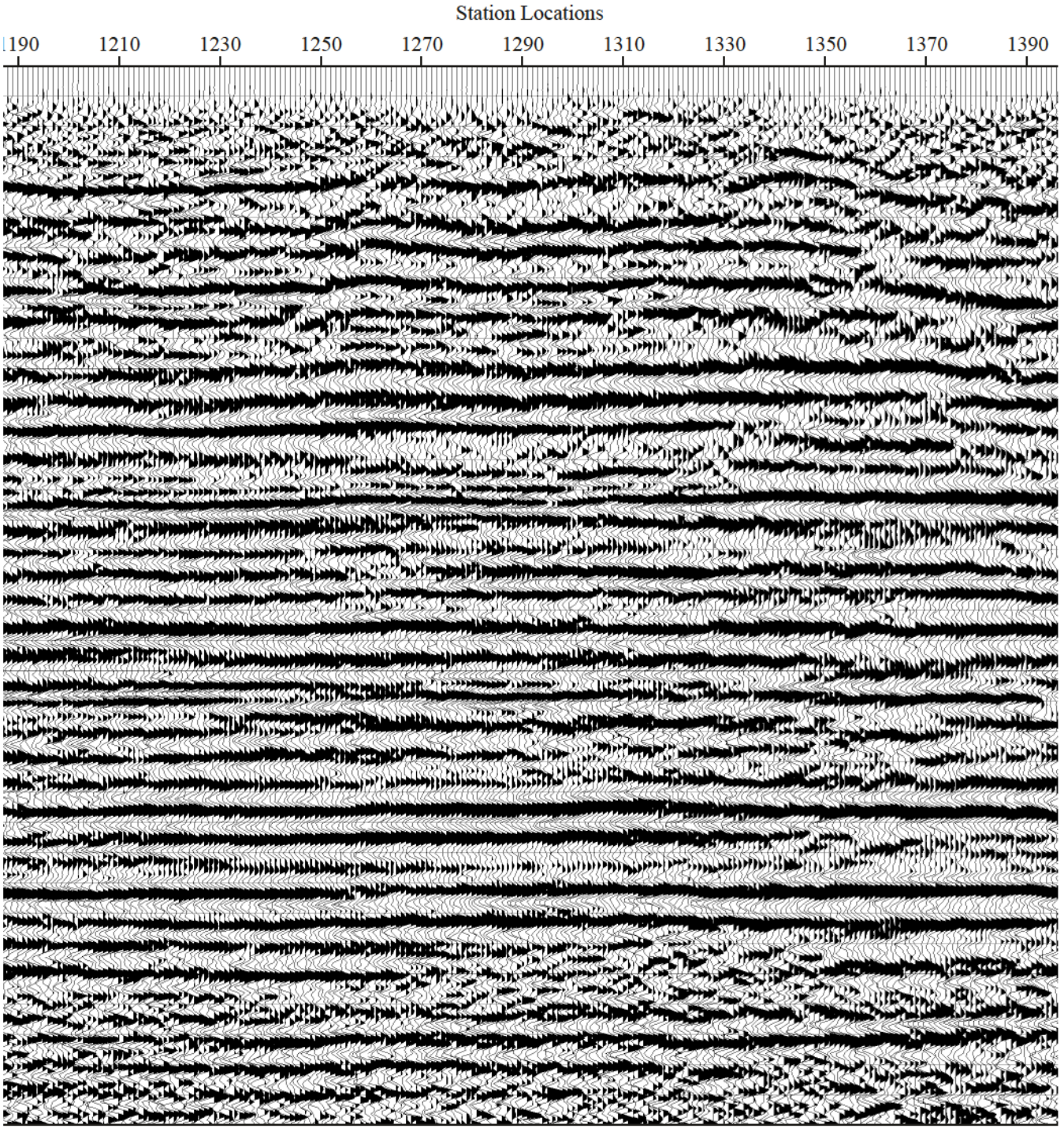
Station Locations
1190
1210
1230
1250
1270
1290
1310
1330
1350
1370
1390

Figure 4b.

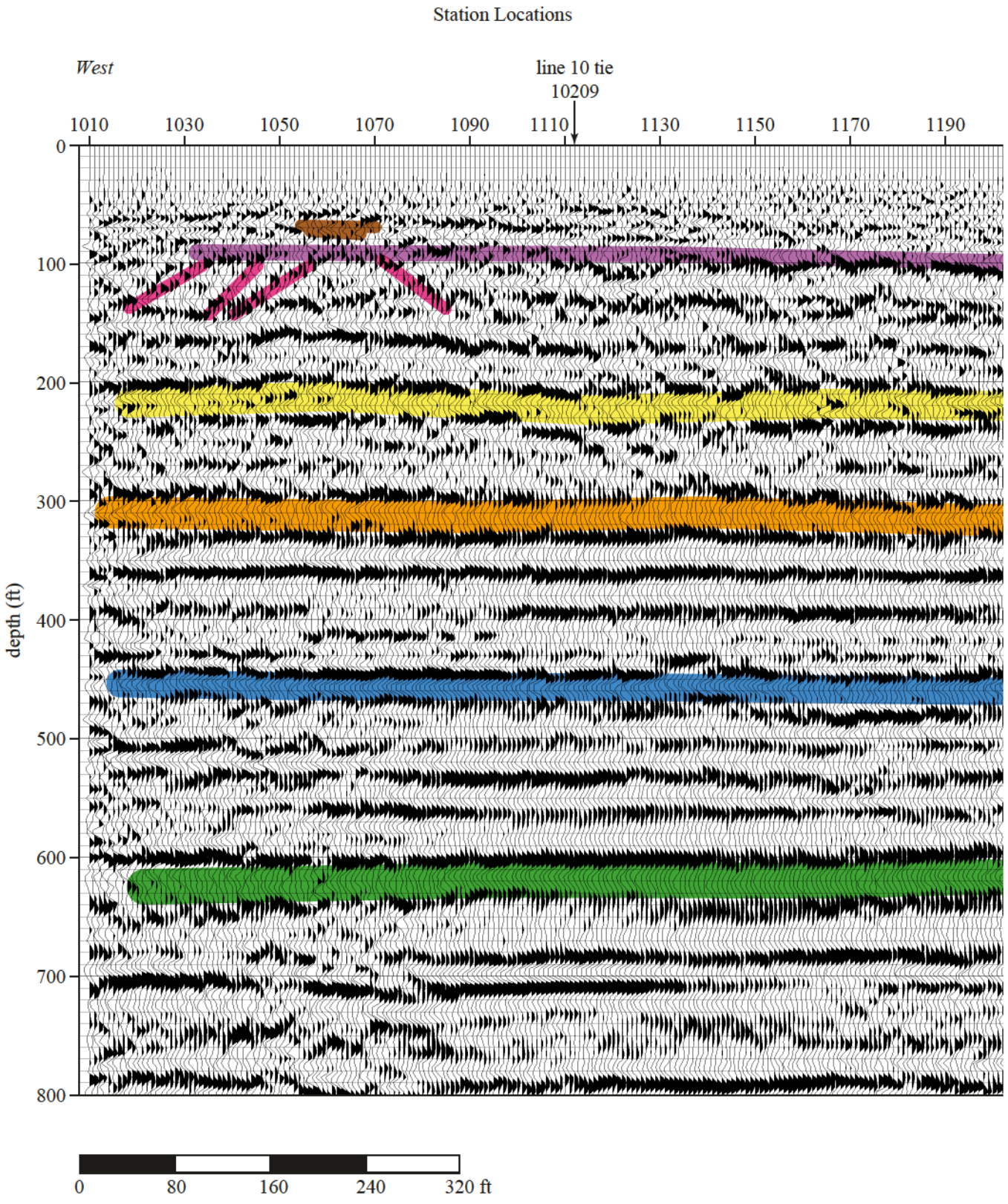

Figure 5a. Interpreted line 1.

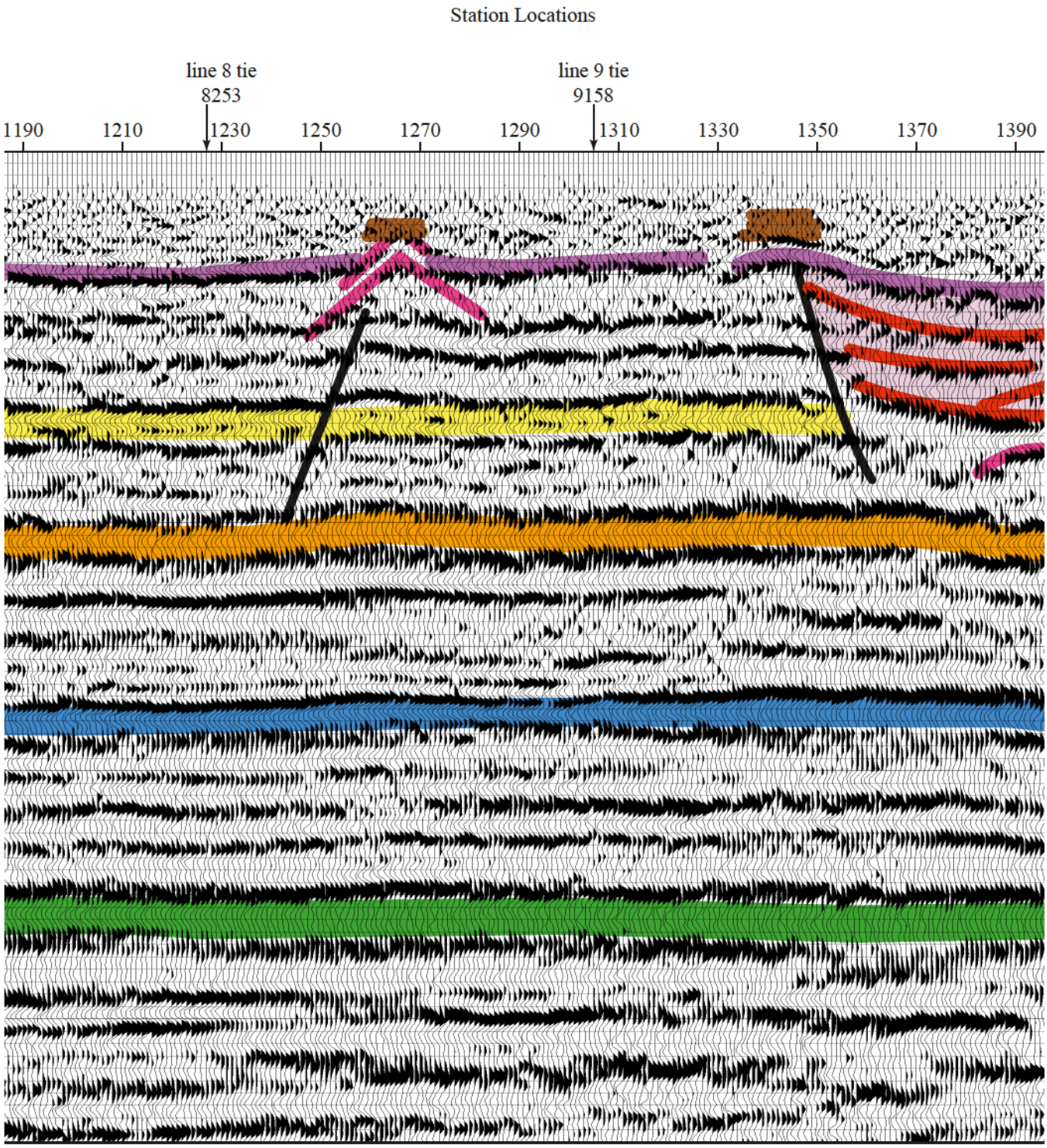
Station Locations
line 8 tie
8253
line 9 tie
9158
1190
1210
1230
1250
1270
1290
1310
1330
1350
1370
1390

Figure 5b..

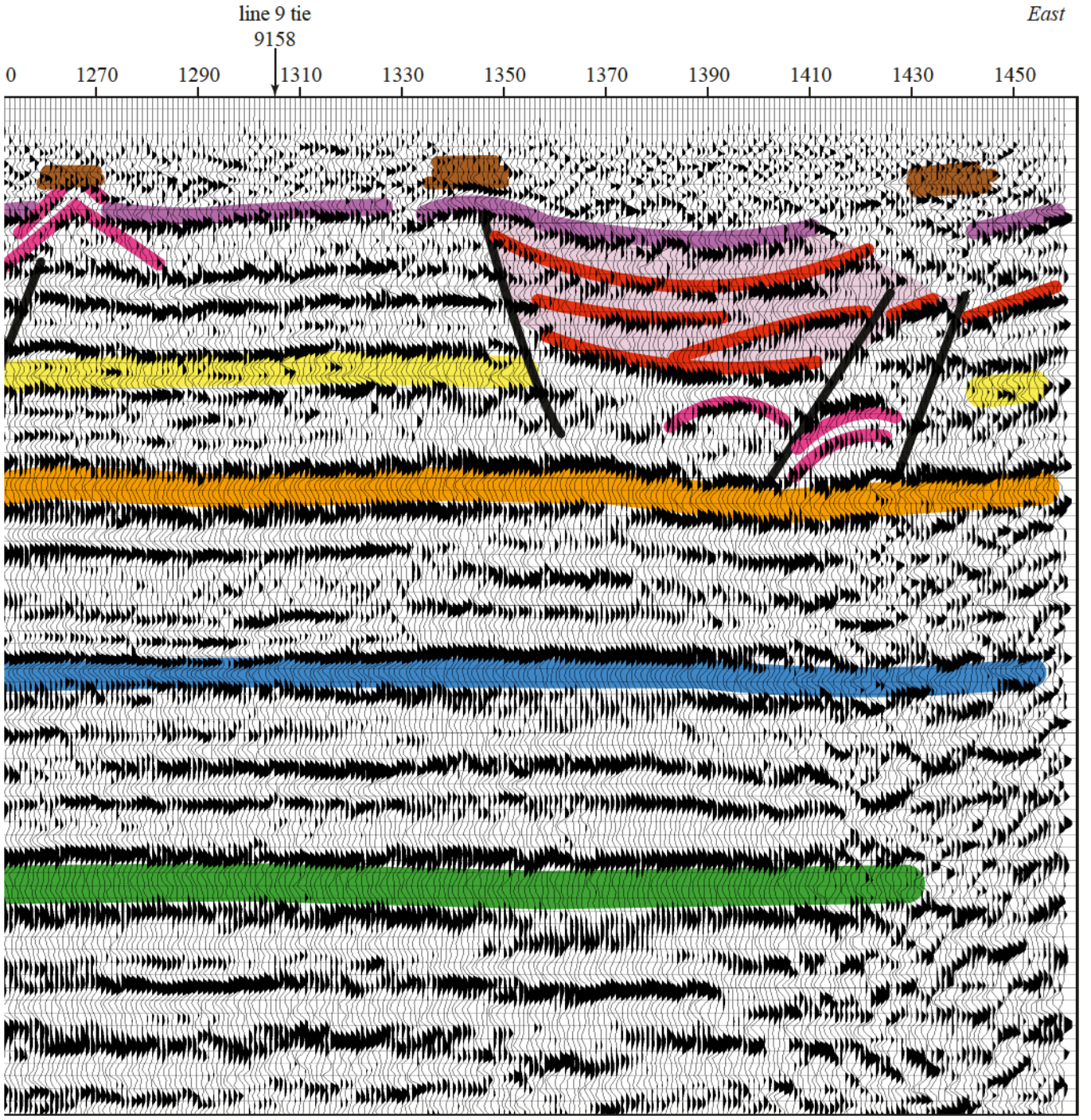
Station Locations
line 9 tie
9158
East
0
1270
1290
1310
1330
1350
1370
1390
1410
1430
1450

Figure 5c..

geometries (tight syncline), small independent blocks, fracture zones, etc. The apexes (centers) of the diffraction events interpreted on these data are at stations 1060 and 1265. Characteristics of the 1060 event are consistent with a dissolution feature. Based on reflection offsets mapped down to around 300 ft beneath the diffraction at 1265, it is reasonable to suggest a fault is responsible for this set of diffraction arrivals. Ending the interpreted faults at about 300 ft of depth was due to insufficient resolution to interpret it below that depth. The fault does extend to greater depth, but the offset is not great enough or the offset is distributed over an area too large to interpret it any deeper.

Surface Wave (Figure 6)

Production of the 2-D shear wave velocity field map of line 1 was accomplished independent of supporting information (drill data, reflection results, etc.). This was done intentionally to insure no bias entered into the initial parameter design of the processing flow. Several distinctive features can be identified that are suggestive of localized zones of very disturbed materials at or just below the bedrock surface. A lower velocity anomaly between station 1030 and about station 1080 from 40 to about 100 ft of depth is consistent with an apparent increasing in depth of the bedrock surface to the west. This low velocity portion of the bedrock is likely smaller than suggested by these data due to the elongation characteristic of this technique discussed previously. It is most likely that a fracture system or void area is present in bedrock beneath surface stations 1050 to 1060 as evidenced by the pulldown in the 1100 and 1200 ft/sec contour near station 1050. This feature is probably less than 30 ft across and extends from the surface of bedrock down to 70 or 80 ft. The tail (downward elongation) of this low velocity zone is directly related to interference of the longer wavelength portions of the ground roll as it passes through the anomaly.

Just east of the low velocity zone beneath surface station 1055 or so is a high velocity closure in the shallow portion of the section. Initial interpretations identified this feature as a drainage culvert crossing under the road. Unless the data set is skewed about 80 ft to the east, this feature cannot be related to the culvert. It is unlikely the culvert represented a large enough contrast to detect. Even more significant than this "bullseye" is the high velocity chimney-looking feature at about station 1080. Even if the high velocity closure at about station 1070 around 10 ft deep is the culvert, this high velocity anomaly is not related to the culvert or the

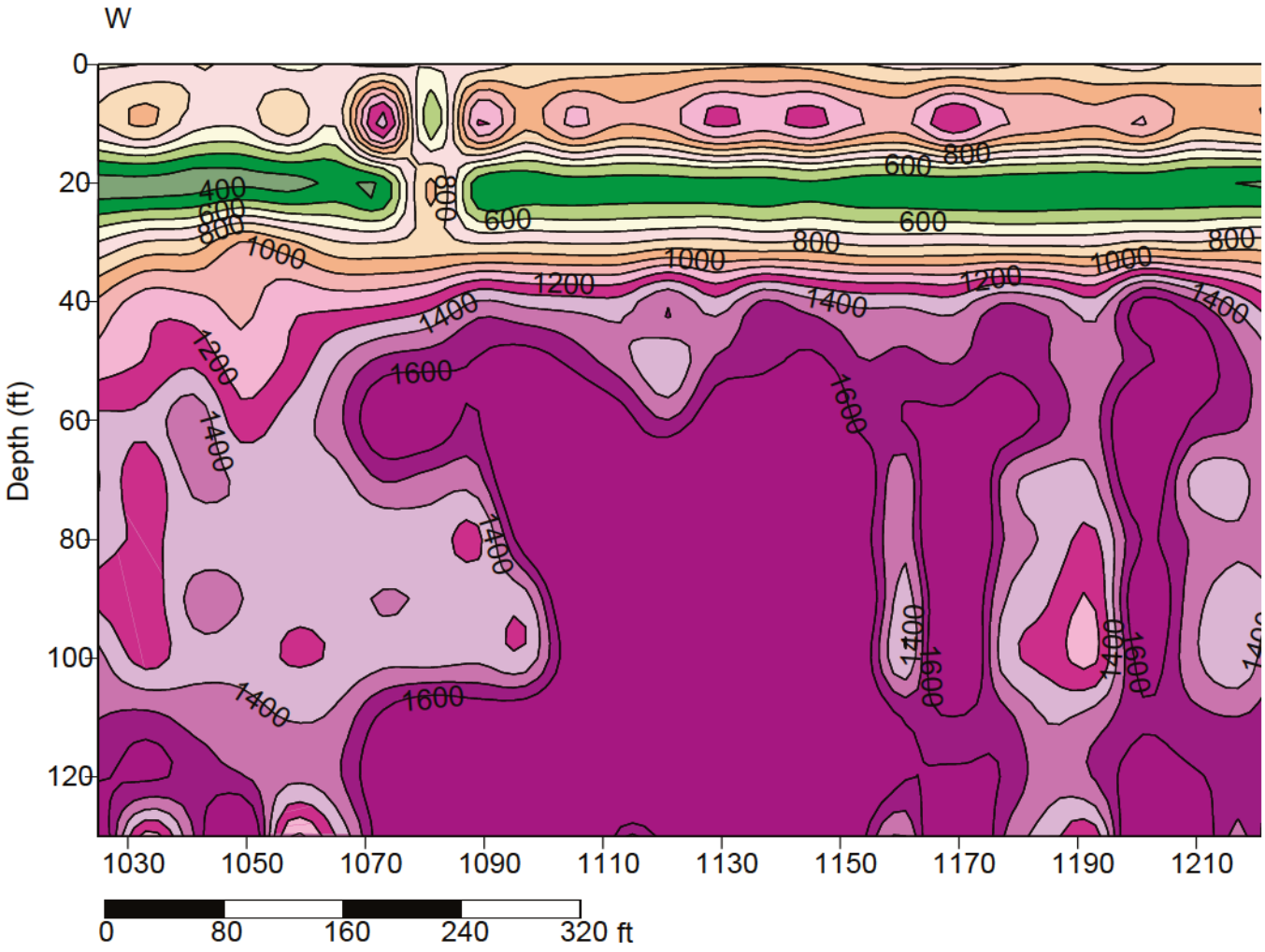

Figure 6a. Shear-wave velocity contour along line 1.

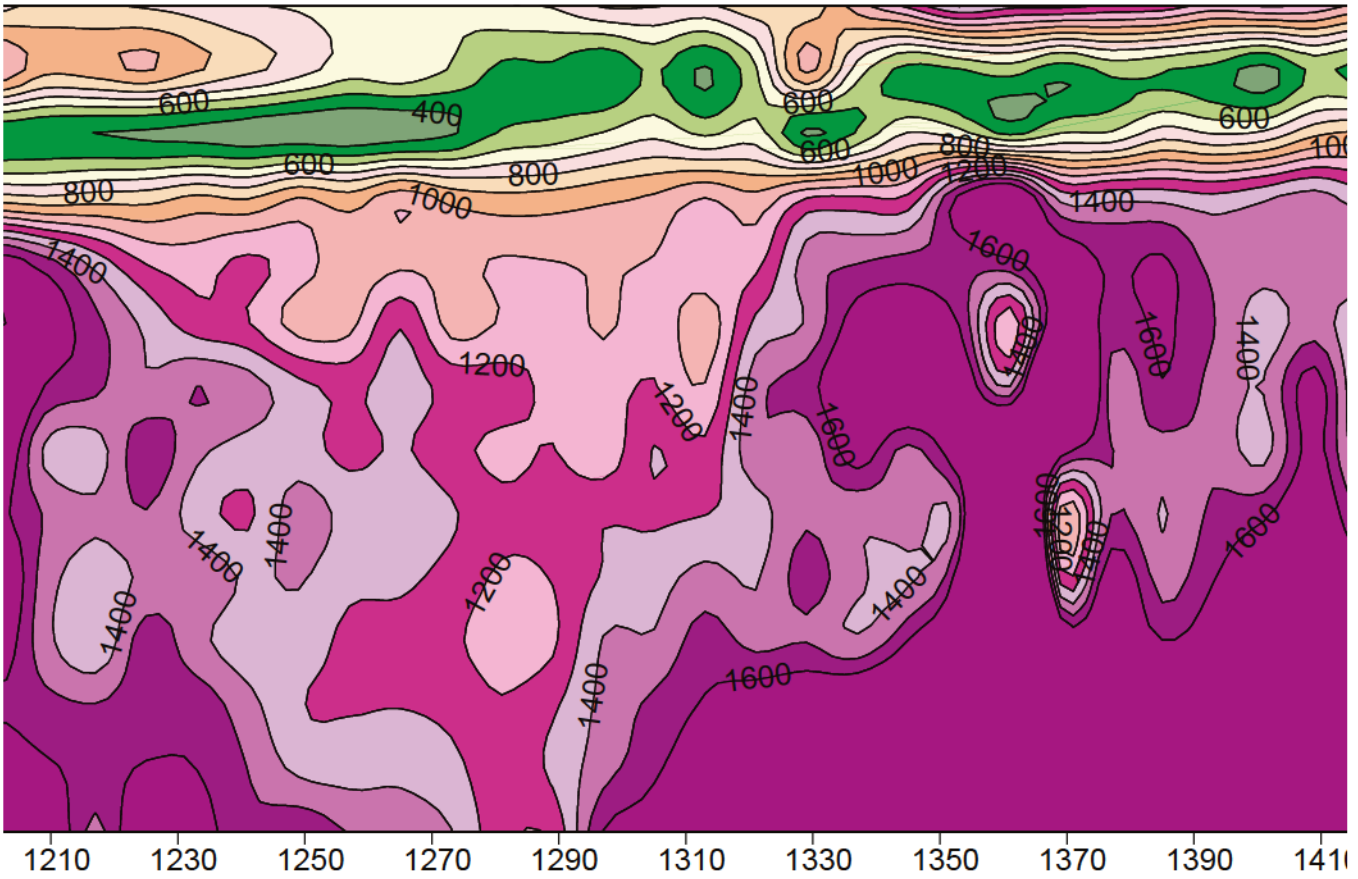

Station Number

Figure 6b.

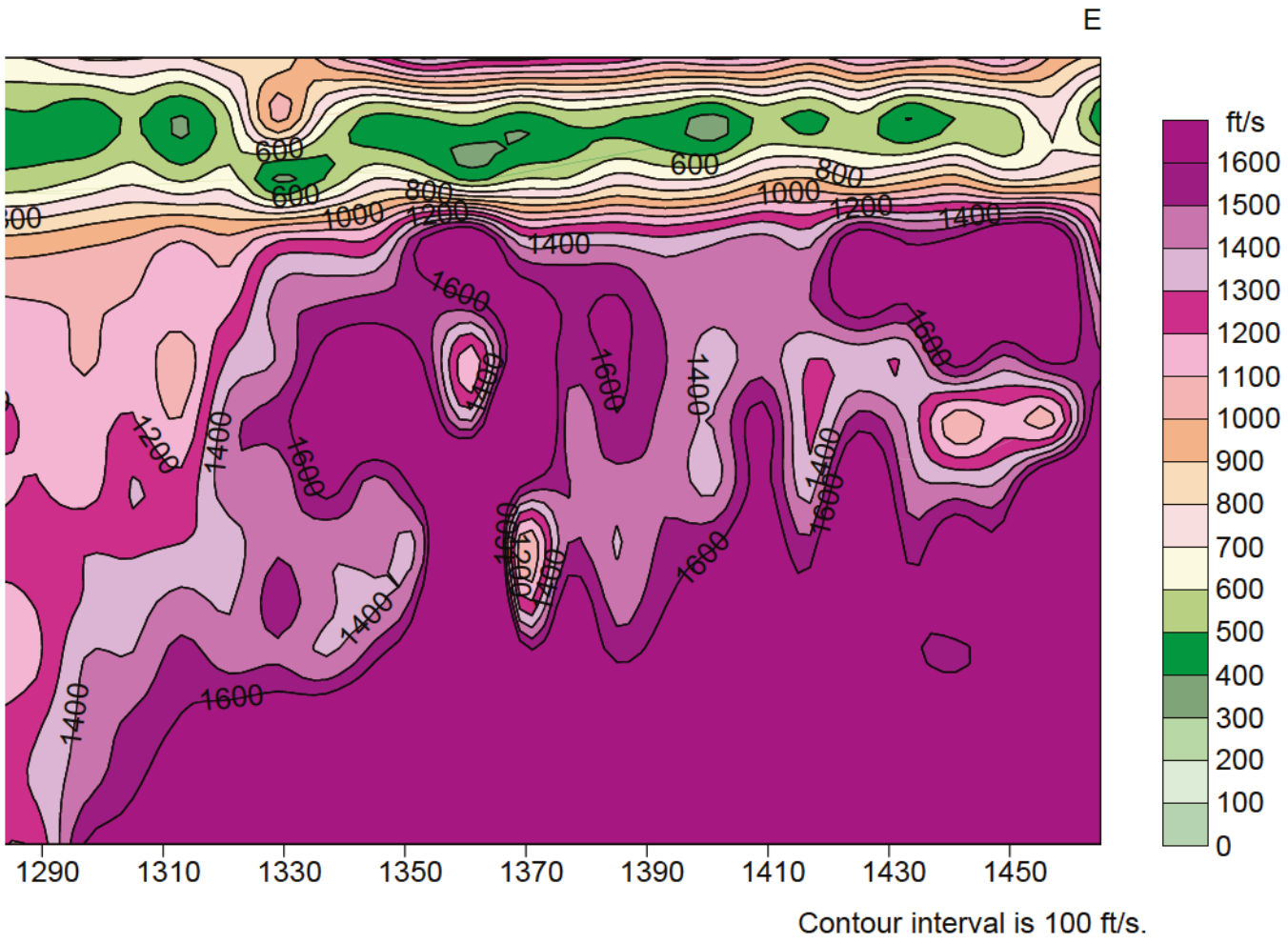
E
ft/s
1600
1500
1400
1300
1200
1100
1000
900
800
700
600
500
400
300
200
100
0
1290
1310
1330
1350
1370
1390
1410
1430
1450
Contour interval is 100 ft/s.
Station Number

Figure 6c.

earthen fill used in making the road. With no indication dissolution has been or is active beneath this feature, it is difficult to interpret it as subsidence induced. It is, however, in close proximity to the anomalous bedrock features below stations 1055 and 1120. Both of these bedrock features are large enough to accommodate the volume of material that may have subsided from this chimney.

A low velocity surface feature correlates quite well with a deep and broad sub-bedrock low velocity zone centered about station 1270. The actual dimensions of this feature are difficult to determine due to the smearing associated with this technique. Without question, the material between the top of bedrock (at about 35 ft) and 90 to 100 ft beneath stations 1280 to 1290 possesses less strength (decreased stiffness, reduced blow counts, etc.) than native materials such as those beneath station 1130. Correlation of this sub-bedrock feature with the shallow anomalous velocity zone (0 to 10 ft) is likely more than coincidence. A clay or clay-rich material responsible for the higher apparent shear wave velocity at 10 ft deep is probably missing between about station 1250 and station 1310. This apparent hole in the confining layer could allow surface and shallow groundwater to migrate vertically in this area at a greater rate than in most other places along this line. The consistent presence of the 800 to 1000 ft/sec contour across this line is not a definitive indication that the bedrock surface is uniform and continuous. Fractures, faults, and lateral discontinuities associated with dissolution and/or erosion would provide a multitude of pathways for vertical water movement and, if small enough, would be undetectable on shear wave contours.

The paleosinkhole interpreted on the stacked reflection section has no clear expression on the shear wave velocity profile. Without a doubt, this lack of expression suggests the subsidence artifacts that define the paleosinkhole are older than the bedrock. With the passing of time, subsidence observed on CMP stacked sections would become more and more difficult to measure using surface wave inversion. The layering evident on the CMP stacked section seems transparent to the shear wave data as a result of time and compaction. Expression of the paleosinkhole may be manifesting itself in the lower velocity anomalies sparsely distributed near the east end of line 1. Features that might correlate to the paleosinkhole are beneath station 1360 at 55 ft, station 1370 at 80 ft, and station 1440 at 60 ft. The uniqueness of these techniques and the advantage of using multiple subsurface imaging techniques to piece together this very compli-

cated geologic situation are illustrated by the lack of consistency in the overlap in the two data sets between 80 and 130 ft of depth.

Line 2

Reflection (Figures 7 and 8)

Stacked data from line 2 have captured the acoustic signature of the paleosinkhole interpreted on line 1. Line 2 intersects line 1 at around station 2070. Subsidence structures on line 2 extend from about station 2030 to station 2130 (a distance of about 400 ft). Two periods of subsidence can be distinguished on these data. The initial and most significant period of subsidence resulted in about 40 to 50 ft of down drop in the deeper reflections from within the sinkhole, while the second episode produced between 20 and 30 ft of layer slump. Two high-amplitude events are interpretable within the "boundaries" of the paleosinkhole. They possess attributes that are inconsistent with the surrounding minimally disturbed rock layers. These higher amplitude and lower frequency arrivals are likely indicative of a more diffuse boundary between different subsidence episodes. The abruptness or sharpness of the interface that separates these different acoustic units within the sinkhole in comparison to those surrounding this feature is controlled by age and compaction. It is reasonable to suggest ground settling due to compaction will be greater in the area over the sinkhole than in the less disturbed areas around this site. Based on lines 1 and 2, the paleosinkhole is elongated along its north-south axis with dimensions of 200 ft by 400 ft and twice dropped around 35 ft during periods of active subsidence.

A feature of particular interest to active dissolution and the associated subsidence poten tial is located beneath station 2235. Offset in otherwise coherent events can be interpreted from the surface down to a depth of around 400 ft. This feature does not seem to extend through the section imaged (deeper than 400 ft), suggesting it is not tectonic in nature. Considering the geology of this area, this offset feature is likely related to dissolution. A disturbed zone about 50 to 60 ft wide extends from about station 2235 to station 2250. Events from within this zone possess distinctively different seismic characteristics when compared to surrounding "native" rock layers. This chaotic zone is a real source of wonderment in terms of its origin and current stability. Subtle features likely related to erosion or dissolution within this zone can be identified

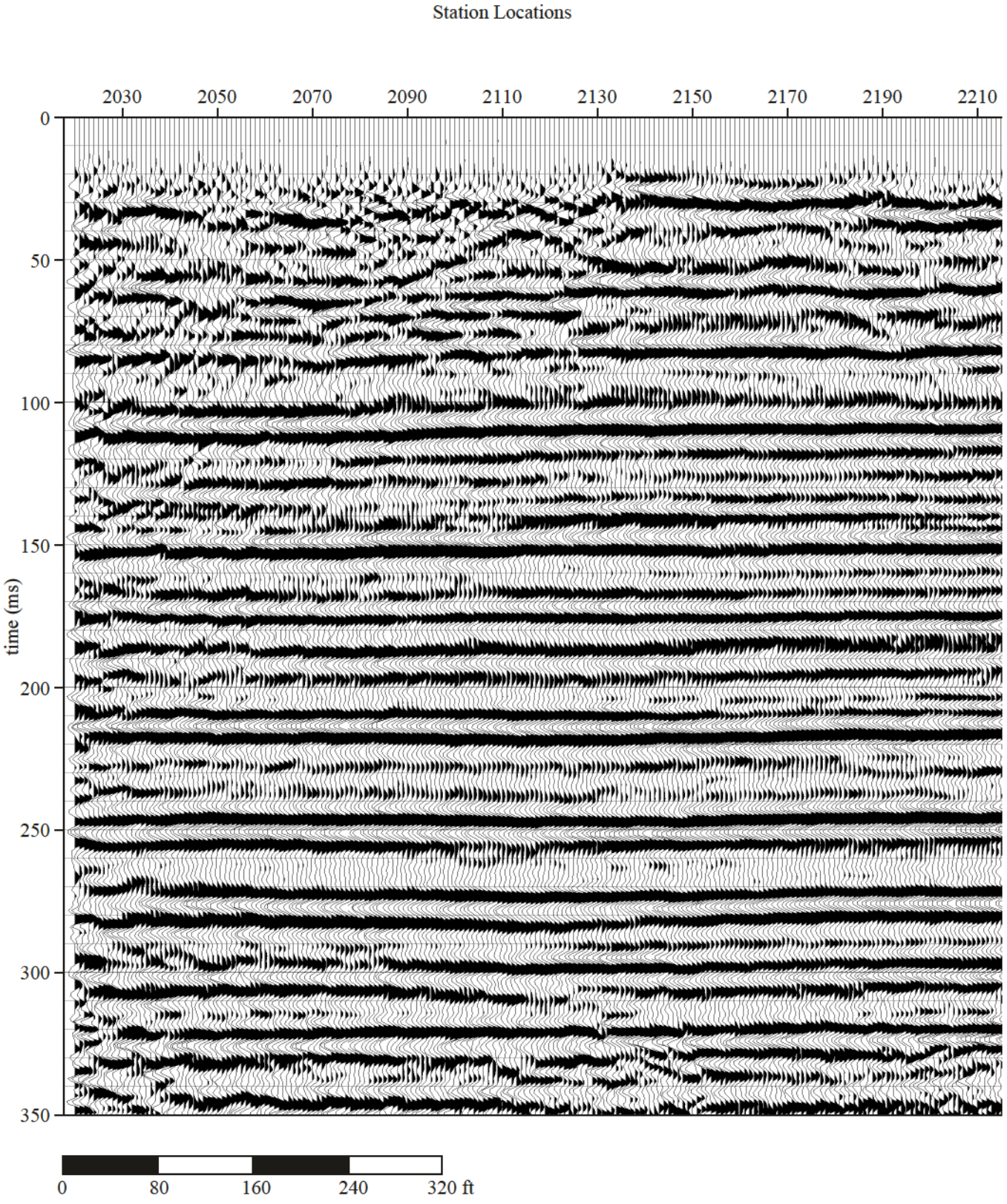

Figure 7a. CMP stacked section of line 2.

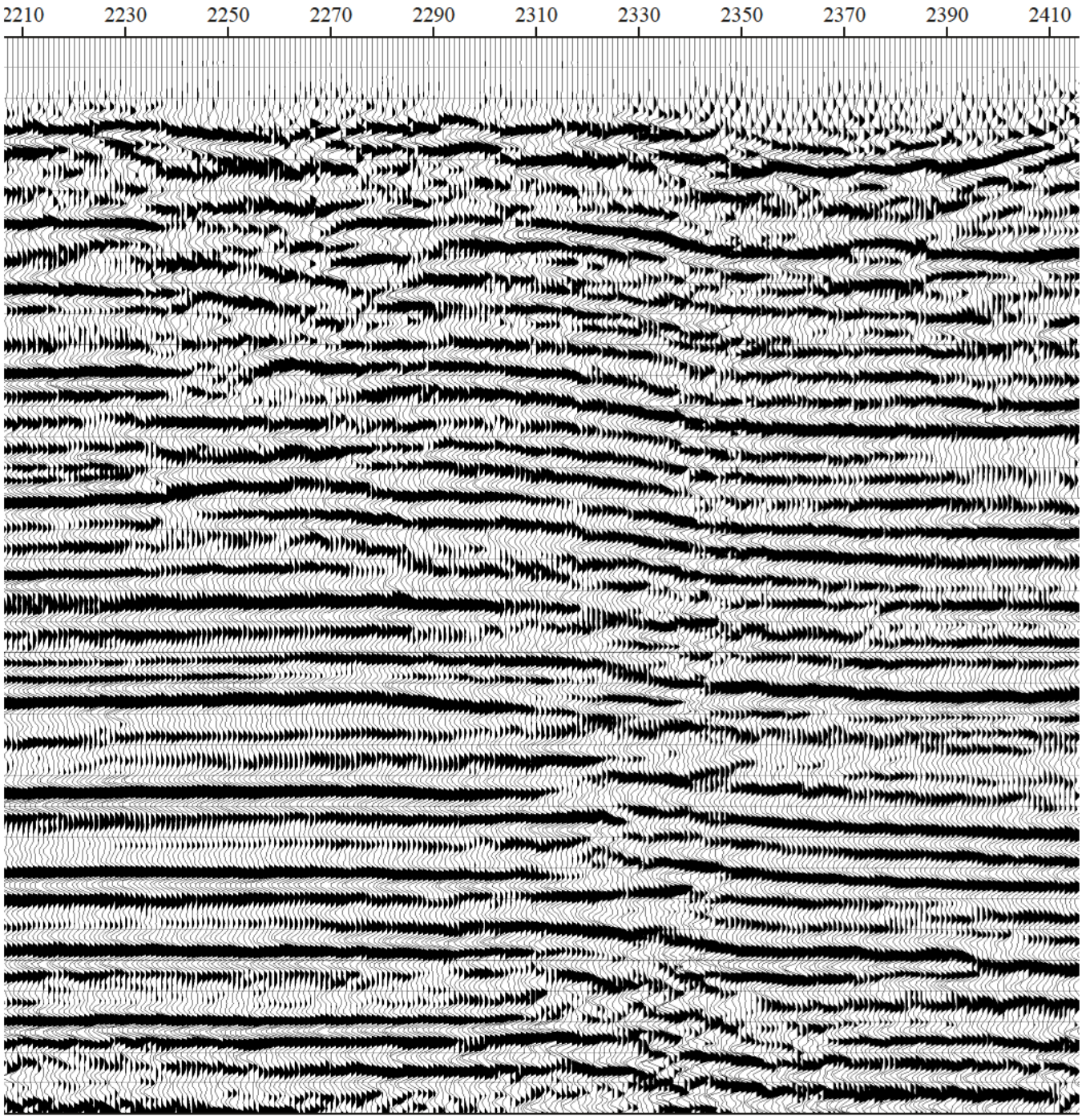
Station Locations
2210
2230
2250
2270
2290
2310
2330
2350
2370
2390
2410

Figure 7b.

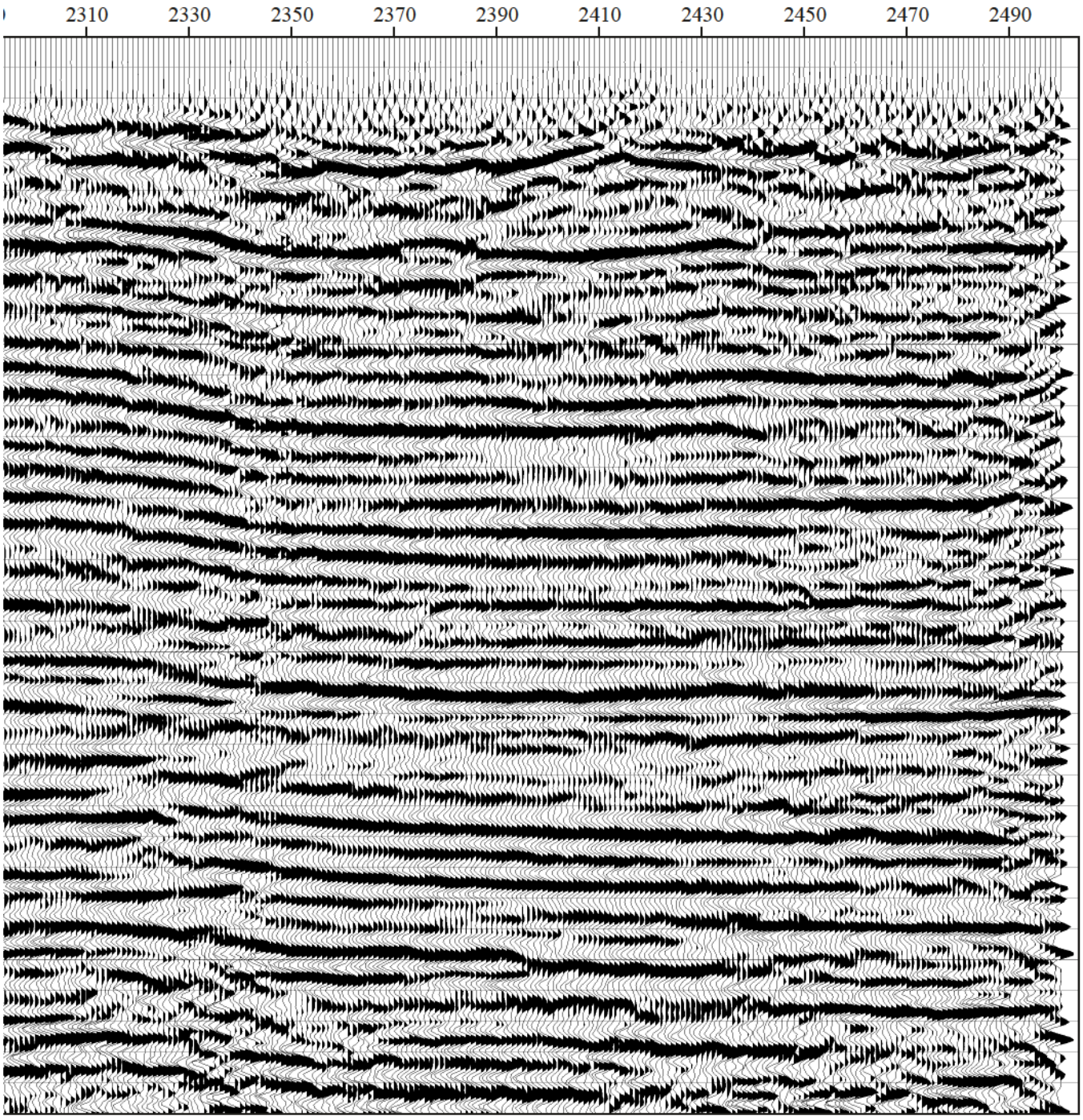
Station Locations
2310
2330
2350
2370
2390
2410
2430
2450
2470
2490

Figure 7c.

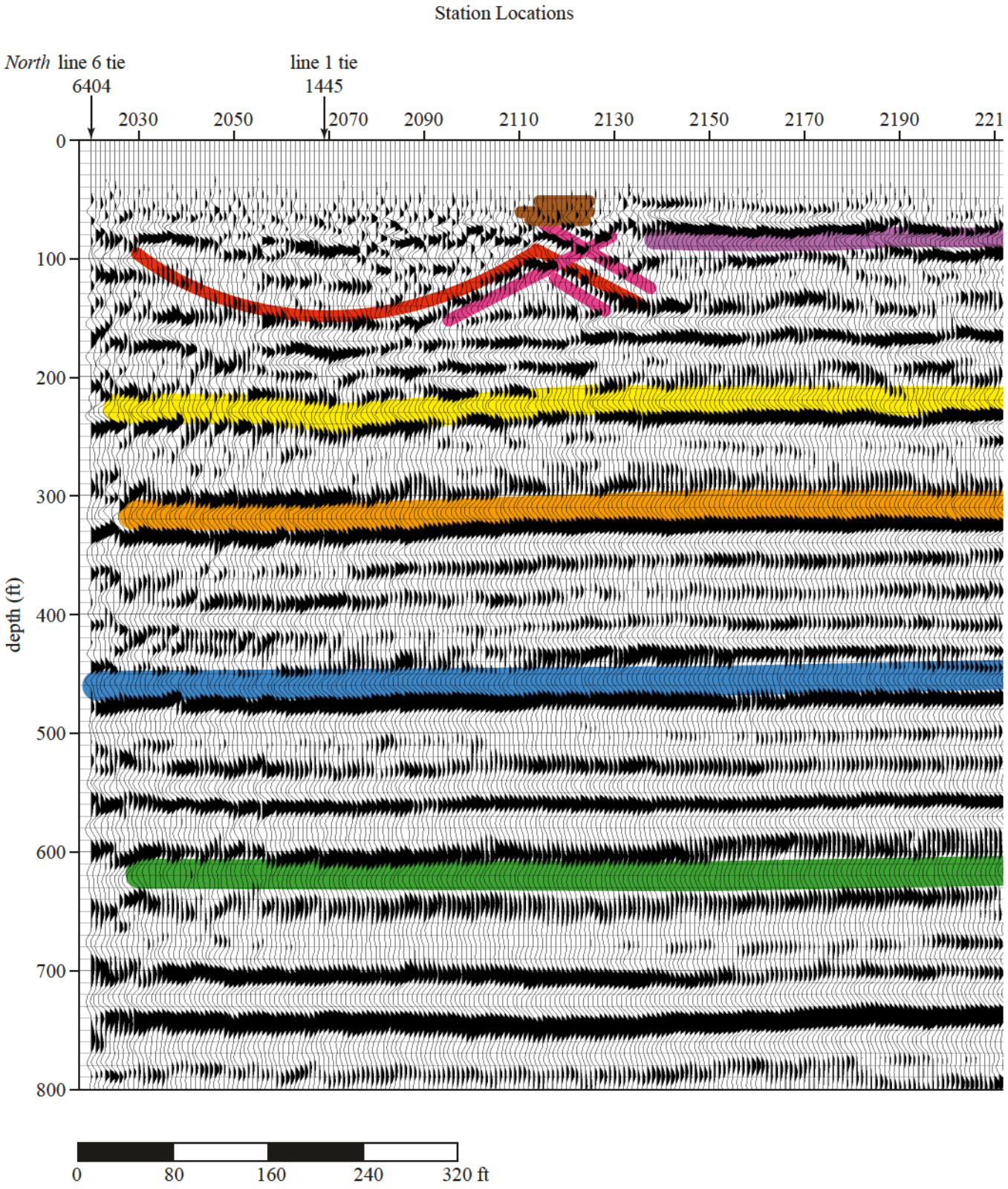

Figure 8a. Interpreted line 2.

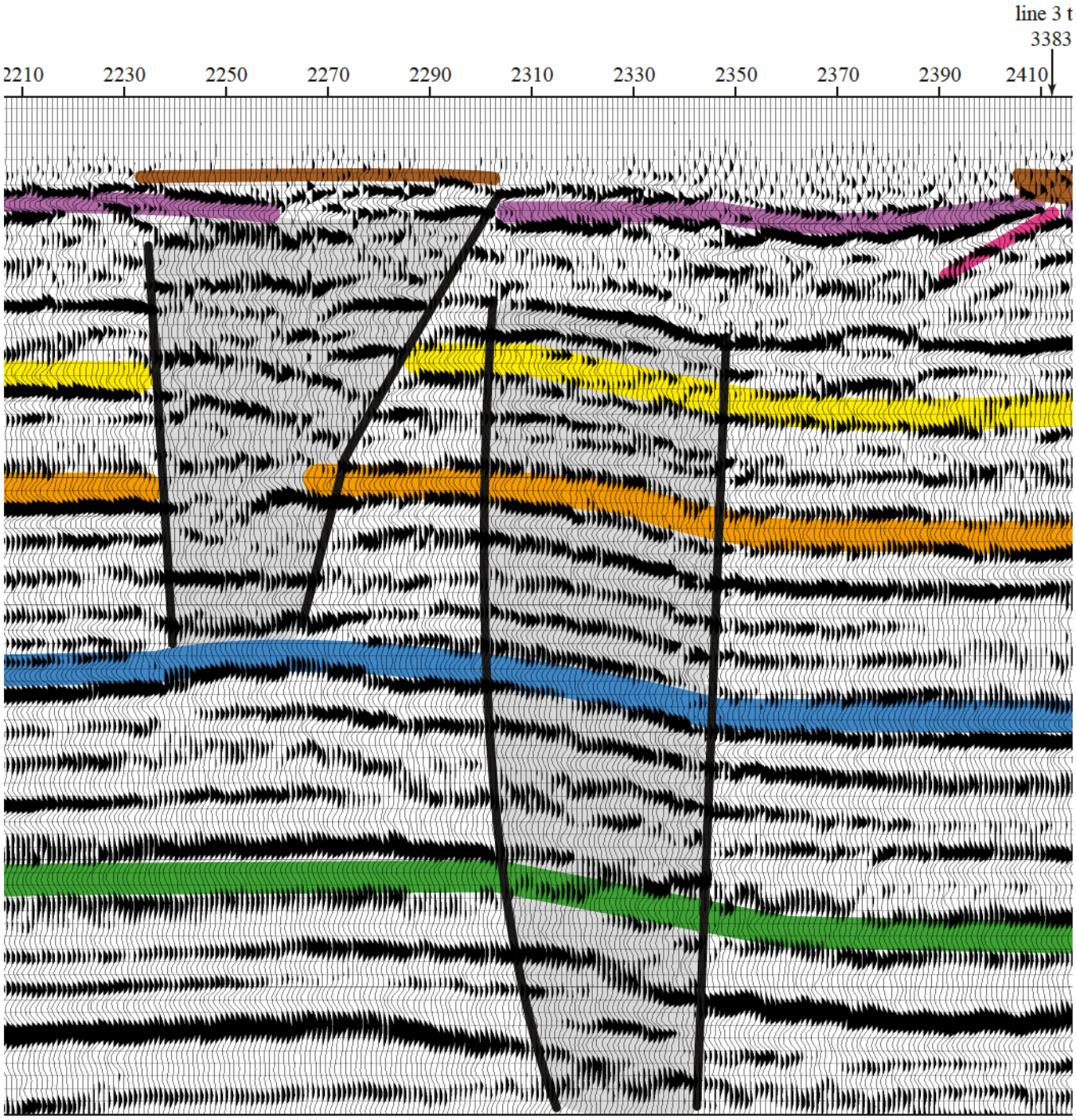
Station Locations
line 3 t
3383
2210
2230
2250
2270
2290
2310
2330
2350
2370
2390
2410

Figure 8b.

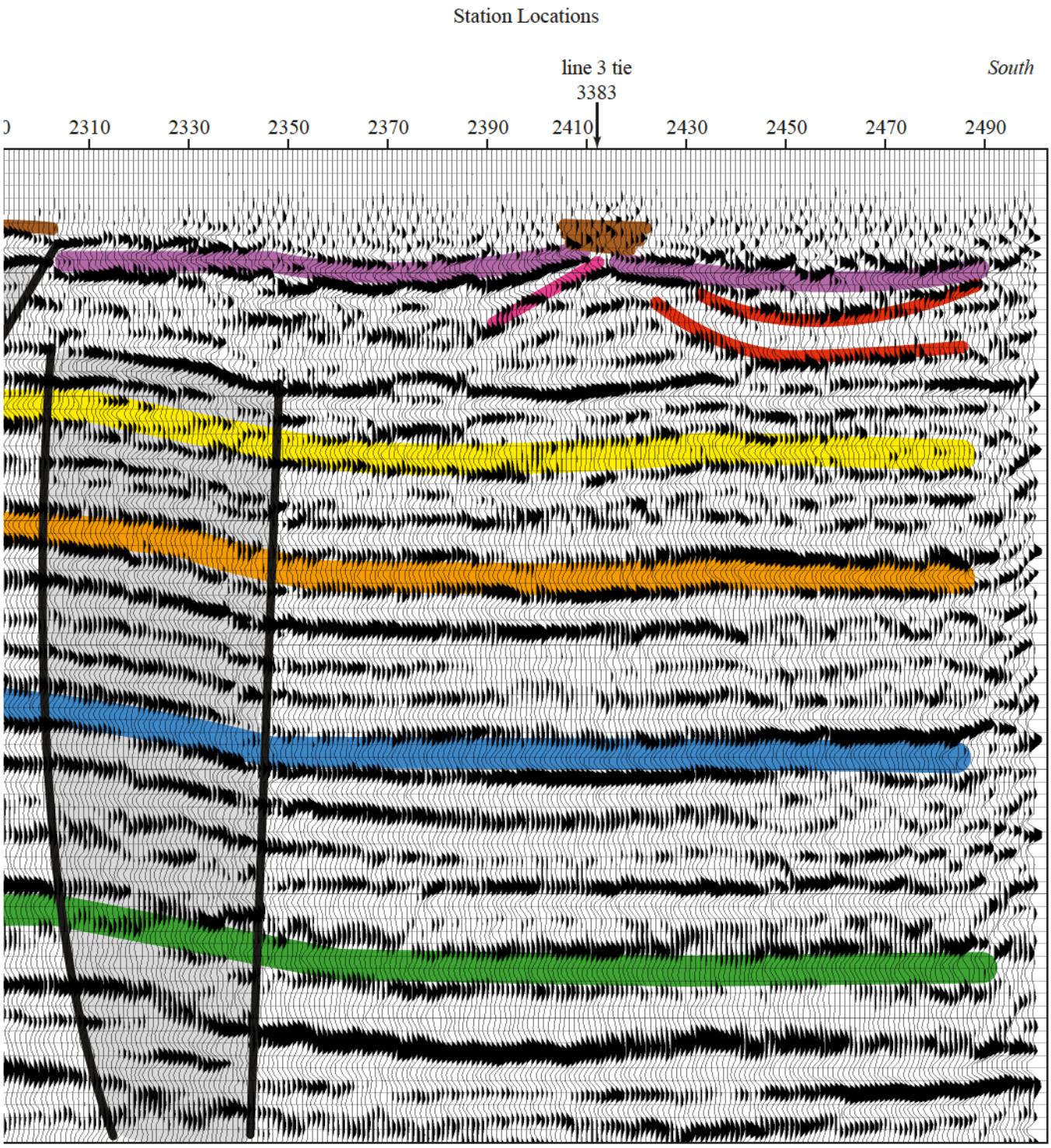
Station Locations
line 3 tie
3383
South
)
2310
2330
2350
2370
2390
2410
2430
2450
2470
2490

Figure 8c.

between the 50 and 300 ft reflections. Distinctive characteristics of this zone include chaotic reflector coherency, synform geometries, and changes in wavelet characteristics.

Features across line 2 with anomalous characteristics include the channel-looking feature beneath station 2130, the reflection with a lens type geometry beneath station 2200 at about 60 ms, as well as the variable geometry events between stations 2335 and 2445 at depths of less than 100 ms. All these reflections with highly variable geometries could be altered during erosion and deposition or as a result of dissolution and subsidence. If dissolution is the cause of these extreme features, it is reasonable to suggest the unconsolidated materials above bedrock may experience settling in areas where these irregularities have been identified.

The monocline located between stations 2290 and 2350 has all the classic characteristics of a normal fault zone, but it may be a static artifact. Processing of these data did not allow a confident determination as to the origin of this feature. The lack of any indication of a fault on other lines generates skepticism as to the possibility of a fault of this size being present. It is possible the apparent structure is related to variation in near-surface compressional wave velocity as a result of the differential compaction that would result from several episodes of subsidence. It is not possible to determine with confidence if this feature is a fault or related to static associated with the paleosinkhole.

Evidence of another paleosinkhole on the south end of this line exists near the intersection with line 3. Draping of the shallow reflections and an apparent diffraction event with an apex around station 2415 is likely the northernmost extreme of this feature and the area where, if more subsidence was to occur on this feature, it would first become evident.

Surface Wave (Figure 9)

Line 2 is our first glimpse of the southern portion of this site. This north-to-south line samples the subsurface under the extreme eastern portion of this site. Evident at the northern portion of the line is the very thin layer of higher velocity material and the extremely disturbed-looking sub-bedrock materials. Clearly, from about station 2260 on to the south the material above bedrock changes in comparison to the northern portion of line 2 as well as most of line 1. Associated with this change in near-surface material is a stunning change in the uniformity of the rock below the bedrock surface. This observation is consistent with the previous suggestion that

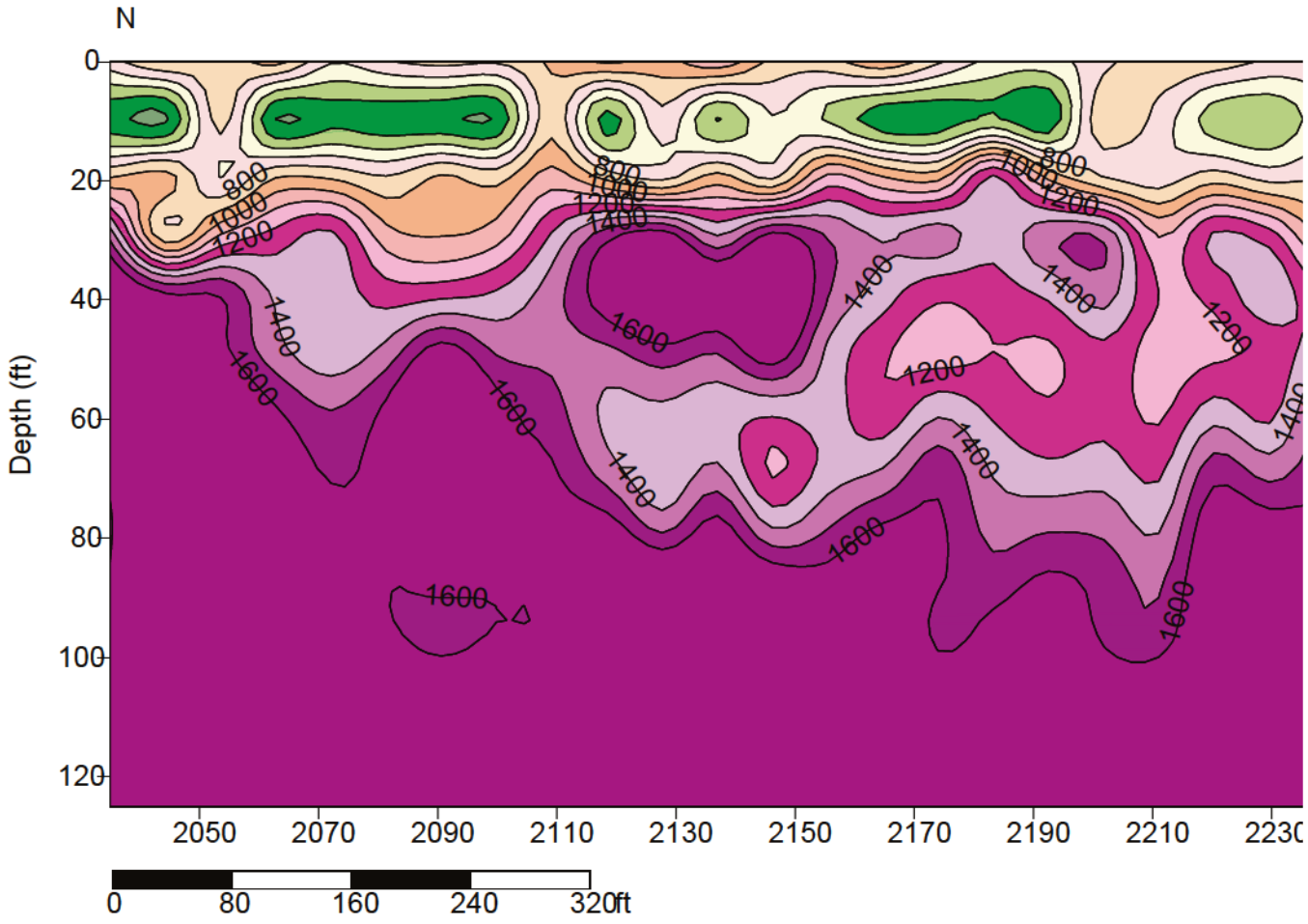

Figure 9a. Shear-wave velocity contour along line 2.

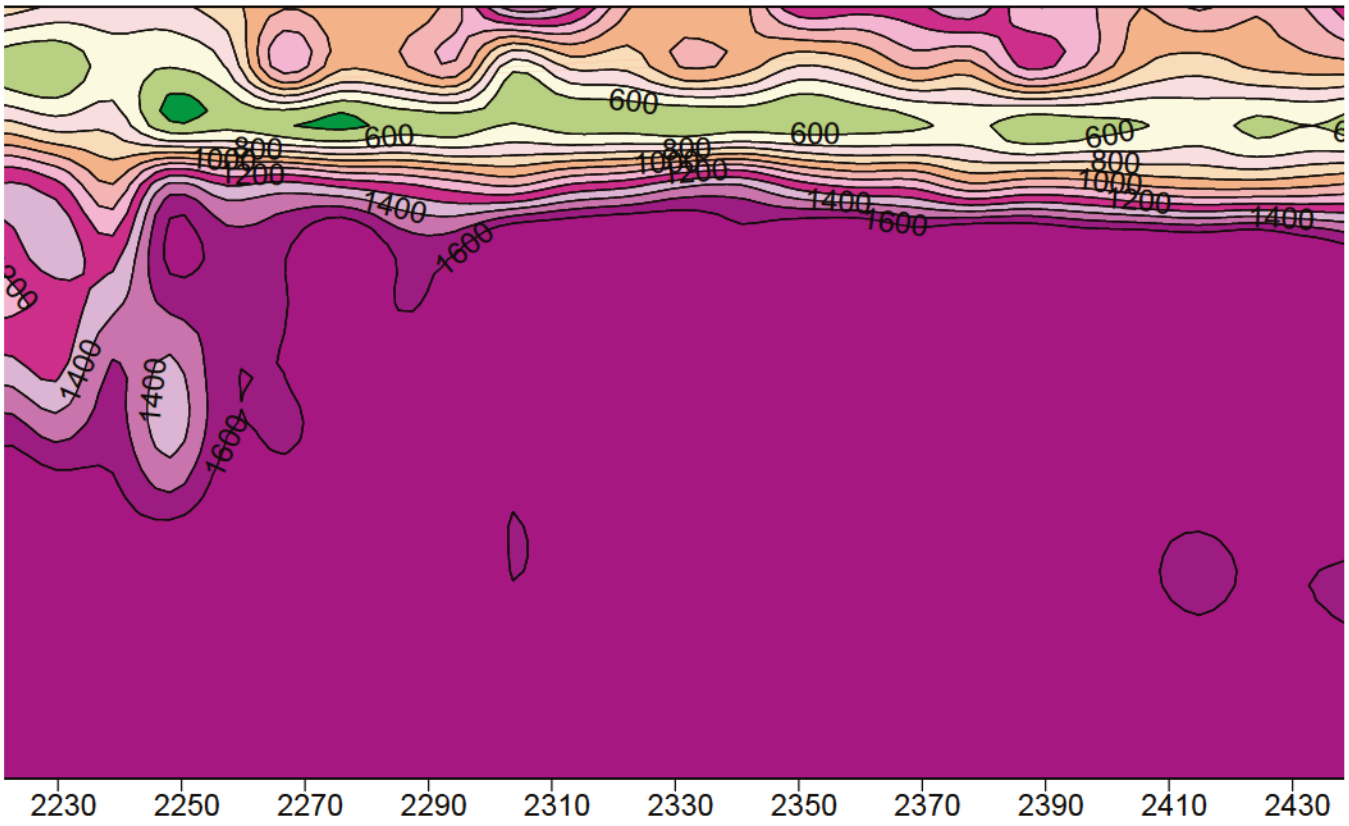

Station Number

Figure 9b.

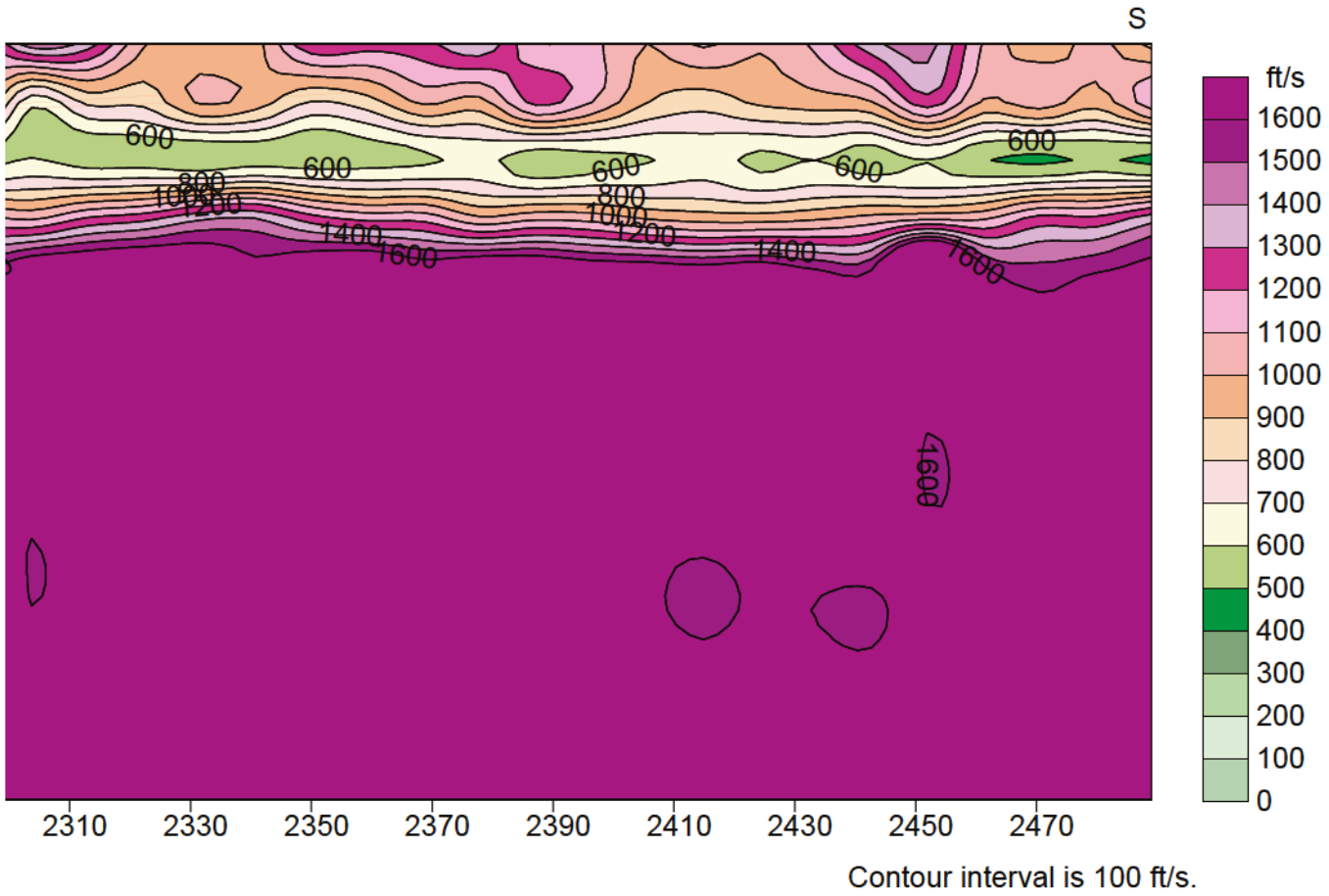

Station Number

Figure 9c.

the large anomalous feature on line 1 beneath station 1270 was likely related to the absence of the higher velocity clay-rich material present in places within the upper 10 ft across this site.

Bedrock appears to be extremely disturbed on the northern end of this line. This very altered appearance is consistent with the interpretation of a paleosinkhole made from the seismic reflection data along line 1. Bedrock lows interpretable at stations 2050 and 2090 are likely subsidence that has occurred in part prior to deposition of the overlying unconsolidated sediments. It is, however, quite noteworthy to speculate about the apparent chimney features beneath stations 2055 and 2110. These high-velocity plugs could be clay-rich materials from shallower layers that infilled sinkholes covering the ground when the layer that is presently at 10 ft was at the ground surface. These sinkholes could easily have been the direct result of subsidence or erosion of bedrock materials evident today as the bedrock lows beneath stations 2050 and 2090.

Another of these chimney features that appears to have been a sinkhole when the lower velocity green layer was exposed at the ground surface is beneath station 2210. Bedrock beneath this anomaly is quite disturbed. The bedrock contour (800 ft/sec) appears to be pulled down just a bit in the proximity of this feature. If the higher velocity zones within the low velocity layer are an infill of younger materials into paleosinkholes that formed by dissolution and/or subsidence of the bedrock surface beneath station 2210, it is likely the sub-bedrock layers are extremely fractured with younger, lower velocity clay-rich materials filling the fractures. From station 2250 on to the south the bedrock layers appear very uniform, with no indication of either stress buildup or anomalous low velocity materials below the bedrock surface.

It is reasonable to assume the large disturbed bedrock zone defined by the lower than surrounding shear wave velocity characteristics of the rock beneath stations 2160 to 2250 is somehow related to the paleosinkhole observed in this general area on reflection sections. This low velocity zone is more current and less devastating than the subsidence that formed that sinkhole. Evidence of paleosinkholes on the shear wave data is very inconsistent in comparison to the reflection data. Two paleosinkholes have been interpreted on the reflection profiles and neither appear on the shear wave data with unique characteristics that would have allowed interpretation of these structures from shear wave data alone.

Several high velocity zones exist above 10 ft of depth on the southern end of the profile. The relative velocity of these zones is consistent with that defined as sub-bedrock units. This

erroneously high velocity is surprising but not completely unexpected. Extremely hard layers were encountered in this part of the site during acquisition of the CMP profile that could easily produce higher shear wave velocities in this area. The surprising aspect revealed by these data is the extent of the shallow high velocity zones.

Line 3

Reflection (Figures 10 and 11)

Reflection line 3 is the only east-to-west reflection profile crossing the southern portion of the site. It contains an excellent set of reflection arrivals between about 40 and 300 ms. The general reflection character of these events is very similar to those on the other seismic lines around this site. Dominant frequencies easily exceed 200 Hz for some reflections within this section. Most events of interest are readily interpretable on this section; probably the most obvious and largest is the paleosinkhole observable across the eastern half of the survey line. Reflection arrivals at depths less than 50 ms (120 ft) on the eastern end of the line appear to possess geometries sculpted during deposition and/or by erosion. These geometries might be the result of dissolution and subsidence, but without supporting data we will assume reflection events with characteristics similar to the eastern portion of this line are the result of dissolution and subsidence while the ones on the west are remnants of erosion and deposition. Reflection arrivals below 120 ft appear relatively flat with no obvious structural character significant to this study.

Reflection arrivals between stations 3190 and around 3400 down to about 100 ms (250 ft) originate within an area interpreted to have layering disturbed by paleo-dissolution and subsidence. Wavelet characteristics, reflection geometries, and apparent depth of this sinkhole area are consistent with the properties and characteristics of the sinkhole interpreted near the intersection of lines 1, 2, and 6. A reasonable estimate of the maximum subsidence at the center of this sinkhole is around 70 ft. This estimate is based on the synclinal structures interpretable on the lower frequency reflection events within the subsidence area. As with the paleosinkhole beneath the northeastern end of this site, there appears to have been at least two unique periods of subsidence. The two periods are defined by the two lower frequency, higher amplitude events. These events probably correlate to the base of the sinkhole when it was exposed to deposition at two different times in the geologic past. Considering the extremely uniform and

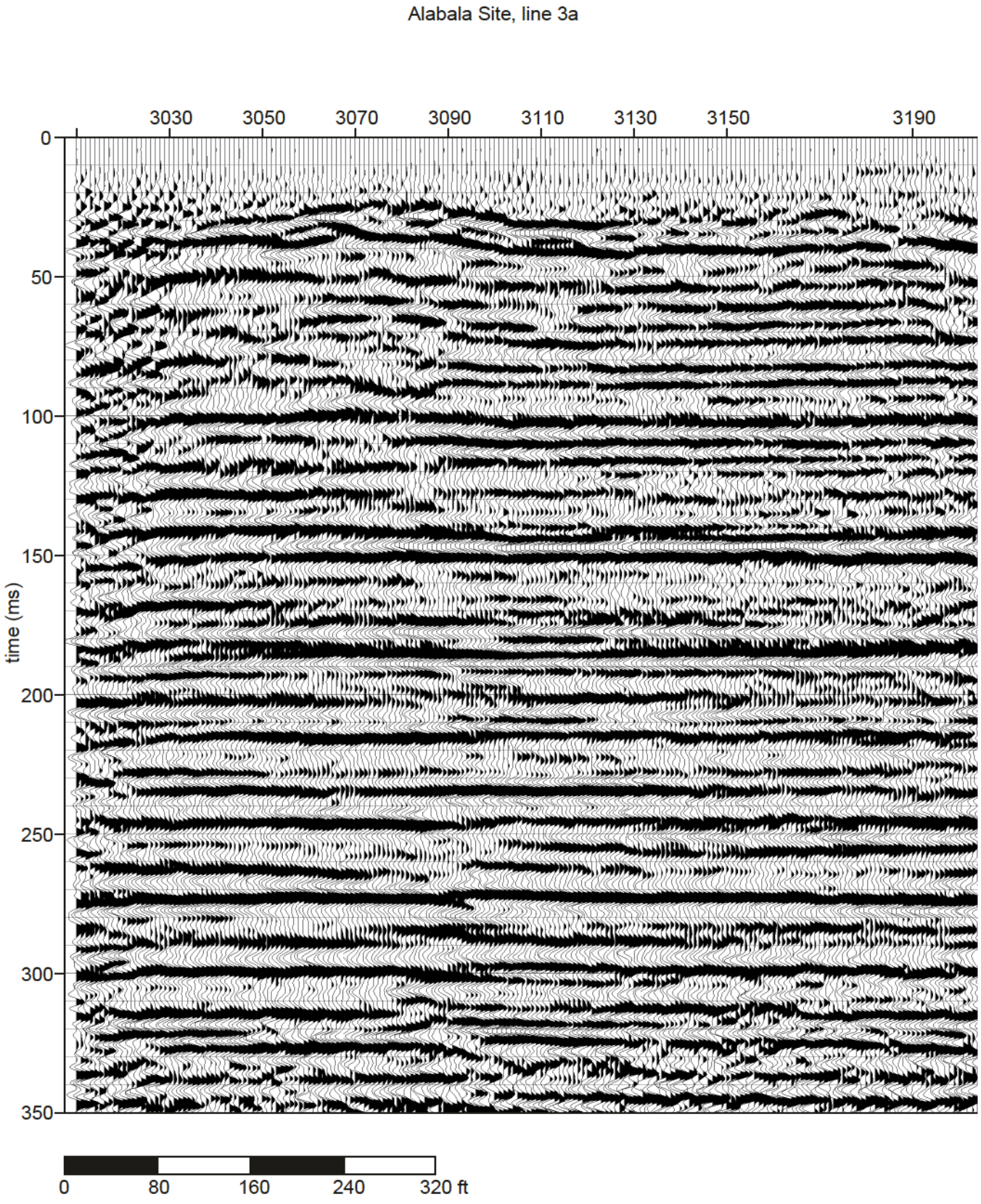

Figure 10a. CMP stacked section of line 3.

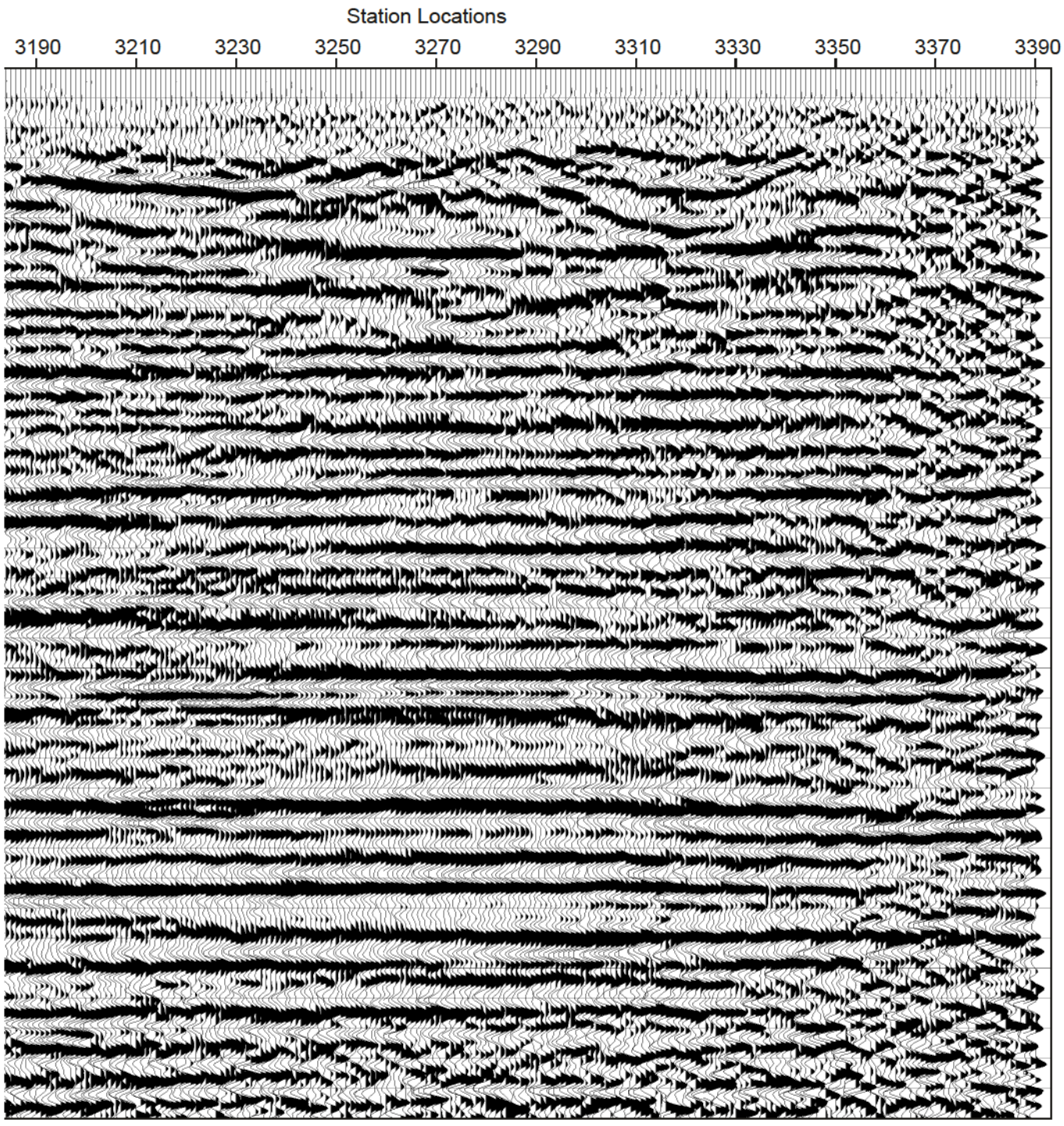
Alabala Site, line 3a
Station Locations
3190
3210
3230
3250
3270
3290
3310
3330
3350
3370
3390

Figure 10b.

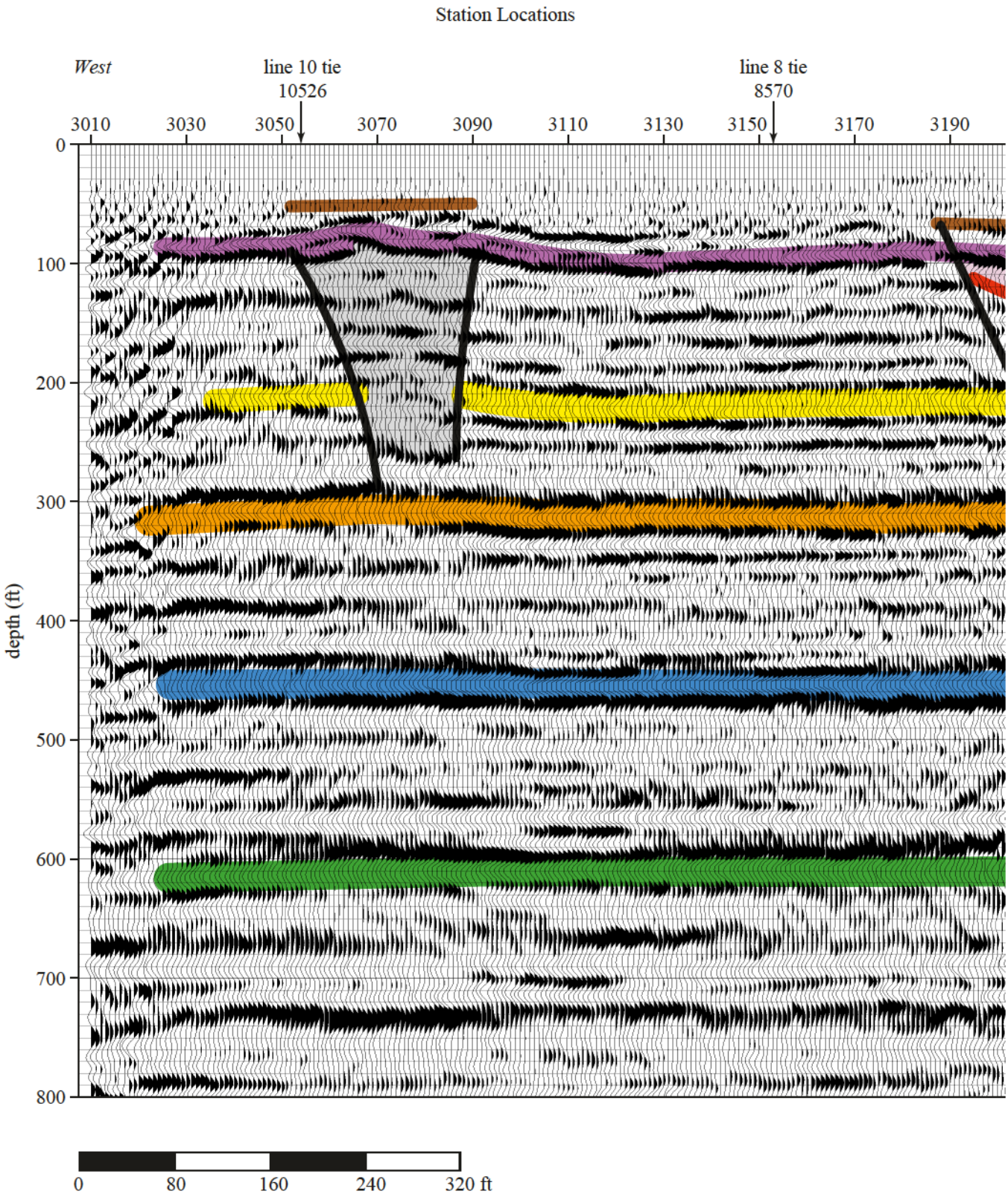

Figure 11a. Interpreted line 3.

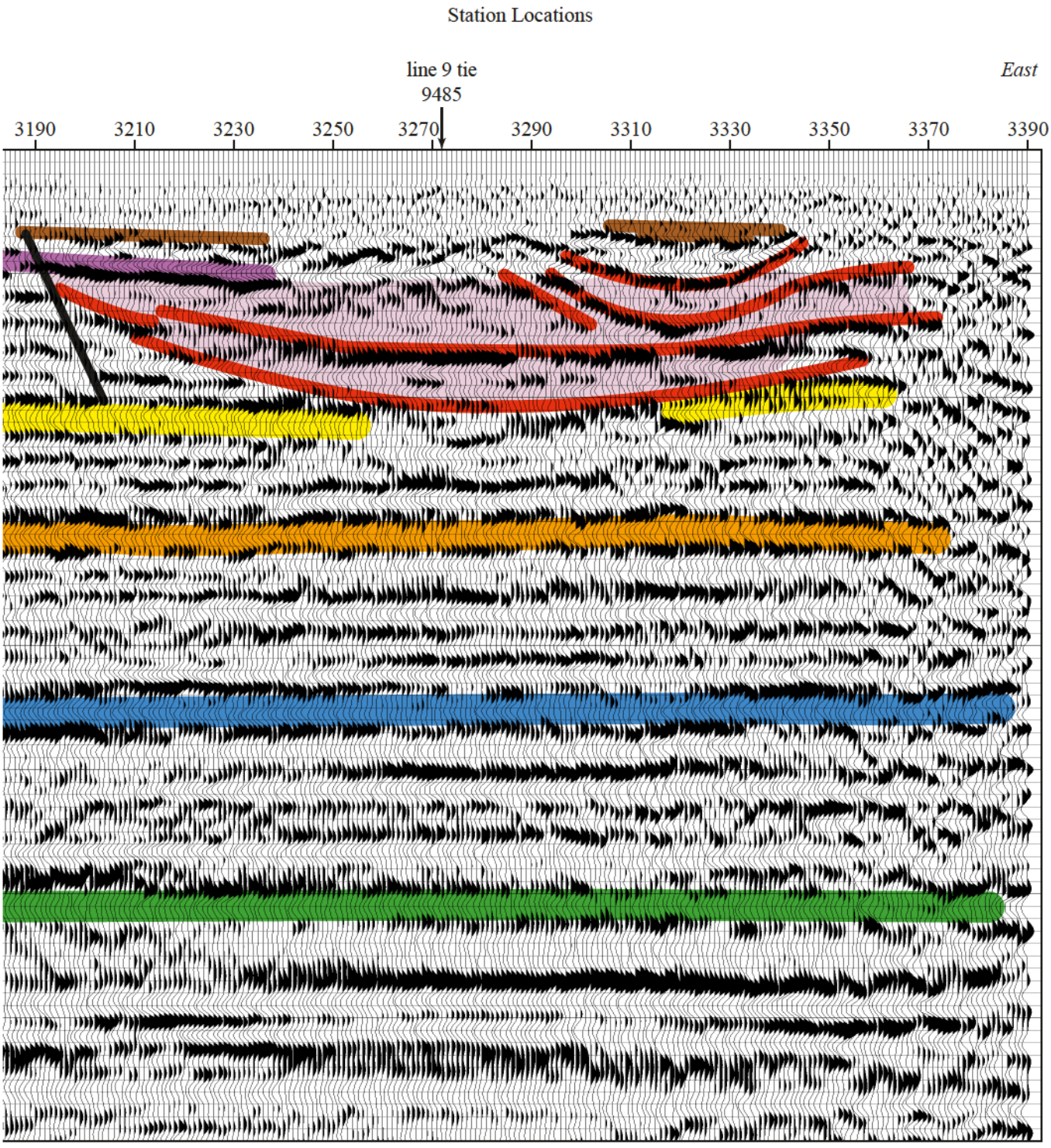
Station Locations
line 9 tie
9485
East
3190
3210
3230
3250
3270
3290
3310
3330
3350
3370
3390

Figure 11b..

undisturbed nature of the shear wave velocity contour above the paleosinkhole interpreted from reflection data it is reasonable to suggest there has been no subsidence activity in association with this paleosinkhole since prior to deposition of the shallowest bedrock materials.

Considering the similarity in reflections between 30 and 70 ms above the sinkhole with reflections outside this interpreted subsidence feature, it is likely dissolution was active throughout this area at this depth and was not isolated to just the area that formed the paleo-sinkhole. None of the dissolution activity outside the paleosinkhole seems to have produced a subsidence feature even close to the size of the one beneath station 3290. This may be why the shear wave velocity field is disturbed east of the paleosinkhole and appears very uniform and unaltered within the sinkhole. Subsidence in the sinkhole may collapse the voids and rubble zones sufficiently that surface waves do not detect any changes in shear wave velocity since the material through compaction has become relatively consistent. Clearly this entire depth interval has been affected by dissolution, or at a minimum there was a time in the past when significant erosional and depositional forces were at work producing the observed geometries.

Within the paleosinkhole expression identified at the eastern end of line 3 is a small channel or subsidence feature. Located beneath station 3320 at between 40 and 60 ms is a small bowl shaped reflection. This steep sided feature is not depositional. It was a secondary subsidence feature that likely formed significantly after the major sinkhole that can currently be traced between stations 3190 and beyond the eastern extreme of the line. This observation is pertinent to reactivation potential in this area.

A small disturbed zone is evident on the depth section with very similar properties and configuration to the disturbed zone identified beneath station 2250 on the line 2 reflection section. This zone is located beneath station 3070 and has the same drop in coherency of reflections and an increase in lower frequency coherent events isolated to this zone. Considering the marshy surface conditions and drill data from the area on line 2 with similar character, it would be reasonable to suggest this area (3070) will or has likely followed similar subsidence routes.

Surface Wave (Figure 12)

Shear wave velocity data from this southernmost east-to-west profile suggest a relatively undisturbed bedrock east of station 3230. This observation is consistent with the interpretation of line 2, which intersects line 3 near its eastern end. Most of the obviously disturbed sub-

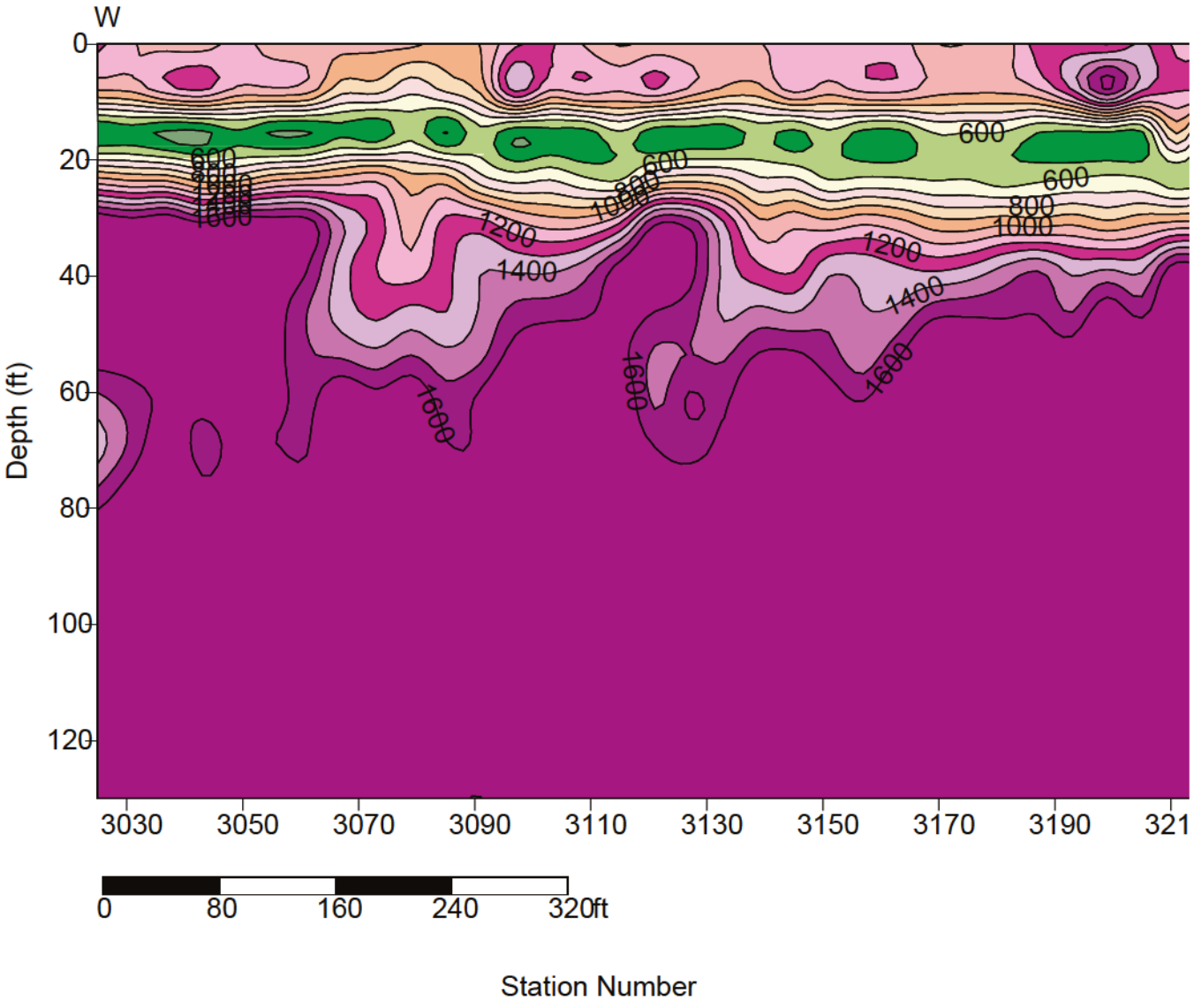

Figure 12a. Shear-wave velocity contour along line 3.

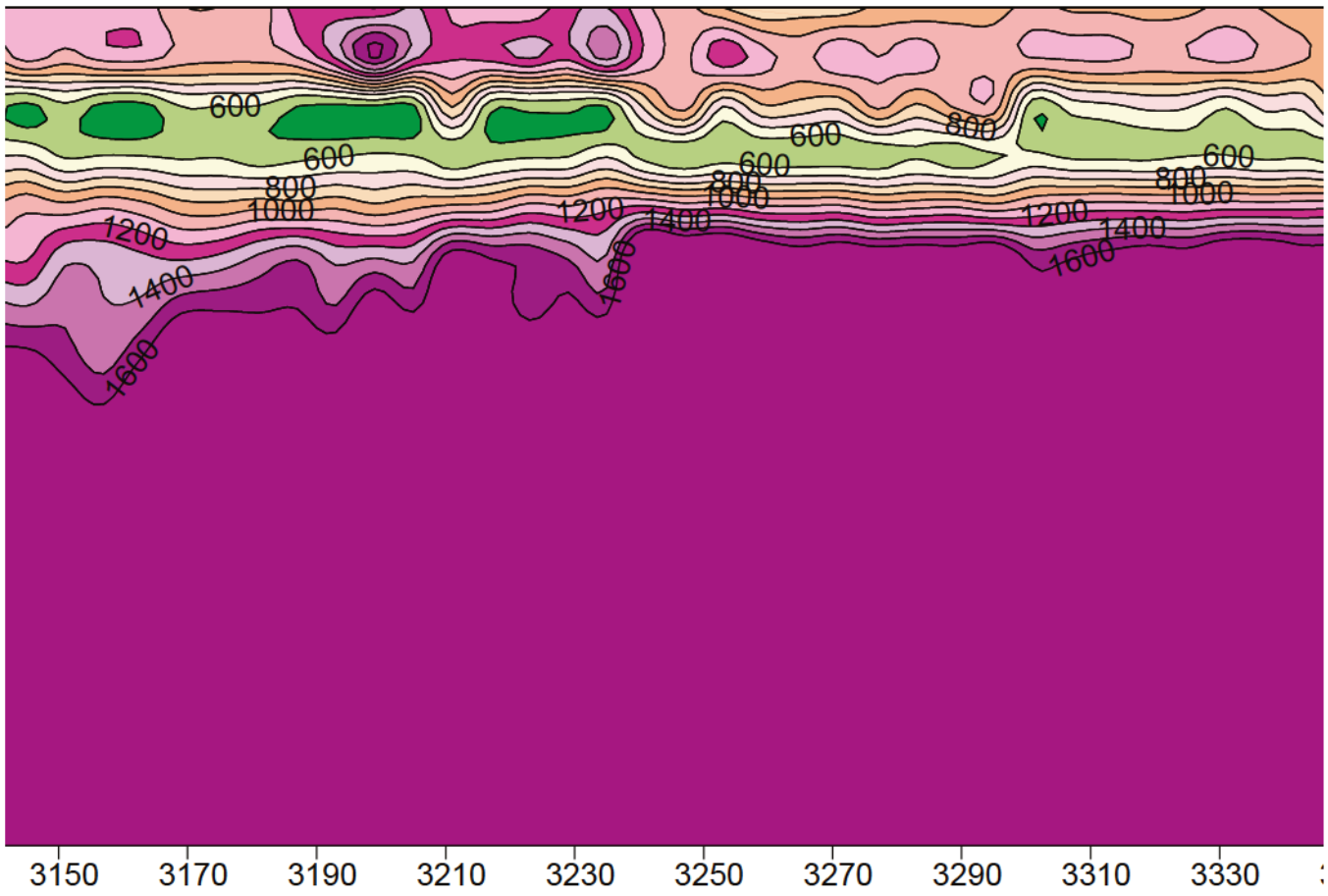

Station Number

Figure 12b.

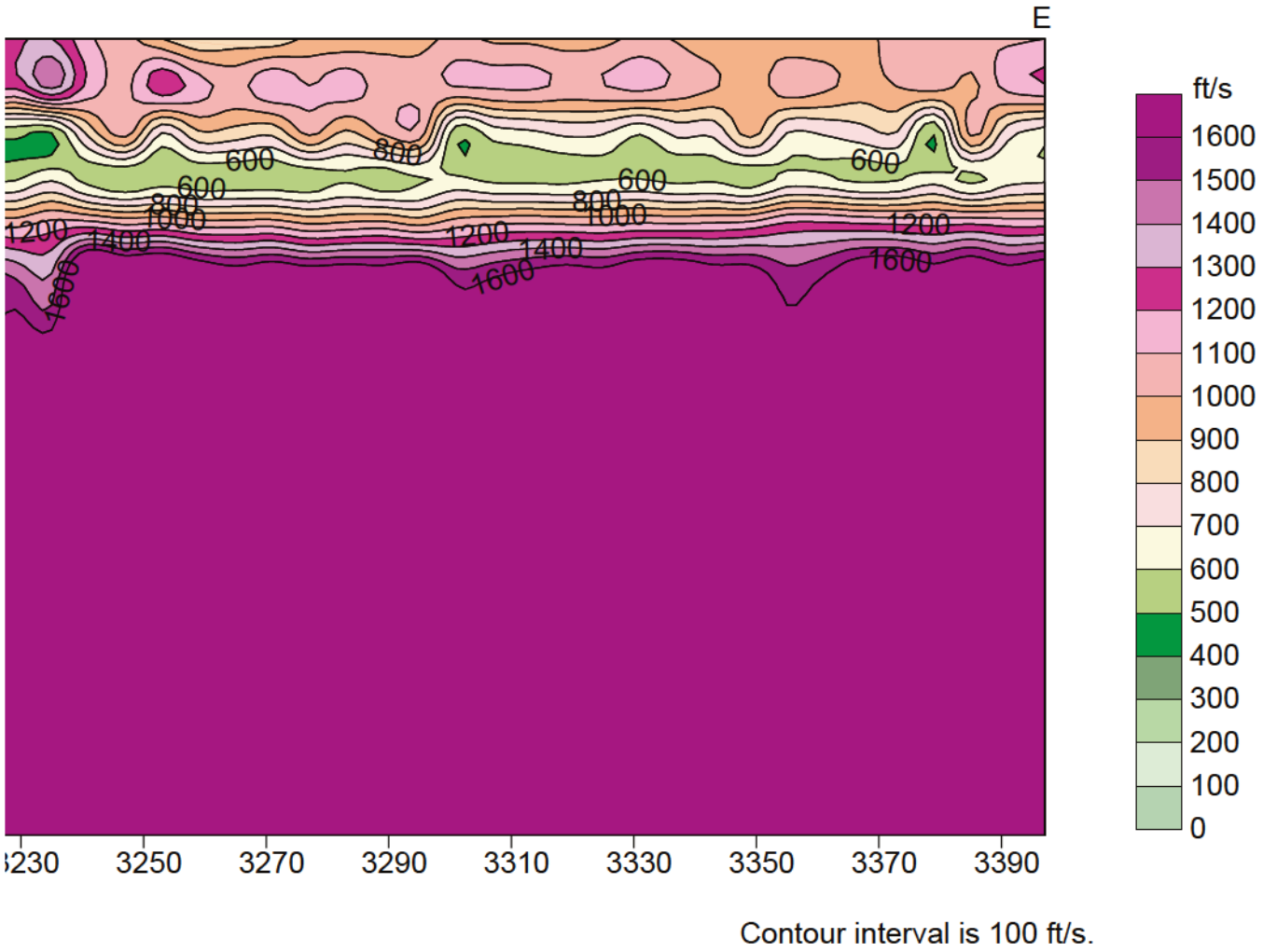
E
ft/s
1600
1500
1400
1300
1200
1100
1000
900
800
700
600
500
400
300
200
100
0
600
800
1000
1200
1400
1600
3230
3250
3270
3290
3310
3330
3350
3370
3390
Contour interval is 100 ft/s.
Station Number

Figure 12c.

bedrock layers are located between stations 3060 and 3230. These disturbed features possess a very abrupt and relatively localized nature in comparison to observations of anomalies on lines 1 and 2. It is reasonable to suggest that these lower velocity zones within bedrock are fracture and/or dissolution related. The very localized nature suggests that dissolution likely produced a series of well-differentiated fracture-looking features that extend from bedrock to about 20 ft below bedrock. With the deposition of the clay unit, found above the bedrock surface across the entire site, these open fractures, fissures, and dissolution joints were infilled, or they could be only partially filled, leaving significant amounts of void or collapse areas present within the bedrock. The location and character of the dissolution patterns are likely related to a zone of inherent weakness in the limestone bedrock.

An interesting anomalous feature less than 10 ft deep between stations 3190 and 3240 is quite suggestive of the sinkhole signatures observed during the feasibility study in the Dixon Forest. It does not have quite as well a defined high velocity closure, but velocities calculated within this zone are anomalously high, with the strong low directly beneath it. As close to the surface as this feature appears, it is unlikely the materials could have supported this much stress buildup without failure already. However, it is possible that several smaller rubble and void areas exist in close proximity to each other, resulting in the observed anomaly.

Line 4

Surface Wave (Figure 13)

Line 4 is within the proposed power block and is characterized by a very diffuse bedrock surface and a low velocity zone just beneath the interpreted bedrock surface. This channel-looking feature beneath station 4220 is likely the result of dissolution. It is reasonable to suggest that bedrock between the western end of the line and station 4250 is gradational from the low velocity sands at around 20 ft through weathered bedrock down to 50 ft or so. A 15 to 20 ft thick layer of weathered bedrock, the remnants of erosion/dissolution activities, are concentrated within this channel between stations 4030 and 4250 at a depth of 40 ft or so. Clay materials that locally overlay bedrock at this site fill the spaces within this rubble zone, leaving this more gradational lower velocity zone between competent bedrock and the unconsolidated material above. This zone is either an ancient bedrock channel or a well developed series of fractures that

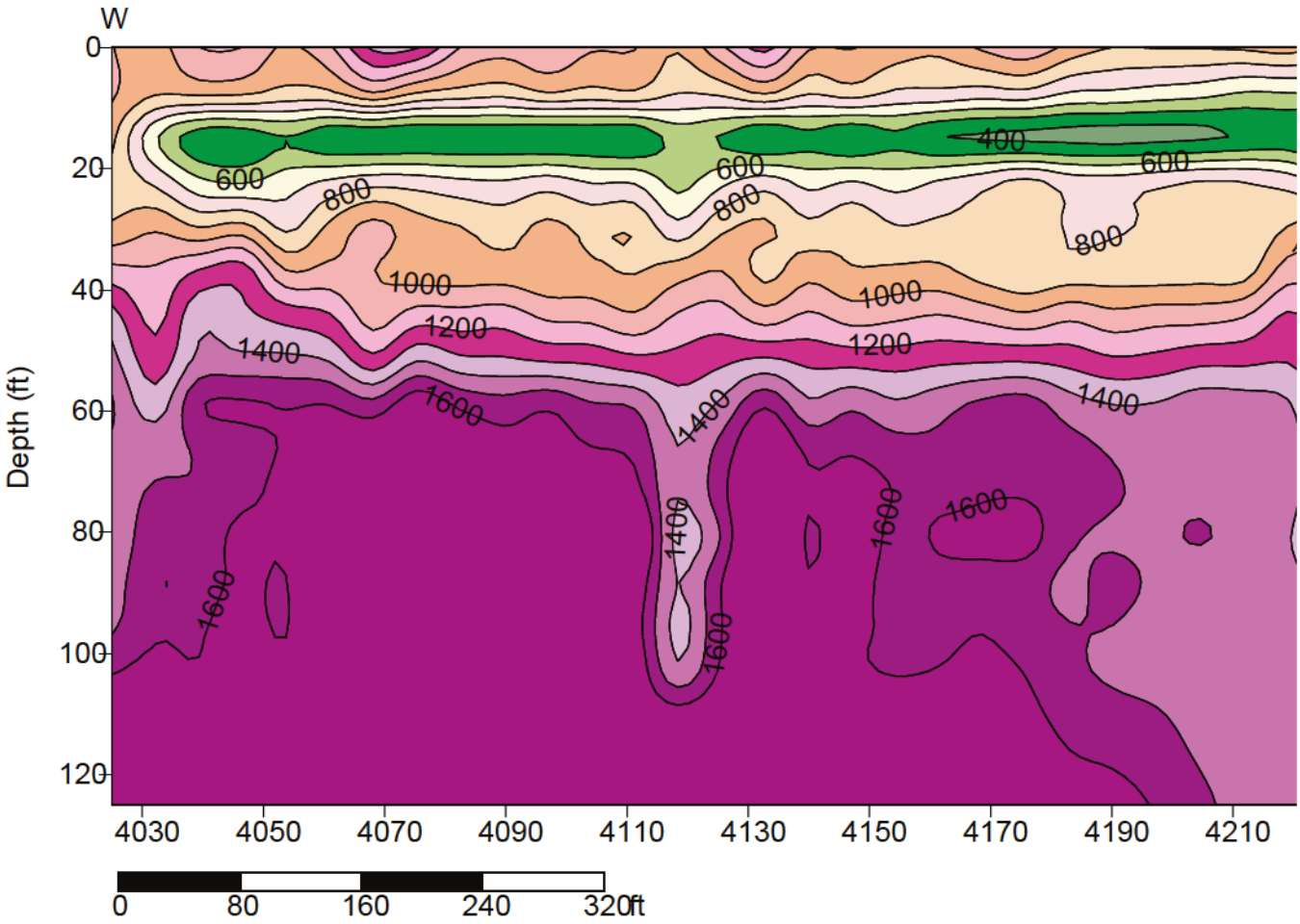

Figure 13a. Shear-wave velocity contour along line 4.

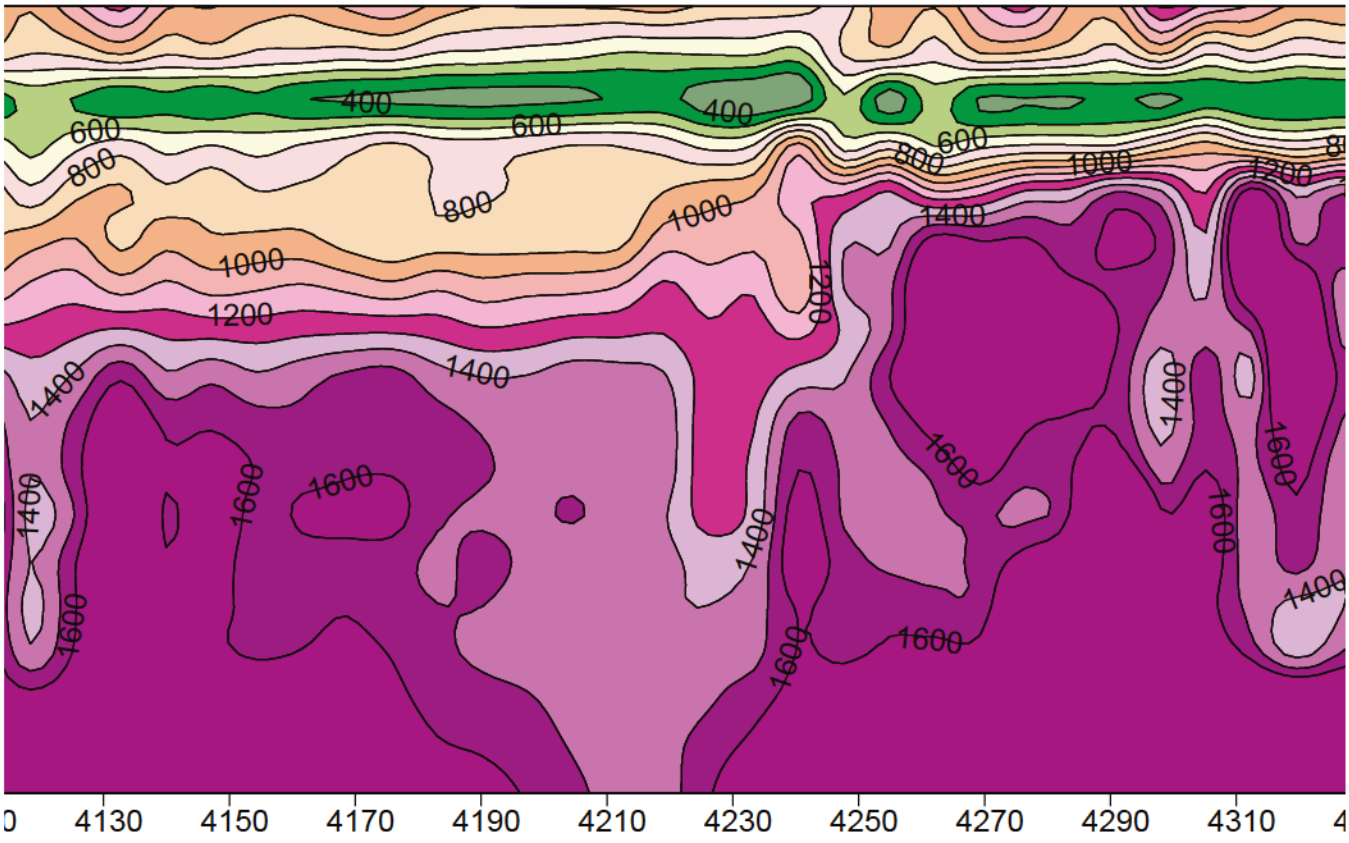

Station Number

Figure 13b.

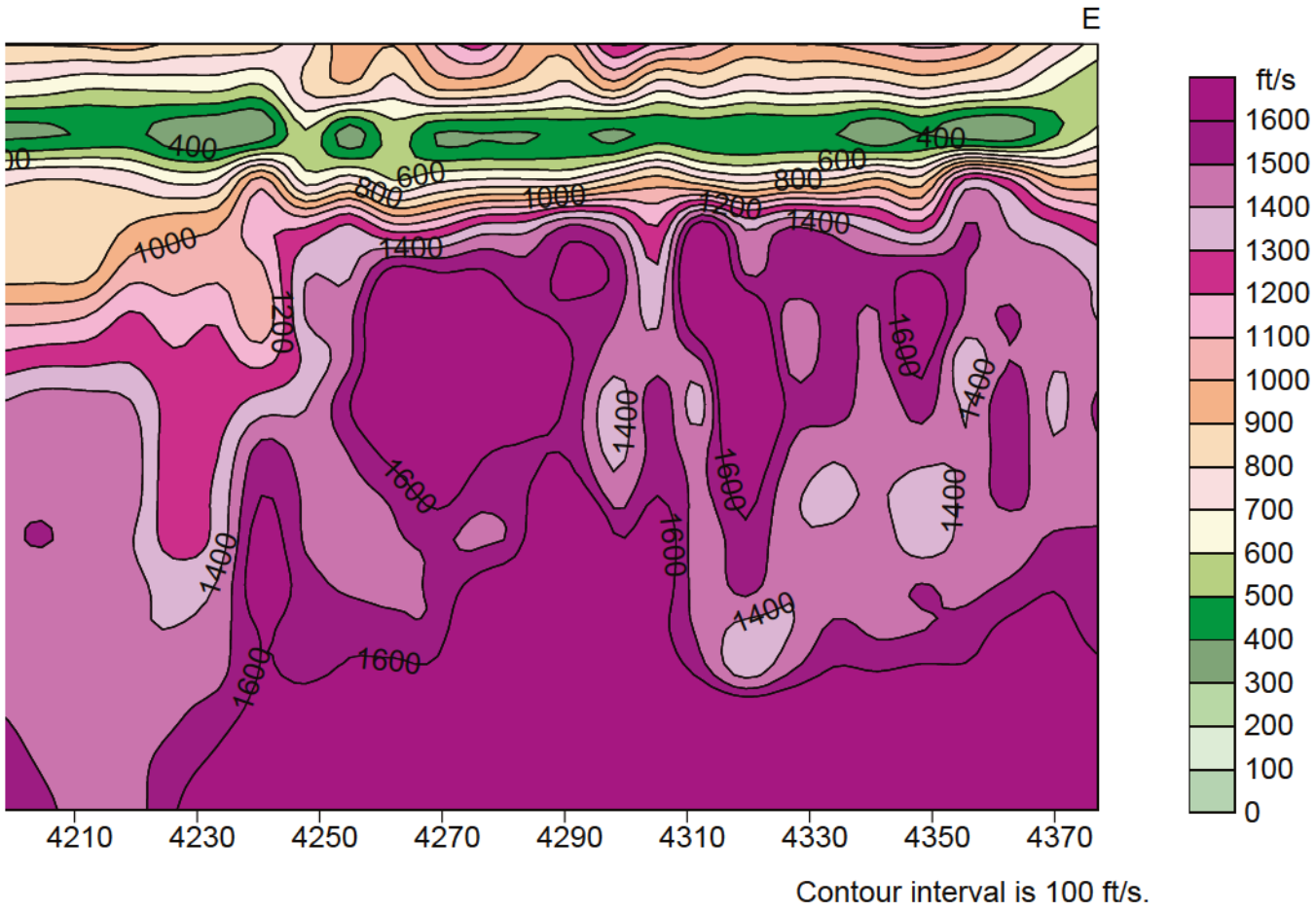

Station Number

Figure 13c.

this profile crosses at an oblique angle. It is again quite defendable to suggest this intra-bedrock structure is directly related to zones of weakness in the bedrock susceptible to dissolution.

In general, the elongated linear lower velocity features such as the one directly beneath station 4120 are indicative of a dissolution joint/fracture that has been infilled with lower velocity material either during joint development or shortly after. Several of these linear anomalous zones can be interpreted along this line. A striking one exists at the very eastern edge of the bedrock channel and has likely had some influence on the eastern extent of the channel feature itself. This vertical low velocity feature beneath station 4220 is very likely related to and connected to similar features evident on other profiles from this area.

Of secondary significance to the bedrock channel is the velocity gradient at the bedrock surface. The high velocity gradient at about 20 to 25 ft at the eastern end of the profile is indicative of an abrupt and rapid change in velocity. The lower velocity gradient within the channel feature represents either a much more gradual transition from the clay material overlaying bedrock and limestone units that make up bedrock or a significant thickness of weathered or fractured bedrock overlaying the more competent "unweathered" bedrock.

Line 5

Surface Wave (Figure 14)

This northernmost west-to-east profile includes one of the more striking anomalous zones in the upper 20 ft anywhere on this site: an extremely high gradient, high velocity closure located beneath surface location 5165. This feature was drilled and determined to correlate with a section of high velocity near-surface materials and a thin void zone over 70 ft deep. It is unlikely that a localized lens of high velocity unconsolidated material can account for this feature. It is more likely that lateral smearing places this feature beneath line 5 when in reality the void truly responsible for this high shear velocity is slightly off-line. It is not possible to determine exactly where the feature is with this single 2-D section. But it is, however, extremely probable that the small void area discovered at 70 ft when drilling this anomaly is related to this feature. This small void area at 70 ft can probably be correlated to the smaller bedrock velocity gradient (700 to 1200 ft/sec contours) beneath station 5160. This is a feature worthy of more study. It clearly is not an artifact or fictitious feature. The question left to answer is: Where is this feature located in the subsurface?

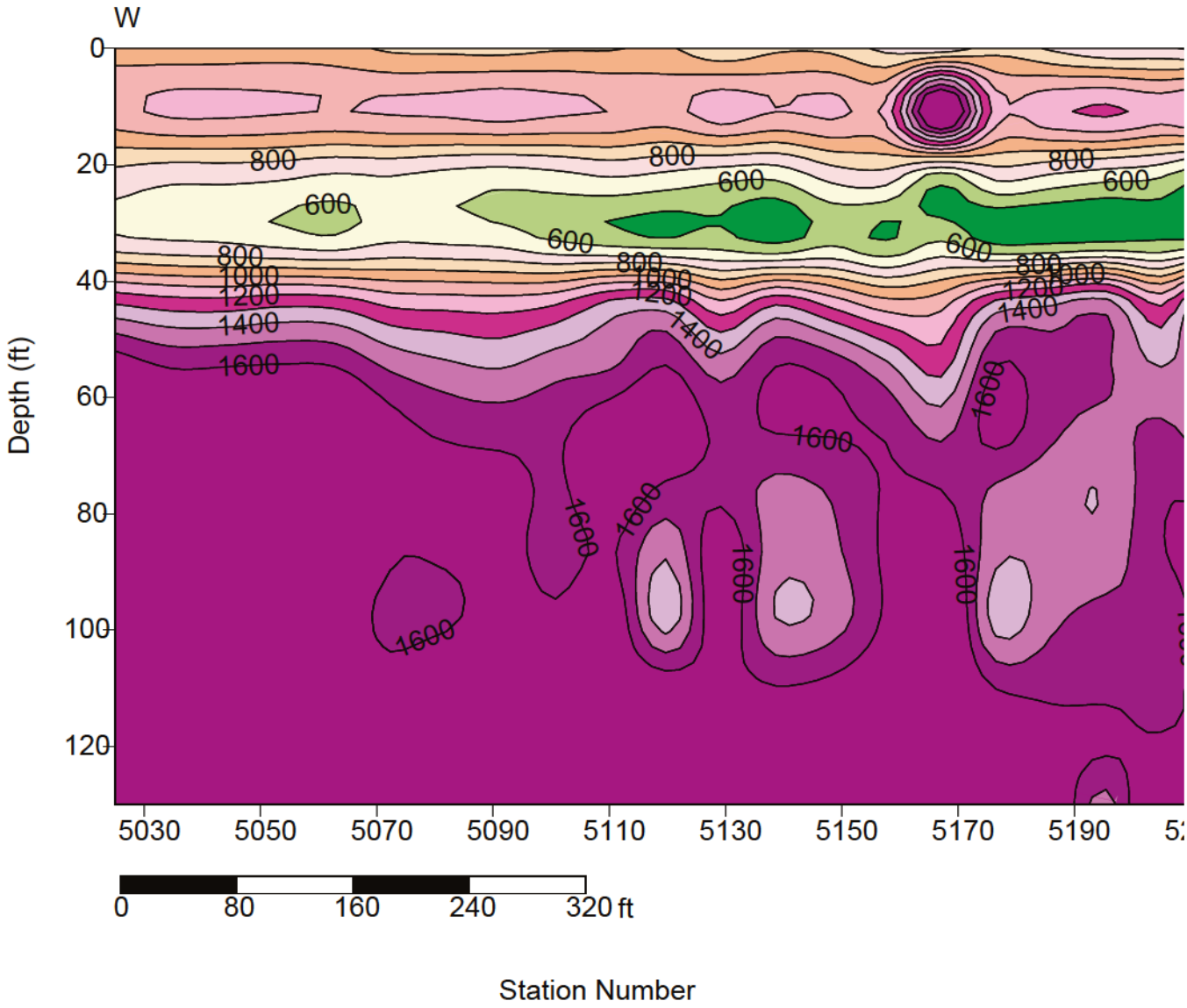

Figure 14a. Shear-wave velocity contour along line 5.

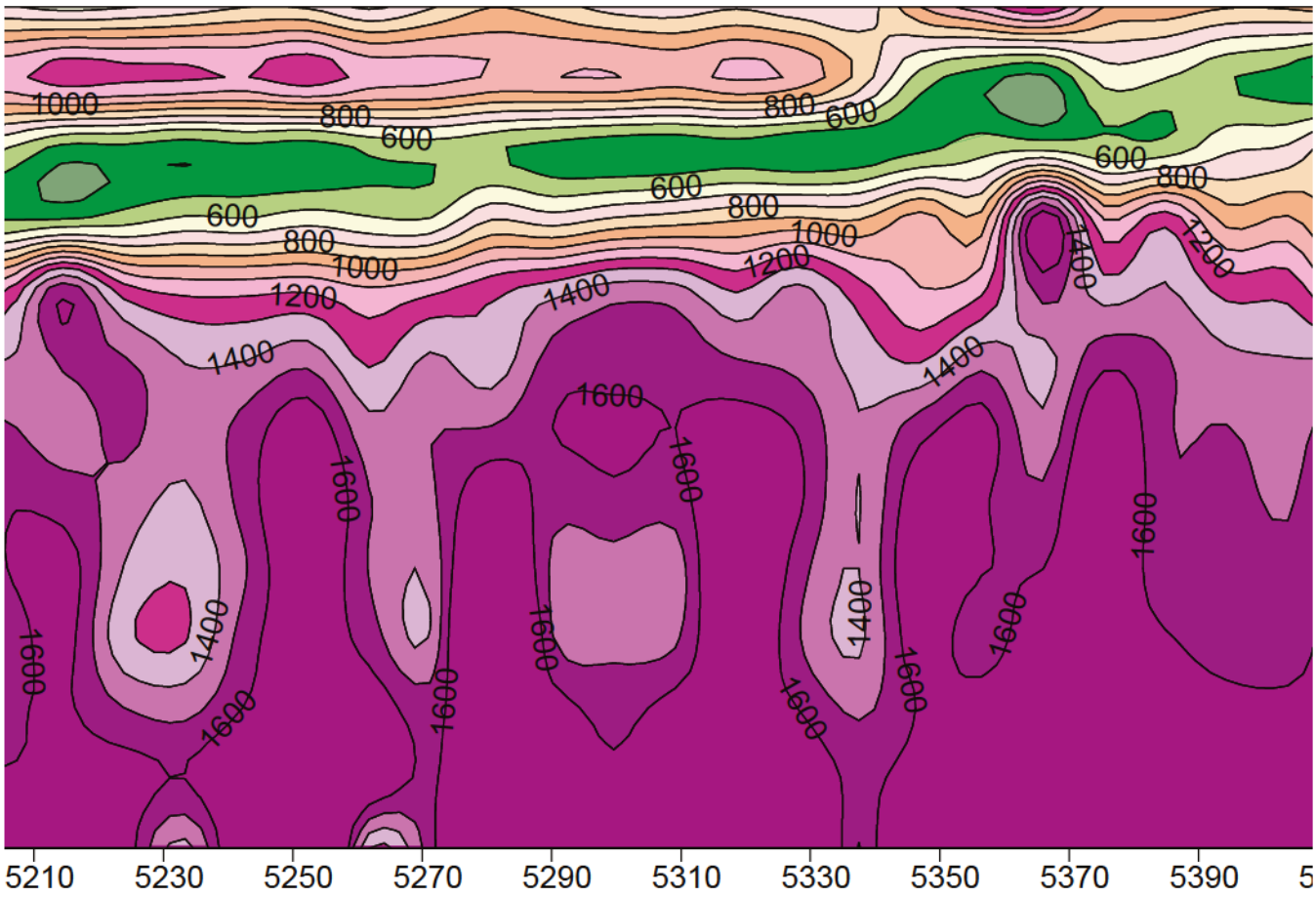

Station Number

Figure 14b.

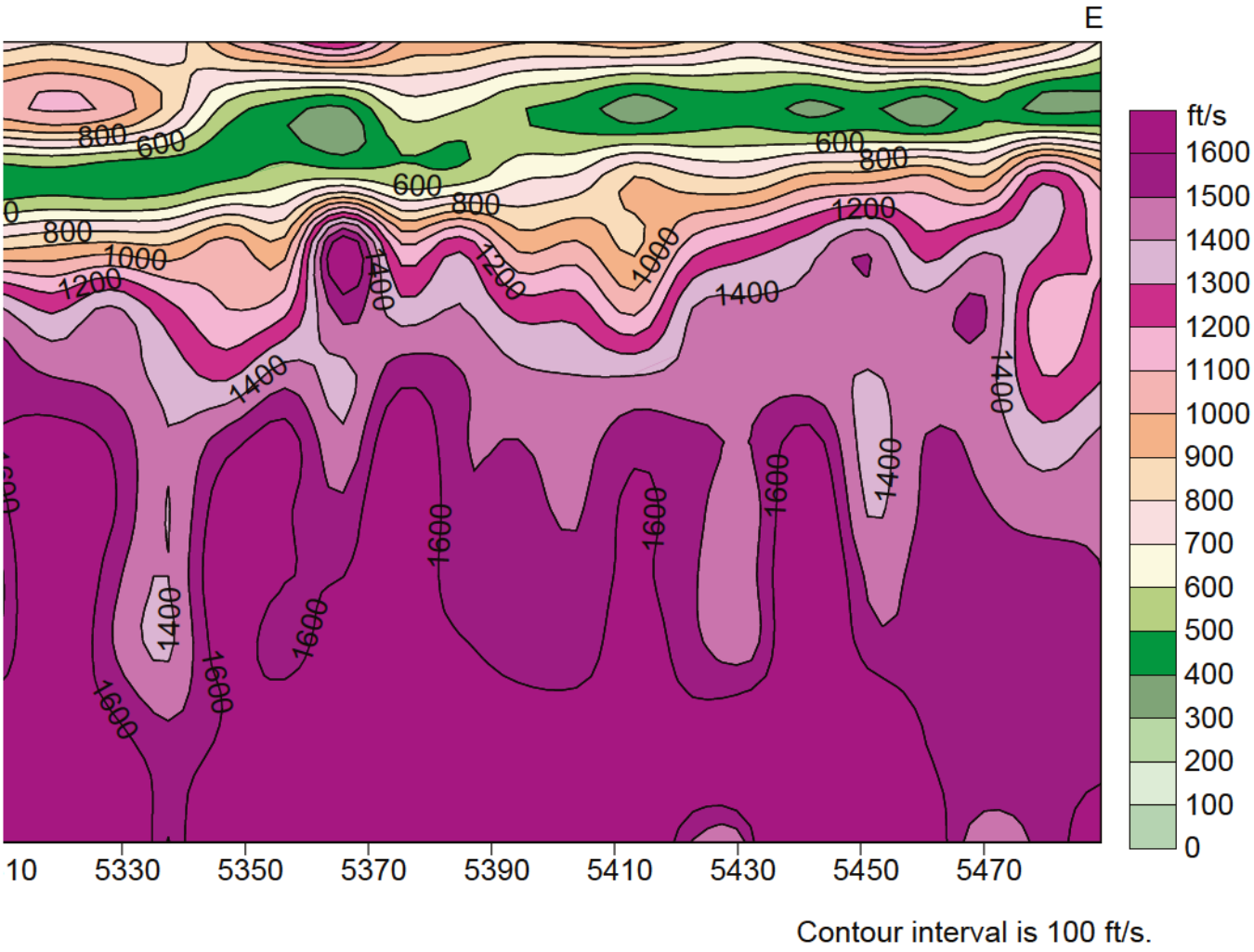
E
ft/s
1600
1500
1400
1300
1200
1100
1000
900
800
700
600
500
400
300
200
100
0
10
5330
5350
5370
5390
5410
5430
5450
5470
Contour interval is 100 ft/s.
Station Number

Figure 14c.

This entire profile is characterized by the same low velocity vertical serrations that have been interpreted as dissolution-related joint/fracture-type features filled with materials that are low velocity in comparison to surrounding sub-bedrock units. Several places exist along the profile where a decrease in the velocity gradient is interpreted to represent weathered bedrock sealed in a clay mortar. This scenario is likely the case beneath stations 5340, 5410, and possibly to a lesser extent at station 5165. The green low velocity layer seems relatively uniform and generally continuous. Based on observation and comparison with other surface wave profiles, the absence of higher velocity chimney features penetrating the low velocity material is synonymous with no subsidence.

Line 6

Reflection (Figures 15 and 16)

Line 6 is the northernmost east-to-west reflection profile. The general seismic character of reflections along this line are consistent with the other reflection profiles. The frequency content of reflections interpretable on this line is quite good, with dominant frequencies above 200 Hz evident from depths in excess of 750 ft. The paleosinkhole imaged on lines 1 and 2 is present and possesses very similar seismic characteristics. From the westernmost extent of the line to about station 6130 the shallowest event interpretable on the stacked data appears to be missing, or at a minimum dramatically reduced in amplitude. This could be indicative of an erosional surface, it could be associated with dissolution, or it could be a stratigraphic change. It does represent a noteworthy change in lithology above 60 ft along that part of the line.

The paleosinkhole evident at the east end of the line ties quite nicely with the interpreted feature on line 2. Based on stacking velocities and inferred spatial resolution, the paleosinkhole underlies an area approximately 200 ft wide with an approximately 70 to 80 ft column of vertically disturbed sediments. The northern end of the sinkholes seems likely to have been active the longest and is the area mostly likely to still have some active subsidence. Considering the expression of the sinkhole on the three lines (1, 2, and 6) that have been interpreted to cross over the feature, it appears to be elongated in a north-south direction and possess relatively uniform dimensions.

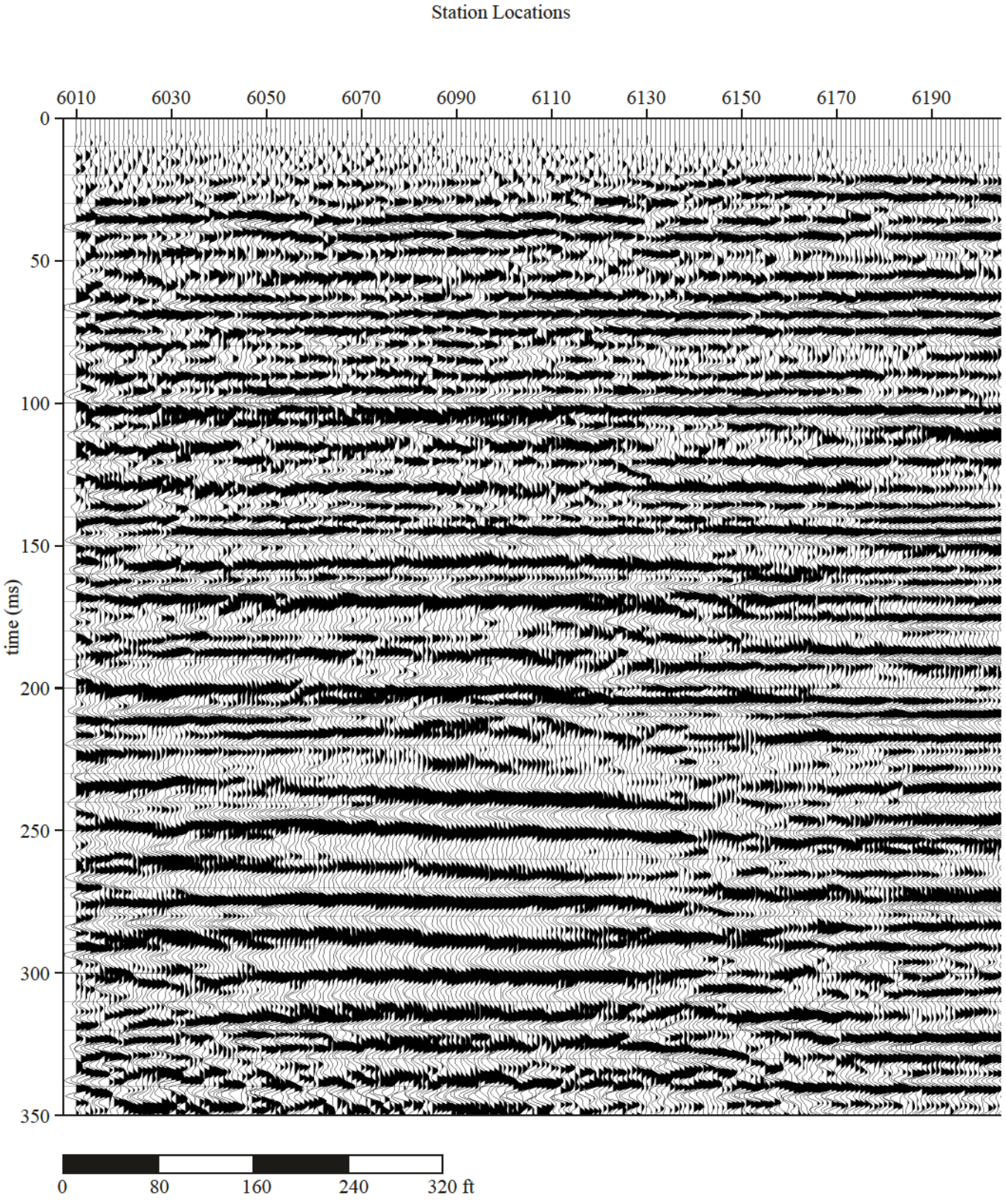

Figure 15a. CMP stacked section of line 6.

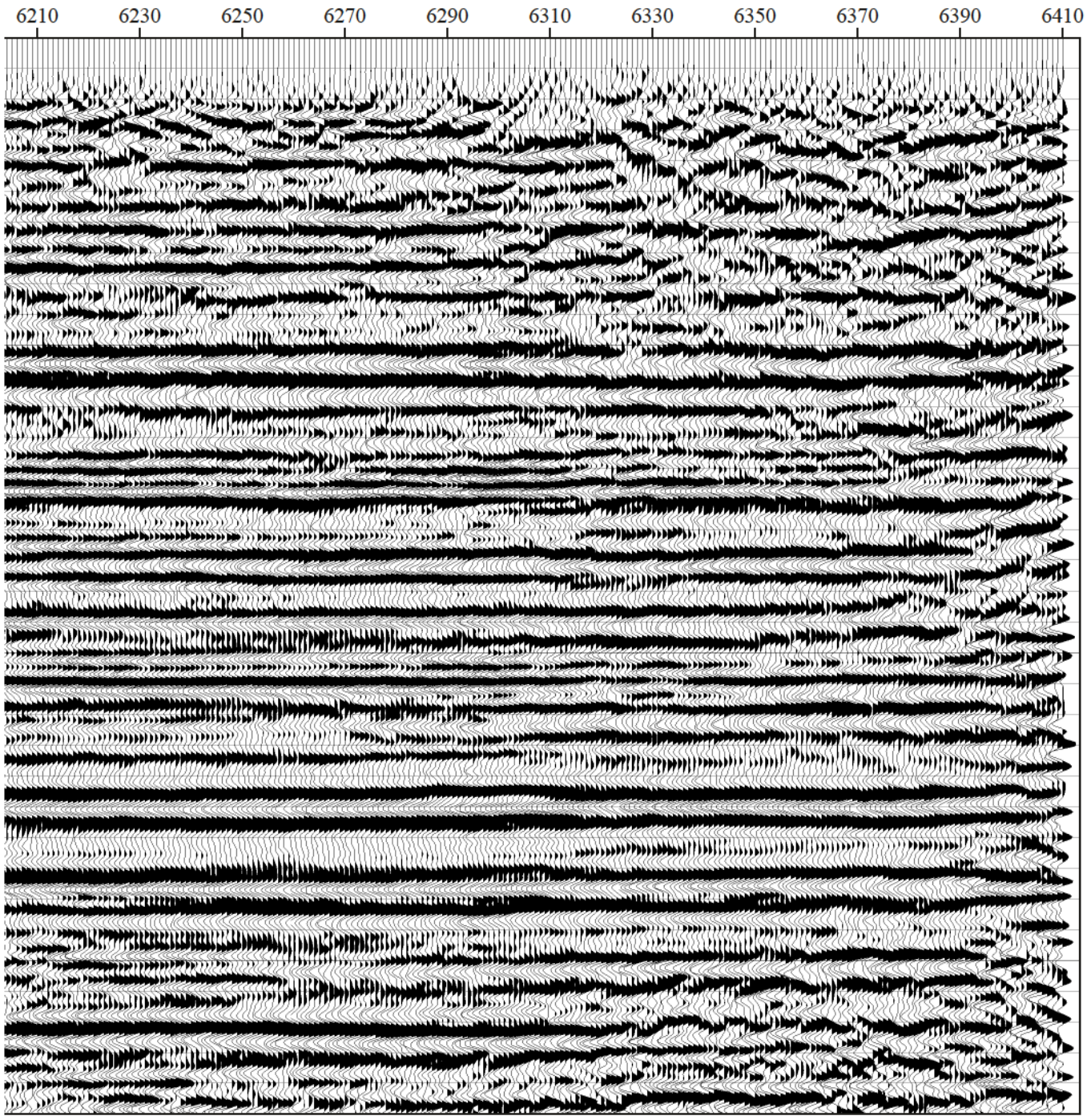
Station Locations
6210
6230
6250
6270
6290
6310
6330
6350
6370
6390
6410

Figure 15b.

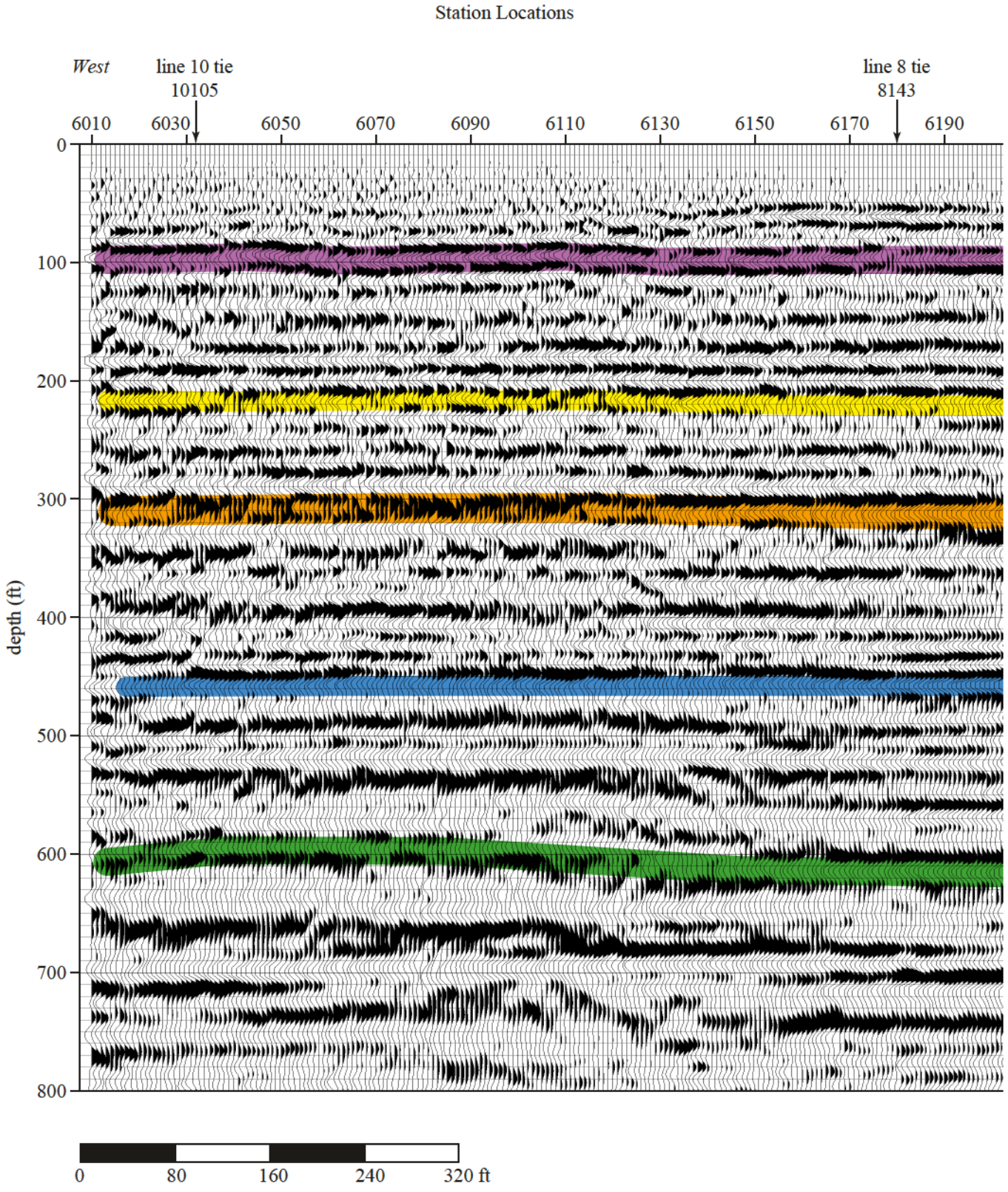

Figure 16a. Interpreted line 6.

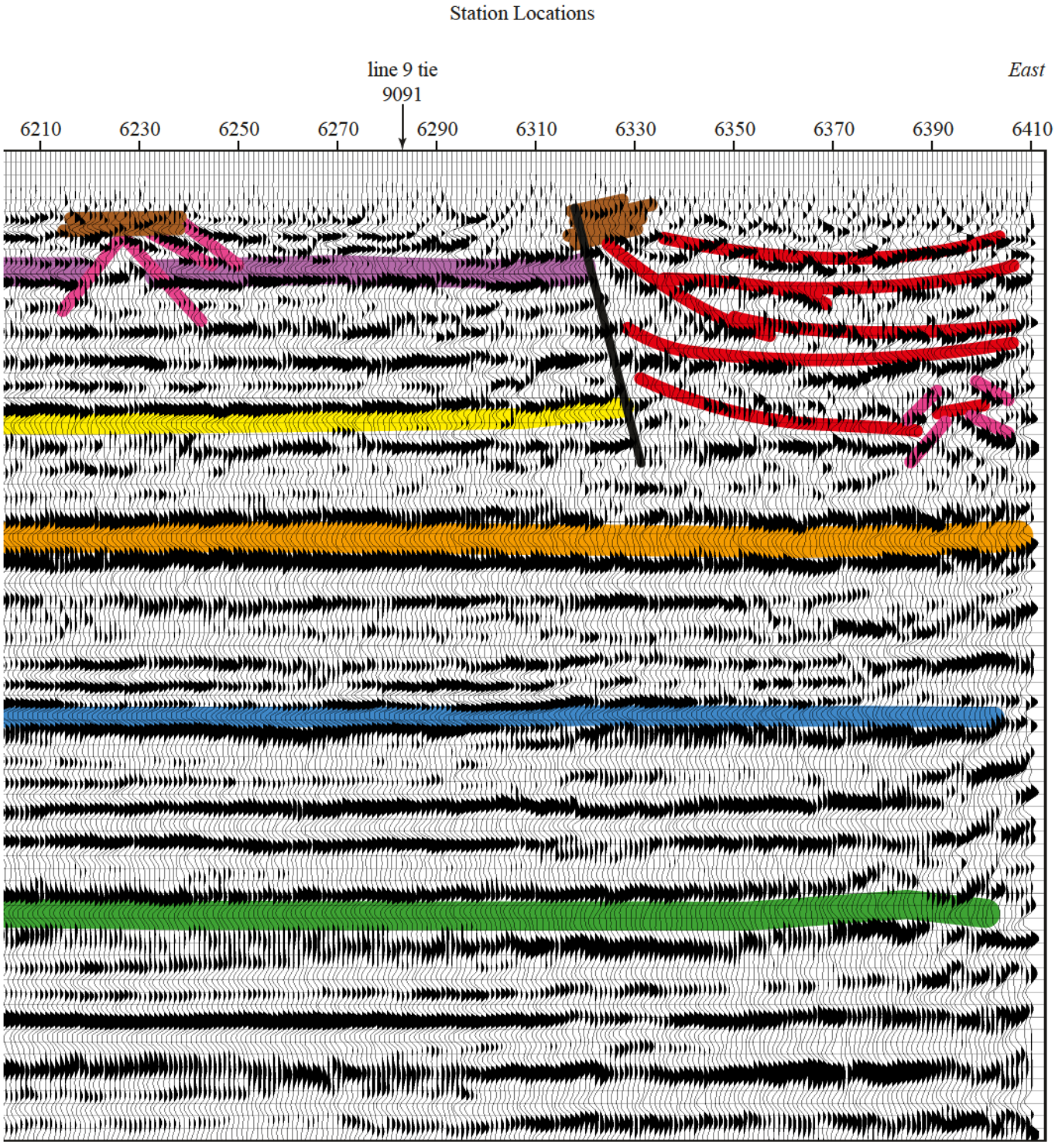
Station Locations
line 9 tie
9091
East
6210
6230
6250
6270
6290
6310
6330
6350
6370
6390
6410

Figure 16b..

Surface Wave (Figure 17)

Surface wave data from along line 6 presents an image suggesting a gentle bedrock dip to the east from about 20 to 25 ft on the east to a maximum depth of around 35 to 40 ft on the west. It is interesting to note the general similarity in patterns observed along all the lines in the north portion of the study area. Two noteworthy anomalous features likely significant to the hydrology of and future engineering at this site are the low velocity infiltrations beneath stations 6150 and 6300 into the otherwise high velocity sub-bedrock layers. These features are quite similar in their general dimensions and degree to others found along the northern group of seismic lines.

The relatively deep, high-gradient low-velocity closure beneath station 6150 is one of the most pronounced and abrupt features of its kind on any of the sections from this survey. Based on the velocity contrast and gradient, this feature has all the key properties to consider it a karst void, or at a minimum an area of very low competence. It is likely, based on the velocity signature of this feature, that it will correlate to an area in the subsurface where the native 1600 ft/sec bedrock materials are missing and infilled with rubble and unconsolidated sediments. This anomaly possesses a geometry consistent with an elongated dissolution joint or fracture (karst) cut deep into bedrock. It is not possible to determine what material fills the karst, but based on its dramatic drop in velocity over such a small area, it could be an open or water-filled cavity. Based on the relatively continuous bedrock contours (700 to 1000 ft/sec), no subsidence has occurred as a result of this feature. It is interesting to note that no expression of this feature can be interpreted on the reflection section.

The second dominant feature on this line that is likely related to karsting is located beneath station 6300. This is one of the few downwardly elongated low velocity areas that affects one of the contours identified as representative of bedrock. This velocity anomaly is probably representative of a dissolution/erosional area extending downward from the bedrock surface to a depth of around 70 ft or so. This bedrock surface anomaly was formed prior to deposition of the low velocity green zone about 20 ft below the ground surface and, based on the general appearance of the feature, it is probably filled with bedrock rubble and clay-rich sediments. Bedrock materials between stations 6280 and 6310 should not be considered as competent (ridge, stiff, mechanically strong) as the bedrock materials under station 6380, for example. This is an area that likely possessed open channels and holes in the upper portion of

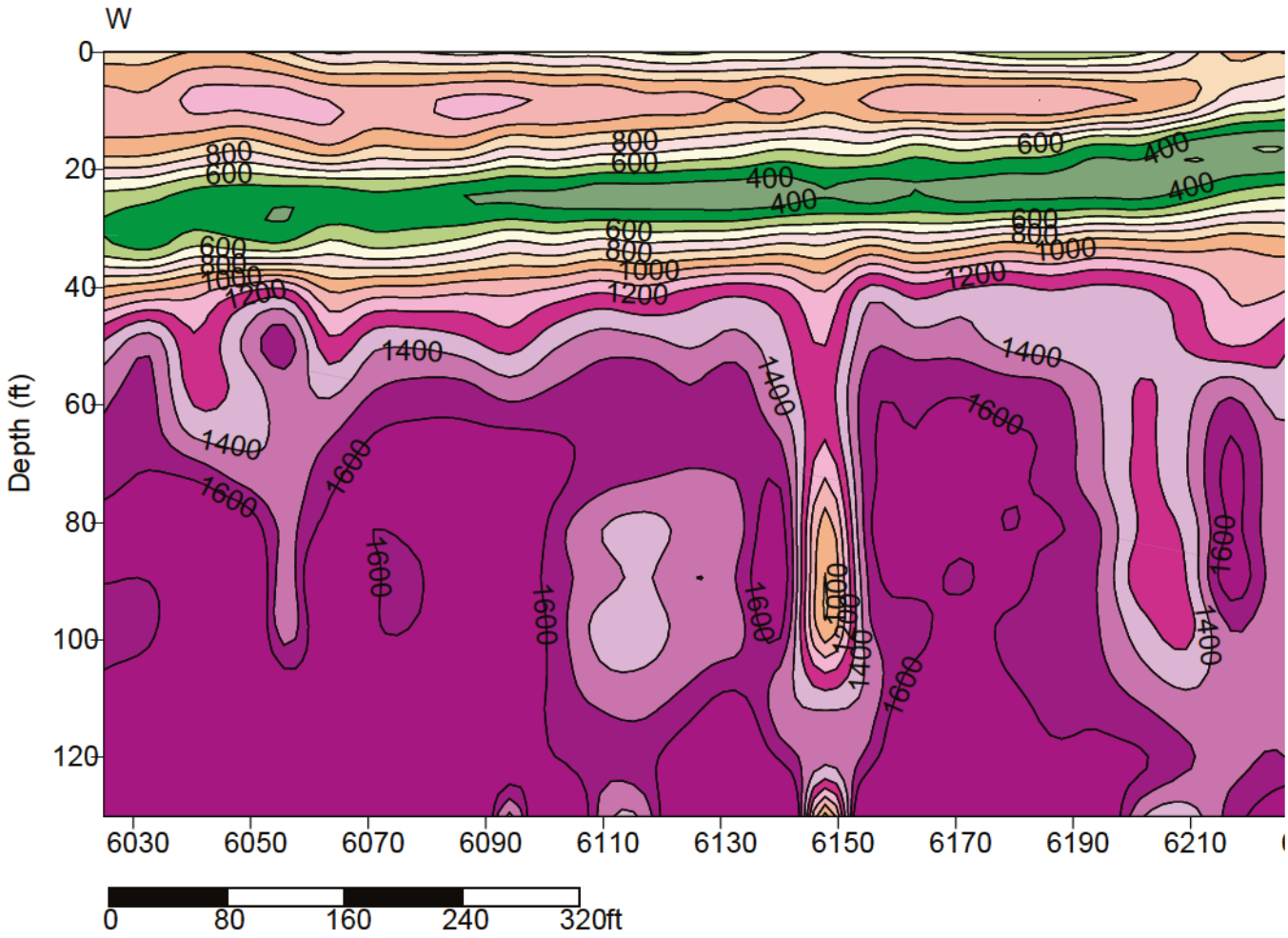

Figure 17a. Shear-wave velocity contour along line 6.

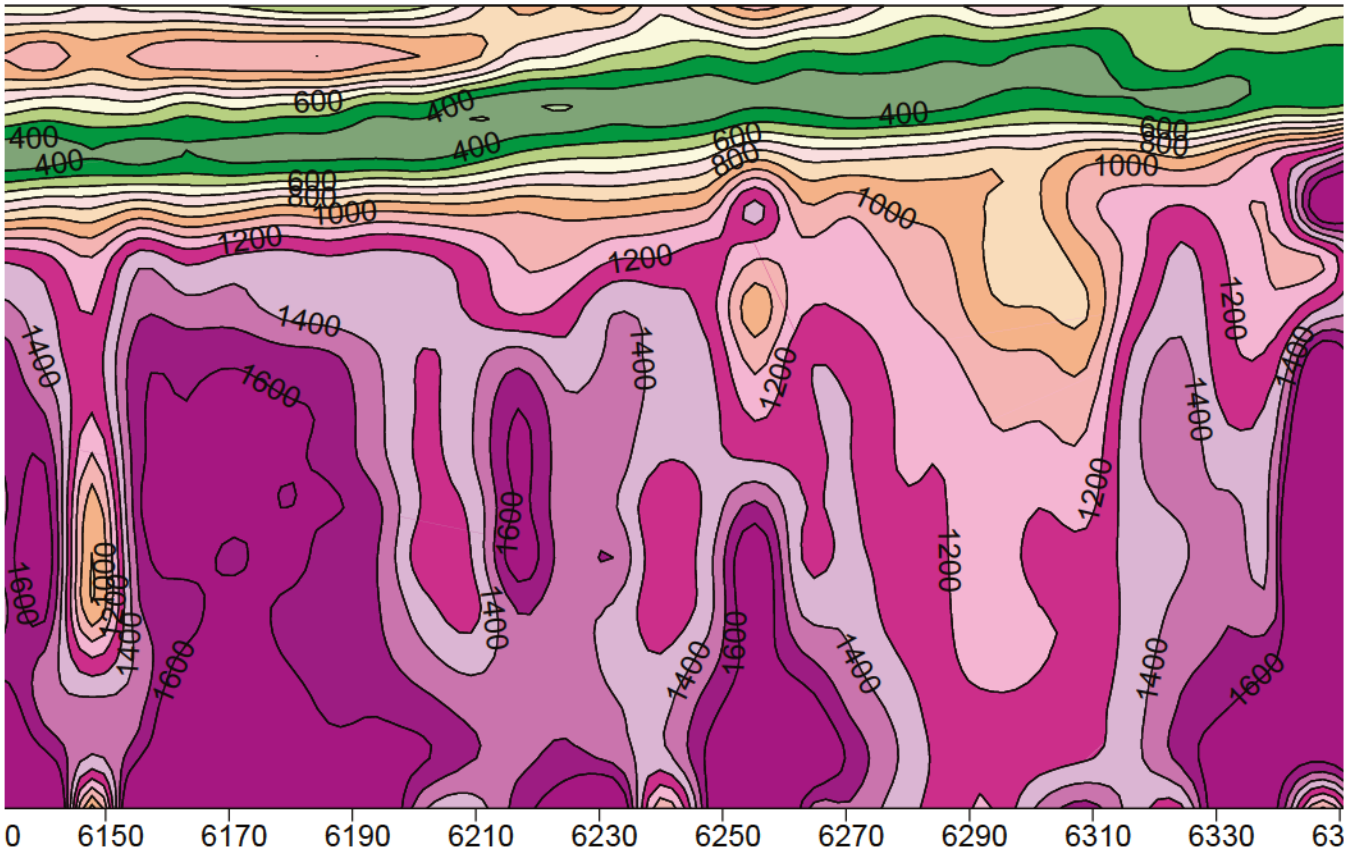

Station Number

Figure 17b.

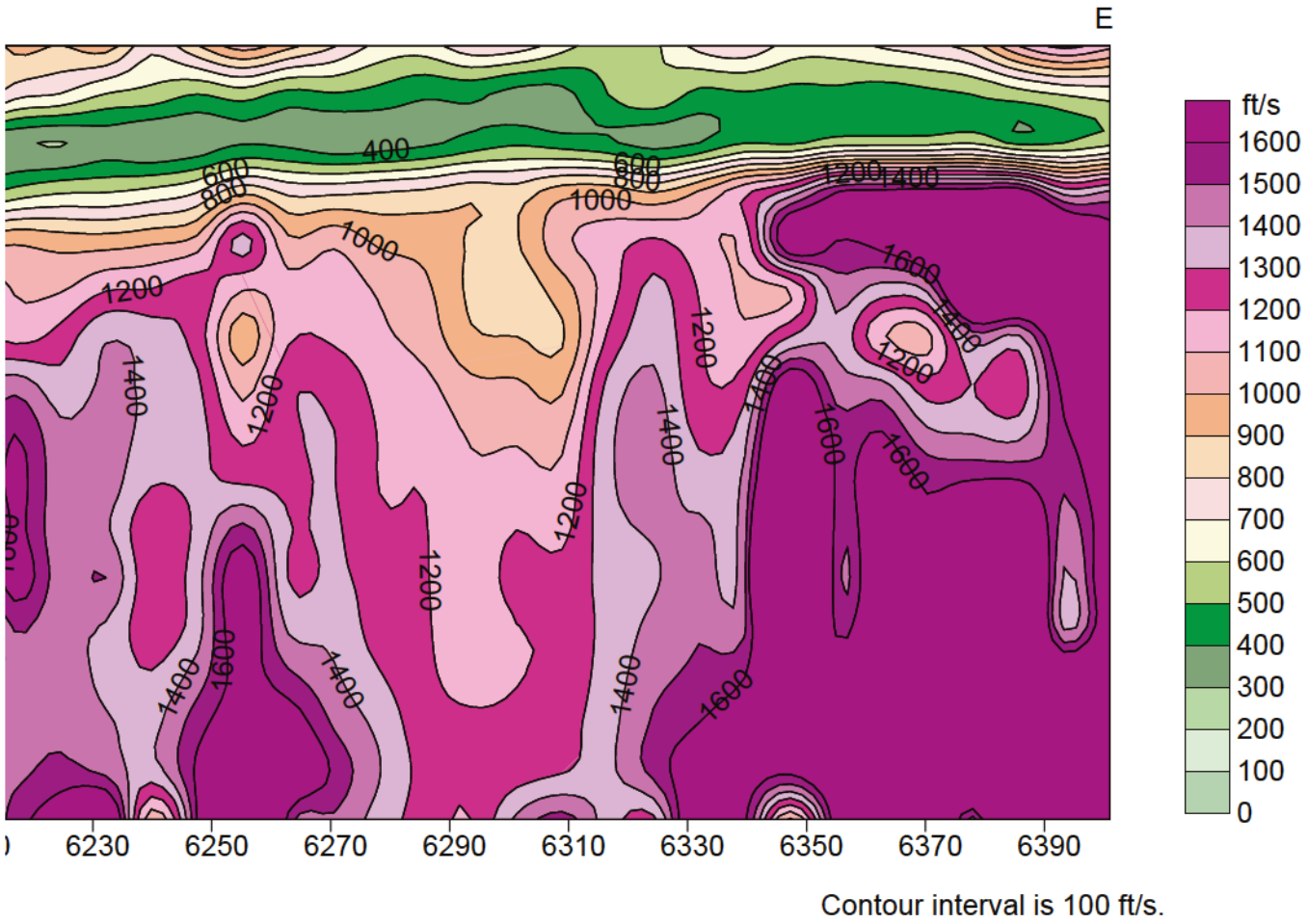

Station Number

Figure 17c.

bedrock due to dissolution prior to infilling with the clay/rubble materials that are likely present in the bedrock "channel" between stations 6280 and 6310.

Uniformity in and minimal deformation of velocity contour lines representing the bedrock surface is the basis for suggesting that features like the one at station 6300 formed prior to the deposition of unconsolidated sediments above bedrock. If these features formed as a result of dissolution after the deposition of the shallow unconsolidated materials, some expression (draping of the velocity contour lines, chimney features within the unconsolidated sediments, etc.) would have been evident at and above the 800 ft/sec bedrock surface contour.

Prior to the deposition of the unconsolidated sediments, the ground surface (bedrock) would have resembled swiss cheese in the northern portion of this study area. It probably closely resembled the karst topography evident at the surface of bedrock observable in outcrop along the river banks and near subsidence and erosion exposure in the Dixon Forest.

Comparing the anomalies and features on both the surface wave and reflection data brings to light an interesting coincidence. The deep velocity low on surface wave data near station 6310 is consistent with the apparent fault-bounded edge of the paleosinkhole delineated by the seismic reflection data. This deep-seated feature has the properties on shear wave data for a highly porous zone and on the reflection data as a highly disturbed zone with minimal continuity in events through the zone. If an area was to be selected that has the potential for fluid movement and structure conducive to subsidence, this would likely be it.

Line 7

Surface Wave (Figure 18)

Line 7 data possess character similar to other northern lines. The bedrock surface and material within 10 or so feet of the top of bedrock are scarred with the effects of dissolution/erosion. Several attributes of these data are noteworthy and are likely indicative of anomalous earth. A few high velocity zones are evident within 5 ft of the surface of the ground. It is unlikely based on a 30 ft wavelength (the shortest processed) that these features can be interpreted with much confidence. The green low velocity layer is relatively continuous and possesses a slight westward dip, which is consistent with the interpreted bedrock dip. An apparent low velocity zone beneath station 7210 is consistent with a dissolution/erosional feature in bedrock that extends to at least 100 ft below ground surface.

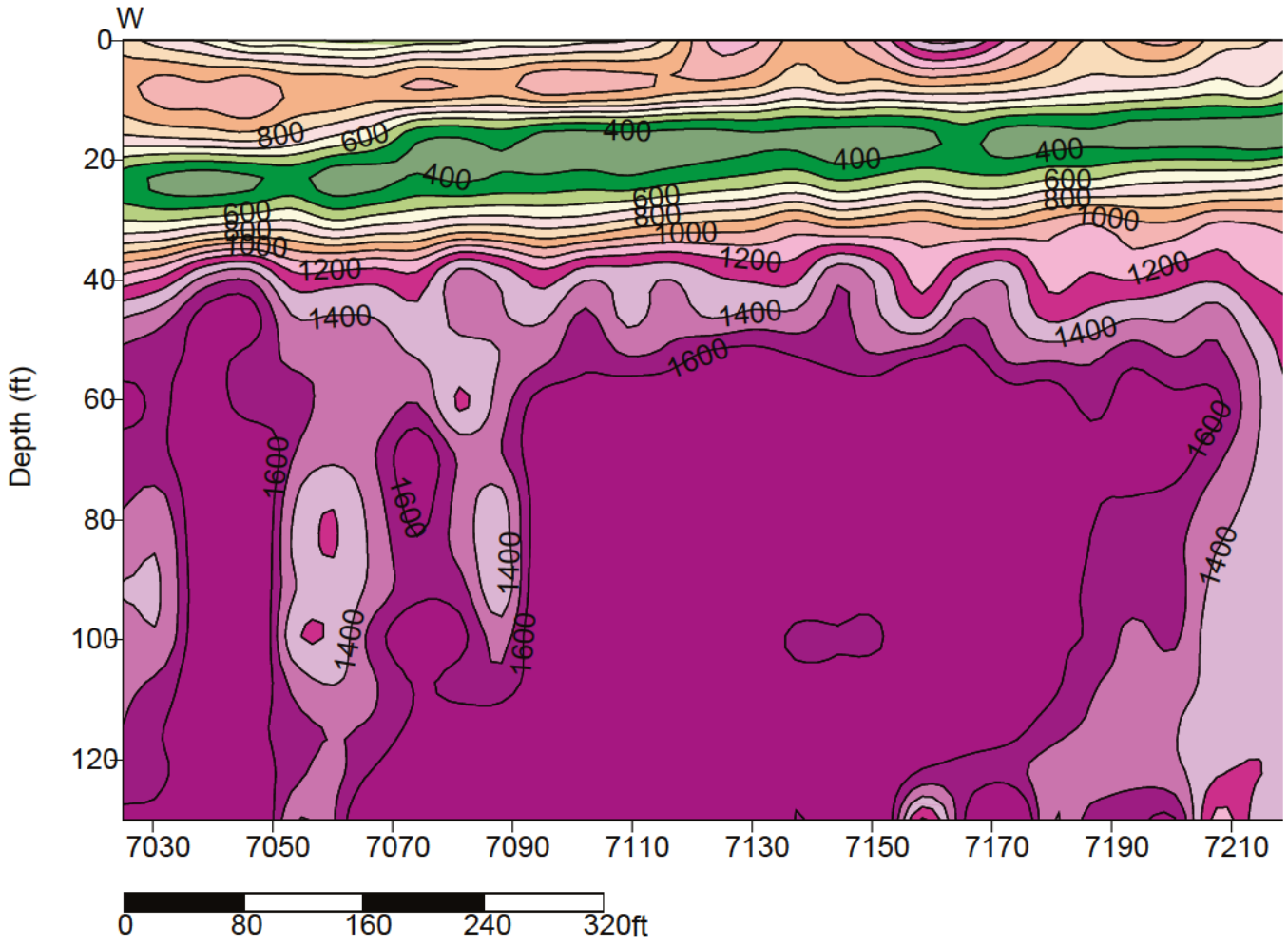

Figure 18a. Shear-wave velocity contour along line 7.

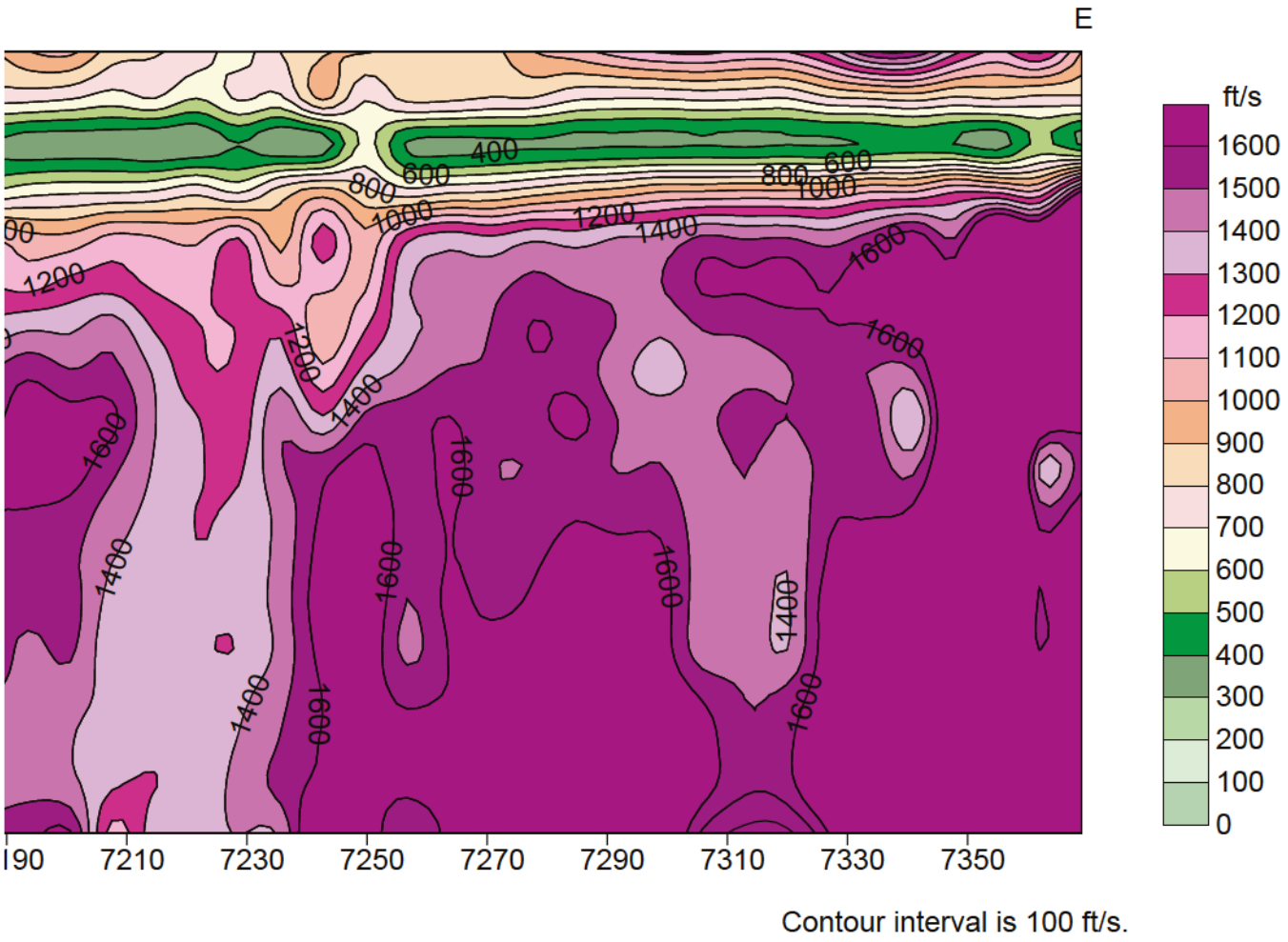
E
ft/s
1600
1500
1400
1300
1200
1100
1000
900
800
700
600
500
400
300
200
100
0
400
600
800
1000
1200
1400
1600
7190
7210
7230
7250
7270
7290
7310
7330
7350
Contour interval is 100 ft/s.
Station Number

Figure 18b.

Consistent with the other lines in this area, a bedrock joint/fracture is identifiable by its chimney-looking low velocity wedge penetrating at least 100 ft into bedrock surrounded by higher velocity native bedrock materials. This vertical bedrock feature lies directly below a higher velocity hole in unconsolidated sediments at a depth of around 20 ft. This pattern is inconsistent with previous suggestions that most bedrock dissolution features were active prior to deposition of the unconsolidated sediments. The low velocity "tongue" extending downward from the top of bedrock is either a dissolution and subsidence feature active predominantly during deposition of the oldest portion of the unconsolidated materials above bedrock, dissolution/erosion when bedrock was exposed to surface activities, or an indication of faulting. Again, as on line 6, this low velocity slice extending over 100 ft into bedrock aligns itself with the extreme edge of the paleosinkhole defined by reflection lines 1, 2, and 6. It is more than a coincidence that low swamp areas are associated with the perimeter of the paleosinkhole.

Line 8

Reflection (Figures 19 and 20)

Reflections from as deep as 300 ms (1300 ft) were imaged along this line. Overlap between the reflection and surface wave data provides improved interpretations between the bedrock and the Ocala Limestone. In general, reflections are relatively flat with little in the way of major structural features. Studying each coherent reflection arrival provides insight into the small-scale complexity of the upper 1000 ft of geology. There are three zones along this line with evidence indicating potential dissolution activity with subsidence potential. These features are somewhat subtle and are likely indicative of past and possibly current dissolution activities.

A small chaotic zone exists around station 8130. Reflection events throughout this zone are flat with little in the way of structure evident. The primary aspect of this area that draws some level of concern is the somewhat unusual wavelet characteristics.

Between stations 8270 and 8350 the general character of the data changes with apparent offset easily interpreted within this zone. This offset feature appears graben-like down to the 290 ms reflection where offset is difficult to confidently interpret. There appears to be just a very subtle indication of offset in this reflection event beneath station 8350. With offsets this small, careful consideration of static effects must come into play during interpretation. It is likely that this graben-like structure is fault controlled, or at least related to fracture zones and

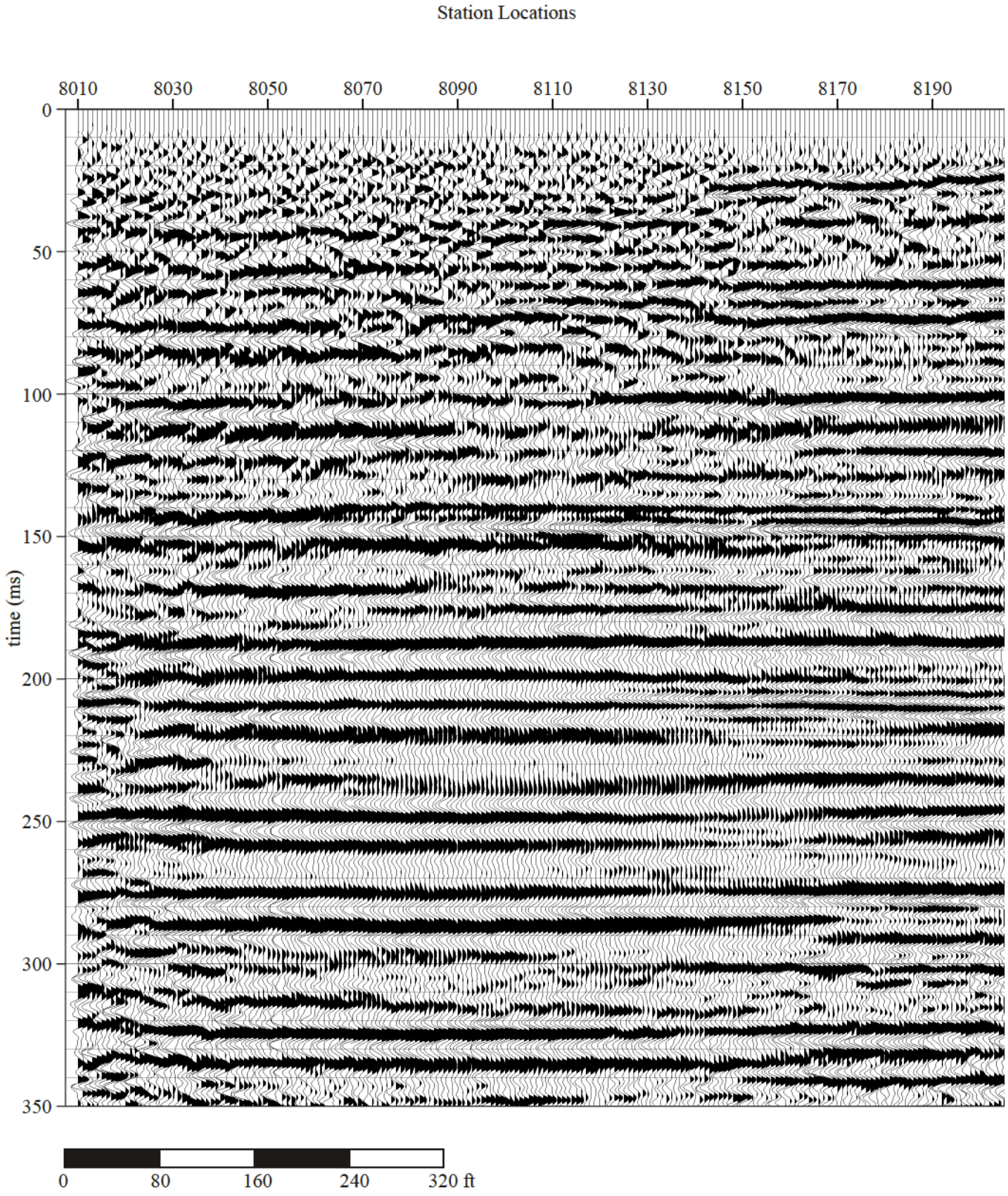

Figure 19a. CMP stacked section of line 8.

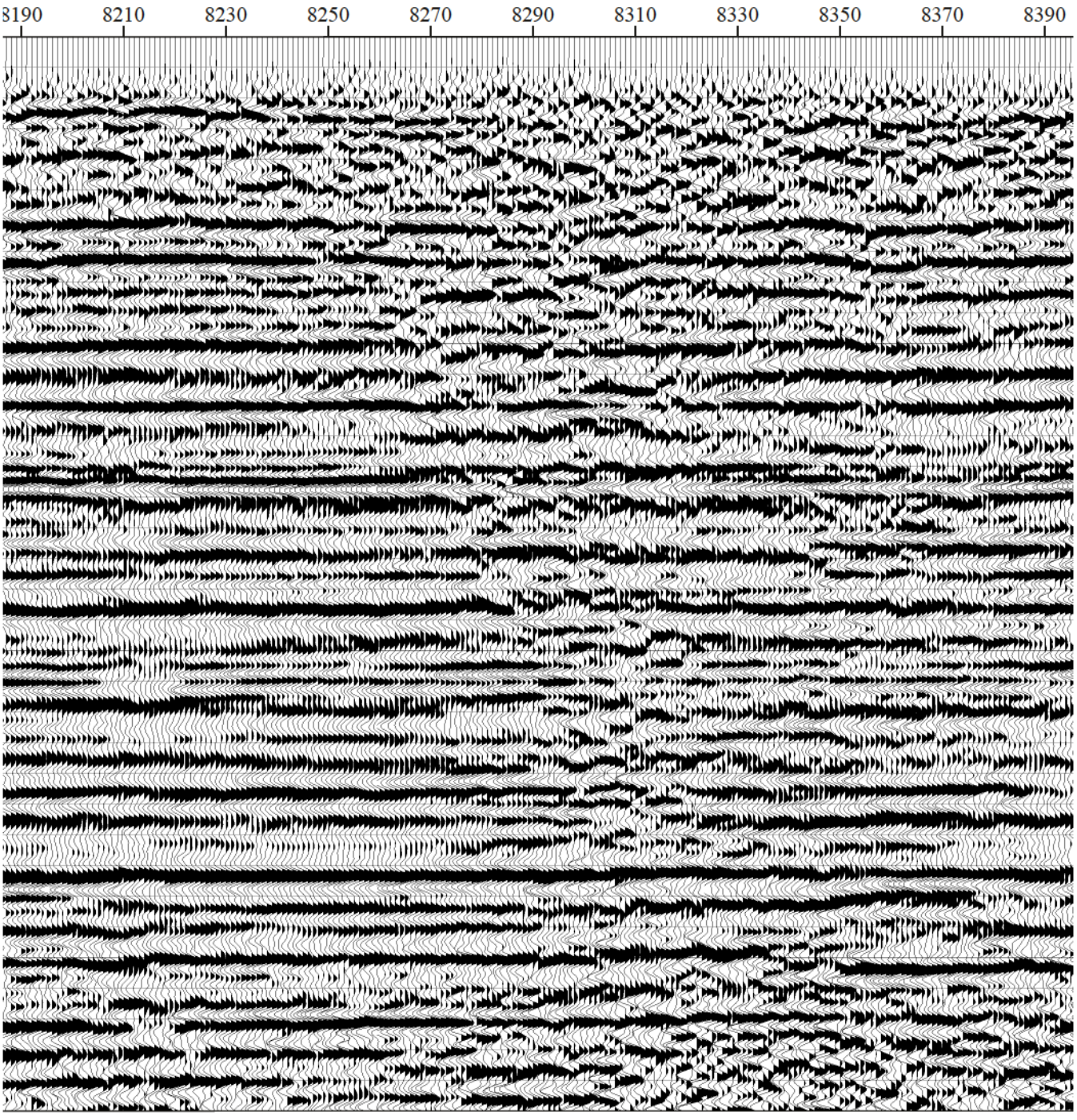
Station Locations
8190
8210
8230
8250
8270
8290
8310
8330
8350
8370
8390

Figure 19b.

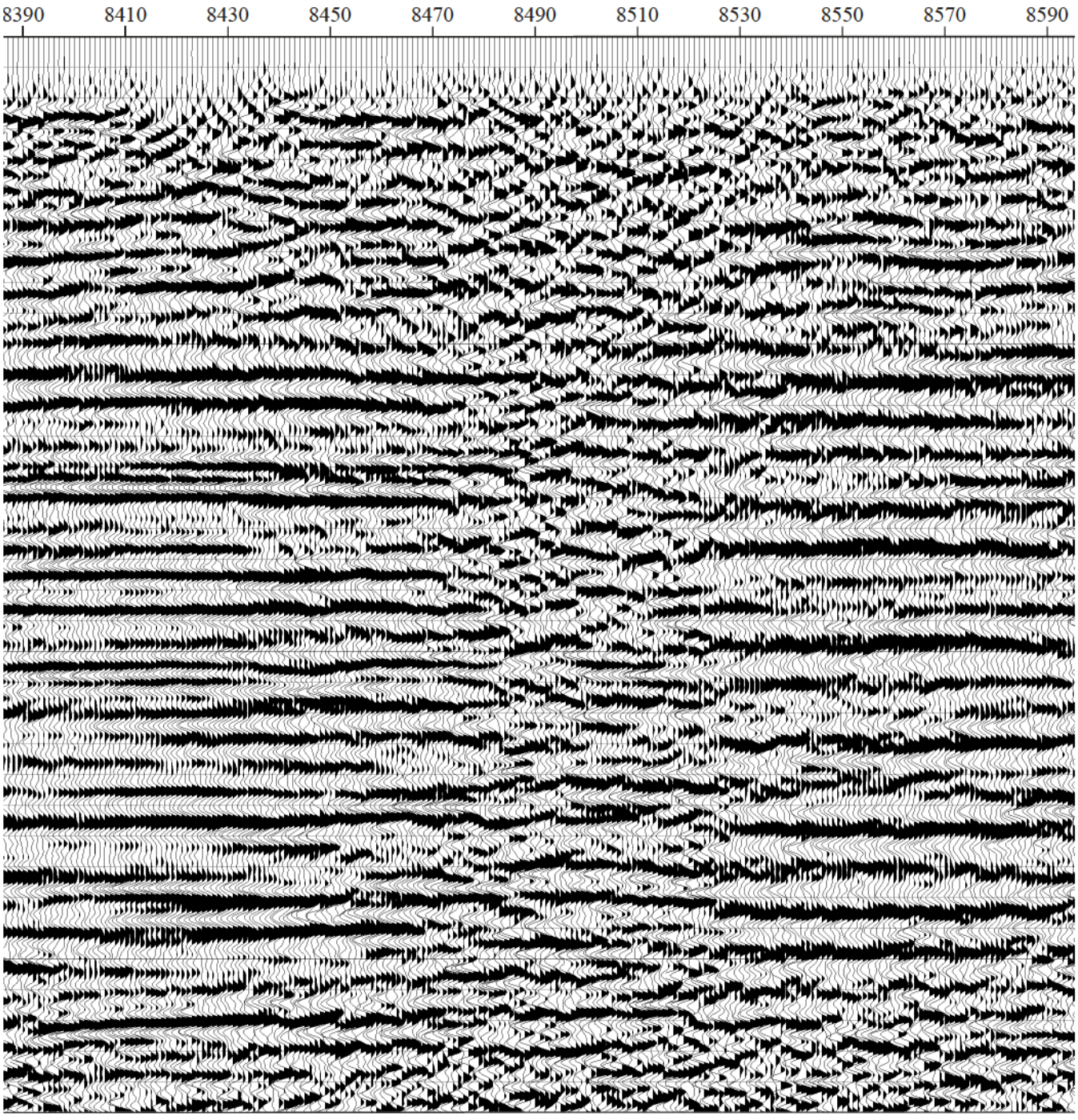
Station Locations
8390
8410
8430
8450
8470
8490
8510
8530
8550
8570
8590

Figure 19c.

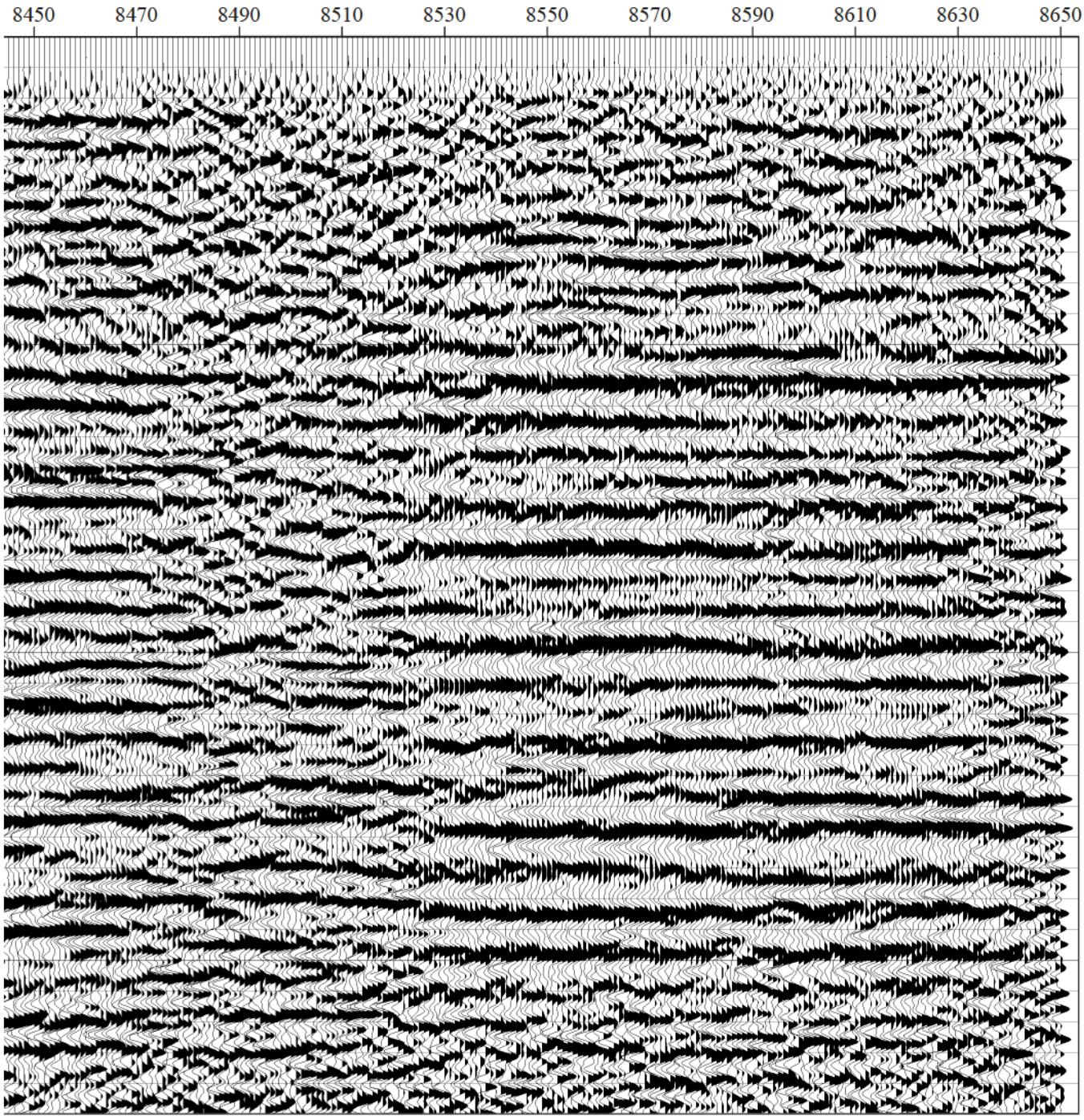
Station Locations
8450
8470
8490
8510
8530
8550
8570
8590
8610
8630
8650

Figure 19d.

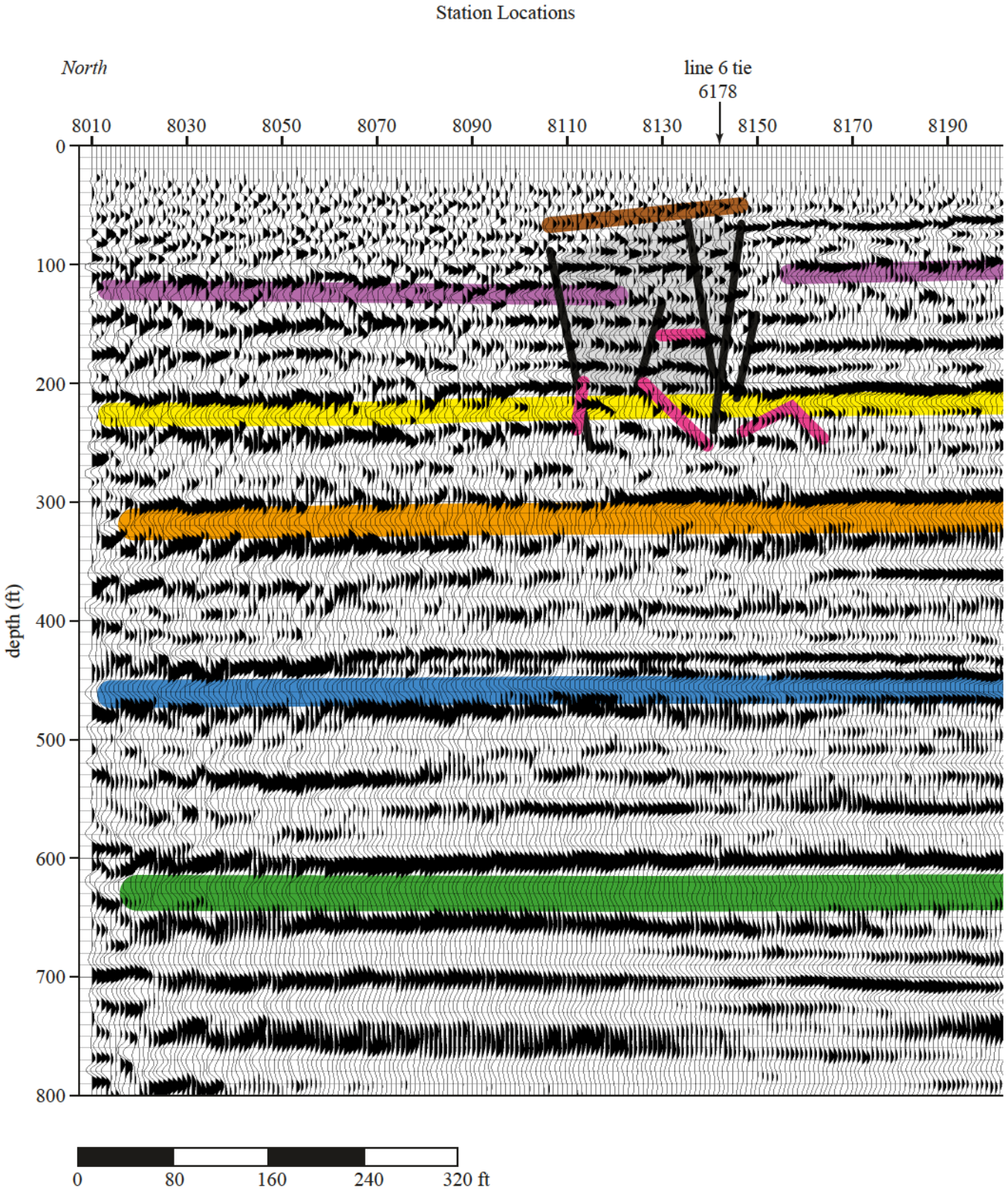

Figure 20a. Interpreted line 8.

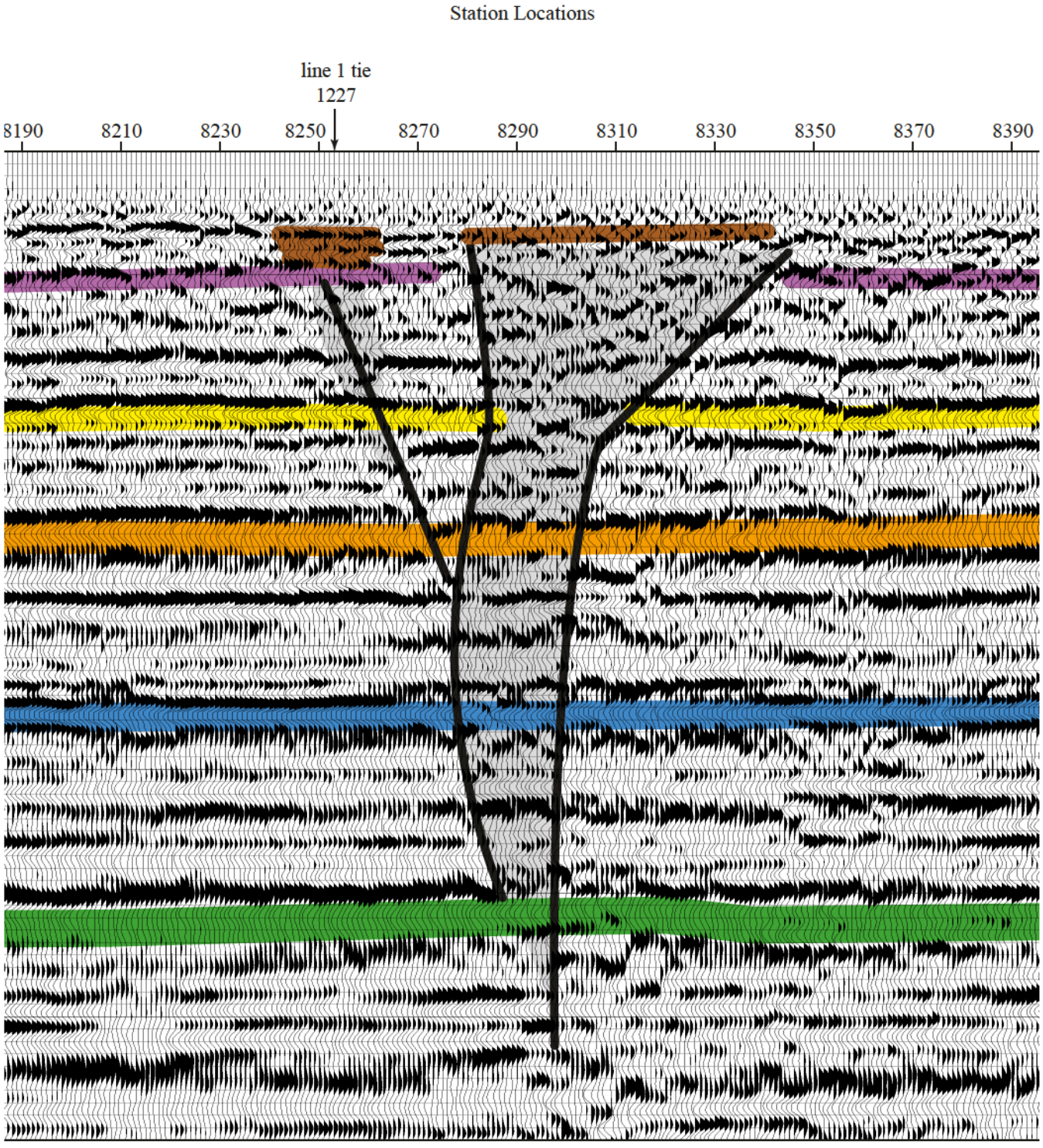
Station Locations
line 1 tie
1227
8190
8210
8230
8250
8270
8290
8310
8330
8350
8370
8390

Figure 20b.

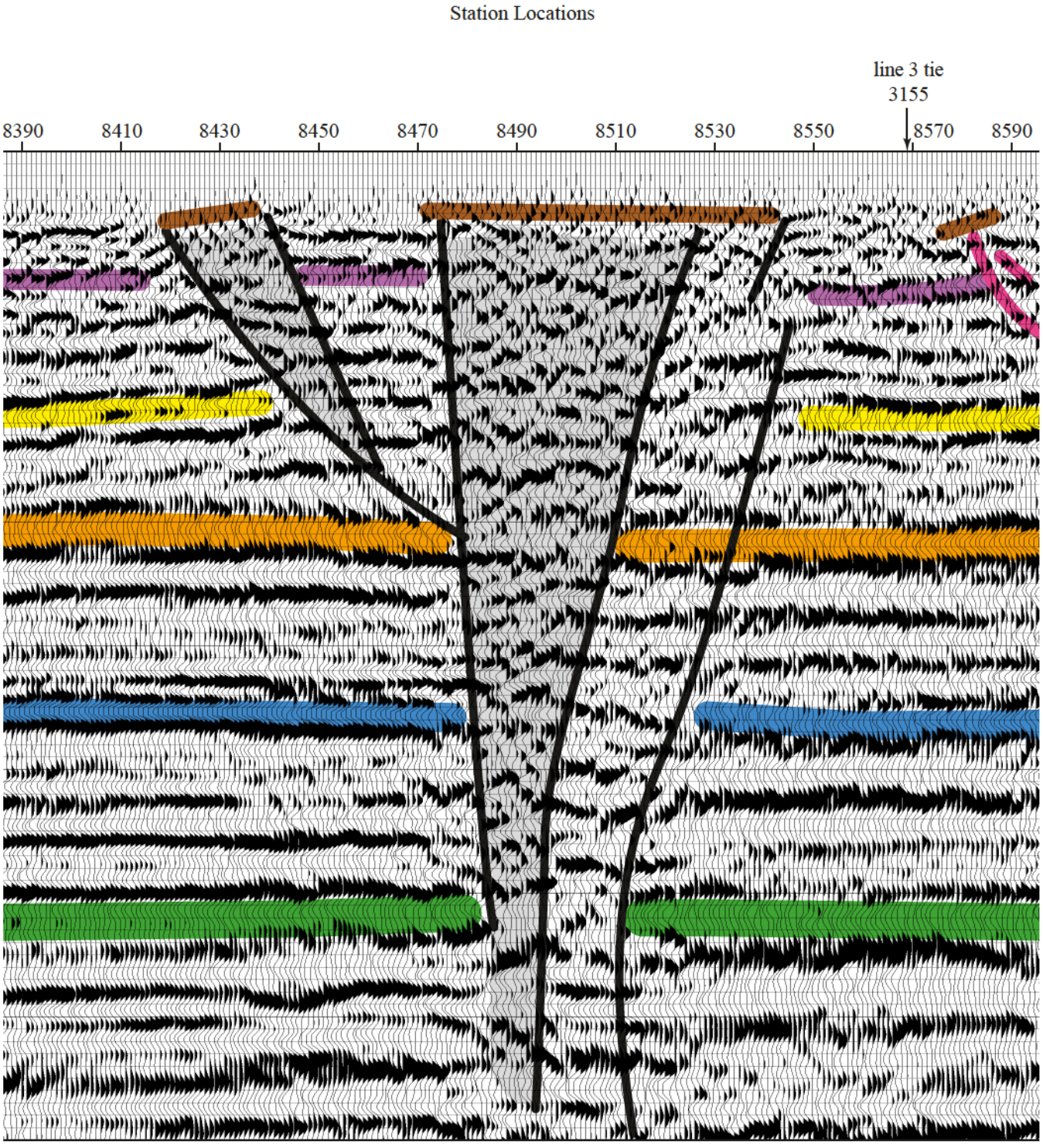
Station Locations
line 3 tie
3155
8390
8410
8430
8450
8470
8490
8510
8530
8550
8570
8590

Figure 20c.

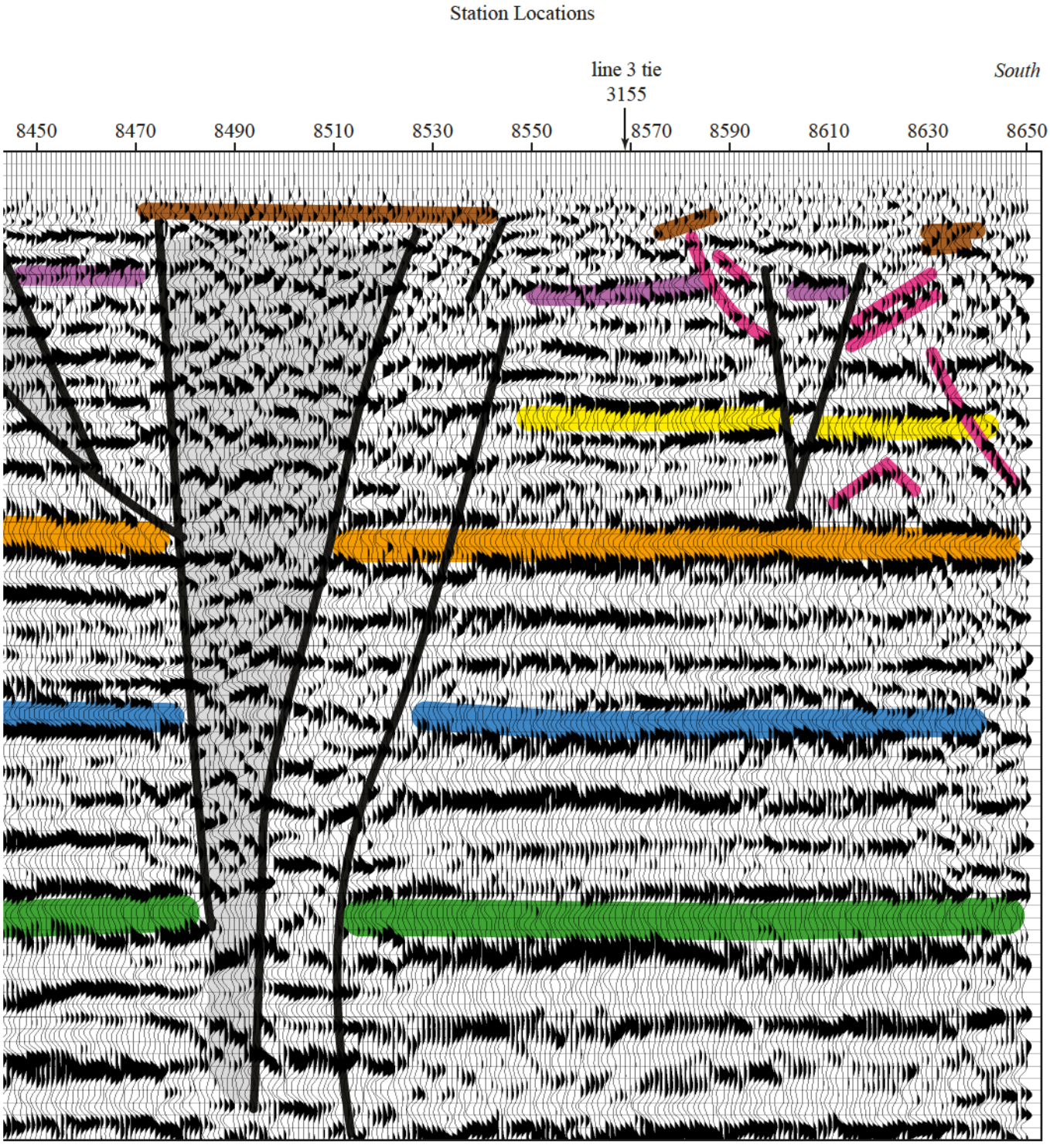
Station Locations
line 3 tie
3155
South
8450
8470
8490
8510
8530
8550
8570
8590
8610
8630
8650

Figure 20d.

orientations, with expression to the top of bedrock. Based on the size, relatively uniform displacement through the mapped section, and non-vertical normal fault characteristics, it is possible this is a faulted area with expression at the bedrock surface and is tectonic in origin. The one reservation that must be addressed is the lack of lateral consistency on adjacent seismic reflection profiles that might cut the fault nearly orthogonally.

Interpreting this series of bed offsets as a fault extending to the surface of bedrock provides some very interesting possibilities with respect to the hydrogeology of this site. Faults that penetrate the bedrock surface, even if they have no topographic expression due to erosion, will act as a conduit for fluid access to materials within the bedrock. Many of the fault-like features that splay from this main zone could all be the result of subsidence in fractured rock.

A lower signal-to-noise and decreased resolution zone is evident between stations 8430 and 8530. This drop in signal and frequency is currently interpreted as related to extremely small displacement faulting. This interpretation is influenced by the fault zone (graben) interpreted just north of this area on the seismic reflection profile.

Surface Wave (Figure 21)

Surface wave data from line 8 detected several anomalous zones within the bedrock but little in the way of subsidence-related features within the unconsolidated materials. Probably the most interesting and significant feature imaged is the low velocity chimney with near vertical walls and an extreme velocity contrast consistent with unconsolidated/consolidated interfaces. This feature resembles many others observed around this site that have been correlated with dissolution joints or fractures infilled with weathered bedrock materials and clay-rich sediments similar to the clays immediately overlaying bedrock. It is very likely the case here, but it is worth noting this feature is probably the most well defined and the deepest of any interpreted at this site. This difference draws in another possible interpretation of this feature: Could this be a fault zone?

Correlating this feature with the reflection profile is the best way to address the possibility that faulting is present at the bedrock surface. Reflection data have been interpreted with a graben that extends from stations 8265 to 8365. This fault expression is somewhat coincident with the low velocity chimney evident on the surface wave data. The eastern fault leg of this graben is coincident on both data sections. It is, therefore, with some degree of confidence that

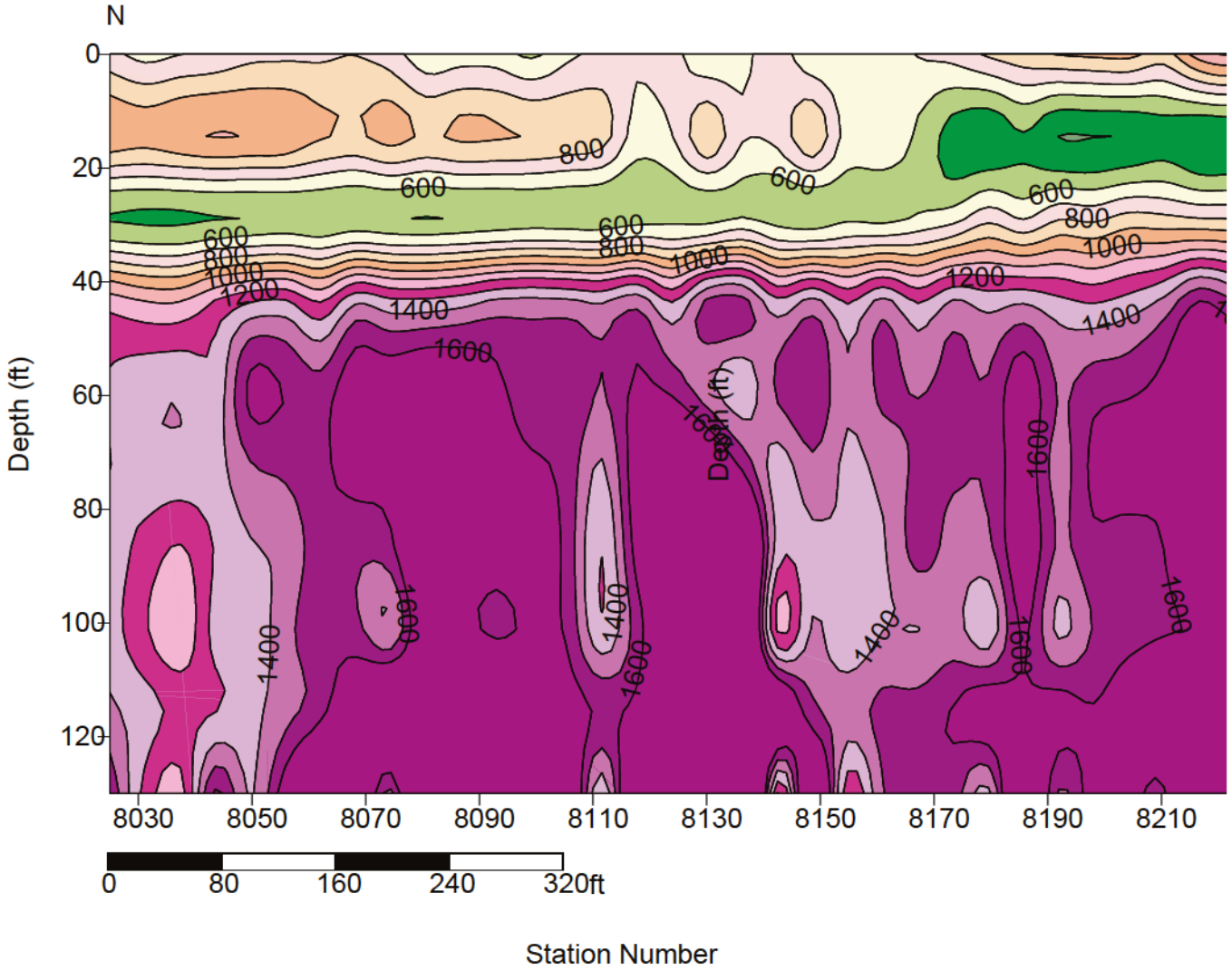

Figure 21a. Shear-wave velocity contour along line 8.

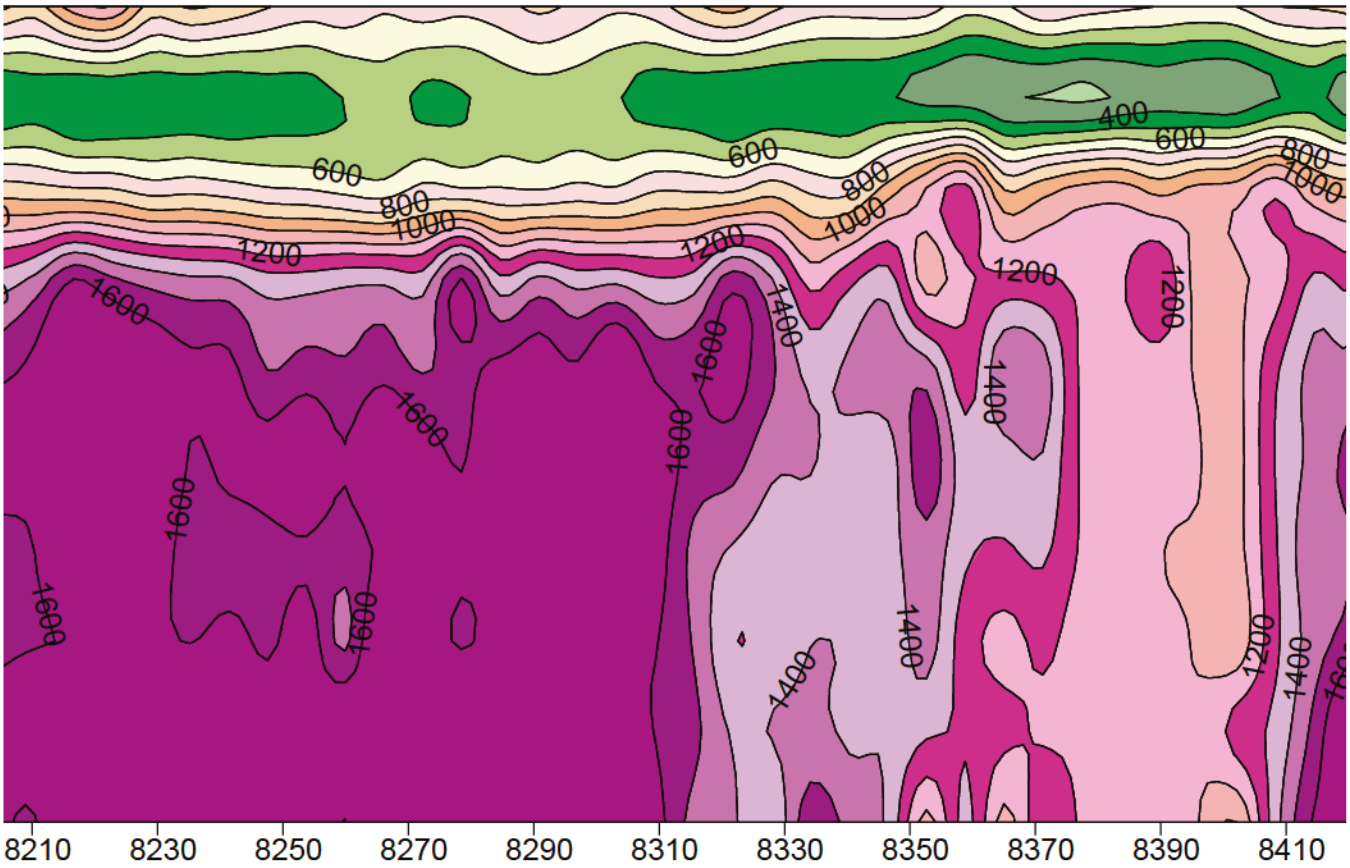
400
600
800
1000
1200
1400
1600
8210
8230
8250
8270
8290
8310
8330
8350
8370
8390
8410
Station Number

Figure 21b.

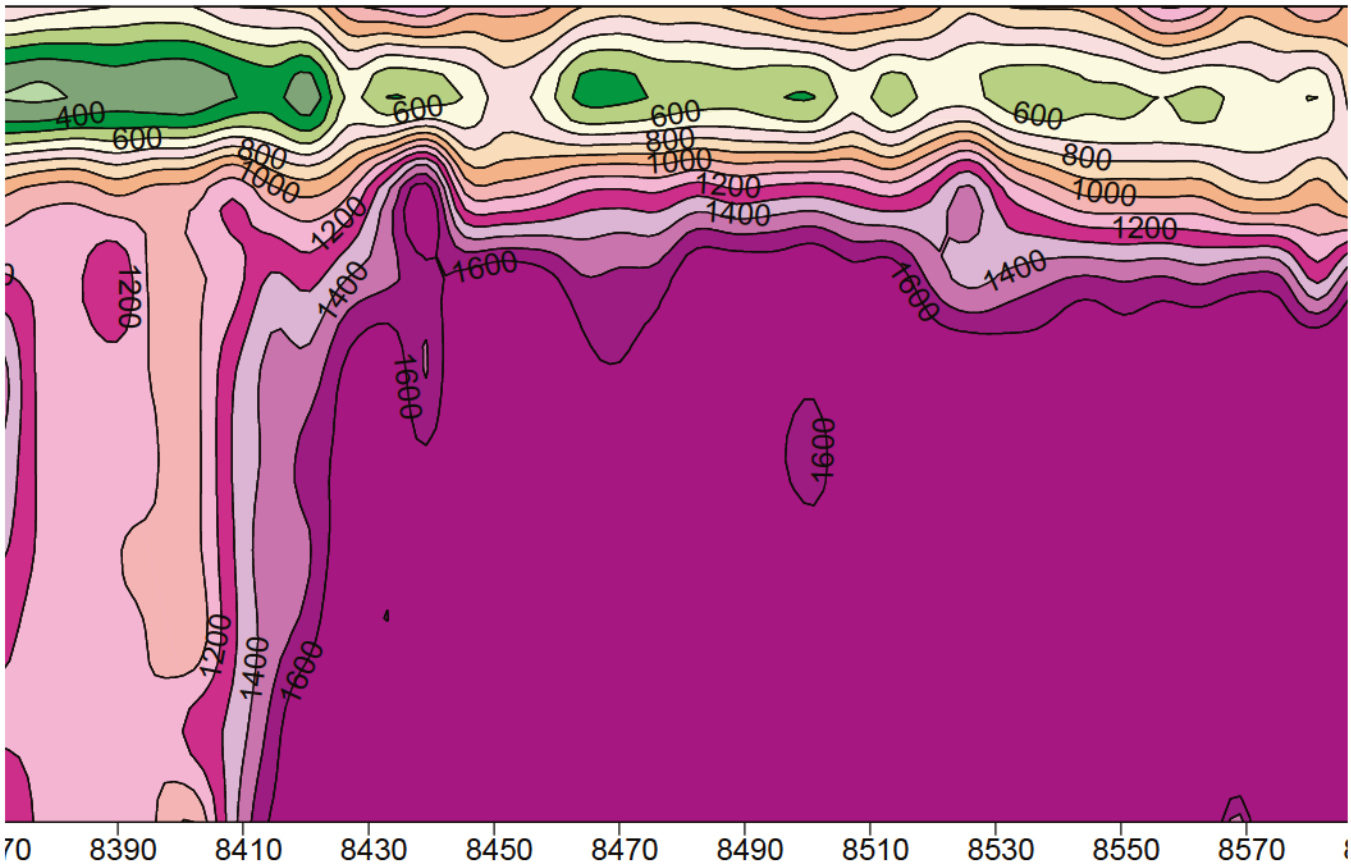

Station Number

Figure 21c.

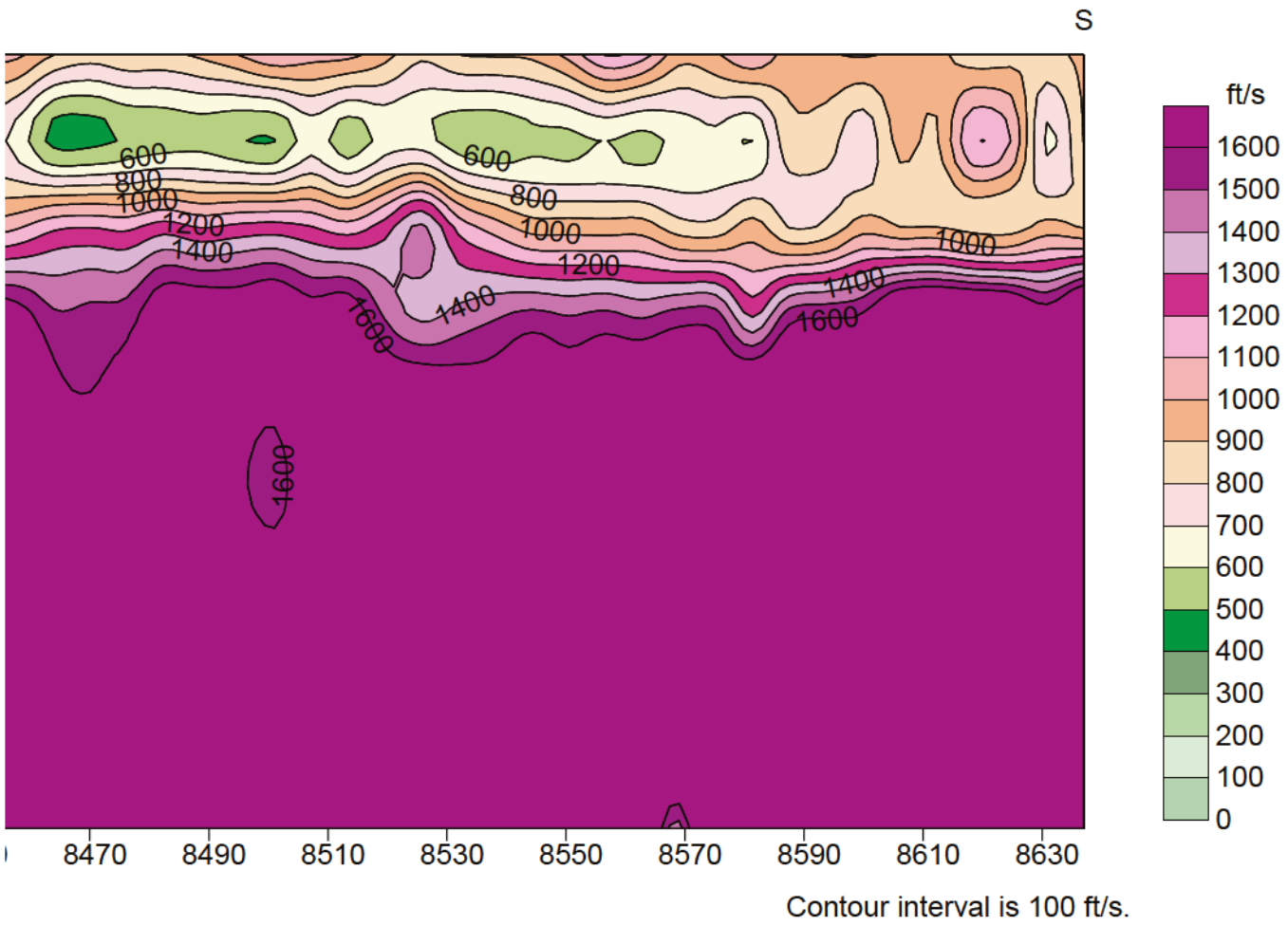
S
ft/s
1600
1500
1400
1300
1200
1100
1000
900
800
700
600
500
400
300
200
100
0
600
800
1000
1200
1400
1600
8470
8490
8510
8530
8550
8570
8590
8610
8630
Contour interval is 100 ft/s.
Station Number

Figure 21d.

these sections are interpreted with fault zones. The highest gradient and lowest velocities are evident between stations 8390 and 8410. Examining surface features in this area brings in another interesting correlation. A shallow pond interpreted to be a sinkhole feature is located at about surface station 8420. Extending this fault to the surface would place the surface expression of the fault at about station 8420.

Seismic reflection data, shear wave velocity field data, and surface investigations are all consistent with the interpretation of fault-controlled dissolution and subsidence in this area. The eastern leg of this graben has provided the most readily accessible pathway for fluid and unconsolidated materials to migrate downward. Based on the extreme depth and degree the shear wave velocity field has been altered beneath stations 8310 to 8410, it is reasonable to assume current surface activities will continue.

If tectonic faulting is ruled out due to the geologic and geophysical setting, the correla tion of these independent data sets supports increased porosity and reduced rigidity of the rock matrix that makes up the upper 200 ft at this location. This feature is very similar to ones on lines 1, 2, 4, 6, and 7. All of these features are at the edge of or just outside the edge of paleo-sinkholes interpreted on reflection data.

Of secondary importance to the subsidence potential at this site are anomalies beneath stations 8030 and 8150. Shear wave velocity field disturbances in these areas within the bedrock are consistent with other features interpreted on shear wave velocity field data from the northern portion of this site. Of particular interest is the feature at station 8030, which correlates with a surface marshy area. This bedrock feature does not appear to tie to the surface, at least in terms of chimney-type features interpreted on surface wave data within the unconsolidated materials above bedrock. These low velocity slices within otherwise uniform bedrock (8030 and 8150) are likely dissolution joints or fractures that have been infilled with weathered bedrock and unconsolidated sediments and have not grown sufficiently to allow subsidence of sediments above bedrock.

Within the overburden several features indicative of potential vertical communication are located beneath stations 8150, 8430, and 8610. Each of these features is correlated by a missing or altered low velocity layer (green). The one at station 8150 overlays a bedrock low velocity zone where no apparent communication seems to exist between the two anomalies. The isolation between these two anomalies is evidenced by the intact, continuous, and unaltered appearance of

the 700 to 1000 ft/sec cluster of contour lines representing the bedrock surface. The feature at station 8430 is interpreted as the subsurface expression of the surface pond determined by surface investigations to be an active sinkhole. Interpreting this feature as an active sinkhole is consistent with this being a major fracture or fault zone. It is also interesting to note that a high velocity bedrock knob is located on the upthrown side of the fault and directly below the surface pond. Finally, the anomaly at station 8610 is in an area without the lower velocity (green) unconsolidated zone at around 20 ft of depth.

Line 9

Reflection (Figures 22 and 23)

Stacked reflections from line 9 are very uniform with little in the way of structure or anomalous features that would relate to variability or irregularities of the type imaged on previous seismic lines. Correlating a fault or fracture system such as the one interpreted on lines 2 and 8 across this site would require a little speculation with reasonable matches in terms of offset and linearity of the trend. A fault or fracture zone similar in size with limited offset can be interpreted on line 9 between stations 9350 and 9400. This fault or fracture system possesses minimal offset and is along a linear trend consistent with lines 2 and 8. The character of this zone is quite a bit different and here lies the reason for some degree of speculation without an extremely high degree of confidence. The zone as depicted here is very reasonable both from an acoustic as well as geologic perspective; it lacks consistency in overall character of the zone.

In support of this zone having some tie to tectonic fault activity is the pronounced break in reflection coherence below the green reflection at station 9370. This abrupt change could easily be interpreted as fault related with this entire zone being the uppermost extension of a growth fault having only minimal activity since deposition of the green reflection.

Several reflection arrivals appear to have a geometry influenced by subsidence. Included in this group of reflection events are arrivals beneath stations 9120 and 9160 at a time of around 50 ms. It is difficult to say with confidence that these features are the result of dissolution and subsidence or are classic cut-and-fill type features. The swarm of diffraction events between stations 9110 and 9170 are indicative of point sources. These can be anything from blocks of rock to fault edges to fracture zones. The dramatic change in reflection character at around station 9350 is significant and does correlate to changes in the near-surface. At this time it is not

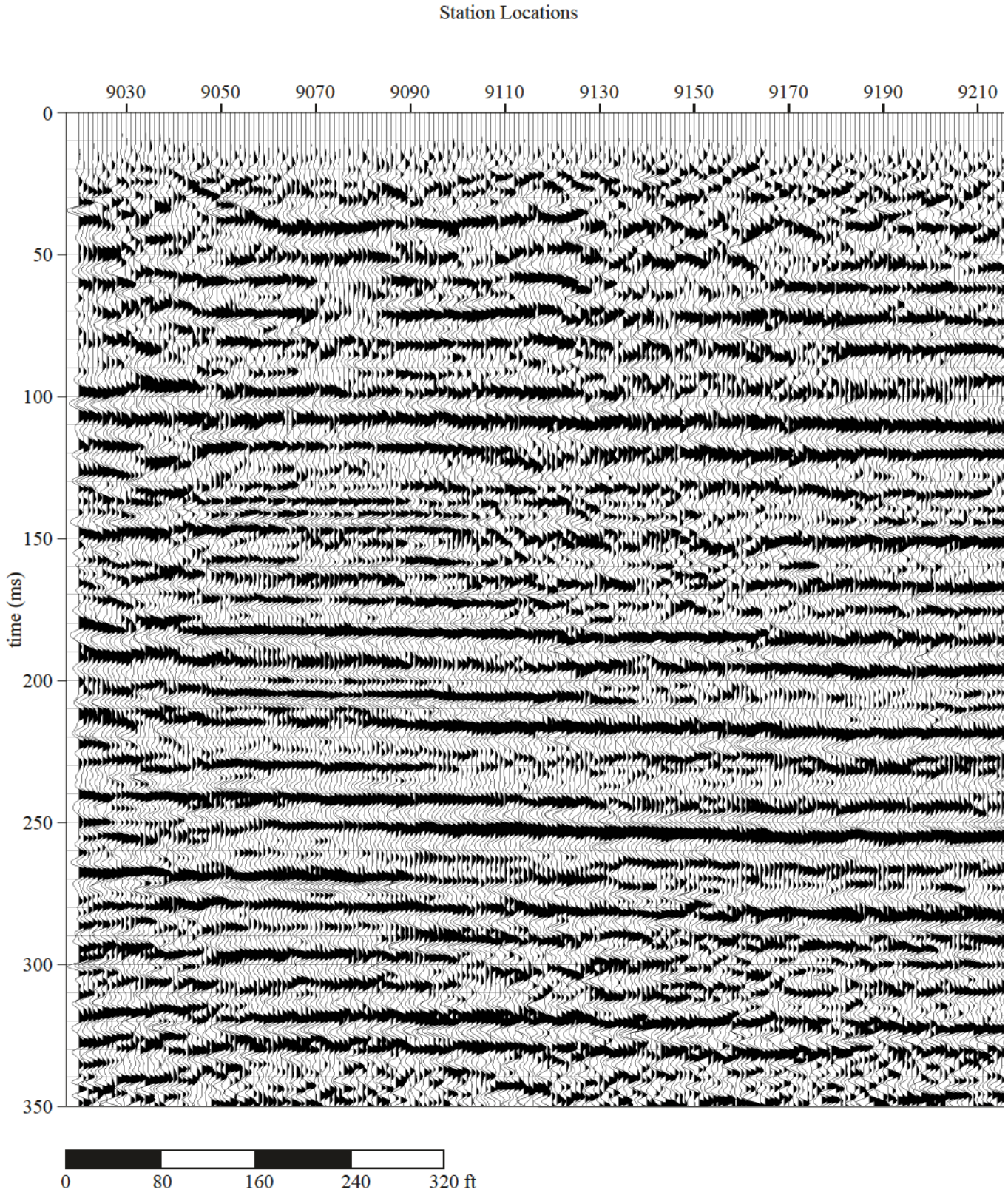

Figure 22a. CMP stacked section of line 9.

Station Locations

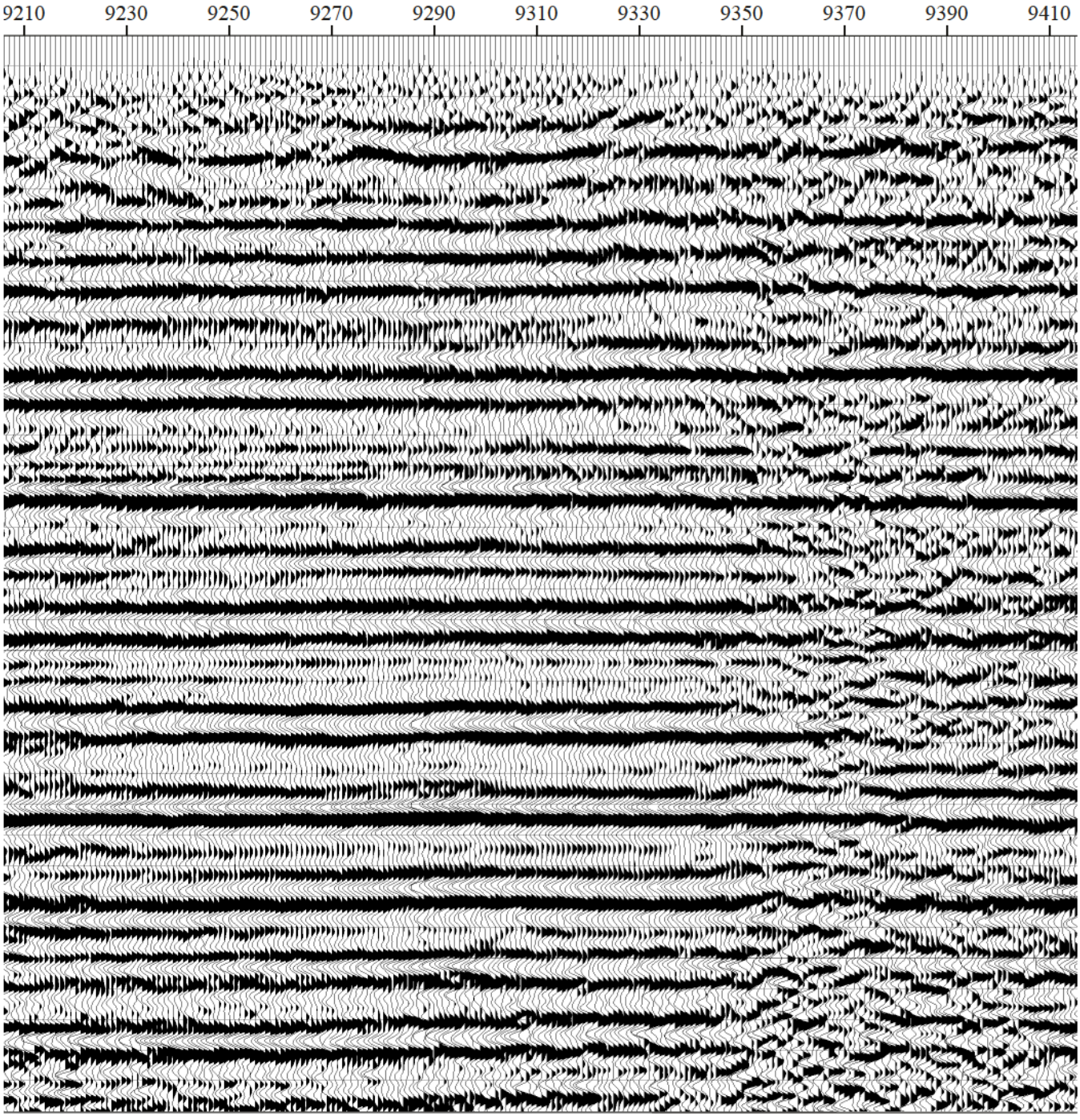

Figure 22b.

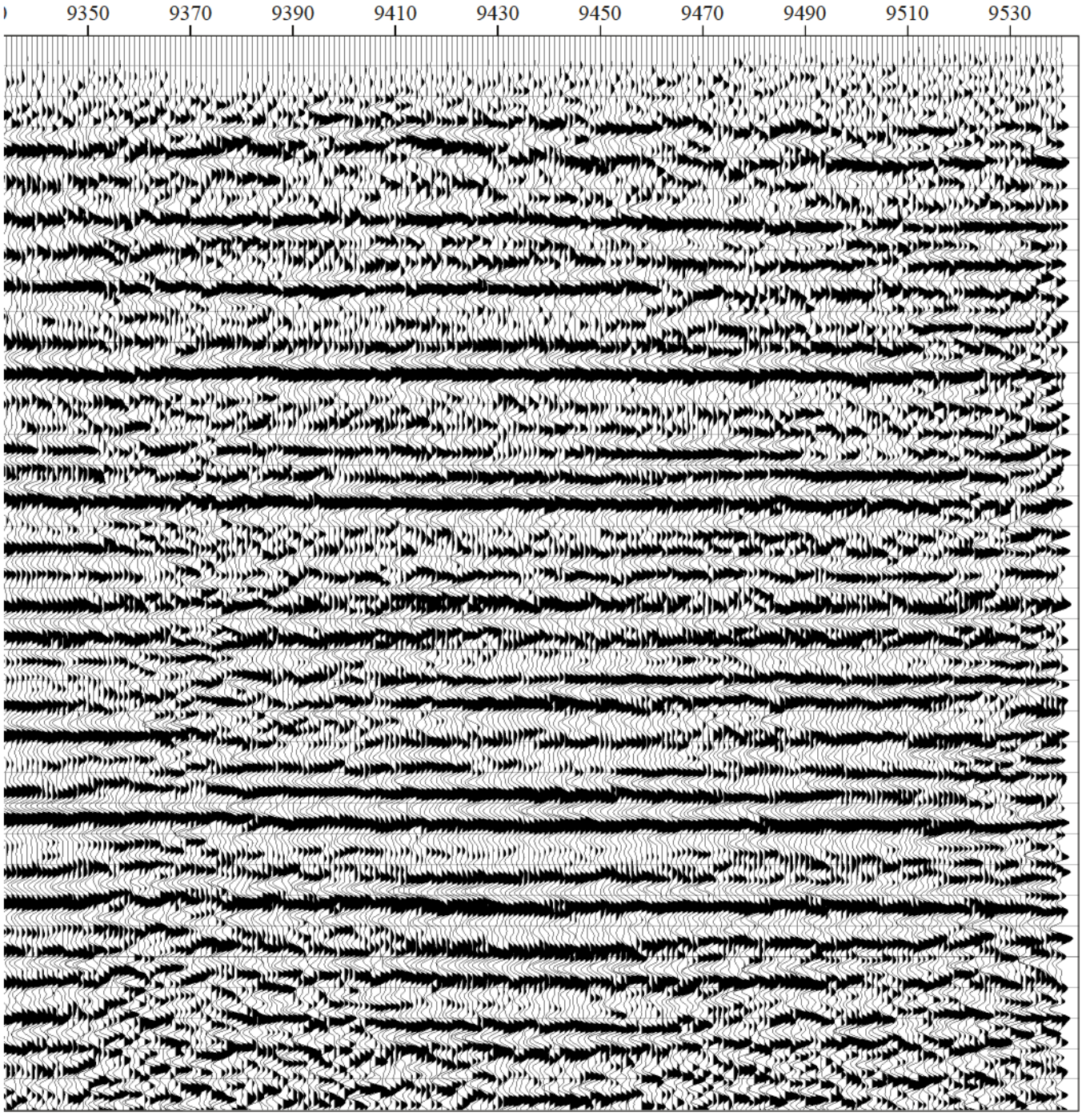
Station Locations
9350
9370
9390
9410
9430
9450
9470
9490
9510
9530

Figure 22c.

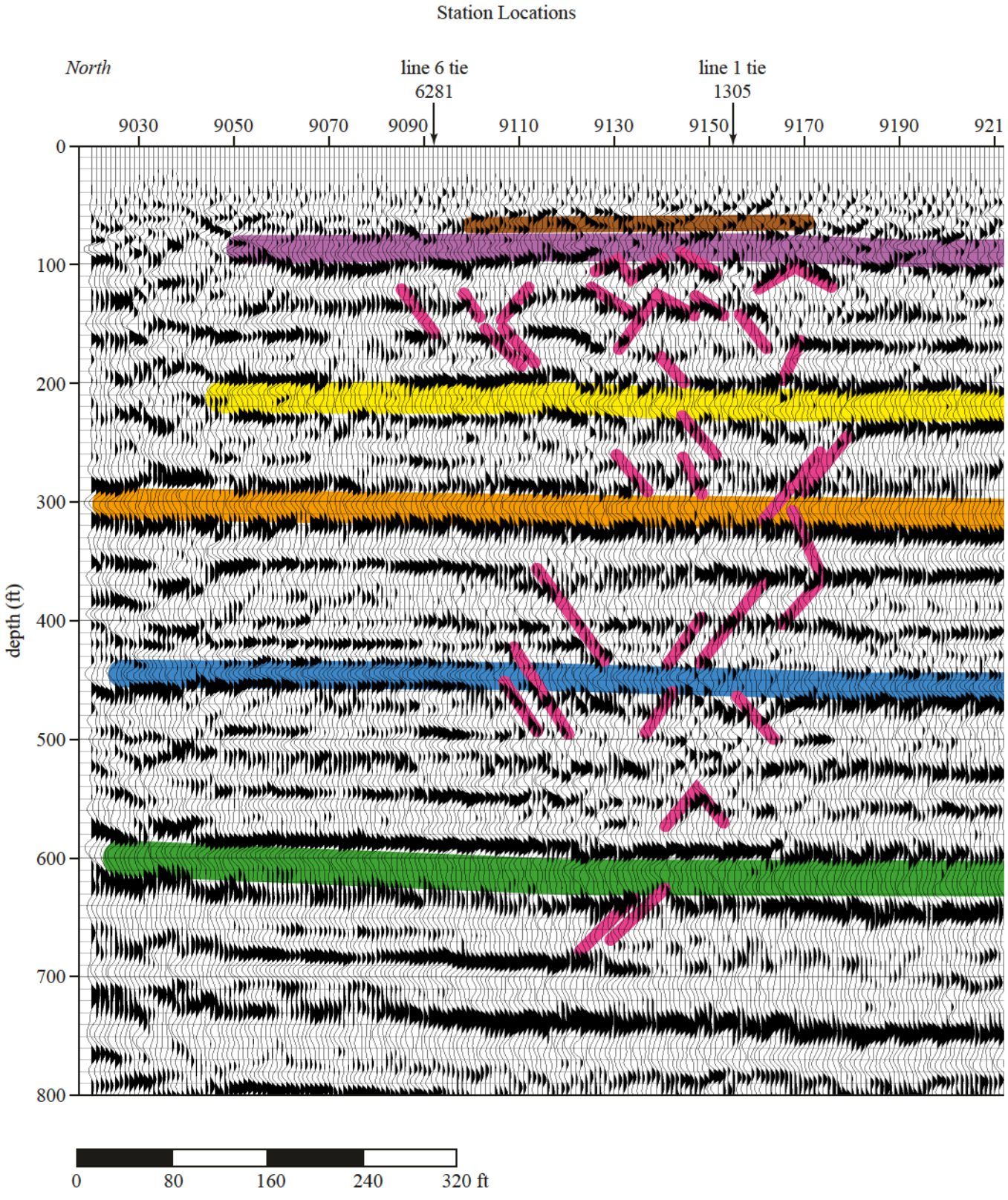

Figure 23a. Interpreted line 9.

Station Locations

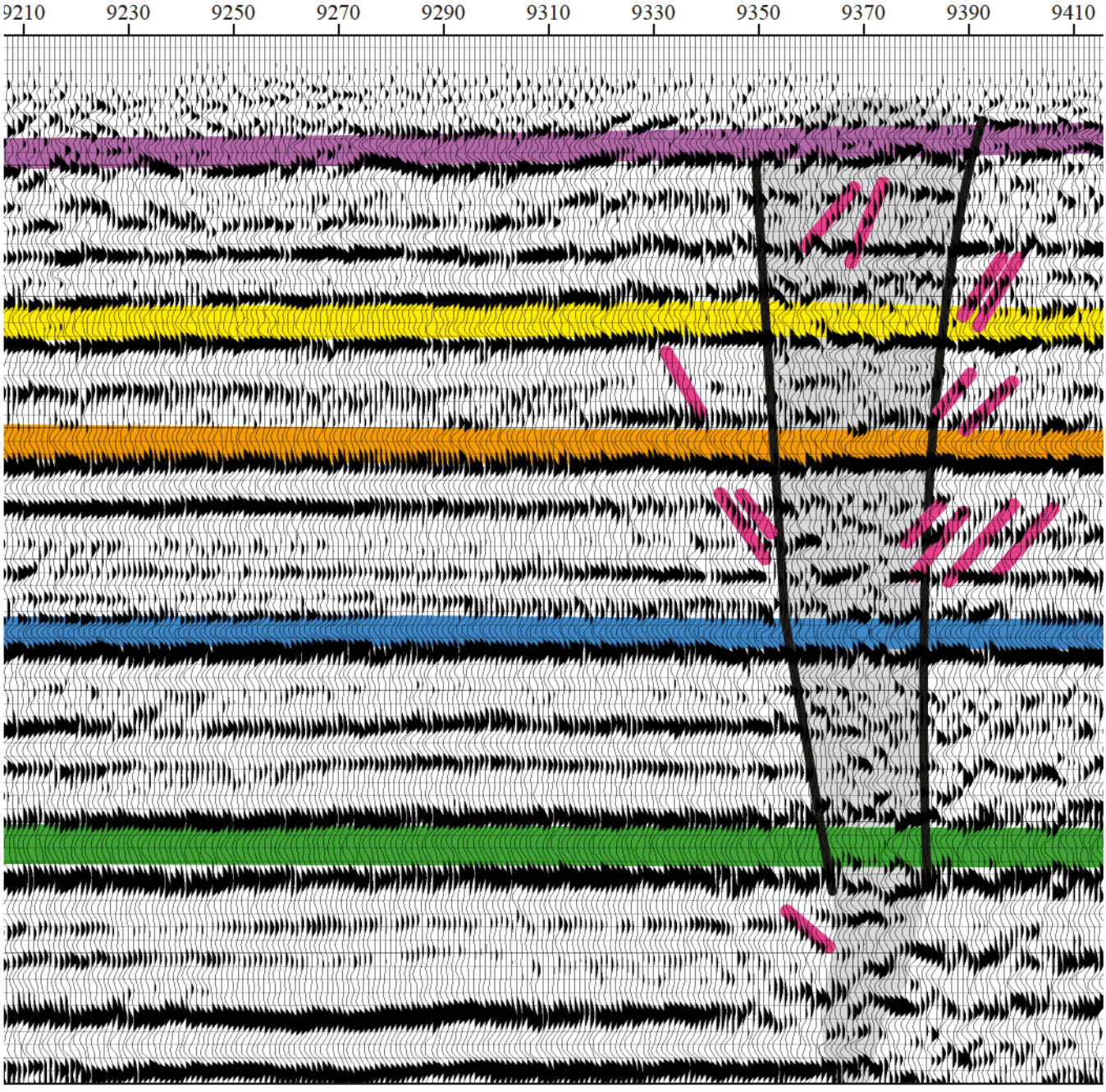

Figure 23b

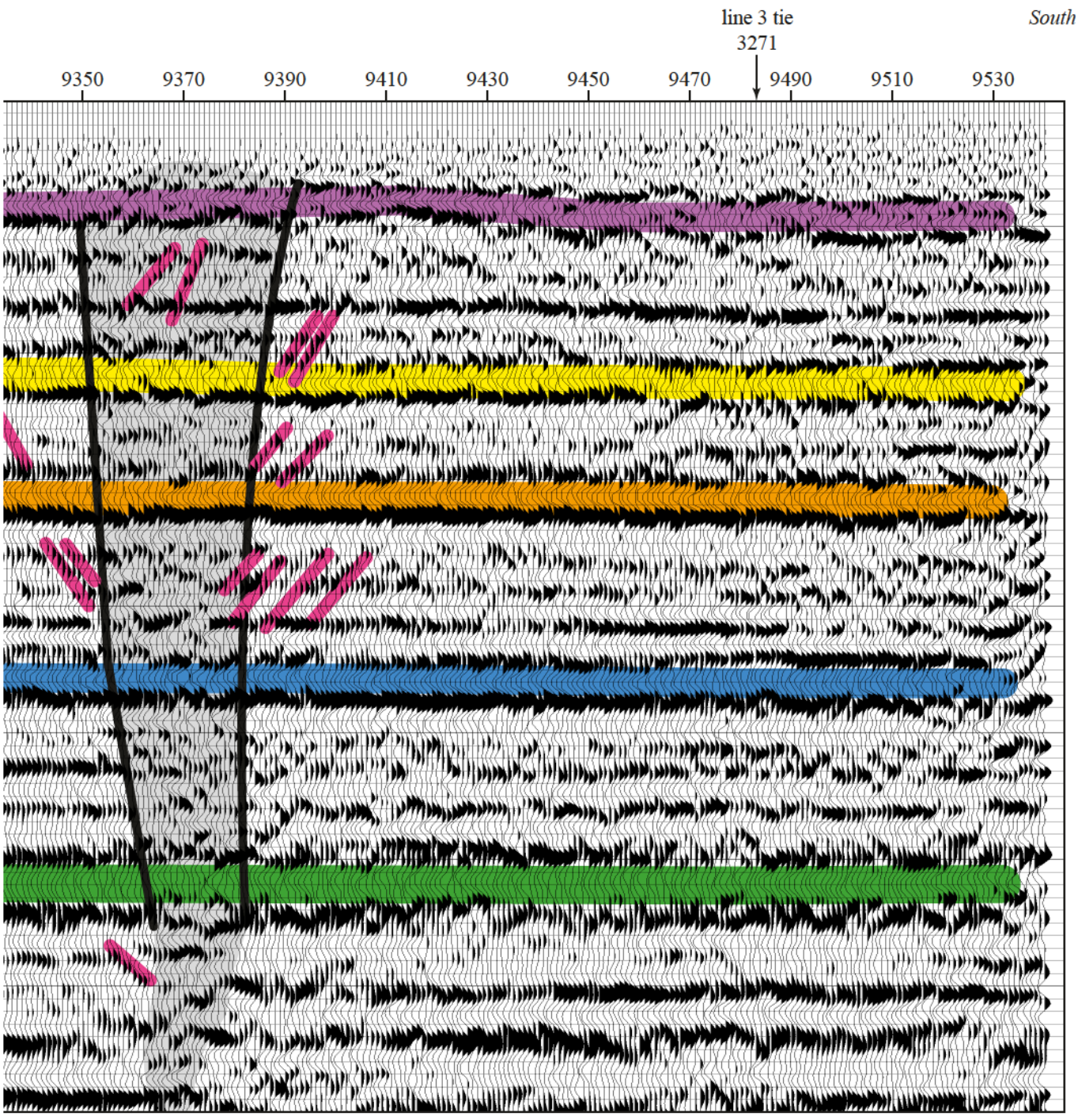
Station Locations
line 3 tie
3271
South
9350
9370
9390
9410
9430
9450
9470
9490
9510
9530

Figure 23c

clear exactly how this disturbance in the reflection waveform, apparent structure, and decrease in signal-to-noise relate to geology.

Surface Wave (Figure 24)

Surface wave data from this site is not consistent with the fault interpretation as described for line 8, but it is consistent with the faulting and described for line 2. A low velocity section of rock below the bedrock surface at station 9300 correlates exceptionally well with the faults interpreted on the stacked section of line 9. This feature as interpreted on both data sets from line 9 matches extremely well with interpretations of a similar faulted feature on both data sets from line 2. Of particular interest to surface structures near the north end of this line is the large and deep velocity low beneath station 9040. This feature is at the extreme north end of the CMP stacked section and therefore can not be interpreted with confidence due to the low fold at the extremes of all reflection sections. Neither of these features appears to have a major impact on the surface of bedrock or the low velocity layer at around 15 ft of depth on this line.

The low velocity feature in bedrock beneath stations 9230 to 9350 matches in character and dimension the features interpreted on several other surface wave lines. Based on surface wave data alone, the bedrock feature centered on station 9300 has expression on the bedrock surface but does not yet appear to have impacted the low velocity green layer within the unconsolidated sediments. The 100+ ft fracture located at station 9240 in conjunction with the sub-bedrock low at station 9300 makes this area susceptible to future and/or continued subsidence.

Line 10

Reflection (Figures 25 and 26)

Reflection data from line 10 are consistent in resolution, signal-to-noise, and event coherency with the other six CMP stacked sections from this site. Events interpreted deeper than about 300 ft seem to be relatively undisturbed by any dissolution-related activities at this site with the exception of a narrow zone between stations 10410 and 10440. Across the southern half of this profile is a complex series of reflection events that have clearly been altered by sub-sidence that has been reactivated, or at a minimum experienced dramatic changes in subsidence rates. These paleosinkholes have expression from the extreme south end of the line northward possibly as far as station 10200. The characteristic synclinal forms of the distorted reflections

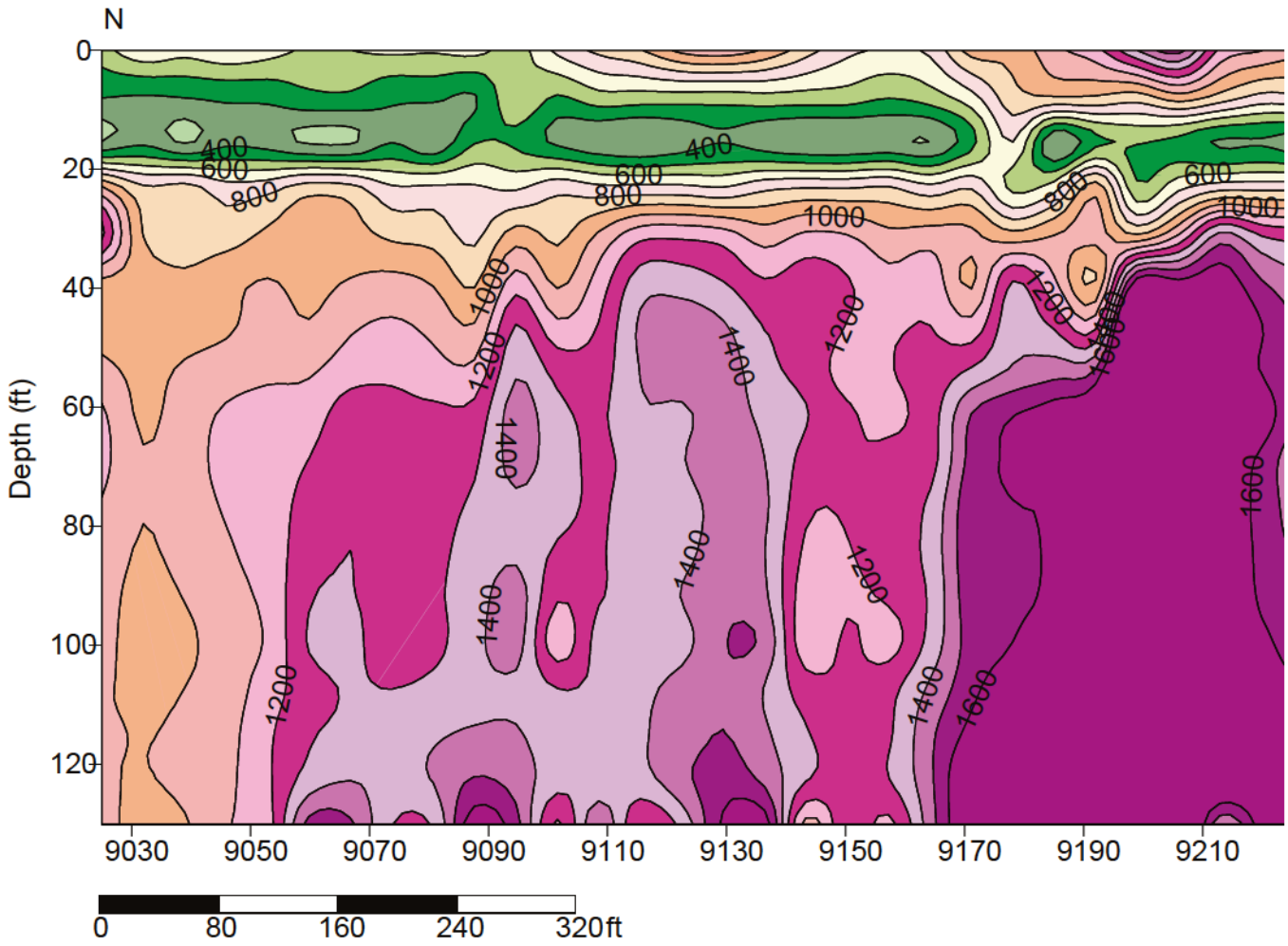

Figure 24a. Shear-wave velocity contour along line 9.

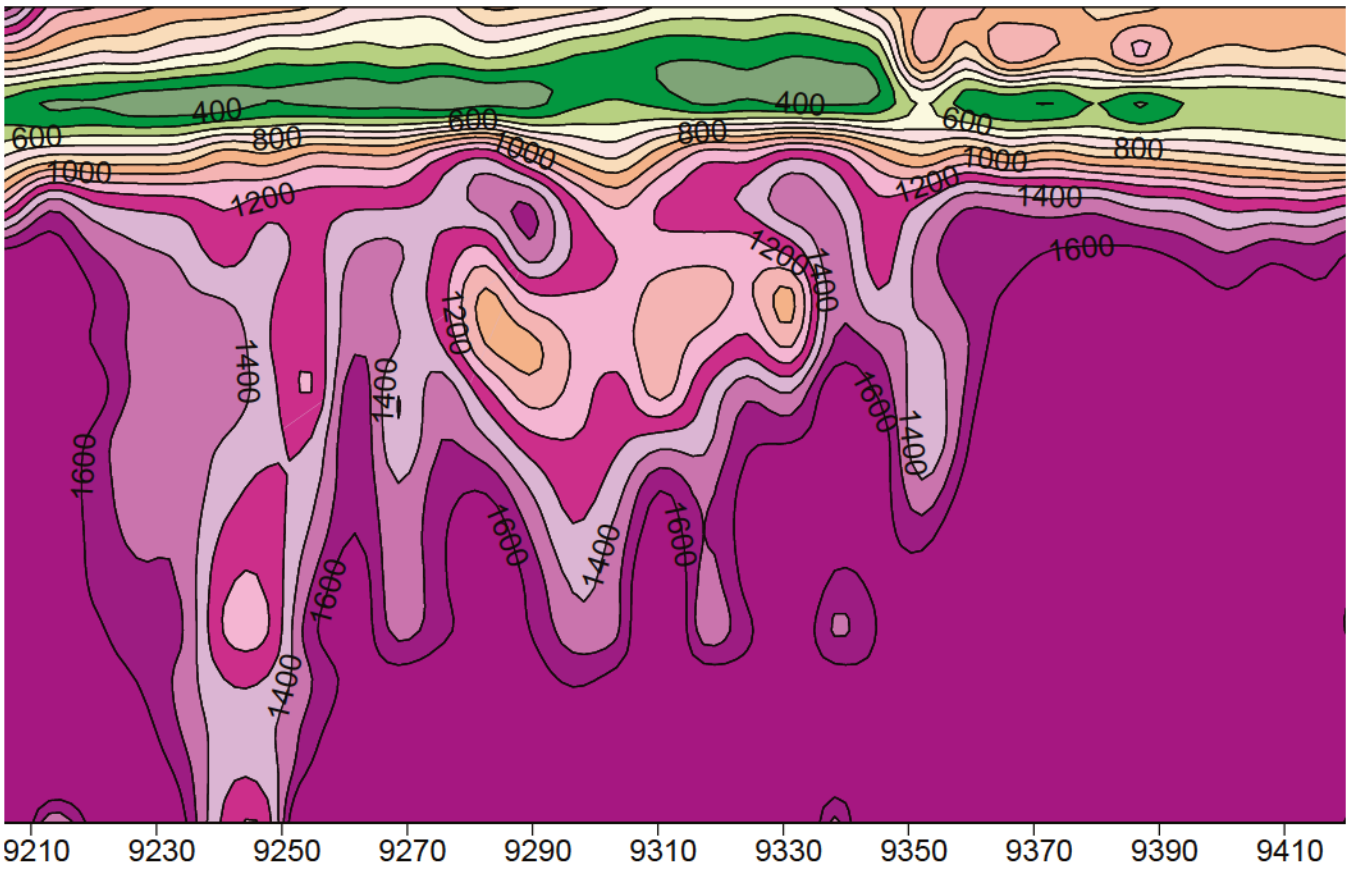

Station Number

Figure 24b.

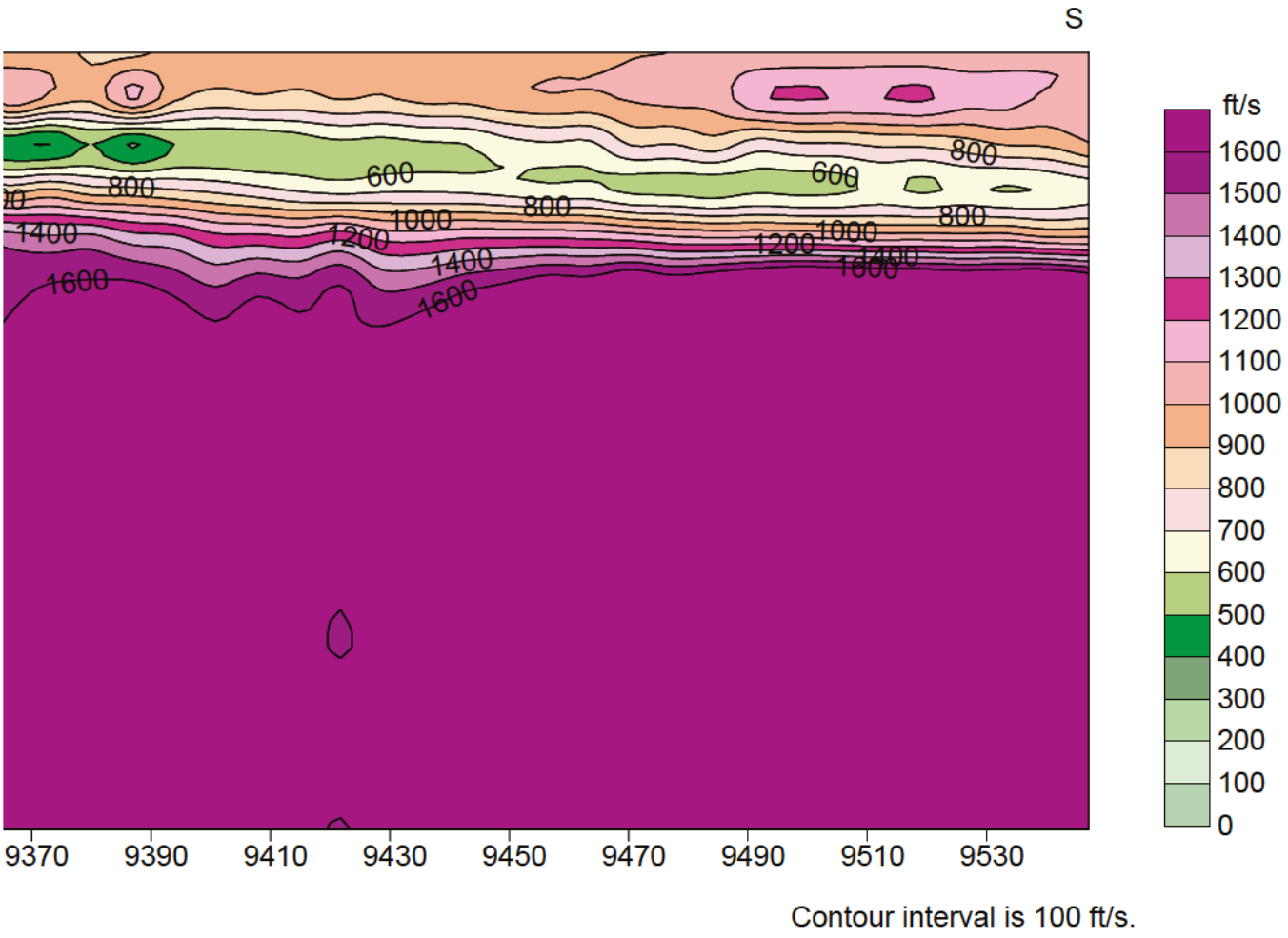

Station Number

Figure 24c.

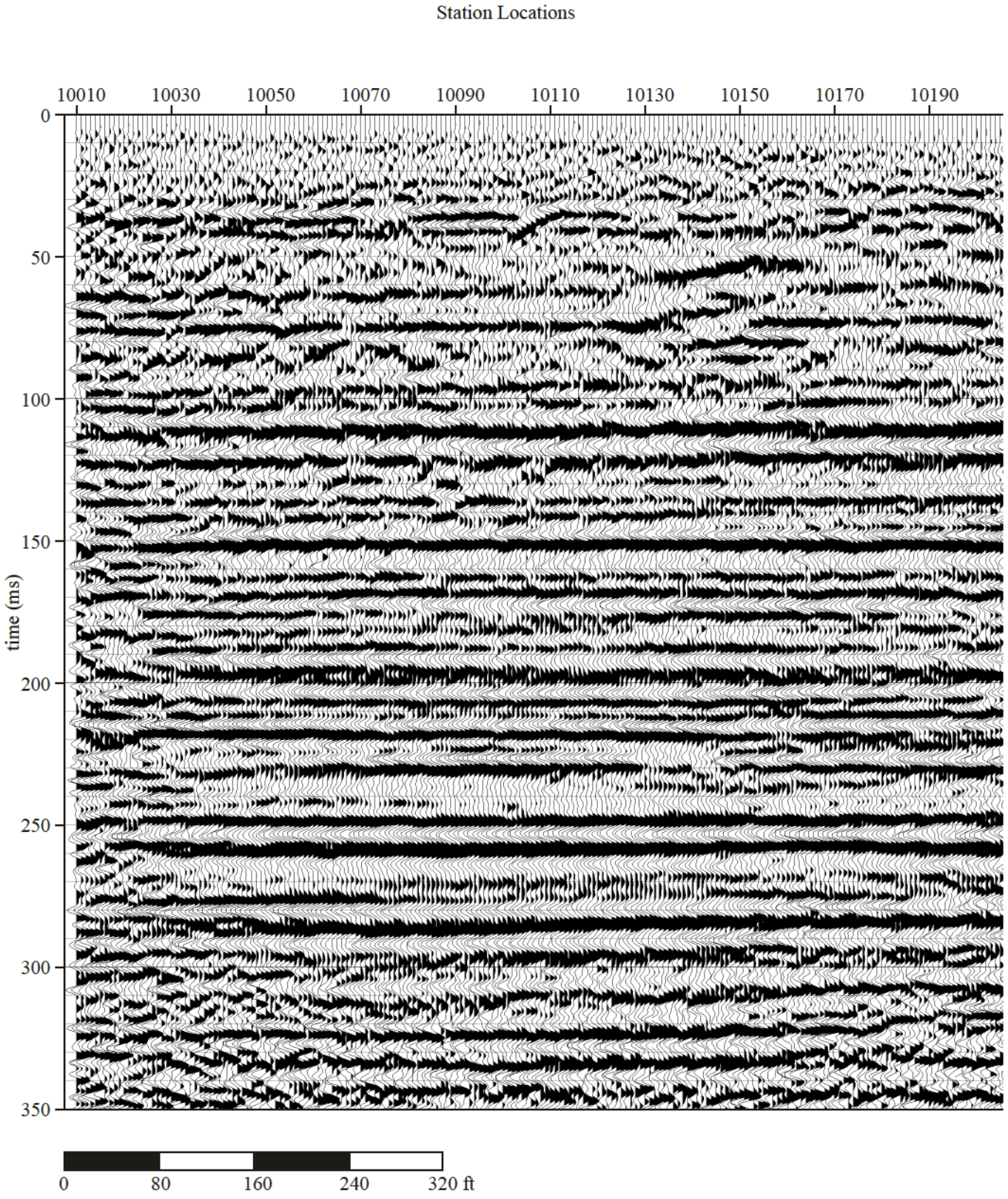

Figure 25a. CMP stacked section of line 10.

Station Locations

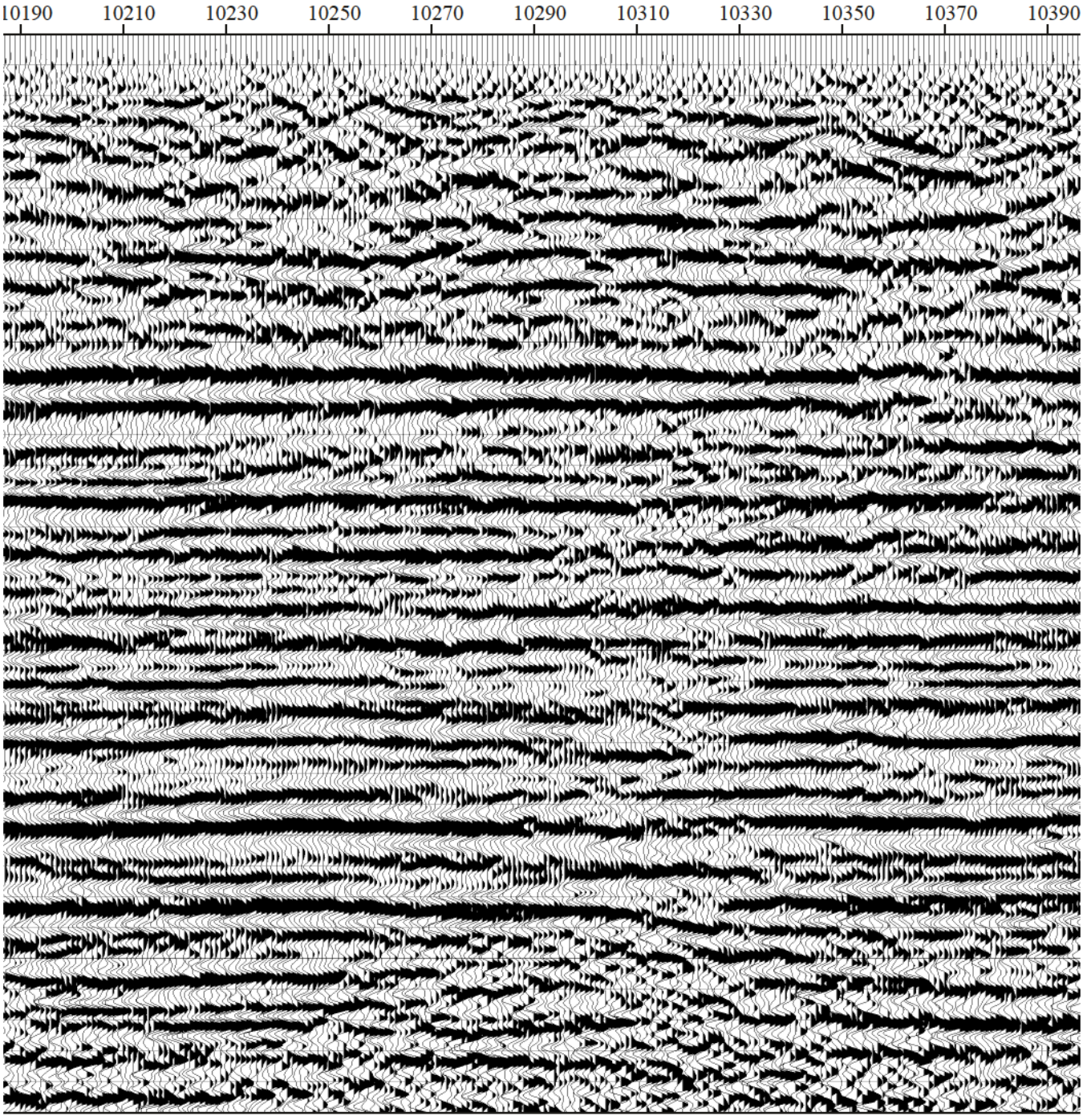

Figure 25b.

Station Locations

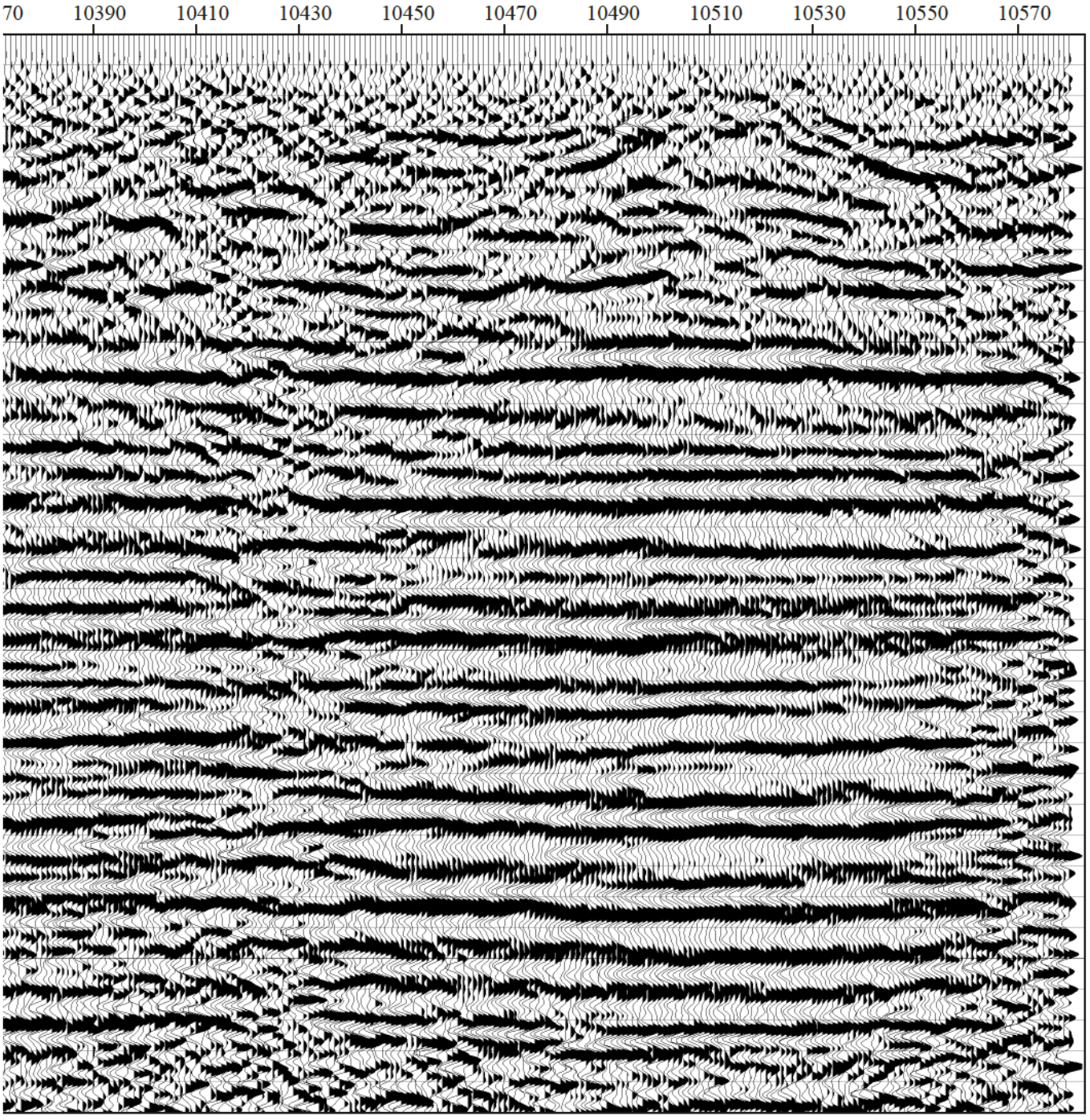

Figure 25c.

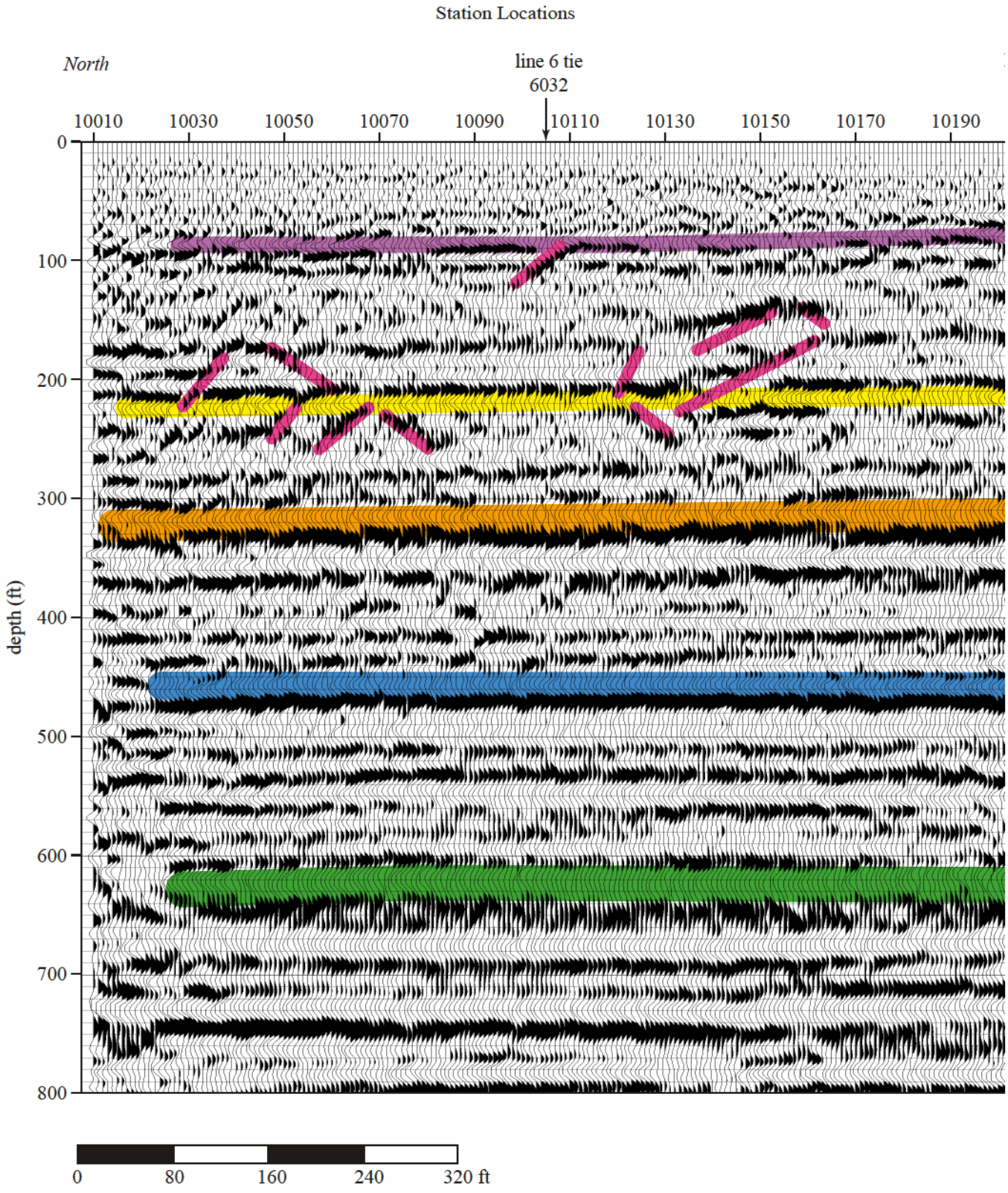

Figure 26a. Interpreted line 10.

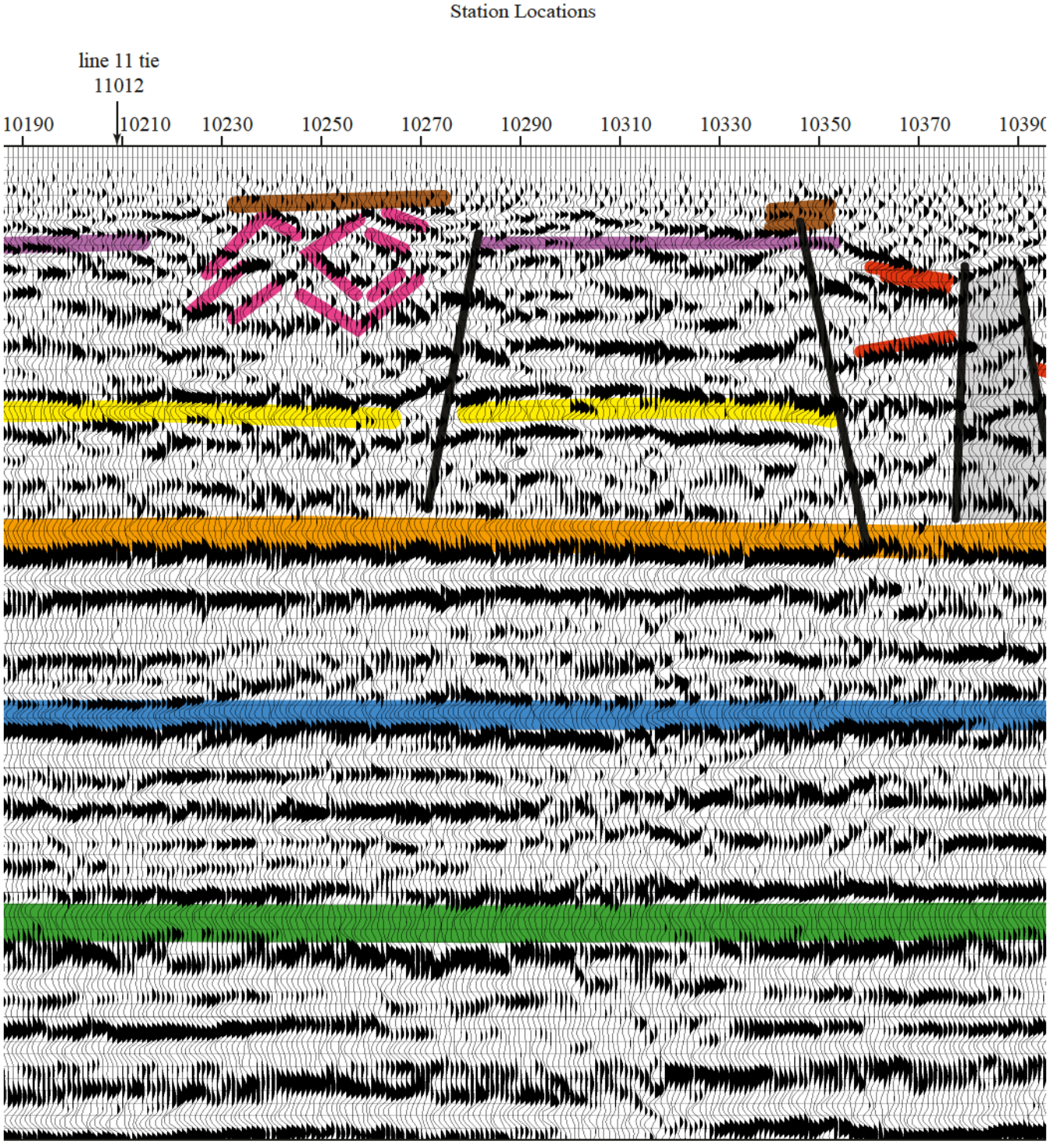
Station Locations
line 11 tie
11012
10190
10210
10230
10250
10270
10290
10310
10330
10350
10370

Figure 26b.

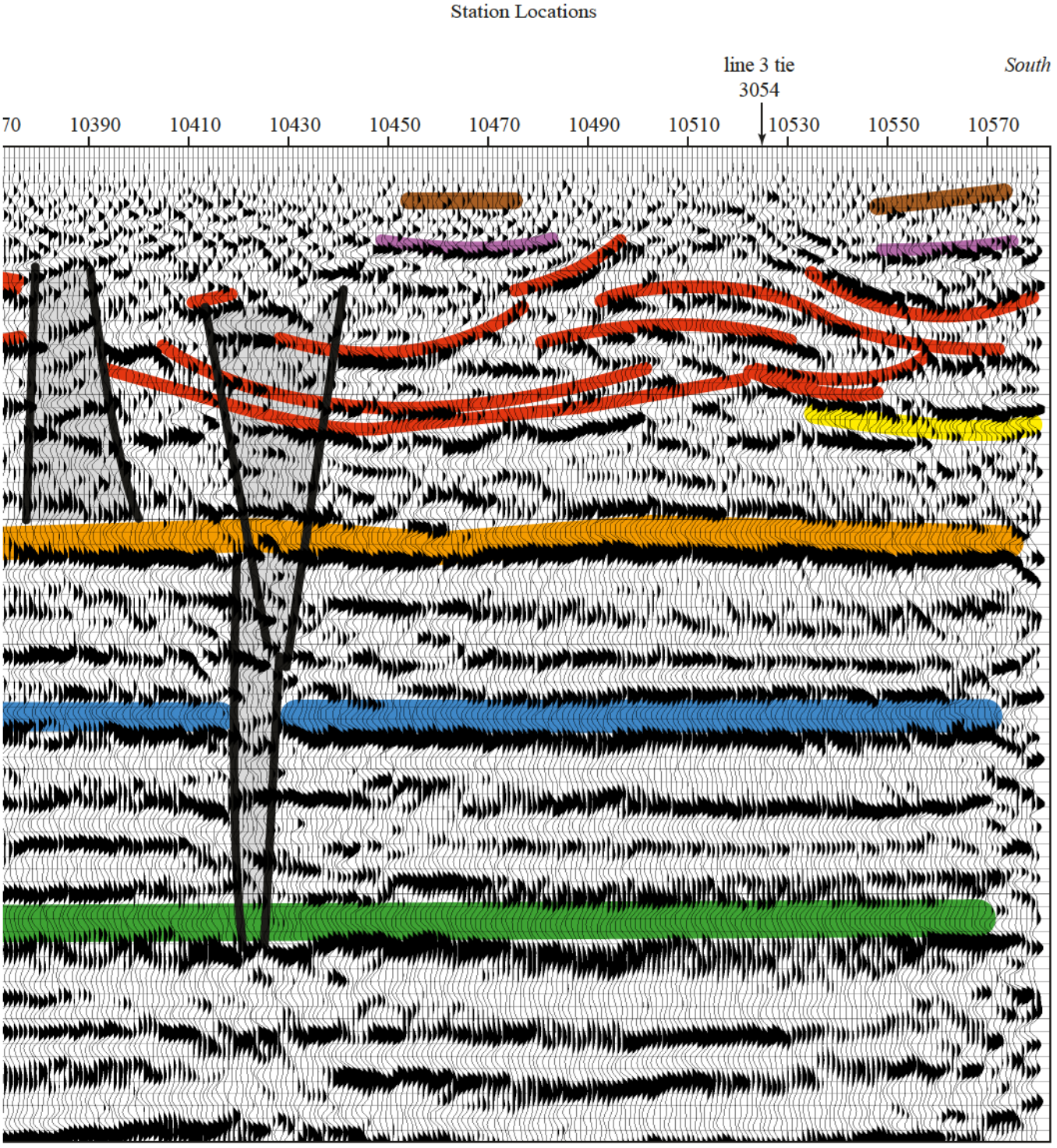
Station Locations
line 3 tie
3054
South
70
10390
10410
10430
10450
10470
10490
10510
10530
10550
10570

Figure 26c.

have been interpreted in red out to about station 10350, but amplitude and frequency attributes of the reflection events between 100 and 200 ft of depth appear diagnostic of paleosinkholes at this site.

Reflection events on the north half of the profile are uniform in frequency, amplitude, and signal-to-noise ratio. Occasionally across the section diffraction or scattered energy might be inferred as the source of the non-linear arrivals. Above 200 ft along the northern end of this line features exist that could be related to previous or possibly current dissolution activities. The 100 ft reflection is relatively undisturbed from the beginning of the line up to about station 10200, where a complex series of diffraction or scatter patterns seem to originate along the northern edge of a linear feature interpreted by bed offset in reflections from 300 ft to the surface. Subdued, or at least very localized, reflection characteristics between stations 10190 and 10270 include synclinal geometries (consistent with subsidence features), a decrease in dominant frequency, and a decrease in lateral coherency, all of which have been used to identify paleosinkholes on other profiles from this site.

The southern half of the profile contains many of the same kinds of geometries and reflection characteristic seen on the previous six profiles. There are seven individual features that justify some discussion. These include the two chaotic zones beneath stations 10385 and 10430, the apparent bridging beneath stations 10460 and 10560, the two reflection discontinuities at stations 10280 and 10350, and finally the area with a concentration of shallow origin scatters/diffractions. The chaotic zones are similar in nature and extent to ones observed on other lines. As in those cases, these are likely areas with a higher probability of fracture or fault controlled enhanced fluid movement conduits. Bridging is a phenomenon observed frequently in association with salt dissolution and is thought to correspond to the rate of dissolution and competence of the roof materials. The bridging observed on this line seems unique to this site and could be an early indicator of subsidence-prone areas where little or no active dissolution is present, but with increased loading could see subsidence related to ancient dissolution activities. Faulting or bed offset is generally considered indicative of relative movement along a plane or fault surface. In this case, with little or no apparent offset below about 300 ft, it is very likely this bed discontinuity is dissolution-induced and is consistent with faulting commonly associated with paleosinkholes. The area in the middle of the section with several point source scatter events has little or no coherent shallow reflection event interpretable and could be a prime

indicator of a shallow subsidence area migrating toward the ground surface or possibly with subdued surface expression that will continue to increase.

Surface Wave (Figure 27)

Three low velocity bedrock features are interpretable on this section. Two of these features (stations 10050 and 10270) extend beyond the maximum depth of investigation for the surface wave survey at this site. The third is a low velocity void-looking feature worthy of a more detailed invasive investigation. The two chimney-type features at stations 10050 and 10270 are likely related to dissolution joints or fractures and, based on interpretations of faulting on lines 2, 8, and 9, either or both of these features could be fault or fracture related. The chimney feature at station 10270 corresponds to an area of increased scattered seismic energy on reflection profiles. It also is consistent with the edge of a paleosinkhole and the bed offset (fault) feature interpreted at the perimeter of all paleosinkholes on this site. Based on the trend of the faulting interpreted on these lines it is very possible that both of these vertical low velocity slices are from the same fault zone that splays between lines 8 and 9.

The character of these features west of line 8 is consistent while the character and general properties of the interpreted faults are similar on data east of line 8. This difference justifies more investigation.

The shallow depth of the low velocity anomaly at station 10390 is intriguing, but does not appear to be a threat for subsidence. The strong anomaly is consistent with a chaotic zone on reflection data. This 800 ft/sec anomaly is the most striking on any surface wave data from this site. At 60 ft of depth, this would be an excellent target for several drill holes. The lack of any indication that shallower rock layers are being affected by this extreme low provides the evidence to suggest that this feature does not present a current threat of subsidence.

Line 11

Surface Wave (Figure 28)

Shear wave velocity field data along line 11 is very uniform. There are no features worth discussion at this stage of the study. Several subtle features are interpretable above bedrock, with a clean undisturbed bedrock surface and upper 10 ft or so of bedrock, no justification exists to suggest any major dissolution activity either past or present along the line.

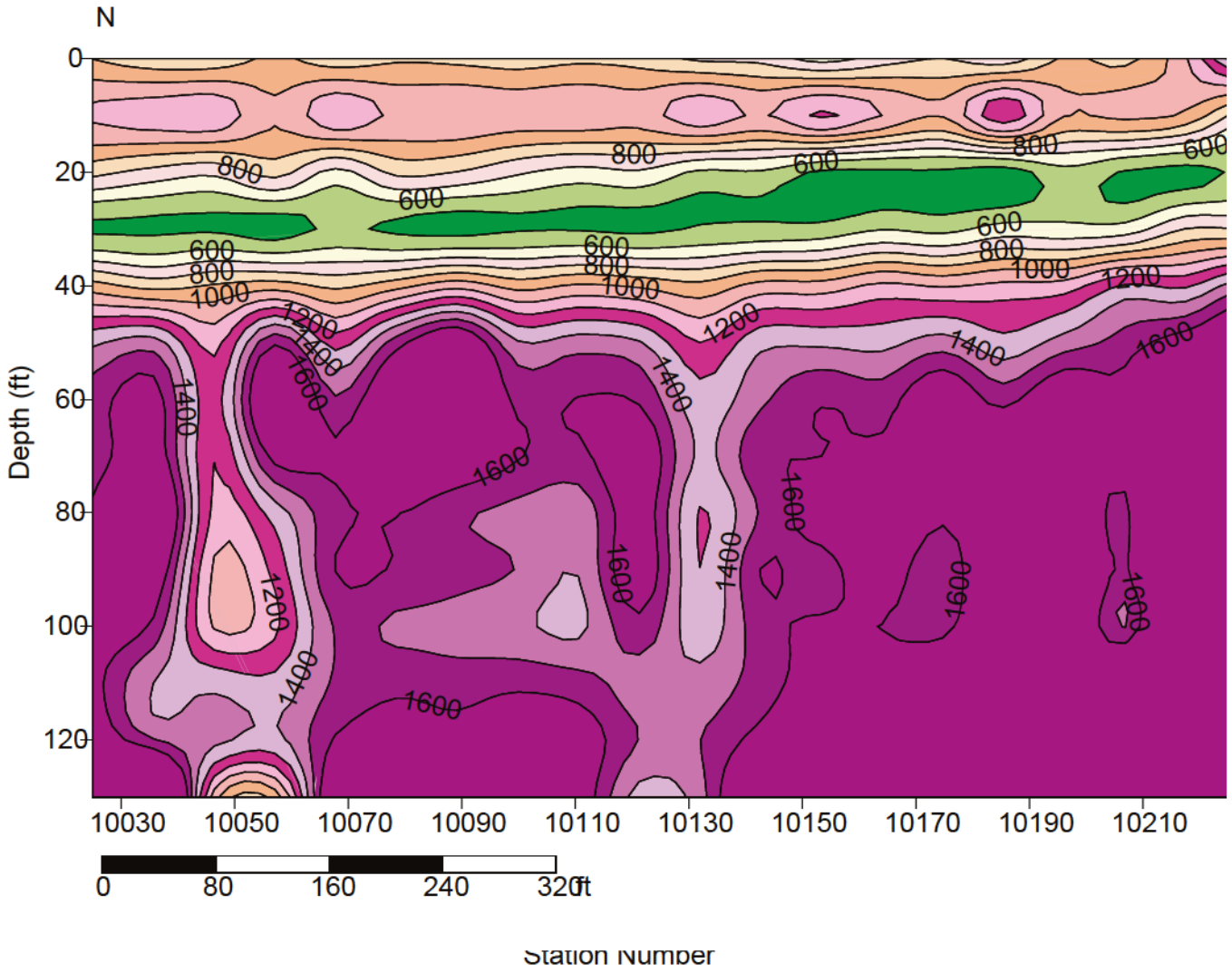

Figure 27a. Shear-wave velocity contour along line 10.

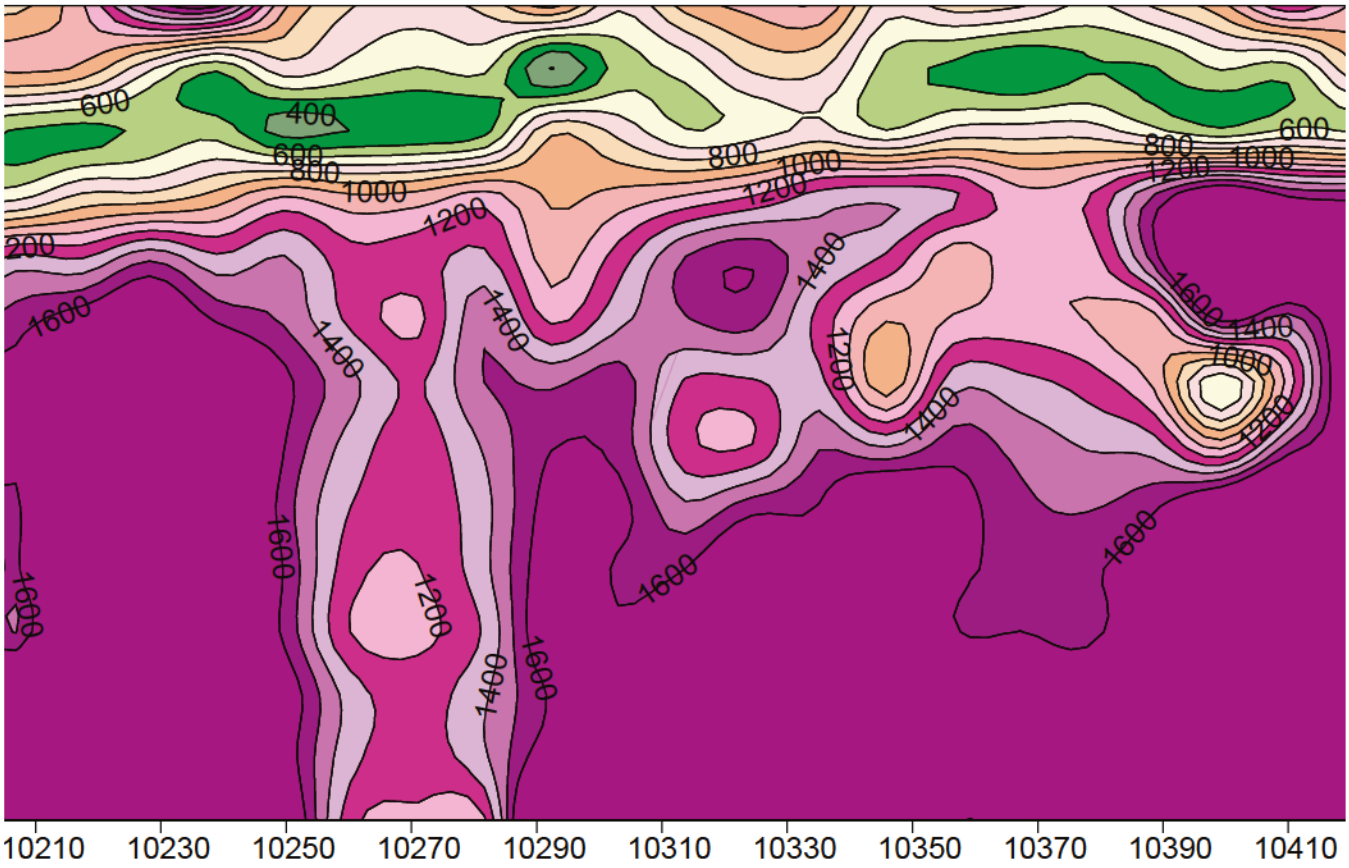

Station Number

Figure 27b.

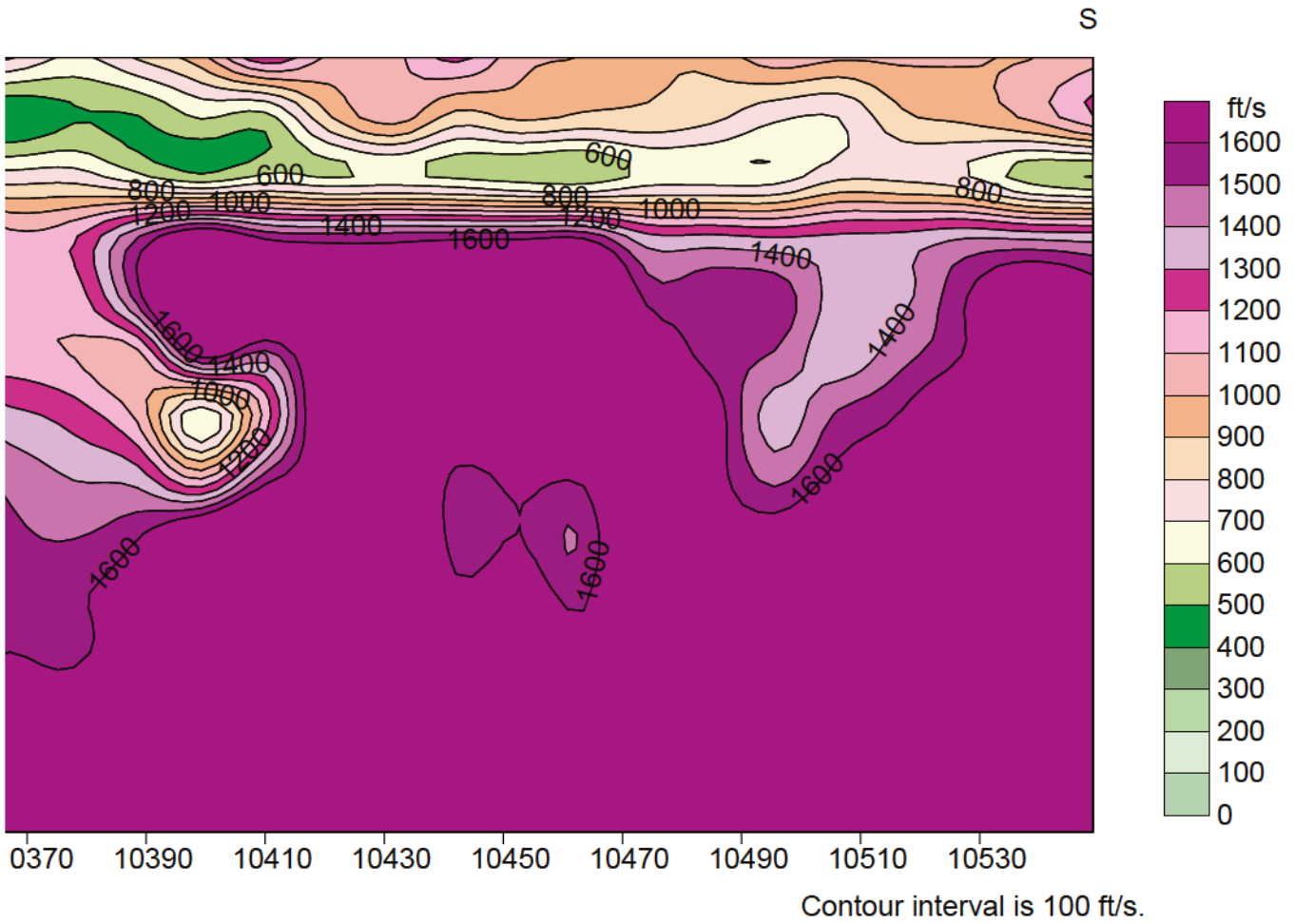

Station Number

Figure 27c.

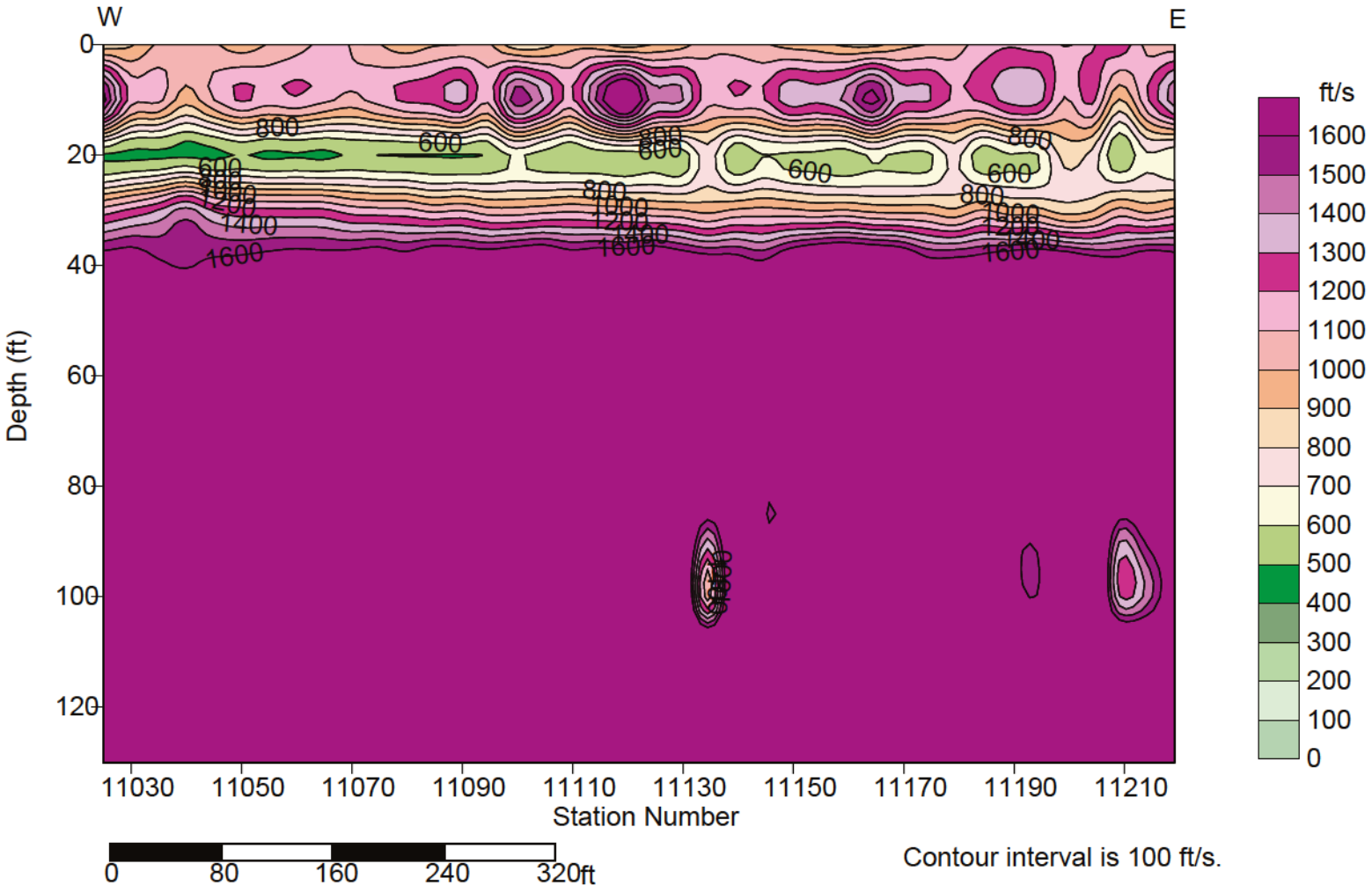

Figure 28. Shear-wave velocity contour along line 11.

Line 12

Surface Wave (Figure 29)

As with line 11, surface wave data on this section compares to anomalous features interpreted on other lines. A very subtle low velocity zone in the bedrock is interpretable beneath station 12190 but it does not seem to correlate to any of the major features interpreted on other lines and does not possess both sub-bedrock and unconsolidated material anomalies. This feature might be associated with the interpreted sinkhole just north along line 8.

Line 13

Surface Wave (Figure 30)

Line 13 crosses a pond that, based on surface investigations, has been suggested to be a sinkhole. Interestingly, shear wave data from this line possess the characteristic high velocity over low that has been suggested to be an indicator of subsurface voids. The feature is not nearly as high gradient as might be expected for a void approaching collapse, but in the case of a gradual subsidence feature this might be reasonable. Correlating the high velocity closure over low velocity closure beneath station 13065 with the surface pond implies a void might be present within the outline of the low velocity zone. Missing from this observation is a pathway between the anomalies at 40 ft and the surface pond. It is possible that the high velocity thickening and the low velocity thinning within the unconsolidated layer beneath station 13080 could represent that tie between the surface pond and subsurface anomalies. Offset between the bedrock feature and unconsolidated sediment features is possible and reasonable considering the fault influence the pond appear to have, as interpreted on seismic line 8.

DISCUSSION

We now look sitewide at the various features and interpretations made from the reflection data, surface wave data, and comparisons of both data sets. Reflection data were interpreted to have paleosinkholes, chaotic zones, disturbed areas with apparent subsidence potential, and some attempt was made to correlate a disturbed zone from line to line. Features interpreted on the reflection data generally had similar characteristics but lack linearity between the lines (Figure 31). This could be indicative of dissolution-induced geometries with little or no tectonic origins. If faulting or regional fracture systems had been responsible for some of these features,

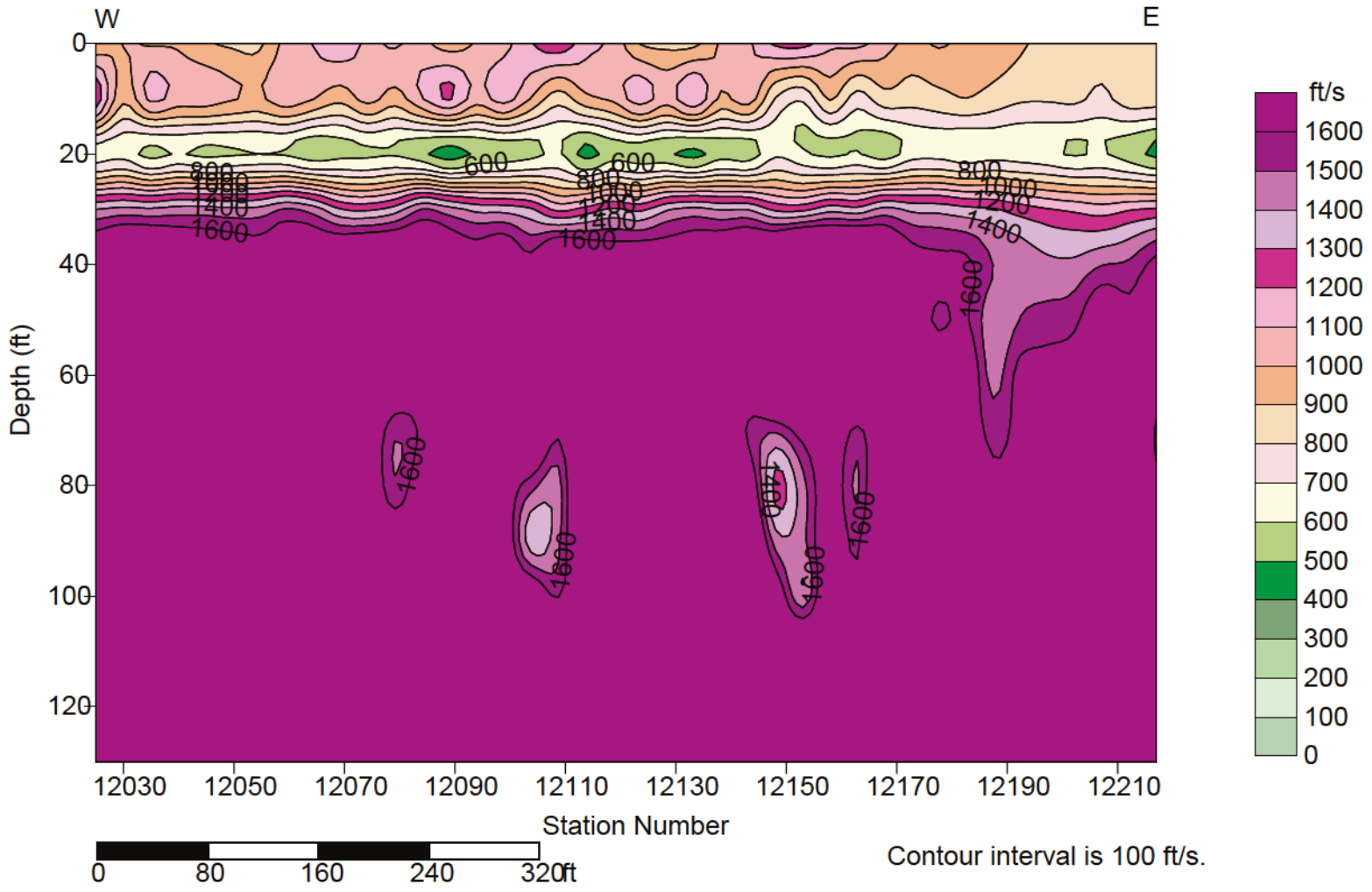

Figure 29. Shear-wave velocity contour along line 12.

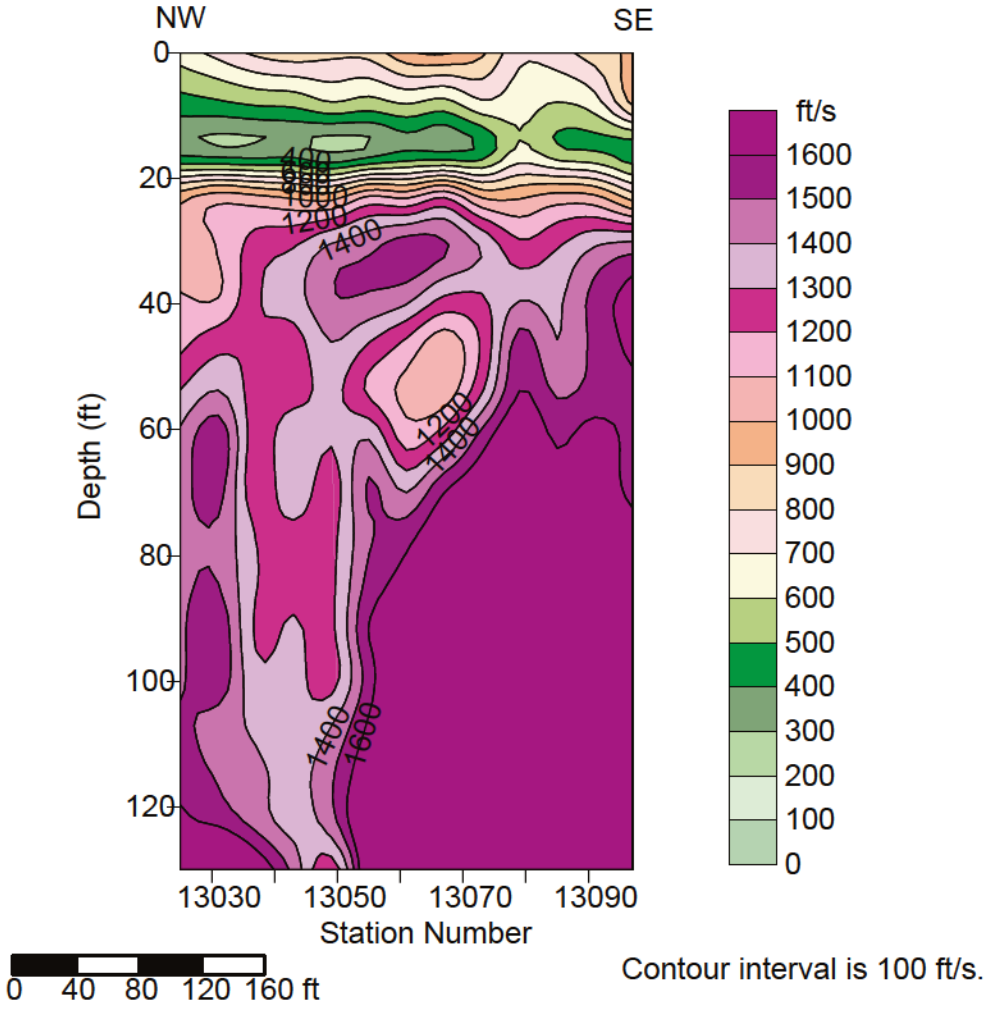

Figure 30. Shear-wave velocity contour along line 13.

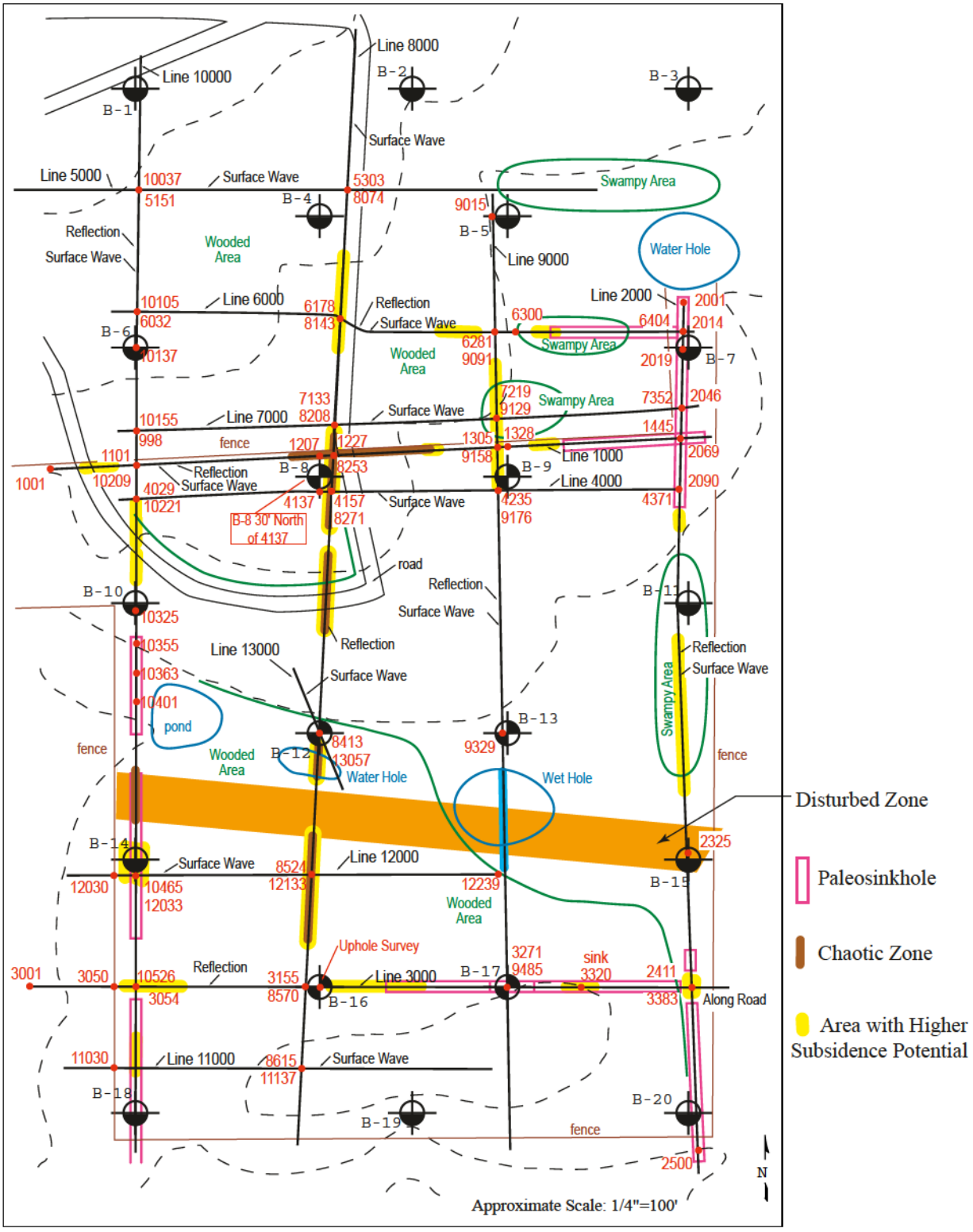

Figure 31. Reflection Interpreted Features. Station location ties between lines and surface features. Lines are located on this diagram in approximate relative locations.

correlating from line to line would have been possible using a simple linear relationship. The lack of linearity is a key indicator that line-to-line ties are possible but fault-controlled structures are likely not what is evident on the data sets. A single linear disturbed zone has been interpreted to cut the site approximately into thirds. The feature that is correlated between the lines possesses a deep rooted (>300 ft) bed offset or chaotic reflection window.

Surface wave data generally possess the least uniformity in the northern half of this site (Figure 32). Using the deeper vertical velocity anomalies as a key indicator of major breeches in the confining and rigidity of the bedrock materials, the northeastern corner of the site immediately west of the paleosinkhole defined on reflection data seems to be an area with the least competence. Several more isolated features can be interpreted where bedrock is clearly deteriorated but most of those would likely resemble swiss cheese if exposed at the surface, without much in the way of lateral or vertical extent.

Combining the interpreted features between the two data sets provides a picture of the subsurface with sitewide coherency of identified anomalies, but does highlight areas with subsurface and in many cases surface expressions that likely relate to areas with reduced bedrock competence (Figure 33). Having both shallow and deep disturbed areas suggests that expression at the ground surface is possible within a small amount of geologic time and there is a potential for conductivity with regional water sources. Future subsidence potential is greatest in areas with both near-surface expression and deeply disturbed rock layers.

Looking at areas on both reflection and surface wave data with the greatest risk of subsidence and a history of subsidence a trend might be observable (Figure 34). At the perimeter of most paleosinkholes defined on reflection data are areas defined by surface wave data with deep seated fault or fracture systems. Combining the locations of these features unique to each data set with surface features such as ponds, wet holes, and swampy areas it is possible to classify areas as "subsidence prone." It is assumed that areas with paleosinkholes might experience some settling, but most dissolution has already been compensated for by subsidence and later sedimentation.

Using only surface wave data a trend can be interpreted that dissects the site west-to-east with all deeper bedrock features north of the lineament (Figure 35). The anomalies interpreted as shallow bedrock disturbances are characterized by a large velocity anomaly with a significant alteration in the bedrock surface contours. Deep bedrock features are the ones that are relatively

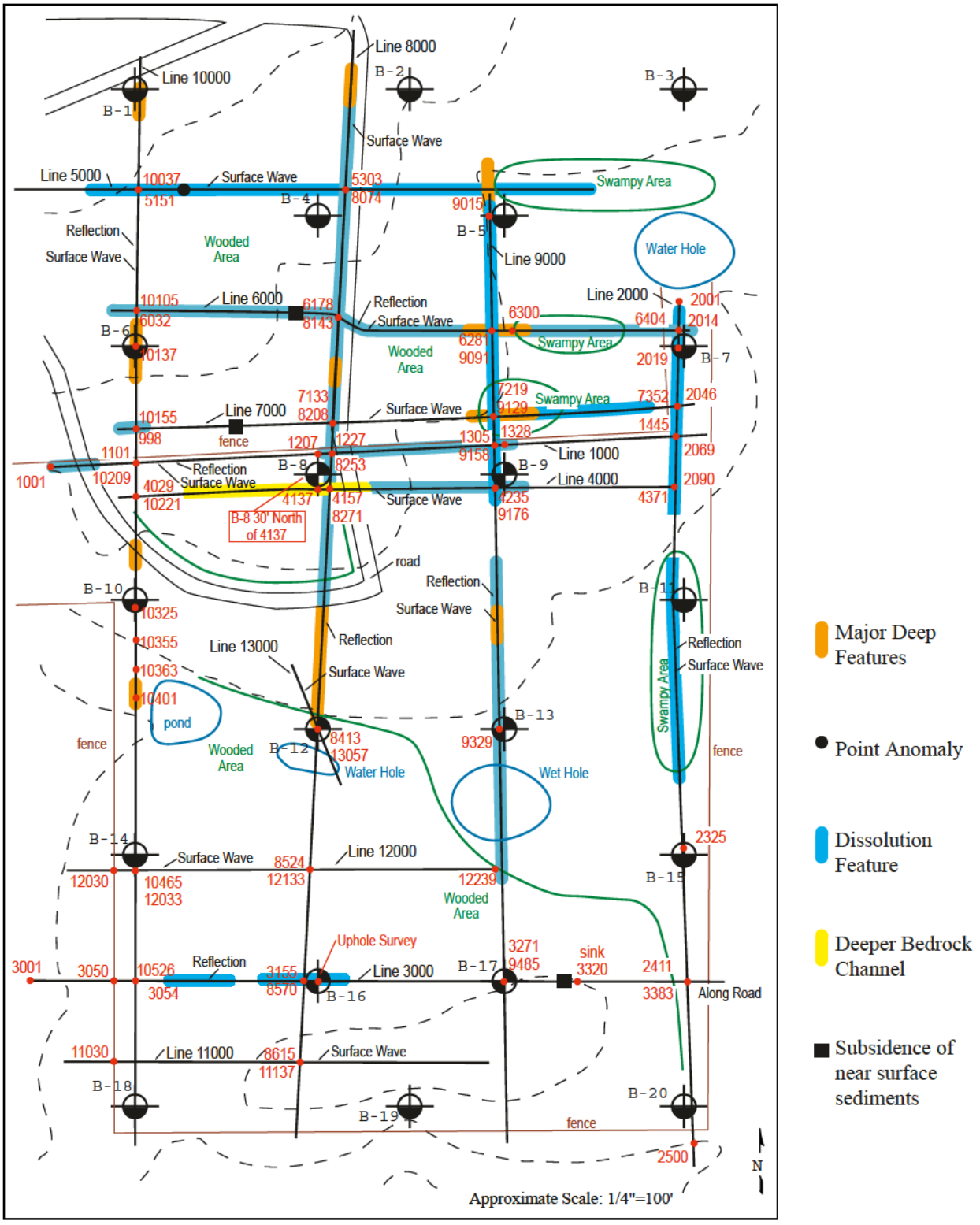

Figure 32. Shear Wave Interpreted Features. Station location ties between lines and surface features. Lines are located on this diagram in approximate relative locations with interpreted features indicated.

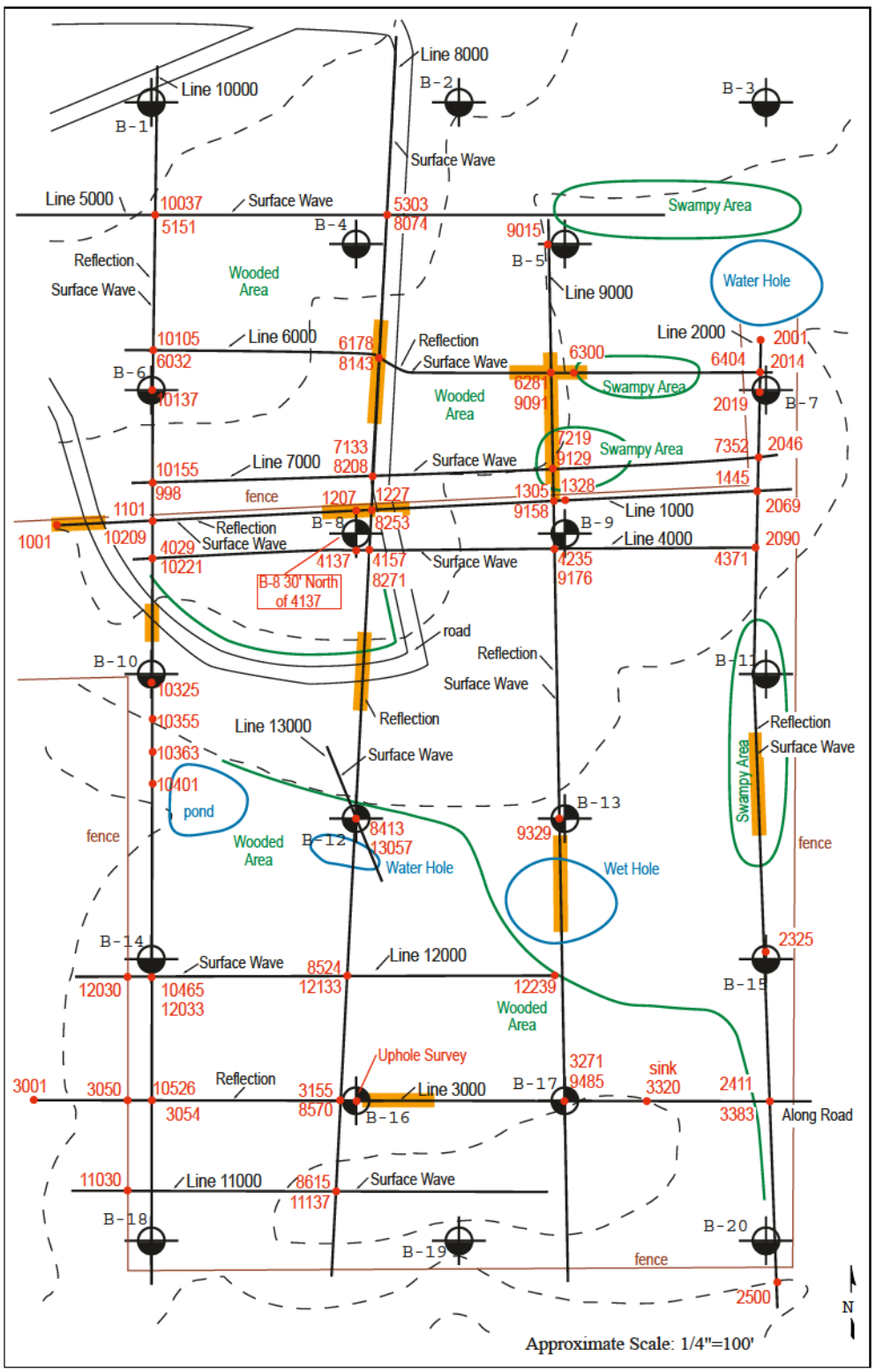

Figure 33. Coincident Features from Reflection and Shear Wave Profiles. Station location ties between lines and surface features. Lines are located on this diagram in approximate relative locations with interpreted features indicated.

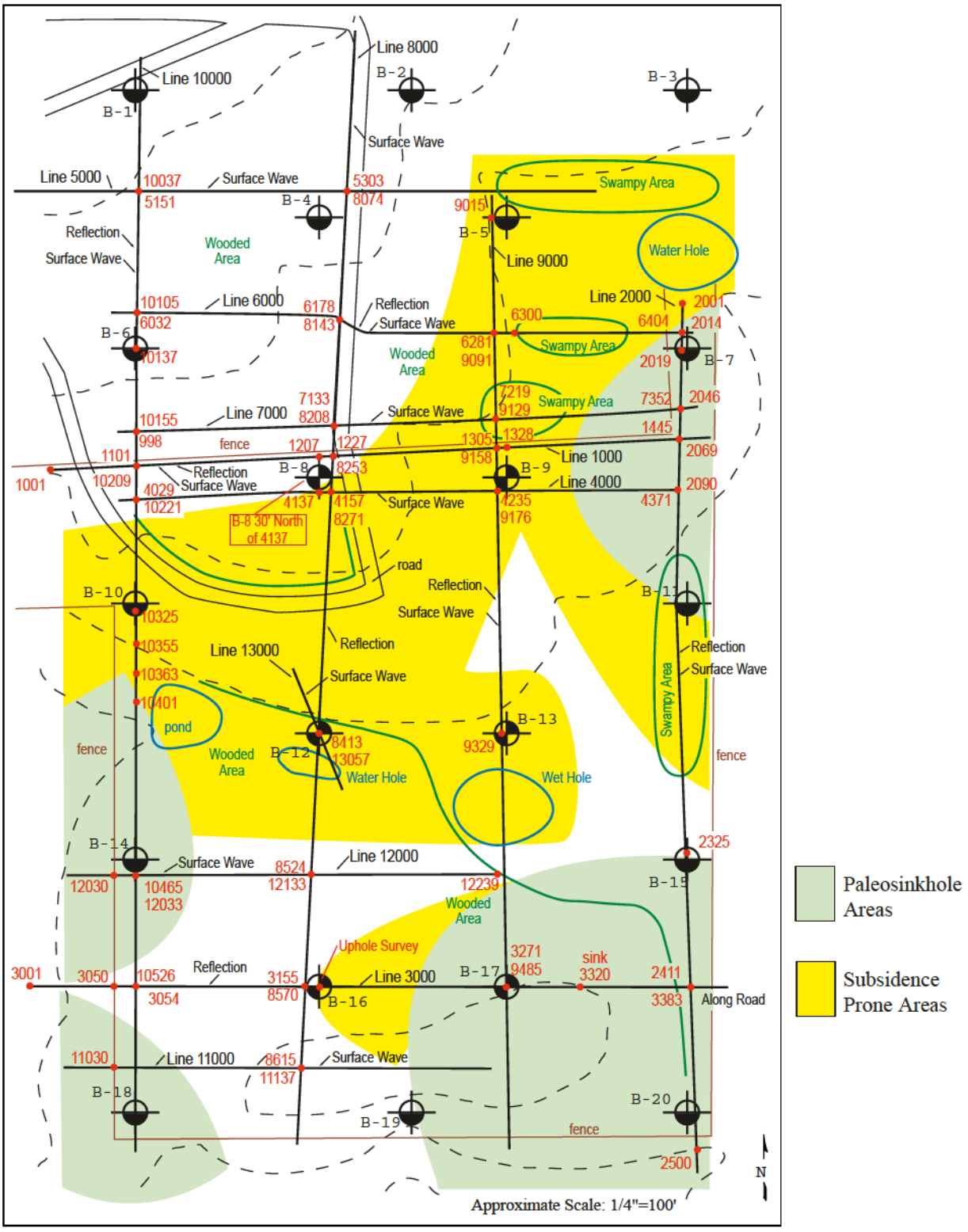

Figure 34. Subsidence Prone Areas and Paleosinkhole Areas. Station location ties between lines and surface features. Lines are located on this diagram in approximate relative locations.

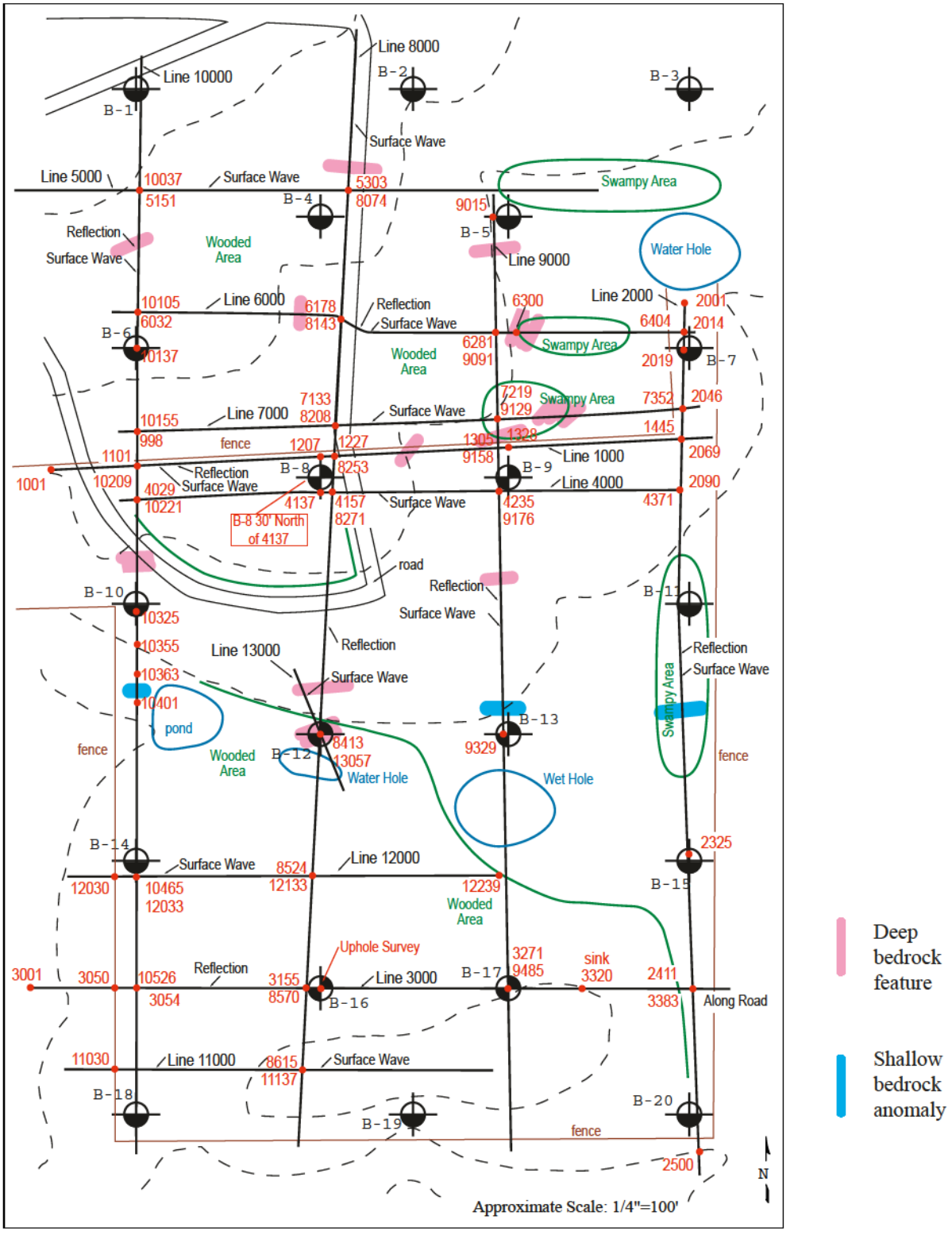

Figure 35. Surface Wave Major Anomalies and Features. Station location ties between lines and surface features. Lines are located on this diagram in approximate relative locations.

narrow and slice throughout the section imaged by the surface wave data. These deep bedrock features usually do not have a strong expression on the bedrock surface. As is evident by examining the distribution of these features, correlating features from line to line is not feasible with the data distribution of this survey. These features could be correlated with several more well-placed profiles.

CONCLUSIONS

Several features have been discovered that are interpreted to either influence dissolution or are the result of dissolution across this site. Features of interest include the fault zone interpreted on lines 2, 8, 9, and 10 as well as the paleosinkholes evident on lines 1, 2, and 3, north of a line that runs almost due east-to-west through boreholes B-12 and B-13.

REFERENCES

Nazarian, S., K.H. Stokoe II, and W.R. Hudson, 1983, Use of spectral analysis of surface waves method for determination of moduli and thicknesses of pavement systems: Transportation Research Record No. 930, p. 38-45.

Miller, R.D., and J. Xia, 1999, Feasibility of seismic techniques to delineate dissolution features in the upper 600 ft at Alabama Electric Cooperative's proposed Damascus site: Kansas Geological Survey Open-file Report 99-3.

Park, C.B., R.D. Miller, and J. Xia, 1996, Multi-channel analysis of surface waves using Vibroseis (MASWV) [Exp. Abs.]: Soc. Expl. Geophys., p. 68-71.

Park, C.B., R.D. Miller, and J. Xia, 1999a, Detection of near-surface voids using surface waves: Proceedings of the Symposium on the Application of Geophysics to Engineering and Environmental Problems (SAGEEP 99), Oakland, California, March 14-18, p. 281-286.

Park, C.B., R.D. Miller, and J. Xia, 1999b, Multi-channel analysis of surface waves: *Geophysics*, v. 64, n. 3, p. 800-808.

stokoe II, K.H., G.W. Wright, A.B. James, and M.R. Jose, 1994, Characterization of geotechnical sites by SASW method, in Geophysical characterization of sites, ISSMFE Technical Committee #10, edited by R.D. Woods, Oxford Publishers, New Delhi.

Xia, J., R.D. Miller, and C.B. Park, 1997, Estimation of shear wave velocity in a compressible Gibson half-space by inverting Rayleigh wave phase velocity [Exp. Abs.]: Technical Program with Biographies, SEG, 67th Annual Meeting, Dallas, Texas, 1927-1920.

Xia, J., R.D. Miller, and C.B. Park, 1998, Construction of vertical seismic section of near-surface shear-wave velocity from ground roll [Exp. Abs.]: Soc. Expl. Geophys./AEGE/CPS, Beijing, p. 29-33.

Xia, J., R.D. Miller, and C.B. Park, 1999a, Configuration of near-surface shear-wave velocity by inverting surface wave: Proceedings of the Symposium on the Application of Geophysics to Engineering and Environmental Problems (SAGEEP 99), Oakland, California, March 14-18, p. 95-104.

Xia, J., R.D. Miller, and C.B. Park, 1999b, Estimation of near-surface shear-wave velocity by inversion of Rayleigh waves: *Geophysics*, v. 64, n. 3, p. 691-700.

Basic principles and concepts of practical shallow seismic reflection profiling

D.W. Steeples and R.D. Miller

Abstract — *Seismic reflection is a powerful geophysical exploration method that has been in widespread use in the petroleum industry for more than 60 years. This paper addresses some basic principles of the method and its application at depths shallower than 30 m (100 ft). Since 1980, the shallow reflection technique has been increasingly used for engineering and environmental problems, such as mapping bedrock beneath alluvium and delineating intra-alluvial features near hazardous waste sites, detecting voids in coal and karst, defining the top of the saturated zone and mapping shallow faults. New applications will be added with improved resolution and increased cost-effectiveness.*

Introduction

This paper describes some of the basic principles of seismic reflection and their significance, as applied to shallow engineering, mining and environmental projects. The seismic reflection method is a powerful technique for underground exploration that has been in use since the 1920s (Waters, 1987; Dobrin, 1976; Coffeen, 1978; Telford et al., 1976; Sheriff, 1978). The use of seismic reflection surveys for imaging targets shallower than 30 m (100 ft) has only been available since the early 1980s. The technique is finding new applications in characterizing the geologic, hydrologic and stratigraphic conditions within 3 to 30 m (10 to 100 ft) of the earth's surface. As research and development continues, higher and higher seismic frequencies will be attainable, allowing practical prospecting for progressively smaller geologic targets.

Seismic reflection techniques depend on the existence of discrete seismic velocity and/or mass density changes in the subsurface, known as acoustic impedance contrasts. Mathematically, acoustic impedance is simply the product of mass density and acoustic wave velocity. Acoustic impedance contrasts occur at natural boundaries between geologic layers, although manmade boundaries, such as tunnels and mines, also represent contrasts. The classic use of seismic reflection is to identify the boundaries of layered geologic units. However, the technique can also be used to search for localized anomalies such as sand/clay lenses and cavities.

Compressional waves (P-waves) propagating through the earth behave similarly to sound waves propagating in air. When sound waves (voices, explosions, horns, etc.) come in contact with a wall, cliff or building (all acoustic contrasts), it is common to hear an echo. When a P-wave comes in contact with an acoustical contrast underground, echoes (reflections) are also generated. P-wave reflections can be thought of as sound wave echoes from underground acoustic impedance contrasts. In the underground environment, the situation is more complex because some P-wave energy impinging on a solid acoustical interface can also be transmitted across the interface, refracted at the interface and/or converted to other types of seismic waves at the interface.

Seismic methods are sensitive to the physical properties of earth materials and relatively insensitive to the chemical makeup of contained fluids in earth materials. Electrical methods are sensitive to contained fluids and to the presence of magnetic or electrically conductive materials. The measurable physical parameters upon which the seismic methods depend are quite different from the important physical parameters for electrical and magnetic methods. In the world of shallow geophysics, there are similarities among seismic reflection, seismic refraction and ground-penetrating radar. There are also similarities with cross-hole seismic tomography and vertical seismic profiling. The similarities with electrical and potential fields methods are substantially less.

The work of Hunter and Pullan and their colleagues at the Geological Survey of Canada (Hunter et al., 1984; Pullan and Hunter, 1985) and Helbig (Doornenbal and Helbig, 1983; Jongerius and Helbig, 1988) and his students at the University of Utrecht in The Netherlands has been instrumental in developing shallow seismic reflection techniques. In particular, the simple data manipulation and display of Hunter's optimum window-common offset makes it a cost-effective method of imaging the shallow subsurface in areas conducive to seismic reflection.

Shallow seismic reflection fundamentals

The simplest case of seismic reflection is a single layer over an infinitely thick medium (Fig. 1). Seismic energy induced into the ground from a point is radiated spherically away from that point in much the same fashion in three dimensions as waves from a pebble tossed into a still pond radiate outward in two dimensions (Fig. 2). An arbitrarily large number of ray paths can be traced outward from the seismic energy source. One particular ray path will direct energy to a subsurface layer, reflect from that subsurface layer and return as an echo to the ground surface first,

D.W. Steeples, member SME, and **R.D. Miller** are associate research director and assistant scientist, respectively, with the Kansas Geological Survey, University of Kansas, Lawrence, KS. SME nonmeeting paper 91-207 B. Manuscript Feb. 22, 1991. Discussion of this peer-reviewed and approved paper is invited and must be submitted, in duplicate, prior to Dec. 31, 1993.

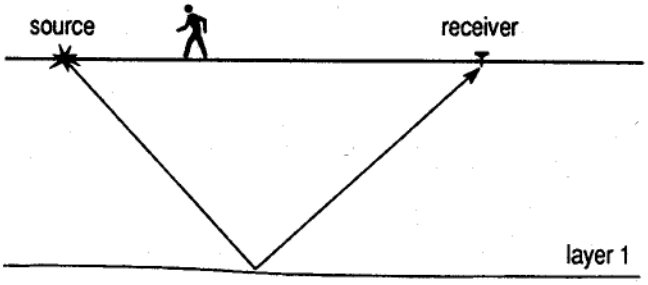

Fig. 1 — Reflection from one subsurface layer. The angle of incidence of the downgoing ray is equal to the angle of reflectance of the upgoing ray.

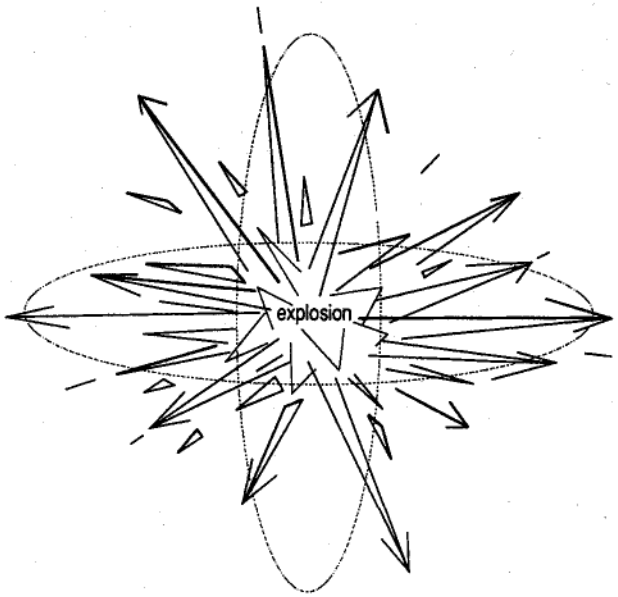

Fig. 2 — Computer simulation of energy radiating out from a subsurface explosion.

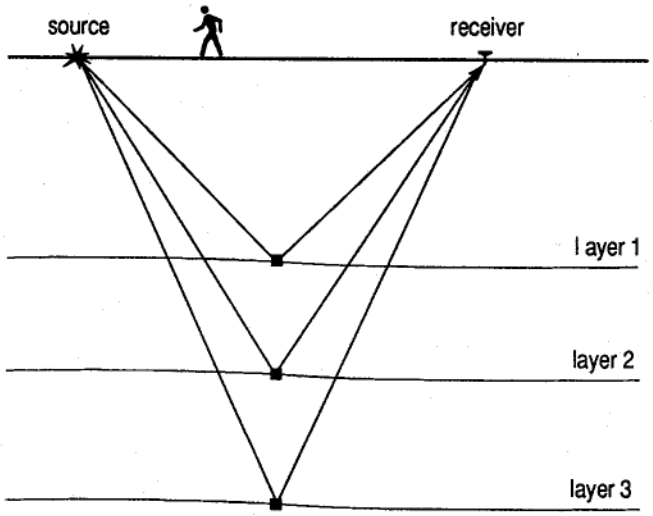

Fig. 3 — Reflection from three subsurface layers. The angle of incidence is different for each layer/ray but the reflecting points are vertically equivalent.

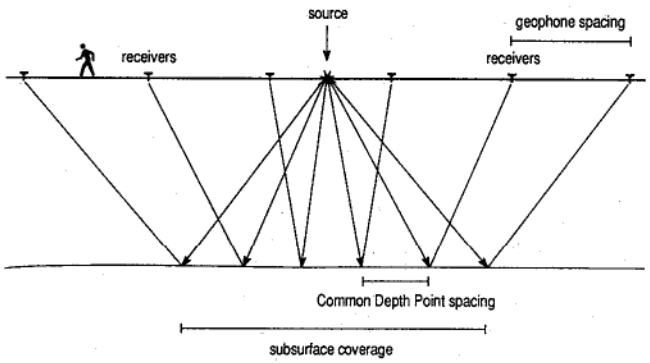

Fig. 4 — Schematic of seismic ray paths for a single shot with a six-channel reflection seismograph.

following Fermat's principle of least travel time. In the case of a single, flat-lying layer and a flat topographic surface (Fig. 1), the path of least time will be from the energy source to a reflecting point midway between the source and the receiver, and then back to the receiver. The incident angle of the down-going ray will be equal to the angle of reflection of the upgoing ray from the subsurface layer.

Several layers beneath the earth's surface are commonly targeted by a single seismic reflection survey (Fig. 3). Seismic data are more complex when several layers are involved. Seismic energy can be converted from one wave type to another at layer interfaces. The simple, one-layer case (Fig. 1) becomes slightly more complicated when considering all the possible raypaths and wave conversions. The apparent complexity of a seismogram directly relates to the variety of types of seismic waves and their associated characteristic velocities and travel paths. Complexity is often increased as well by the presence of seismic energy that has bounced more than one time off layers in the subsurface (multiple reflections). Reflected energy from successively deeper and deeper boundaries appears on a seismic trace at greater and greater time.

Expanding the multilayer case of Fig. 3 to multiple receivers allows travel path vs. arrival time determinations and comparisons (Fig. 4). Rays reflected from different points in the subsurface are recorded by receivers appropriately spaced on the ground surface. The distance between these subsurface reflecting points is exactly half the distance between receivers, providing a closer subsurface sampling interval than the surface receiver spacing. The recording of multiple receiver-channel locations for each individual shot allows determinations of apparent velocity (travel path-arrival time) and apparent reflector dip.

Source and receiver locations can be placed so that path S1-R2 reflects from the same location in the subsurface as path S2-R1 (Fig. 5). The subsurface point that is in common for both source and receiver pairs is called a common reflection point (CRP) (Mayne, 1962), a common depth point (CDP) or a common midpoint (CMP), depending on the preference of the author (Fig. 5).

The power of the CDP method is in the redundancy in sampling of a particular subsurface location. By gathering traces in a computer according to CMP and time-adjusting them for different travel-path lengths, traces with the same CMP can be added to enhance the reflection signal. The degree of redundancy or multiplicity of data at a particular

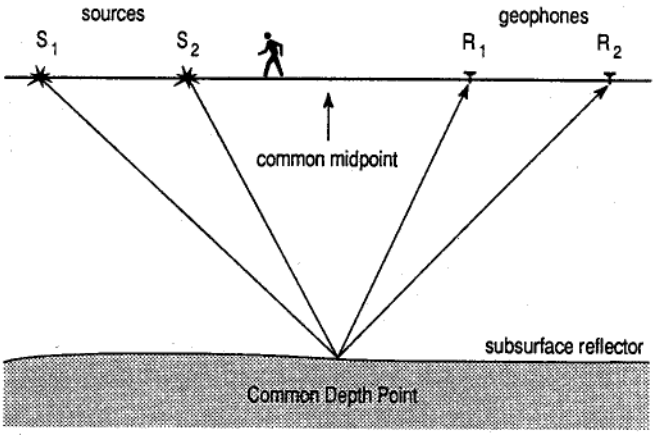

Fig. 5 — The concept of common depth point (CDP). Note that ray paths from two different shots (SI and S2) reflect from a common point in the subsurface.

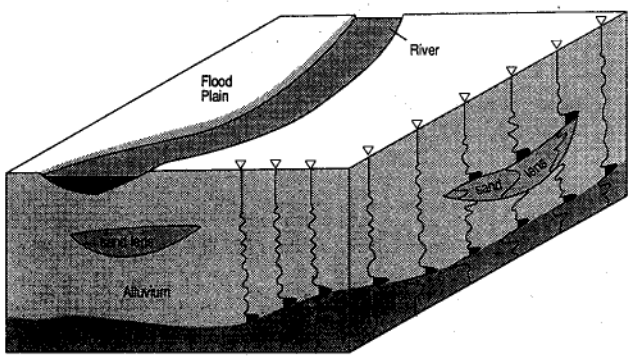

Fig. 6 — Schematic showing a seismic section relating to real-world geology.

point is known as "CDP fold." A 24-channel seismograph, for example, is typically used to gather 12-fold CDP data. From a theoretical standpoint, signal-to-noise ratio of reflections improves proportionally to the square root of the CDP fold. For shallow reflection data in particular, it is important to remember that one-fold of good data is better than many-fold of bad or marginal data.

The seismic reflection method is generally used to determine the spatial configuration of underground geological interfaces. Displaying all the CDP stacked traces consistent with their spatial locations results in a reflection-time cross-section of a portion of the earth (Fig. 6). The peaks of the seismic reflections (wiggles) are generally blackened to assist in interpretation. This schematic example (Fig. 6) is a very simple version of typical near-surface geology that depicts a buried sand lens in a river valley. Resolving a fixed-size target becomes more difficult with increasing depth below the ground surface, but the physical principles remain the same. Resolving power is a linear function of increasing the frequency and bandwidth of the seismic reflection data.

Obtaining high quality shallow seismic reflection data is still somewhat of an art, where an individual's ability improves with experience. Improving the quality of shallow reflection data depends on careful, meticulous procedures based on sound scientific observation and theory, step-by-step data analysis, stringent quality control during all aspects and avoiding invalid assumptions during the acquisition, processing and interpretation of shallow reflection data.

Practical shallow reflection surveying

Seismic reflection surveys routinely involve three basic parts: acquisition, processing and interpretation. A variety of selectable parameters and methods are possible at each of these three distinct stages. Pronounced differences exist between shallow and conventional seismic reflection techniques during the acquisition and processing stages. The basic principles of interpretation for shallow and conventional seismic reflection are consistent, except for scale differences. The underlying theoretical basis for the seismic reflection method is consistent for conventional and shallow applications.

Acquisition

The basic instrument for seismic studies is a seismograph, which is analogous to a stereo music system. The better the music system, the more detail the listener can ascertain from subtle background instruments. Likewise, the better a seismograph's dynamic range, the more the potential for distinguishing subtle geologic features. A stereo music system has variable controls to enhance high frequencies (like a flute) or low frequencies (like a tuba). A seismograph has similar selective capabilities for emphasizing recorded sound frequencies. A seismograph that can record and enhance high frequency sound waves is necessary to detect small geologic features. The use of high frequency seismic waves (>80 Hz) in reflection seismology is known as "high resolution" seismic exploration (Sheriff, 1991).

A stereo system also has an amplifier volume control where a seismograph has amplifier gain control, either fixed (selectable) or floating point (automatic). Selection of the frequencies to be enhanced and the amplifier gain necessary to maximize the recorded relevant geologic information depends on the depth and size of the underground geologic features of interest and the acoustic properties of the near-surface material.

Receivers for detecting reflected acoustic signals in the ground are called geophones. These are very specialized microphones similar in principle to those used in voice recording. The operation of a geophone is based on the voltage induced in a coil of wire when it moves through a magnetic field. For most geophones, a magnet is rigidly attached within the geophone case. A coil of wire mounted on a spring surrounds the magnet. When the case experiences movement, the coil moves relative to the magnetic field (set up by the magnet), which in turn induces a voltage proportional to the velocity of the ground motion. Selection of the appropriate geophone for a particular survey should be based on dominant frequency and amplitude of the signal.

The most site-dependent part of the acquisition system is the acoustic energy source. A variety of sources have been developed and are in routine use on shallow seismic reflection projects. As a human voice is a source of acoustic energy, so is an explosion, a book dropped onto the floor, a car horn or an electric razor. The method of generating and transmitting acoustic energy into the ground is what determines the quality of a source at any particular site.

There are two types of sources: impulsive and vibratory. Impulsive sources are the predominant type of shallow seismic source while vibratory sources are the predominant conventional seismic source. The frequency-limited nature

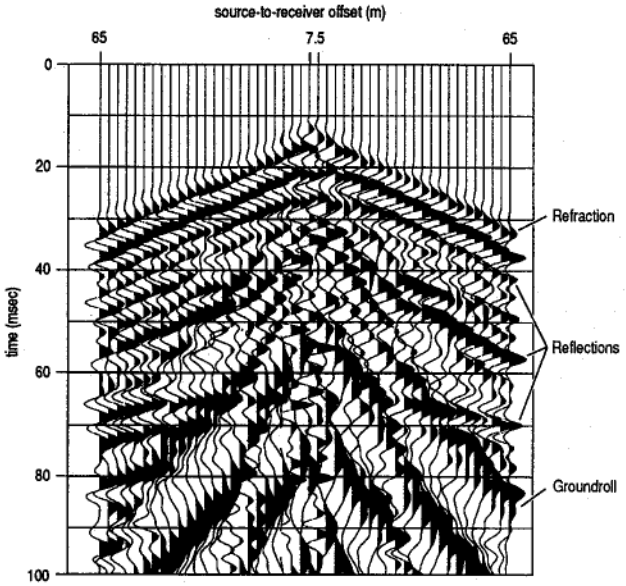

Fig. 7 — 48-channel field file acquired in a split-spread format. The source is located between two sets of 24 channels.

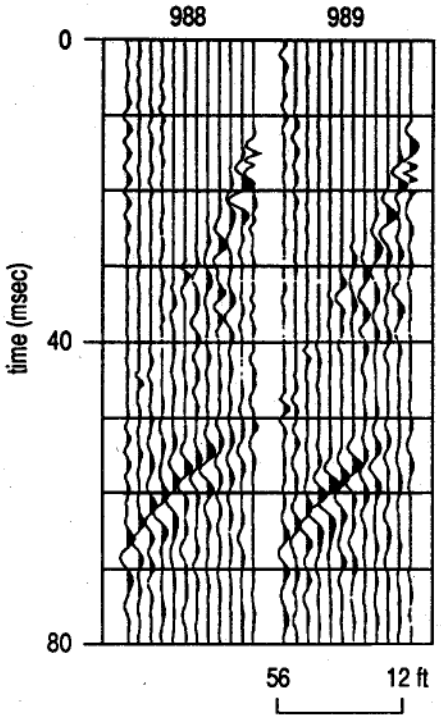

Fig. 8 — Two CDP gathers from a 24-channel seismograph. The hyperbolic curvature of the reflection arrival is easily identified.

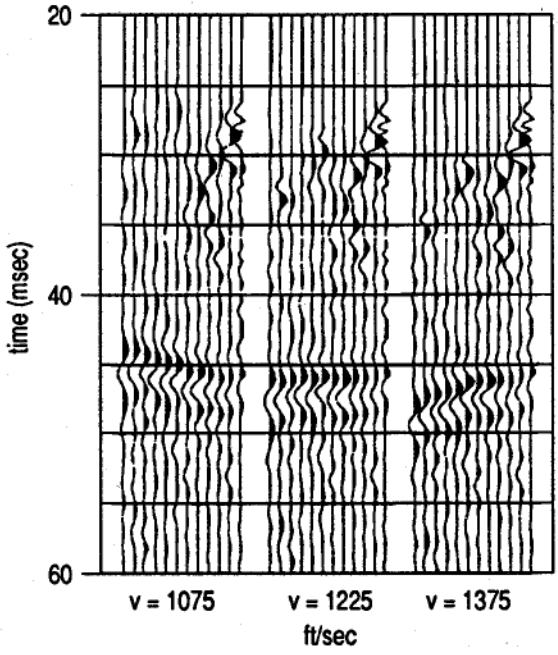

Fig. 9 — CDP gathers from Fig. 8 moved out at various velocities.

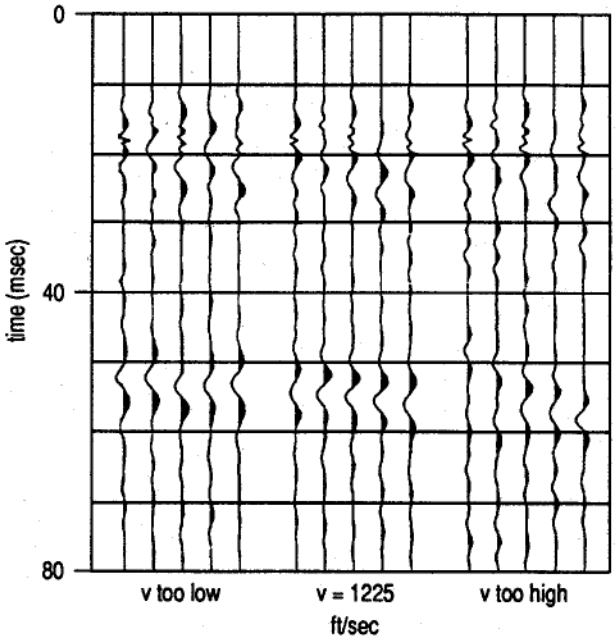

Fig. 10 — The effects of an improper stacking velocity.

of vibratory sources is what has held them to very limited used on shallow reflection surveys. Most shallow reflection surveys employ weight drop (accelerated) or explosives as the source of acoustic energy.

Processing shallow reflection data

The purpose of acquiring and processing seismic reflection data in a CDP format is to enhance reflections at the expense of everything else. There are a variety of filtering, display and static correction techniques that can be employed to improve the quality of the reflections. Discussion here is limited to only those techniques that are necessary to understand the fundamentals of CDP processing. There are many places in the scientific literature to obtain more details (Waters, 1987; Yilmaz, 1987; Robinson and Treitel, 1980).

Raw seismic data are in a field file or shot gather format, with each seismograph channel or seismic trace for a particular shot ordered according to channel number (Fig. 7). The number of seismic traces within each shot gather is equal to the total number of seismograph channels. Before gathering or sorting the data into a CDP format, dead or unacceptably noisy traces are removed and the location of each station is defined in three dimensions. A CDP gather, from a simplistic point of view, is a collection of seismic traces that have a common midpoint in the subsurface.

Before stacking (adding) seismic traces with equivalent subsurface sample points, it is necessary to compensate for different travel-path lengths (arrival time of the reflection) and localized variability in the near-surface material. The arrival pattern of reflection wavelets across receivers with linearly increasing distance from the source is a hyperbolic function (Fig. 8). This hyperbolic arrival pattern, or normal moveout curve, is a result of the nonlinear increase in travel path for a ray traveling down to a reflector and back to the surface with a linear increasing in distance from source to receiver.

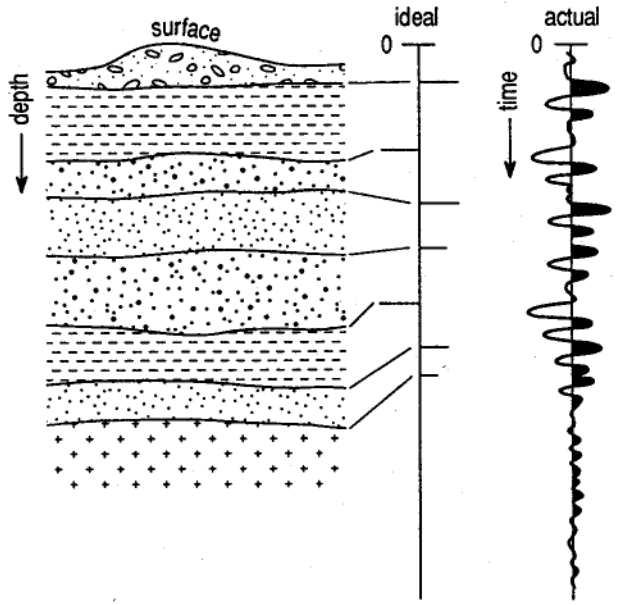

Fig. 11 — Actual seismic trace (with simulated noise) that would result from a reflection survey over the geologic model. The spike or ideal trace represents the acoustic impedance contrasts at each interface.

To properly correct for different ray path lengths, the average velocity above the reflector must be known (Fig. 9). The simplest procedure to determine the seismic velocity for good seismic reflection data is to fit a hyperbola (x^2,t^2) to the data. The degree of curvature of the hyperbola or normal moveout curve of the reflection arrival (assuming horizontal surfaces) is dictated by the average seismic velocity above the reflector, depth to the reflector and distance between geophones.

Once corrected, the data emulate what would be observed with zero distance between shot and geophone, known as zero-offset (vertical incidence). Proper time adjustment to correct for offset allows traces with common midpoints to be directly added without sacrificing any wavelet properties. The correct velocity gives the highest frequency and the best coherency on the stacked data (Fig. 10).

Variations in the velocity and thickness of the near-surface material cause errors known as statics, which uncorrected, can produce apparent geologic structures that have no geologic significance. Static variations are most commonly determined using cross-correlation techniques, such as surface consistent statics, residual statics, common offset statics and refraction statics. Correcting static variations is accomplished through whole-trace time shifts representative of variability in the near-surface, generally in a relatively localized area.

A variety of filtering, scaling, display and analysis techniques much less significant to the understanding of shallow data CDP processing are routinely used to improve overall data quality. The basics of CDP processing discussed here should provide a general understanding of what is most significant to the generation of high quality stacked sections.

Interpretation

Seismic reflection data can be displayed in many forms including CDP stacked section, shot gather (field file), CDP gather and common offset section. Data displayed in any of these formats have features that require special considerations when trying to interpret the significance of the wiggles. First, with shallow reflection data, not every wiggle necessarily has special geologic significance. Noise is present on any seismic data set, and overly optimistic interpretations that draw meaning from every wiggle will eventually lead to misinterpretations.

CDP stacked sections are corrected to represent vertically incident time arrivals . Therefore, of all the data display formats, CDP stacked data most closely equate to a geologic cross section. Common offset data are similar to CDP in the similarity to a geologic cross section. However, common offset data generally are not corrected from nonvertical travel paths. Conversions from time to depth must compensate for the increased time of arrivals.

Data in either shot gather or CDP gather format are generally ordered according to distance from shot to receiver. In this arrangement, a single reflecting interface will be recorded at ever-increasing times at longer offsets. Interpretations based on shot or CDP gathered data are generally limited to approximate reflector depths and occasionally the inference (in a qualitative sense) of faulting or dipping beds. Seismic reflection data are almost always displayed relative to two-way travel time, which can be converted in a general sense to depth if velocity is known.

Seismic reflection data in a CDP stacked or common offset format can be thought of as the time equivalent to a highway road cut where geologic units are exposed for viewing. The accuracy of the conversion of a time seismic reflection section to a depth geologic cross section depends on how well the average velocity from the surface to each reflector is known. The wiggles on a reflection seismogram represent amplitude (loudness from a sound wave perspective) of an echo that arrived at the geophone at a particular time. That time, when multiplied by the average seismic velocity within the earth, equates to twice depth. If the travel time of an acoustic pulse from the surface to a variety of depths in the subsurface can be determined from borehole geophones, conversion of time to depth can be very accurate.

If, on the other hand, no borehole seismic velocity information is available, the NMO velocity must be used to approximate depth. NMO, or stacking velocity, is always 0 to 20% greater than the real average velocity. Reflector depths estimated from NMO or stacking velocities cannot be more than 20% deeper than the actual reflecting interface.

The nature of seismic energy is responsible for the representation of recorded signal in the form of a wave (wiggle) (Fig. 11). Extracting discrete geologic boundaries or anomalies from the series of wiggles present on seismic data requires the actual or inferred removal of the source wavelet or characteristic sound of a source. Seismic data recorded using the perfect source (flat frequency spectrum from zero to infinity) have spikes that represent each acoustic imped-

ance contrast with the height of a spike directly related to the acoustic impedance contrast at the interface.

Unfortunately, since no perfect source exists, the spikes of the perfect source are spread out in time and become waves whose appearance or characteristics are related to the unique spectral properties of the actual source. The narrower the bandwidth of the source the farther from a spike and the 'ringier' the reflection wavelets become. In some cases, a reflection may be represented by a wavelet with as many as three zero crossings (three positive and three negative deflections). The interpretation of seismic data requires a good understanding and working knowledge of the source wavelet for a particular source and experience with distinguishing interference between wavelets from two closely spaced reflectors.

Conclusion

Seismic reflection is a powerful geophysical tool for exploration of the subsurface. Applications of the technique to engineering, environmental and ground water problems has only recently become cost-effective. As with any geophysical technique, as long as the basic principles and limitations are understood and no assumptions are made, shallow seismic reflection can provide subsurface continuity not possible by any other means at some locations. ♦

References

Coffeen, J.A., 1978, *Seismic exploration fundamentals*, PennWell Publishing Co., Tulsa, Okla., 277 pp.

Dobrin, M.B., 1976, *Introduction to geophysical prospecting*, McGraw-Hill Book Co., New York.

Doornenbal, J.C., and Helbig, K., 1983, "High-resolution reflection seismics on a tidal flat in the Dutch Delta-Acquisition, processing, and interpretation," *First Break*, May, pp. 9-20.

Hunter, J.A., et al., 1984, "Shallow seismic reflection mapping of the overburden-bedrock interface with the engineering seismograph — some simple techniques," *Geophysics*, Vol. 49, pp. 1381-1385.

Jongerius, P. and Helbig, K., 1988, "Onshore high-resolution seismic profiling applied to sedimentology," *Geophysics*, Vol. 53, pp. 1276-1283.

Mayne, W.H., 1962, "Horizontal data stacking techniques," supplement to *Geophysics*, Vol. 27, pp. 927-938.

Pullan, S.E., and Hunter, J.A., 1985, "Seismic model studies of the overburden-bedrock reflection," *Geophysics*, Vol. 50, pp. 1684-1688.

Robinson, E.A., and Treitel, S., 1980, *Geophysical signal analysis*, Prentice-Hall, Inc., Englewood Cliffs, N.J., 466 pp.

Sheriff, R.E., 1978, *A first course in geophysical exploration and interpretation*, International Human Resources Development Corp., Boston, 313 pp.

Sheriff, R.E., 1991, *Encyclopedic dictionary of exploration geophysics*, 3rd ed., Society of Exploration Geophysicists, Tulsa, Okla., 376 pp.

Telford, W.M., et al., 1976, *Applied geophysics*, Cambridge University Press, New York, 860 pp.

Waters, K.H., 1987, *Reflection seismology — A tool for energy resource exploration*, 3rd ed., John Wiley and Sons, New York, 538 pp.

Yilmaz, O., 1987, *Seismic data processing*; S.M. Doherty, Ed.; *Investigations in Geophysics* series, No. 2, E.B. Neitzel, Series Ed., Society of Exploration Geophysics, Tulsa, OK.

GEOPHYSICS, VOL. 64, NO. 3 (MAY-JUNE 1999); P. 800–808, 7 FIGS.

APPENDIX B

Multichannel analysis of surface waves

Choon B. Park , Richard D. Miller , and Jianghai Xia

ABSTRACT

The frequency-dependent properties of Rayleigh-type surface waves can be utilized for imaging and characterizing the shallow subsurface. Most surface-wave analysis relies on the accurate calculation of phase velocities for the horizontally traveling fundamental-mode Rayleigh wave acquired by stepping out a pair of receivers at intervals based on calculated ground roll wavelengths. Interference by coherent source-generated noise inhibits the reliability of shear-wave velocities determined through inversion of the whole wave field. Among these nonplanar, nonfundamental-mode Rayleigh waves (noise) are body waves, scattered and nonsource-generated surface waves, and higher-mode surface waves. The degree to which each of these types of noise contaminates the dispersion curve and, ultimately, the inverted shear-wave velocity profile is dependent on frequency as well as distance from the source.

Multichannel recording permits effective identification and isolation of noise according to distinctive trace-to-trace coherency in arrival time and amplitude. An added advantage is the speed and redundancy of the measurement process. Decomposition of a multichannel record into a time variable-frequency format, similar to an uncorrelated Vibroseis record, permits analysis and display of each frequency component in a unique and continuous format. Coherent noise contamination can then be examined and its effects appraised in both frequency and offset space. Separation of frequency components permits real-time maximization of the S/N ratio during acquisition and subsequent processing steps.

Linear separation of each ground roll frequency component allows calculation of phase velocities by simply measuring the linear slope of each frequency component. Breaks in coherent surface-wave arrivals, observable on the decomposed record, can be compensated for during acquisition and processing. Multichannel recording permits single-measurement surveying of a broad depth range, high levels of redundancy with a single field configuration, and the ability to adjust the offset, effectively reducing random or nonlinear noise introduced during recording.

A multichannel shot gather decomposed into a swept-frequency record allows the fast generation of an accurate dispersion curve. The accuracy of dispersion curves determined using this method is proven through field comparisons of the inverted shear-wave velocity (v_s) profile with a downhole v_s profile.

INTRODUCTION

In most surface seismic surveys when a compressional wave source is used, more than two-thirds of total seismic energy generated is imparted into Rayleigh waves (Richart et al., 1970), the principal component of ground roll. Assuming vertical velocity variation, each frequency component of a surface wave has a different propagation velocity (called phase velocity, C_f) at each unique frequency (f) component. This unique characteristic results in a different wavelength ($_f$) for each frequency propagated. This property is called dispersion. Although ground roll is considered noise on body-wave surveys (i.e., reflection or refraction profiling), its dispersive properties can be utilized to infer near-surface elastic properties (Nazarian et al., 1983; Stokoe et al., 1994; Park et al., 1998a). Construction of a shear (S)-wave velocity (v_s) profile through the analysis of plane-wave, fundamental-mode Rayleigh waves is one of the most common ways to use the dispersive properties of surface waves (Bullen, 1963). This type of analysis provides key parameters commonly used to evaluate near-surface stiffness—a critical property for many geotechnical studies (Stokoe et al., 1994). As well, the near-surface v_s field can provide useful information about statics during body-wave data processing (Mari, 1984).

Presented at the 66th Annual Meeting, Society of Exploration Geophysicists. Manuscript received by the Editor August 15, 1997; revised manuscript received November 23, 1998.
Kansas Geological Survey, University of Kansas, 1930 Constant Avenue, Campus West, Lawrence, Kansas 66047-3726. E-mail: park@kgs.ukans.edu; rmiller@kgs.ukans.edu; jxia@kgs.ukans.edu.

In the early 1980s, a wave-propagation method to generate the near-surface v_s profile, called spectral analysis of surface waves (SASW), was introduced (Nazarian et al., 1983). SASW uses the spectral analysis of ground roll generated by an impulsive source and recorded by a pair of receivers. This method has been widely and effectively used in many geotechnical engineering projects (Stokoe et al., 1994). The single pair of receivers is configured and reconfigured (based on wavelength calculations made during acquisition) as many times as necessary to sample the desired frequency range. Data are analyzed in the frequency domain to produce a dispersion curve by calculating the phase difference between each deployment of receiver pairs. The inclusion of noise during SASW measurements occasionally can be controlled using a set of empirical criteria tailored for each site investigated (Gucunski and Woods, 1991; Stokoe et al., 1994). Optimizing these criteria is challenging because of the degree of changes possible in near-surface materials. Besides the uniqueness of each site, inherent difficulties exist when evaluating and distinguishing signal from noise with only a pair of receivers. The necessity of recording repeated shots into multiple field deployments for a given site increases the time and labor requirements over a multichannel procedure. Multichannel analysis of surface waves (MASW) tries to overcome the few weaknesses of the SASW method.

The entire process classically used to produce a v_s profile through spectral analysis of surface waves involves three steps: acquisition of ground roll, construction of dispersion curve (a plot of phase velocity versus f), and backcalculation (inversion) of the v_s profile from the calculated dispersion curve. Broadband ground roll must be produced and recorded with minimal noise to accurately determine the v_s profile. A variety of techniques have been used to calculate dispersion curves (McMechan and Yedlin, 1981; Stokoe et al., 1994), each having its own unique advantages and disadvantages. Backcalculation of the v_s profile (inversion of the dispersion curve) is accomplished iteratively, using the measured dispersion curve as a reference for either forward modeling (Stokoe et al., 1994) or a least-squares approach (Nazarian, 1984). Values for Poisson's ratio and density are necessary to obtain a v_s profile from a dispersion curve and are usually estimated from local measurements or material types.

A variety of wave types are produced during the generation of planar, fundamental-mode Rayleigh waves. Among these are body waves, nonplanar surface waves, backscattered waves, and ambient noise. Body waves can manifest themselves on a shot record in a variety of ways. Refracted and reflected body waves result from interactions between body waves and acoustic impedance or velocity contrasts in the subsurface, while direct body waves travel, as the name implies, directly from the source to a receiver. Also of consequence are surface waves that have propagated only a short distance from the source. These waves usually behave in a complicated nonlinear pattern and cannot be treated as plane waves (Stokoe et al., 1994). Backscattered surface waves can be prevalent on the shot gather if horizontal discontinuities such as building foundations, earth berms, or retaining walls exist nearby (Sheu et al., 1988). Relative amplitudes of each noise type generally change with frequency and distance from the source (source offset). Each noise type normally has distinct velocity and attenuation properties that can be identified on multichannel records by the coherency pattern, arrival time, and amplitude of each.

Decomposition of recorded wavefields into a swept-frequency format permits identification of most noise by frequency phase and source offset. Decomposition can therefore be used in association with multichannel records to make adjustments to minimize noise during acquisition. Selection of data-processing parameters such as the optimum frequency range for the phase-velocity calculation can be made more accurately from multichannel shot records. Once shot gathers are decomposed, a simple multichannel coherency measure applied in the time (Yilmaz, 1987) or frequency domain (Park et al., 1998b) can be used to calculate phase velocity with a frequency. Phase velocity with frequency are the two variables (x, y) that make up the dispersion curve. It is also possible to determine the accuracy of the calculated dispersion curve by analyzing the linear slope of each frequency component of the ground roll on a single shot gather. In this way, MASW allows the optimum recording and separation of broad bandwidth and high S/N ratio Rayleigh waves from other acoustic energy. A high S/N ratio ensures accuracy in the calculated dispersion curve, while the broad bandwidth improves resolution and possible depth of investigation of the inverted v_s profile (Rix and Leipski, 1991).

GENERAL PROCEDURE

Ground roll is easily generated by either a swept source like a vibrator or an impulsive source like a sledgehammer. Raw uncorrelated data are optimum for multichannel analysis; therefore, swept sources are preferred if they can be frequency and amplitude optimized for the target. Impulsive source data, on the other hand, need to be decomposed into a swept-frequency format to expose phase velocity-frequency relationship of dispersive ground roll. The basic field configuration and acquisition routine for MASW is generally the same as that used in conventional common midpoint (CMP) body-wave reflection surveys. Some rules of thumb for MASW are inconsistent with reflection optimization. This commonality allows development of near-surface velocity field variations using MASW that can be used for accurate statics corrections on reflection profiles. MASW can be effective with as few as twelve recording channels connected to single low-frequency geophones (<10 Hz).

Near offset

Even with the dominance of ground roll on seismic data, optimal recording of ground roll requires field configurations and acquisition parameters favorable to recording planar, fundamental-mode Rayleigh waves and unfavorable to all other types of acoustic waves. Because of undesirable near-field effects, Rayleigh waves can only be treated as horizontally traveling plane waves after they have propagated a certain distance (offset x_1) from the source point (Richart et al., 1970). Plane-wave propagation of surface waves does not occur in most cases until the near-offset (x_1) is greater than half the maximum desired wavelength ($_{max}$) (Stokoe et al., 1994):

$$x_1 \quad 0.5 \ _{max}. \tag{1}$$

On a multichannel record displayed in a swept-frequency format, near-field effects manifest themselves as a lack of linear

coherency in phase at lower frequencies. This effect manifests itself as arrivals with increased frequencies that lack coherency (Figure 1b). Different investigators have reported different optimum ratios between x_1 and $_{max}$ (Gucunski and Woods, 1991; Stokoe et al., 1994). The normally accepted axiom is that the penetration depth (z) of ground roll is approximately equal to its wavelength ( ) (Richart et al., 1970), while the maximum depth (z_{max}) for which v_s can be reasonably calculated is about half the longest wavelength ($_{max}$) measured (Rix and Leipski, 1991). Rewriting equation (1) to represent maximum depth,

$$x_1 \quad z_{max} \tag{2}$$

provides a good rule of thumb for selecting near-offset distances.

Far offset

As with all acoustic energy traveling in the earth, high-frequency (short-wavelength) components of surface waves attenuate quite rapidly with distance away from the source (Bullen, 1963). If the maximum receiver offset is too large, the high-frequency components of surface-wave energy will not dominate higher-frequency components of the spectrum—specifically, body waves. Contamination by body waves because of attenuation of high-frequency ground roll at longer offsets is referred to here as the far-offset effect. Far-offset effects manifest themselves as a decrease in ground roll slope (increased apparent phase velocity) or reduction in the linear coherency of a band of arrivals because of interference between low-velocity ground roll and high-velocity body waves (Figure 1c). Far-offset effects initially are evident at far-offset traces, spreading inward with increasing frequency to near-offset traces. This effect limits the highest frequency (f_{max}) at which phase velocity can be measured. When the initial layer model is created according to the half-wavelength criterion, f_{max} usually designates the uppermost thickness (H_1) imaged for a particular measured phase velocity (Stokoe et al., 1994):

$$H_1 \quad 0.5 \ _{min} = 0.5C_{min}/f_{max}, \tag{3}$$

where C_{min} and $_{min}$ are phase velocity and wavelength, respectively, corresponding to a particular f_{max}. Although the final inverted v_s profile may possess shallow layers thinner than H_1, calculated v_s values for these layers should be considered unreliable (Rix and Leipski, 1991). Equation (3) can be used as a rough estimation of the minimum definable thickness of the shallowest layer. If a smaller H_1 is sought, the receiver spread and/or offset from the source needs to be reduced (decrease x_1 and/or decrease receiver spacing dx). To avoid spatial aliasing, dx cannot be smaller than half the shortest wavelength measured.

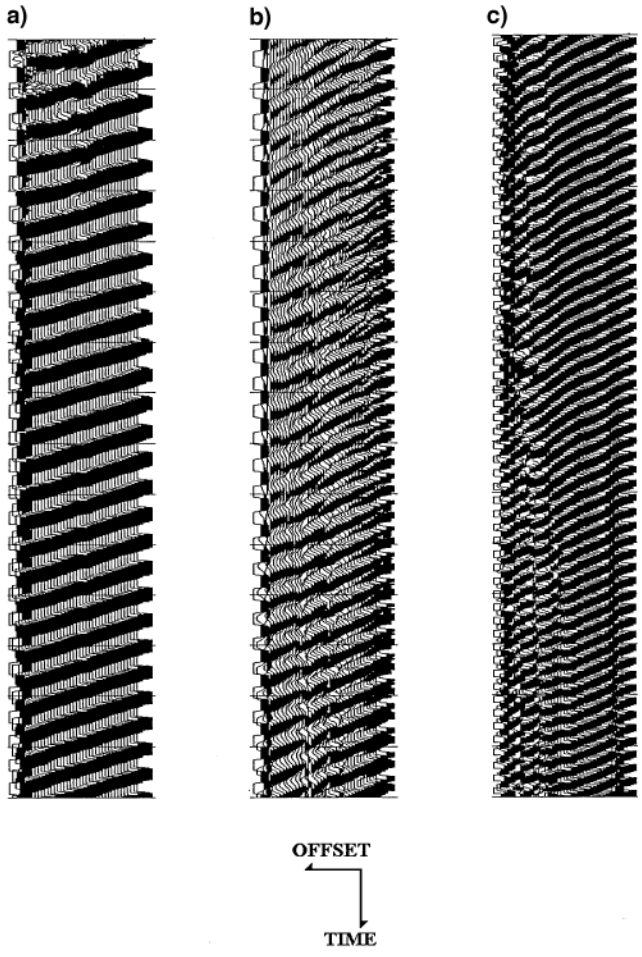

FIG. 1. Field data examples of different quality in recorded ground roll obtained using Vibroseis. [The first trace represents the sweep used.] Ground roll is shown with distinctive coherency over most traces in (a), indicating a good quality, whereas it suffers from (b) near-field effect that is identified by either weak energy or reduced coherency with fragmented energy packets and (c) far-offset effect that is identified by decreased slopes in comparison to earlier lower-frequency components or reduced coherency. The distance (x_1) of the nearest receiver from the source is (a) 27 m, (b) 1.8 m, and (c) 89 m.

Swept-frequency record

A swept-frequency record can be obtained either directly (an uncorrelated Vibroseis field record) or indirectly (an impulsive record passed through a stretch function). Three parameters need to be considered when preparing a swept-frequency record: the lowest frequency recorded (f_1), the highest frequency recorded (f_2), and length (T) of frequency-time plot or stretch function. Optimum selection of these parameters should be based on a series of rules of thumb.

It has been suggested that the lowest frequency (f_1) analyzed determines the maximum depth of investigation z_{max} such that

$$z_{max} = C_1/(2f_1), \tag{4}$$

where C_1 is phase velocity for frequency f_1 (Rix and Leipski, 1991). The lowest frequency recorded is usually limited by the natural frequency of the geophone and source type/configuration. If z_{max} is not sufficient to meet the depth requirement, a different type of source should be tested that has the potential to generate more low-frequency energy and/or lower-frequency geophones should be used.

The highest frequency to be analyzed (f_2) should initially be chosen higher than likely necessary (several times higher than the apparent frequency of ground roll) and lowered to the optimal value after noise analysis.

Length (T) of the swept-frequency record should be as long as feasible or possible, allowing detailed examination of changes in ground roll frequency. A longer T is necessary when near-surface properties change rapidly with depth. When f_1

and f_2 are properly selected, a T of no more than 10 s is sufficient.

Stretch function

An impulsive record $r(t)$ obtained by using a source such as a sledgehammer or weight drop can be transformed into the swept-frequency record $r_s(t)$ by convolution of $r(t)$ with a stretch function $s(t)$ (Coruh, 1985):

$$r_s(t) = r(t) \; s(t), \tag{5}$$

where denotes the convolution operation. The stretch function $s(t)$ is a sinusoidal function with changing frequency as a function of time. A linear sweep similar to those commonly used in Vibroseis surveys (Waters, 1978) is a good choice for $s(t)$:

$$s(t) = \sin \quad 2 \quad f_1 t + \frac{(f_2 \quad f_1)}{T} t^2 \quad , \tag{6}$$

where f_1, f_2, and T are lowest, highest, and length of $s(t)$. These parameters can be optimized using the previously outlined procedure.

Dispersion curve

Generation of a dispersion curve is one of the most critical steps for eventually generating an accurate shear-wave velocity profile. Dispersion curves are generally displayed as phase velocity versus frequency. This relationship can be established by calculating the phase velocity from the linear slope of each component of the swept-frequency record. The accuracy of a dispersion curve can be enhanced by the analysis and removal of noise on ground roll data. With the excellent isolation potential of each frequency component, a multichannel coherency measure (Yilmaz, 1987) can be applied to a ground roll seismogram. A frequency-domain approach (Park et al., 1998b) to calculating the dispersion curve can also be used on impulsive data.

Inversion

The v_s profiles are calculated using an iterative inversion process that requires the dispersion data and estimations of Poisson's ratio and density. A least-squares approach allows automation of the process (Xia et al., 1999). For the method used here, only v_s is updated after each iteration, with Poisson's ratio, density, and model thickness remaining unchanged throughout the inversion.

An initial earth model needs to be specified as a starting point for the iterative inversion process. The earth model consists of velocity (P-wave and S-wave velocity), density, and thickness parameters. Among these four parameters, v_s has the most significant effect on the reliable convergence of the algorithm. Several methods are reported to ensure the reliable and accurate convergence after calculating the initial v_s profile (Heukelom and Foster, 1960; Vardoulakis and Vrettos, 1988). An initial v_s profile should be defined such that v_s at a depth z_f is 1.09 times (Stokoe et al., 1994) the measured phase velocity C_f at the frequency where wavelength $_f$ satisfies the relationship

$$z_f = a \quad _f, \tag{7}$$

where a is a coefficient that only slightly changes with frequency and is based on extensive modeling (Figure 5c). One inversion method (Xia et al., 1999) guarantees the process procedure converges to a reliable result for a wide range of initial models.

FIELD TEST WITH SWEPT SOURCE

An IVI Minivib was used to generate swept surface-wave (ground roll) data at a test site near the Kansas Geological Survey in Lawrence, Kansas. The main purpose of this field test was to produce a v_s profile using the MASW procedure. The site consists of a thick (>50 m) layered shale sequence overlying a repetitive section of Kansas cyclothems (Moore, 1964). The surface topography was relatively flat with only subtle relief, <1 m across the 100-m-long site. The weathered-zone thickness was known to be about 3 m.

Forty-one of the 48 channels available on a Geometrics Strataview seismograph were connected to a group of three 10-Hz Geospace geophones with each group separated by 1 m. During the survey design, the thickness of the uppermost layer to be resolved was chosen to be about the same as the thickness (3 m) of the weathered zone. The minimum offset (x_1) was chosen to be 1.8 m to allow observation of the near-field effect. A 10-s linear upsweep from 10 to 50 Hz was recorded with a 1-ms sampling interval. A maximum depth of investigation was chosen not in advance but after noise analysis was assigned, so as to be consistent with the lowest measured frequency (10 Hz).

Shot gathers from our test site suffer from severe near-field effects at low frequencies (<about 25 Hz), as indicated by the lack of ground roll coherency (Figure 2). The slightly curved nature of the coherent ground roll events is believed to be from a slight topographic high (<1 m) near the center of the line or a laterally variable velocity structure. Far-offset effects are noticeable at higher frequencies (>about 40 Hz) and longer offsets. Subsequent processing suggests these effects do not adversely affect the accuracy of calculated phase velocities at the higher frequencies. The lowest observed phase velocity was about 200 m/s at 50 Hz, equating to a minimum wavelength of 4 m. Half this minimum wavelength is comparable to the expected thickness of the uppermost layer, or the shallowest depth of investigation for this data.

Subsequent noise analysis attempts were designed to estimate the highest recorded phase velocity without near-field effect. A minimum offset x_1 was chosen large (89 m) to enhance these effects. Good coherency is observed (Figure 3) for frequencies from about 20 Hz down to near the natural frequency of the geophones (10 Hz). The reduced coherency evident near 10 Hz (near 500 ms recording time) is not because of the near-field effect but is rather from the purposely tapered drive force of the vibrator at the start of the sweep (necessary because of physical limitations of the vibrator) and ambient noise. The highest phase velocity was about 800 m/s for frequencies very near 10 Hz. At later times, traces at this site suffer from high-amplitude body waves, backscatter from nearby buildings, and surface waves from vehicle traffic. Based on the previous two noise analyses, the approximate range of phase velocities measurable at this site is estimated to be 200–800 m/s,

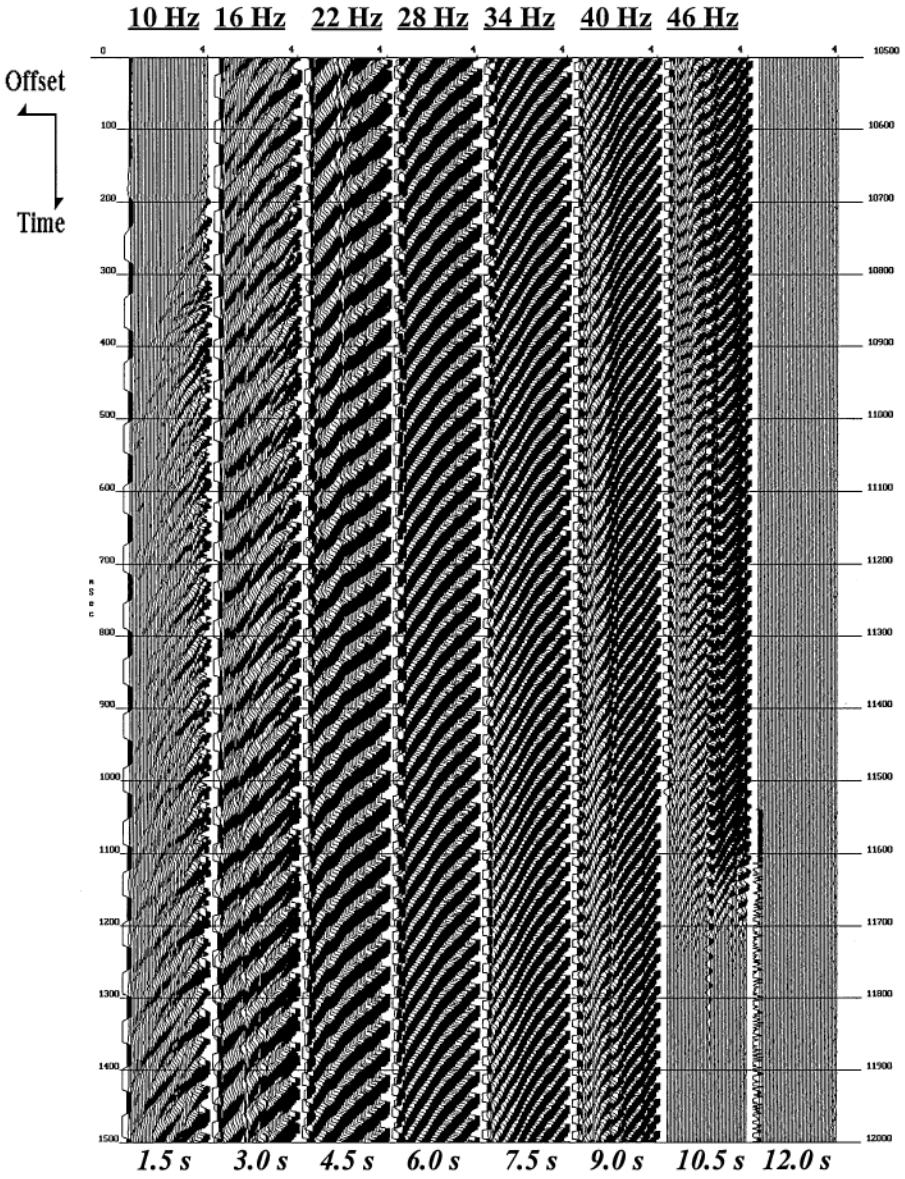

FIG. 2. Uncorrelated field record obtained using a source offset (x_1) of 1.8 m. A sweep of 10–50 Hz with 10-s sweep length was used and represented in the first trace. The record is displayed in 1.5-s segments because of the long record length. On the top and bottom of each segment are shown the sweep frequency and the time at the corresponding part of the record.

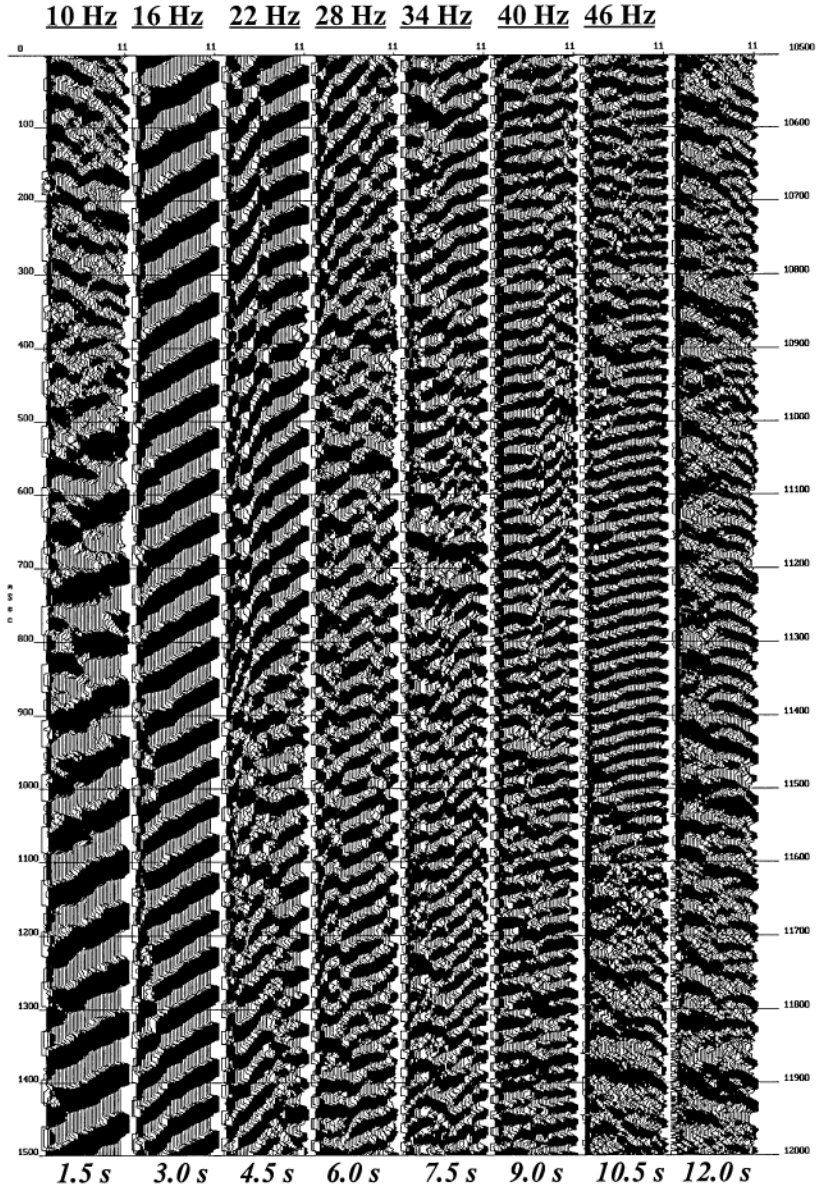

FIG. 3. Uncorrelated field record obtained by using a source offset (x_1) of 89 m.

corresponding to a wavelength range of 4–80 m and resulting in a 40-m maximum depth (z_{max}) of investigation.

A third record (Figure 4) was acquired with an x_1 (27 m) smaller than suggested by equation (2). This was done for two reasons. First, from the two previous noise analyses the optimum ratio between x_1 and $_{max}$ (avoiding near-field effects [equation (1)]) turned out to be about 0.3 (instead of the predicted 0.5). Second, the dominance of far-offset effects increased rapidly with offset, indicating the farthest offset needs to be closer to the source. This third record possesses a broadband ground roll spectra and suffers the least from near-field and far-offset effects of the three records from this site (Figures 2–4). Far-offset effects at frequencies higher than about 35 Hz did not affect the calculated phase velocities, indicative of a minimal noise environment (Park et al., 1998b).

The inverted v_s profile compares quite well with a nearby downhole-measured v_s profile (Figure 5a). A test well located near the end of the geophone spread was used to produce the measured downhole v_s profile using a three-component downhole receiver and a sledgehammer source. The downhole profile was calculated to be consistent with the thickness model used in the inversion process. Less than a 7% overall deviation can be observed between the inverted v_s profile and the downhole v_s profile. The close match between the inverted earth model and the measured data in terms of dispersion property is quite encouraging and provides a reasonable measure of ground truth (Figure 5b).

FIELD TEST WITH IMPULSIVE SOURCE

The flexibility of this technique is demonstrated by impulsive data acquired at Geometrics' San Jose, California, test site (Figure 6a). Data from this site were recorded using a sledgehammer source and 4.5-Hz geophones. A swept-frequency record can be transformed from the impulsive record (Figure 6b). The first trace in this record represents the stretch function used

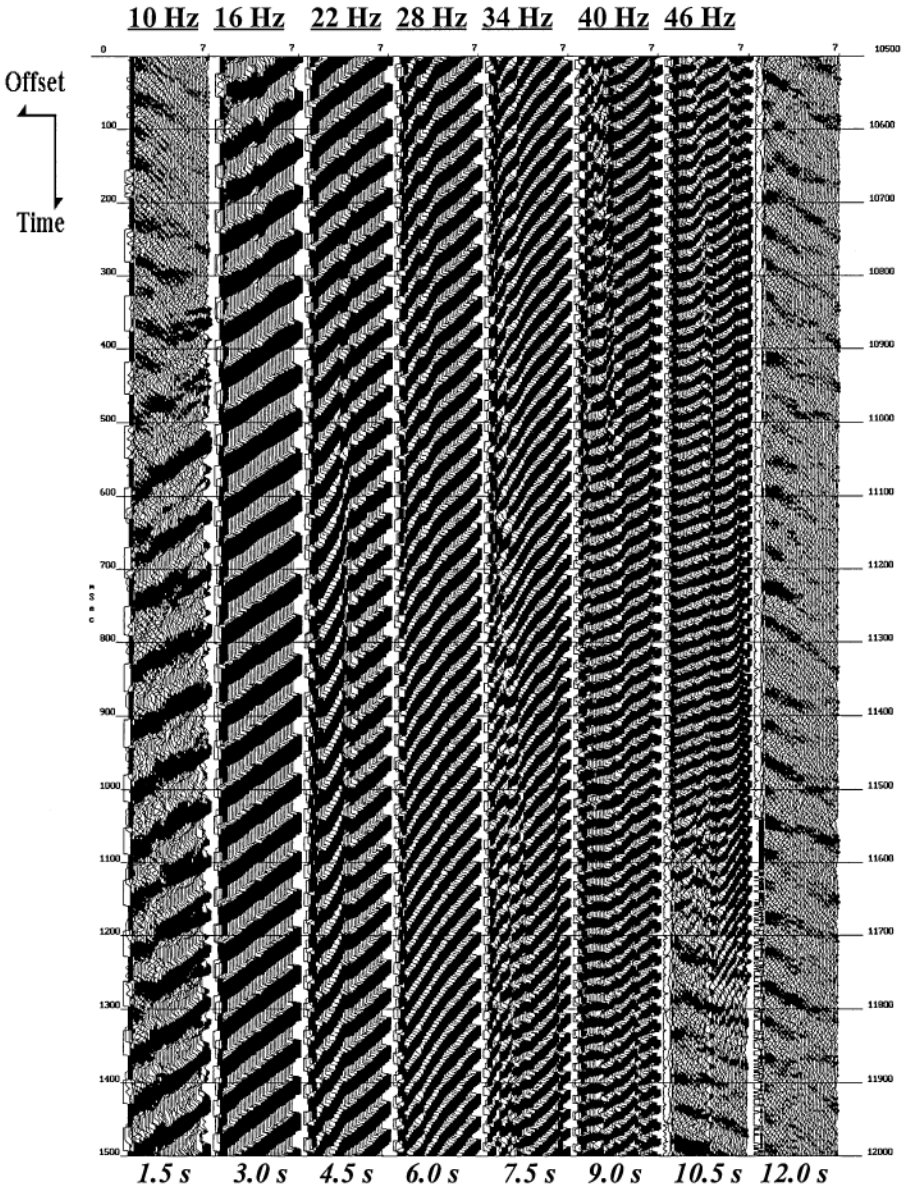

FIG. 4. Uncorrelated field record obtained by using a source offset (x_1) of 27 m.

to linearly separate frequencies from 5 to 55 Hz across the 2.5-s record. Near-field effects are obvious at low frequencies (<10 Hz) on these data. Little energy appears to have propagated to far-offset (>50 m) traces. Far-offset effects are obvious at high frequencies (>25 Hz) as well on these data. Far-offset effects manifest themselves on these data as severe attenuation (25–45 Hz) and body-wave contamination (>45 Hz) on longer-offset (>30 m) traces. For these reasons, near-offset (4–30 m) and far-offset (30–60 m) traces were digitally separated for phase-velocity calculations. This would be equivalent to acquiring and processing two shot gathers with fewer traces and into different spreads. The calculated dispersion curve (Figure 7a) obtained by analyzing only the far-offset traces shows a reasonable trend at the lower frequencies (<15 Hz), but body-wave contamination corrupts the trend at higher frequencies. The lowest analyzable frequency in this dispersion curve is around 3 Hz. The dispersion curve (Figure 7a) obtained by analyzing only near-offset traces provides a realistic trend for most frequencies above 6 Hz.

The two dispersion curves (Figure 7a) were combined to form a composite dispersion curve (Figure 7c), which was used to generate the v_s profile (Figure 7b).

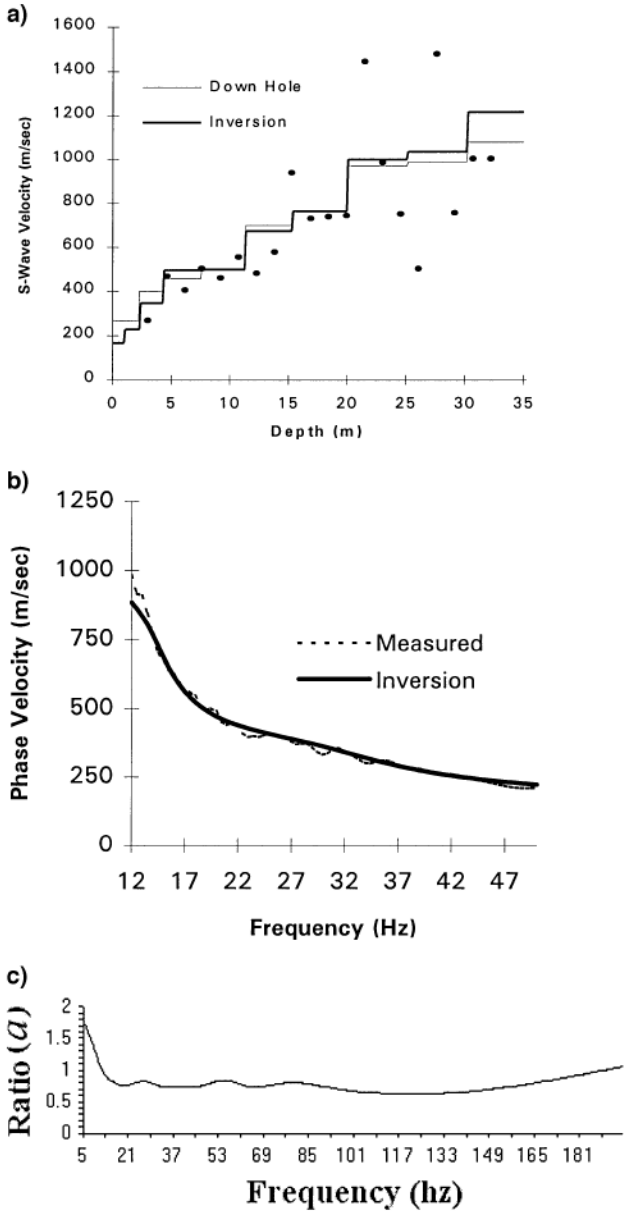

FIG. 5. Inversion results from a field test of (a) a v_s profile and (b) the corresponding dispersion curve in comparison with a downhole v_s profile and measured dispersion curve. Dots in the displayed v_s profile in (a) represent the data points actually measured during the downhole survey. The downhole profile was recalculated from these data according to the thickness model used in the inversion process. (c) The ratio a in equation (7) that was used during construction of the initial v_s profile.

DISCUSSIONS

The MASW method emphasized the minimization of near-field and far-offset effects, acquisition speed, sampling redundancy, and overall data accuracy. Minimization of near-field and far-field effects is achieved through optimum field configuration and/or a selective offset and frequency processing.

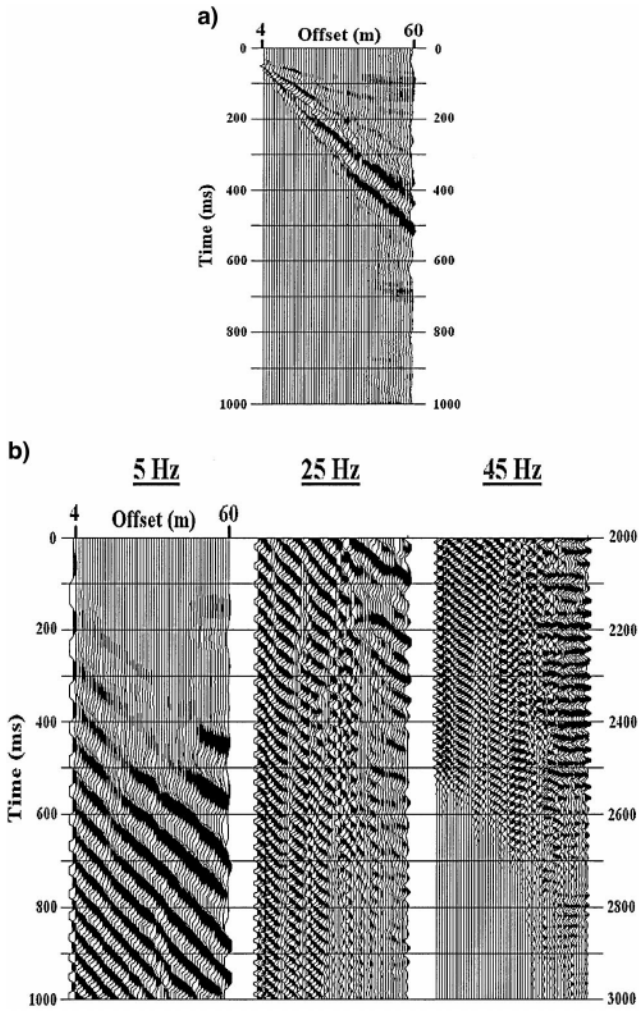

FIG. 6. (a) A shot gather obtained using a 12-lb sledgehammer as the source at a soil site in San Jose, California, and (b) its 3-s-long swept-frequency display after transformation using a stretch function (first trace). The swept-frequency record is displayed in 1-s segments. On top of each segment are shown the frequencies of the stretch function at the corresponding parts of the record.

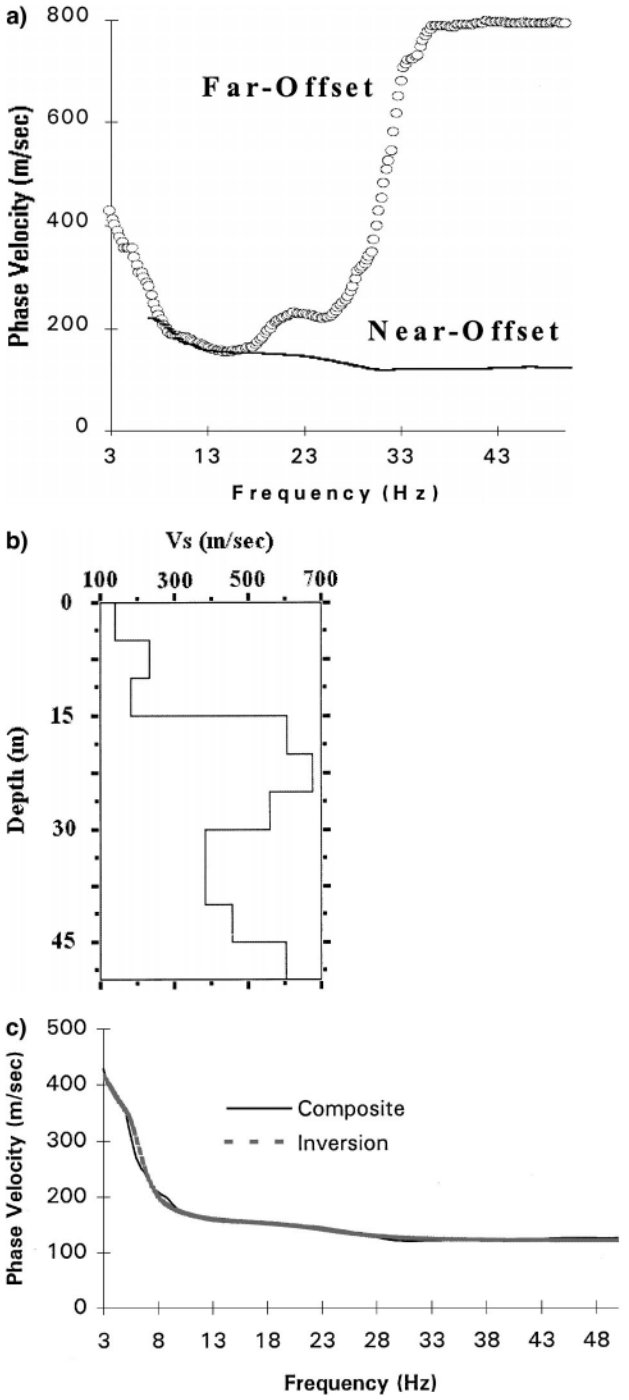

FIG. 7. (a) Dispersion curves obtained by processing near-offset (4–30 m) traces and far-offset (30–60 m) traces of the record in Figure 6a separately. (b) A v_s profile obtained from the inversion of a composite dispersion curve created by integrating the two curves. (c) The composite dispersion curve in comparison with the dispersion curve corresponding to the inverted v_s profile in (b).

Sampling redundancy is obtained by the relatively large number and tight spacing of all receivers. Accuracy of the MASW method was tested through ground truth comparisons with borehole measurements.

MASW assumes that the nature of near-surface materials can be treated implicitly as a layered earth model with no lateral variation in elastic properties. It is therefore important to keep the entire spread as short as possible to maximize the validity of this assumption if lateral variations are suspected. From an empirical perspective, this assumption is valid as long as good linear coherency is observed on decomposed or swept shot records.

We do not see any appreciable difference in the overall effectiveness, whether using a swept source or an impulsive source. Considering the relative importance of lower frequencies for deeper penetration, a heavy impulsive source seems to be an effective and economic choice. Because of this dependence on depth of penetration in the lower frequencies, we recommend always using high-output, low-frequency geophones with no recording filters. As far as the stretch function or Vibroseis sweep is concerned, we see no difference in the resulting v_s profile between up or down sweeps.

A frequency-continuous approach makes the swept-frequency display more useful when analyzing the interaction between several different types of seismic events, as compared with conventional filter panels. The optimum offset and lowest usable frequency outside the ground roll can be established more effectively using a swept-frequency display than from the impulsive record alone. This makes decomposition of frequencies a potentially useful tool for compressional surveys as well.

An indication of the overall speed of the MASW process is revealed by the production of a ten-layer v_s profile in less than 5 minutes on a 100-MHz Pentium-based PC from a 48-channel, 12-s-long swept-frequency record.

CONCLUSIONS

When ground roll is acquired using a multichannel recording method and displayed in a swept-frequency format, different frequency components of Rayleigh waves can be identified by distinctive and simple coherency. This leads to a seismic surface-wave method that provides a useful noninvasive tool, where information about elastic properties of near-surface materials can be effectively obtained for two reasons:

1) The integrity of each single Rayleigh wave frequency can be readily examined for contamination by coherent noise, making adjustments possible to improve S/N ratio during data acquisition and processing steps, and
2) A highly accurate dispersion curve can be obtained and inverted to produce a v_s profile with high confidence and consistency using ground roll recorded on a single shot gather.

ACKNOWLEDGMENTS

We thank Joe Anderson, David Laflen, and Brett Bennett for their commitment during the field tests. A special thanks to Lee Gerhard, director of the Kansas Geological Survey (KGS), and Kathy Sheldon, chief of operations at KGS, for giving permission to acquire vibroseis data at the KGS test site. Finally, we thank Mary Brohammer for her help in the preparation of this manuscript.

REFERENCES

Bullen, K. E., 1963, An introduction to the theory of seismology: Cambridge Univ. Press.
Coruh, C., 1985, Stretched automatic amplitude adjustment of seismic data: Geophysics, **50**, 252–256.

Gucunski, N., and Woods, R. D., 1991, Instrumentation for SASW testing, *in* Bhatia, S. K., and Blaney, G. W., Eds., Recent advances in instrumentation, data acquisition and testing in soil dynamics: Am. Soc. Civil Eng., 1–16.

Heukelom, W., and Foster, C. R., 1960, Dynamic testing of pavements: J. Soil Mechanics and Foundations Div., **86**, no. SM1, 1–28.

Mari, J. L., 1984, Estimation of static corrections for shear-wave profiling using the dispersion properties of Love waves: Geophysics, **49**, 1169–1179.

McMechan, G. A., and Yedlin, M. J., 1981, Analysis of dispersive waves by wave field transformation: Geophysics, **46**, 869–874.

Moore, R. C., 1964, Paleoecological aspects of Kansas Pennsylvanian and Permian Cyclothems: Kansas Geol. Bull., **169**, no. 1, 287–380.

Nazarian, S., 1984, In situ determination of elastic moduli of soil deposits and pavement systems by spectral-analysis-of-surface-waves method: Ph.D. dissertation, Univ. of Texas, Austin.

Nazarian, S., Stokoe, K. H., II, and Hudson, W. R., 1983, Use of spectral analysis of surface waves method for determination of moduli and thicknesses of pavement systems: Transport. Res. Record, **930**, 38–45.

Park, C. B., Xia, J., and Miller, R. D., 1998a, Ground roll as a tool to image near-surface anomaly: 68th Ann. Internat. Mtg., Soc. Expl. Geophys., Expanded Abstracts, 874–877.

———1998b, Imaging dispersion curves of surface waves on multichannel record: 68th Ann. Internat. Mtg., Soc. Expl. Geophys., Expanded Abstracts, 1377–1380.

Richart, F. E., Hall, J. R., and Woods, R. D., 1970, Vibrations of soils and foundations: Prentice-Hall, Inc.

Rix, G. J., and Leipski, E. A., 1991, Accuracy and resolution of surface wave inversion, *in* Bhatia, S. K., and Blaney, G. W., Eds., Recent advances in instrumentation, data acquisition and testing in soil dynamics: Am. Soc. Civil Eng., 17–32.

Sheu, J. C., Stokoe, K. H., II, and Roesset, J. M., 1988, Effect of reflected waves in SASW testing of pavements: Transportation Res. Record, **1196**, 51–61.

Stokoe, K. H., II, Wright, G. W., James, A. B., and Jose, M. R., 1994, Characterization of geotechnical sites by SASW method, *in* Woods, R. D., Ed., Geophysical characterization of sites: Oxford Publ.

Vardoulakis, I., and Vrettos, C., 1988, dispersion law of Rayleigh-type waves in a compressible Gibson half space: Internat. J. Numerical and Analytical Methods in Geomechanics, **12**, 639–655.

Waters, K. H., 1978, Reflection seismology: John Wiley & Sons, Inc.

Xia, J., Miller, R. D., and Park, C. B., 1999, Estimation of near-surface shear-wave velocity by inversion of Rayleigh wave: Geophysics, **64**, 691–700, this issue.

Yilmaz, O., 1987, Seismic data processing: Soc. of Expl. Geophys.